OPTICAL PROPERTIES OF SOME SURFACES FOR SOLAR ENERGY APPLICATION

by

ALIA H. MUSA, B.Sc., M.Sc.

A Thesis submitted to the
University of Aston in
Birmingham for the Degree
of

Doctor of Philosophy

Department of Physics
November 1980

TO MY FATHER AND MOTHER

STATEMENT

Title of Ph.D. Thesis: Optical Properties of Some
Surfaces for Solar Energy
Application

I hereby certify that no part of the work described in this thesis was done in collaboration, unless specifically so described, and that the work has not been submitted for any other academic award.

November 1980

CONTENTS

PAGE

OPTICAL PROPERTIES OF SOME SURFACES FOR SOLAR ENERGY APPLICATION

ALIA H. MUSA Ph.D., 1980

SUMMARY

The present work is a study of the optical properties of some surfaces, in order to determine their applications in solar energy utilisation. An attempt has been made to investigate and measure the optical properties of two systems of surfaces: moderately selective surfaces like thermally grown oxide of titanium, titanium oxide on aluminium and thermally grown oxides of stainless steel; and, selective surfaces of five different coloured stainless steel (INCO surfaces) and of black nickel foil.

A calorimetric instrument based on the steady state method for measuring directly the total emittance has been designed.

Chapter 1 is an introductory survey of selective surfaces. It also includes a brief review of various preparation techniques in use since 1955.

Chapter 2 investigates the theory of selective surfaces, defining their optical properties and their figures of merit. It also outlines the method of computing the optical properties (i.e. absorptance, $\underline{a}$, and emittance, $\underline{e}$), which have been adopted for the present work.

Chapter 3 describes the measuring techniques and the modes of operation of the equipment used in the experimental work carried out.

Chapter 4 gives the results of the experimental work to measure the optical properties, the life testing and chemical composition of the surfaces under study.

Chapter 5 deals with the experimentation leading to the design of a calorimetric instrument for measuring the total emittance directly.

Chapter 6 presents concluding remarks about the outcome of the present work and some suggestions for further work.

KEY WORDS

selective surface/absorptance/emittance/reflectance

ACKNOWLEDGEMENTS

The Author would like to thank her supervisor, Professor W.E.J. Neal, for valuable help and encouragement at all stages of the work.

My grateful thanks are due also to Professor B.O. Seraphin and his colleagues, in the Optical Sciences Center at Arizona University, U.S.A., for the use of the many facilities which were put at my disposal, and for making my work and stay there such a pleasure.

I am indebted to all the technical staff in the University who have kindly given me all the help I needed at various stages of my project. I am particularly grateful to Mr F. Lane and H. Arrowsmith in the Physics Workshop, for constructing the calorimetric instrument.

My thanks are due to Miss S. Al-Hilly and Mr H. Nasr for their assistance and help in the use of the computer, and Miss I. Hindy for help in final thesis preparation.

I am grateful to the Government of the Republic of Iraq for their financial assistance.

Finally, for the patience, support and encouragement given by my parents and family, I shall always be grateful.

TABLES PAGE

PAGE

FIGURES PAGE

PAGE

CHAPTER 1

INTRODUCTORY SURVEY OF SELECTIVE SURFACES

Whether the sun eventually becomes a source of commercially useful energy of some significance depends to a great extent on whether we will be able to make solar energy economically competitive with energy from other sources. The current trend, however, appears to favour solar energy as a potential renewable energy source. To increase the probability further means improving the energy collection and retention efficiency of existing solar system designs and at the same time reducing the cost.

An obvious area where further improvements can be realized is in the use of spectral selective surfaces.

A surface in this context means a system which consists of at least one thin layer on a substrate. Spectral selectivity means possessing particular radiation properties as defined in section 2.1 ; namely high solar absorptance (over the wavelength range 0.3 μm to 2.5 μm) and low emittance of thermal radiation (over a wavelength range ≥ 2 μm). For all practical purposes, all selective surfaces are based upon a metal substrate. This provides a low thermal emittance as well as good heat transfer characteristics.

A survey of selective surfaces suggests that four main types can be distinguished:

1. Intrinsic material surfaces.
2. Absorber-reflector tandem.
3. Interference stacks of alternating dielectric and metals, and
4. Topological coatings.

The intrinsic materials are substances that have selectivity naturally, without the need for any other material to augment the optical behaviour. For example, hafnium carbide (HFC), whose thermal infrared reflectance is in the order of 0.90, but whose absorptance is only about 0.70.

Since no single material has been found which exhibits both high absorptance and a low enough emittance, practical selective surfaces therefore have to be synthesized.

The absorber reflector tandem can be fabricated either by overcoating a metal, having infrared reflectance with semiconductor layers, or by subsequence layers of metal-dielectric film called interference filters.

Semiconductor layers - there are two classes of selective surfaces in which a thin semiconductor coating may be distinguished:

Class 1. A solar-absorbing layer on a metal substrate.
Class 2. A solar-transparent layer on a black substrate.

Almost all of the selective surfaces described to date are of the first class. The first selective surfaces were introduced and developed by Tabor (1955, 1967). Tabor produced CuO/Al by dipping the anodised aluminium plate into a hot acidic solution (90°C) of $Cu(NO_3)_2$-$KMnO_4$ for ten minutes. The plate was then dried and baked for 5 to 10 minutes. The reddish brown colour turned to nearly black cupric oxide. This surface gave an absorptance, a = 0.85 and emittance e = 0.11 and was stable up to 200°C.

Hottel and Unger (1959) prepared CuO/Al by spraying a dilute $Cu(NO_3)_2$ solution on to hot aluminium plate and then heating to above 170°C. The process produced black cupric oxide where a = 0.93 and e = 0.11.

Edwards et al (1962) used Ebanol C on copper which gave coatings largely of CuO where a = 0.91 and e = 0.16.

Close (1962) reported a copper black on copper by treating copper with a solution of NaOH and $NaClO_2$ (commercial process); such a surface gave values of a = 0.89 and e = 0.17.

Mattox and Sowell (1974) prepared blackened copper by using Ebanol C or NaOH/$NaClO_2$ which was normally burnished after treatment. The surface mostly consisted of CuO with some Cu_2O. This showed a dendritic structure and gave a as 0.91 and e as 0.16.

Blattner et al (1977) prepared copper on silver on a glass microscope slide. They thermally oxidised the copper at 380°C to form CuO. This surface gave a = 0.95 with e = 0.045, but after heat treatment at 540°C the silver migrated towards the surface from where it vaporized into the surroundings.

Gillette [1960] prepared cobalt oxide on polished copper or polished nickel. This surface was prepared by plating the copper with pure cobalt and then anodizing the surface. The absorptance of this surface was found to be, $\underline{a} = 0.93$ and its emittance, $\underline{e} = 0.23$.

Kokoropoulos et al [1959] reported on the preparation of cobalt oxide on silver by deposition and oxidation. The cobalt layer was deposited electrolytically in a cobalt sulphate bath on polished silver, followed by air oxidation in an oven at 400°C for a few hours. Values of $\underline{a} = 0.90$ and $\underline{e} = 0.27$ were found.

Leig [1979] prepared cobalt oxide on bright nickel, [40 μm thick] electroplated on polished steel 37. The best film was produced at a bath temperature of 55°C and a current density of 400 A/m^2. The plating time used was 90 secs, with a solution pH value of 2.3. This surface gave $\underline{a} = 0.93$ and $\underline{e} = 0.09$. If the pH was 2.3 but the current density changed to 800 A/m^2 with a 60 sec. plating time, then $\underline{a}$ was found to be 0.95 with $\underline{e} = 0.11$. The coating consisted of CO_3O_4 in addition to some traces of pure cobalt.

McDonald [1975] reported on a 'black chrome' selective surface which was a commercially electroplated decorative finish on bright nickel plated steel (Harshow Chemical Co.

or E. I. DV point Co., i.e. Chromonyx]. The deposition conditions were as follows: a current density of 24 A/m^2 and a voltage of 24 V for 3 minutes. The coating consisted of black chrome and its oxide Cr_2O_3. For this type of surface, a was found to be 0.87 and e was 0.09.

Fan [1976] reported on black chrome deposited on copper by electroplating. The coating consisted of polycrystalline Cr_2O_3 and amorphous Cr. This surface was stable up to 200°C giving a = 0.94 and e = 0.04.

Mattox [1976] investigated the optimum thickness of black chrome in a range [150 - 180] nm thick which gave a = 0.96 with e = 0.09 on nickel-plated steels. This coating was stable to 350°C. At temperatures higher than 450°C all of the Cr was converted to Cr_2O_3 and the nickel base oxidized causing failure.

Driver et al [1977] reported chrome black on nickel plated copper substrate. The best film gave a = 0.92 with e = 0.08. They found that those plated for 20 - 50 secs. were specular with interference colours ; those plated for 50 - 60 secs. looked non-specular and grey and those plated for periods greater than 60 secs. were specular and black.

Recently Gogna and Chopra [1979] prepared black chrome on bright and etched nickel-plated steel and studied the effect of substrate roughness. The coating produced a = 0.94

with e = 0.14 on etched nickel-plated steel. The bath used was chromium trioxide and sulphuric acid. The electroplating was carried out at a current density of 0.40 A/cm^2 and a temperature of about 30°C for a period of 1 to 4 minutes. They concluded that the rougher substrate gave higher absorptance, even at large angles of incidence.

Czanderna et al [1979] produced black chrome by reactive evaporation of chromium in oxygen-18. The thickness range was up to 110 nm thick and the layer consisted of Cr in a Cr_2O_3 matrix. They found that the possibility of varying the mixture of Cr in Cr_2O_3 depended on the deposition pressure in a steady state flow of oxygen-18. The surface was smooth but porous. They concluded that the desired ratio of Cr_2O_3 to Cr could be obtained by varying the oxygen partial pressure during reactive evaporation.

Pettit and Sowell [1979] studied the stability of electroplated 'black chrome' obtained from the Harshow Chemical Co. [Chromonyx bath] as a function of various parameters. They concluded that when the trivalent chromium concentrate was reduced from 16 gm/l to 8 gm/l, the absorptance value of the coating did not change even after aging at 350°C in air for over 1800 hours. For this surface, a = 0.98 with e [300°C] = 0.30, while the absorptance value of the depositing coating from 16 gm/l decreased by 8% when heated above 300°C in air.

Lampert and Washburn (1979) studied the stability of the chrome black (from a chromonyx bath) coating at different temperatures and atmospheres. They found that the coating was stable up to 400°C with $\underline{a}$ = 0.93 and $\underline{e}$ = 0.08; the coating consisted of Cr/Cr_2O_3. Above 400°C, in a vacuum and in air, the coating showed the growth of Cr_2O_3 at the expense of Cr and was responsible for the failure.

The early work on black nickel on nickel was done by Tabor (1961) and Tabor et al (1961) on galvanised iron. The deposited film thicknesses were in the range of 0.025 to 0.10 μm. In addition, the films were smooth when deposited on smooth surfaces and this led to the optical interference phenomena. It was Tabor who first discovered that a change in the plating current density during film deposition led to better absorbers. For example, a current density of 0.5 mA/cm^2 gave an optical constant equal to 1.85 - 0.83 i, but this changed to 1.68 - 0.35 i with a current density of 1.5 mA/cm^2. This meant that the chemical composition changed, i.e. one range of current density gave films that were nickel rich, whilst another range gave films that were zinc rich. This raised the possibility of optimizing the absorptance and the emittance of the coating. The double layer nickel black on polished nickel gave rise to $\underline{a}$ = 0.94 with $\underline{e}$ = 0.1 and $\underline{a}$ = 0.885 with $\underline{e}$ = 0.18 on galvanised iron. However, problems were encountered with adhesion failure.

Silo and Mladinik [1969] investigated coatings of 'black' nickel on zinc and found optimum values of current density, time of deposition and electrolyte composition of best selectivity. Their recommended electrolyte was a variation of one used for many years in the electroplating industry, [Cf. Ollard and Smith, 1964] and consisted of nickel ammonia sulphate [$NiSO_4[NH_4]_2SiO_4.7H_2O$] 60 gm/l, zinc sulphate [$ZnSO_4.7H_2O$] 75 gm/l and potassium thiocyanate [KCNS] 15 gm/l. This 'black' nickel was actually a mixture of nickel sulphide and zinc sulphide, the proportions of each varying with deposition parameters [Tabor et al, 1961].

Peterson and Ramsey [1975] fabricated nickel black [NiS & ZnS] coatings on nickel plated substrates. These double layer coatings deposited at first with a low and then a high current density, gave improved selectivity and remained unchanged if heated at 280°C for one week or subjected for up to 1400 cycles between temperatures of 20°C to 70°C at 90% relative humidity once a day.

Pettit and Sowell [1976] developed the black nickel by electroplating from both sulphate and chloride baths. They found that the sulphate bath gave no stable coatings. Those from chloride were deposited on bright nickel and mild steel substrate and were stable. Black nickel coatings on nickel foil substrate were obtained by varying the electroplating time while keeping the current density of 0.5 mA/cm^2 at a bath temperature of 25°C. They obtained a surface black nickel with a = 0.8 to 0.88 and e = 0.13. As the film thickness was increased such that the first-second and a high order interference reflectance minimum were located in the middle of the solar spectrum, a was shown to equal 0.95.

Wright and Mason [1978] developed and marketed selective nickel foil with a black surface oxide layer coating (unknown process) with a = 0.98 and e = 0.1 ± 0.03 at 100°C.

Recently a black nickel coating prepared on a zinc surface by chemical conversion was reported by Gogna and Chopra [1979]. The chemical bath consisting of nickel and ions of thiocyanate and ammonium was prepared to deposit the black nickel on galvanised iron. These surfaces gave a = 0.93 and e = 0.1.

Other selective surfaces with metal oxide have been prepared by chemical oxidation. Iron oxide on steel was prepared by Mattox and Sowell [1974]. Fe_3O_4 coating formed on carbon steel type 1018 using Ebanol S, (a = 0.88 with e = 0.1). They reported on the chemical blackening of 304 stainless steel using Ebanol SS. (This was called Ebanol SS on 304 SS). This coating formed Fe_3O_4 and exhibited no change in surface morphology and was stable in air up to 230°C. This coating gave a = 0.91 with e = 0.1.

Trombe et al [1961] reported the selectivity which could be produced by a simple method, i.e. by the oxidation of stainless steel between 250°C and 600°C. This gave extremely thin surfaces of coloured oxides. For 16% Cr stainless steel, after a 3 hour heating period at 600°C, a = 0.75 and e = 0.1; the colour was blue. With 18% Cr and 8% Ni, after heating at 600°C for three hours, a = 0.70 and e = 0.1. The cost of such treatment remained very low. The same method has been used by Edwards et al (1962) for thermally oxidized titanium (AMS 4901) heated for 300 hours at 450°C in air and gave a = 0.80 eith e = 0.21 and for 410 stainless steel heated to 750°C in air gave a = 0.76 with e = 0.13. Edwards used Ebanol S on steel dipped for 5 minutes in a 127°C boiling solution and produced a surface of a = 0.85 with e = 0.1.

Intrinsic semiconductors such as silicon (Si), germanium (Ge) and lead sulphide (PbS) have also been investigated as possible spectral-selective materials. They showed a high solar reflectance and they needed anti-reflection layers for proper use.

Edwards et al (1962) prepared a silicon layer of 0.5 mm thick on evaporated aluminium. This surface gave a = 0.50 and e = 0.12. With an additional layer of 83 mm of SiO_2 to antireflect the silicon, the combination gave a = 0.65 and e = 0.12.

Gilbert et al (1978) reported on black germanium produced by rf sputtering. This surface gave a = 0.90.

Williams et al [1963] reported on selective surface made of PbS crystals [34 nm thick] deposited on aluminium substrates. These coatings were dendritic in structure, so the optical absorption was a combination of the intrinsic absorption of the lead sulphide and particular scattering. Their sulphide crystallites were bonded to the substrate by a silicone resin binder. The absorptance, $\underline{a}$, for lead sulphide with the binder = 0.89 and $\underline{e}$ = 0.2 to 0.3.

MacMahon and Jasperson [1974] prepared some tandem layers with PbS using vacuum evaporated coatings on evaporated [100 nm thickness] aluminium. These coatings were polycrystalline and did not show specular reflectance in the visible region of the spectrum. They used a much thinner layer of PbS (about 0.12 μm] as compared to Ge or Si thicknesses which are in the range of [1 - 10 μm]. The a/e ratio of about 43 was reported with this type of layer and $\underline{a} \approx 1$ over the solar range and the transition from high to low absorption was confined to the range of wavelengths 1.0 - 2.5 μm.

Marchini and Gandy [1978] determined the optimum thickness of PbS that gave a maximum a/e ratio. They found that the optimum a/e is in the lead sulphide thickness range of 30 to 80 nm. These surfaces survived heating to 300°C. The coatings must be used in a non-oxygen atmosphere and the ultra violet irradiation in air converted the films to $PbSO_4$ via photo-oxidation, as shown by Mattox and Sowell [1974].

Pettit and Sowell [1976] prepared three surfaces by a spraying technique to a polished 1018 stainless steel substrate. The paint was then cured in air at 150°C for over 2 hours. The first one with PbS paint particle of size 10 - 15 nm gave $\underline{a}$ = 0.96 with $\underline{e}$ = 0.70. The second one with Ge particles [325 mesh] gave $\underline{a}$ = 0.90 and the third one with Si particles [325 mesh] gave $\underline{a}$ = 0.83. These particles were a mixed in 3:1 volume ratio of particles to binder.

The multilayer stack with silicon as a core material on a silver substrate as reported by Seraphin [1976] was produced by chemical vapour deposition [CVD]. This tandem was composed of a silver layer and 1 - 2 μm thick layer of silicon and two additional layers [SiO_2/Si_3N_4] were used as antireflecting layers. In addition a Cr_2O_3 layer was used as a diffusion barrier and agglomeration inhibitor between the silver and the silicon. This multilayer gave an a/e ratio of 15 at room temperature. Donnadieu and Seraphin [1978] improved on the above converter by adding a layer of Ge, 0.5 μm thick; the $\underline{a}/\underline{e}$ ratio increased to 22. The above tandem was produced for use at 450°C to 600°C.

A good example of class [2] selective surfaces is that of a fluorine doped tin dioxide layer on black enamelled steel. Leig [1979] prepared the above surface by a spraying technique with a $[CH_3]_2$ $SnCl_2$-H_2O-HCl solution in which 100% mole NH_4F relative to the tin salt was added. The spraying occurred at a substrate temperature of 520 - 570°C. This convertor gave $\bar{a}$ = 0.91 with $\bar{e}$ = 0.15. By adding a thin antireflection coating of silicon resin (Dow Corning 805) on the SnO_2 surface, the absorptance increased to 0.93 but the emittance increased as well to 0.17.

Another example reported recently relates to TiO_2-Ag-TiO_2 complex used as a heat mirror by Fan and Bachner (1976)

The interference stack of alternating dielectric and metals. These are called interference filters. These stacks usually consist of a number of metal-dielectric films. The physical principle is that by optical interference of thin layers of an alternating low and high refractive index, the absorptance at certain wavelengths can be maximized. This method depends on the optical properties of the individual layers and on the film thickness to wavelength ratio. This method requires very careful control and in a vacuum deposition process is likely to be expensive and not easily applicable to large areas.

A good example is the (Al_2O_3-Mo-Al_2O_3-Mo) coating, developed by Schmidt and Janssen (1965) and Peterson and Ramsey (1975). This coating was built of at least two layers of Mo-Al_2O_3 on a stainless steel substrate and seems to be the most stable (thermally) system at high temperature $\approx$ 800°C, which has been produced up to the present time. Its absorptance $\bar{a}$ = 0.85 - 0.91 and emittance $\bar{e}$ = 0.11

measured at 500°C. The same system has been deposited on a molybdenum substrate. This failed at 1050°C while the former failed at 900°C. Auger analysis revealed in both cases that this was due to the out-diffusion of iron and chromium from the steel substrate. The limitation of this system is the need for the deposition of the films by a vacuum evaporation technique.

Another example of an interference filter was reported by Meinal et al (1975). This consisted of four-layer coatings using $Ag/Al_2O_3/Cr/Al_2O_3$ and gave a double reflection minimum in the solar region of the spectrum with a sharp transition leading to high infrared reflectance. The measured absorptance ranged between 0.90 and 0.95 and the emittance between 0.02 and 0.04. This system survived heating for 1000 hours at 150°C in air. Other interference filters were reported by Long (1965) and Kadryashova (1969).

Topological coatings; this type of coating could be classified into:

a. macro case, i.e. corrugated surfaces and
b. micro case, i.e. control of the morphology of the surface.

Topological coatings provide different properties for short wavelength and long wavelength radiation and this can be achieved if the surface textured profile could discriminate between the pencil-beam character of the solar input and the hemispherical wavefront of thermal radiation. The underlying mechanism differs accordingly to the size and separation of the structural elements as compared to the wavelength of light and accordingly to properties and distribution of the inhomogeneties.

Good examples for the macro-case are the corrugated surfaces such as a series of vees so that any beam of incident light - within a given range of angles of incidence - will suffer more than one reflection before emerging from the vee [Tabor, 1955 and Close, 1963]. A 'Gothic arch' was suggested by Tabor [1967] to ensure two reflections for a beam at any angle of incidence.

Hollands [1963] concluded that the vee-corrugated specular surface is directionally selective and the selectivity of the specular spectrally selective surface can be improved by vee-corrugating to make it directionally selective also.

In micro-case coating, the surface roughness has dimensions of the order of a micron or so. The surface may act as an array of adjacent cavity absorbers for short wavelengths [i.e. as a strong absorber], whilst appearing substantially flat for long wavelengths, so that the material surface has an intrinsically low emissivity [i.e. a metal]. The nett result is a selective surface in the sense discussed.

Examples of this approach are the dendritic, microporous surfaces and surfaces provided with very small holes or meshes.

Cuomo et al [1975] prepared a dendritic surface of tungsten by [CVD] from $W[CO_3]$. This process involved hydrogen reduction of tungsten at temperature 500°C. The authors could distinguish between the dendritic form - which looked black [$\underline{a} \approx 0.96$] and a shallower 'hillock' form which appeared grey [$\underline{a} \approx 0.75$]. By anodizing the surface to reduce surface reflectivity, the $\underline{a}$ value improved and approached unity and the e values of 0.2 - 0.3 were measured. The 'hillock' type surface anodized [Distefano et al 1978] in 0.1 N phosphoric acid produced a surface where $\underline{a}$ 0.95 to 0.98 and $\underline{e}$ = 0.12 to 0.18. This last figure was very similar to the 'best' values for nickel-black and chrome black. Costs were high for this type of surface.

In an attempt to reduce the costs, Grimmer et al [1978] produced nickel dendrite as in the tungsten case by CVD from $Ni[CO_4]$ on aluminium substrate. Values of $\underline{a}$ = 0.90 to 0.95 and $\underline{e}$ = 0.2 to 0.4 were found.

Horwitz [1974] has proposed an approach in which the topology is made by providing very small holes or meshes that distinguish between optical and thermal wavelengths. High a/e ratios are predicted on theoretical grounds, but practical surfaces have not yet been obtained.

Small metal particles embedded in a dielectric matrix [which is infrared-transparent], prepared by vacuum evaporation, can yield selective microporous surfaces. Some examples of this technique are the gold black deposits of McKenzie [1976]. Fan and ZaVracky [1976] prepared cermet films of MgO/Au by radio frequency sputtering on Mo [100 nm] coated stainless steel. MgO and Au in this coating were both crystalline and gave measurements of a = 0.93 and e = 0.1. This coating showed stability up to 400°C for 64 hours.

Tests on cermet films of Cr_2O_3/Cr have been published by Fan [1978] and these were stable up to 300°C. Their optical properties were found equal to that produced by electroplating.

Fan [1978] also prepared Ni/SiO_2 and MgO/Ni film by pressing tablets of MgO powder and Ni powder and then evaporating by an electron beam on quartz substrate. The surface gave a in ranges 0.88 to 0.90 and e from 0.13 to 0.18.

Grangvist et al [1979] developed Ni/Al_2O_3 films on aluminium substrates. This surface was blackened by ac electrolysis in a bath containing $NiSO_4$ and it showed stability when heated at 300°C for two weeks. The measured values of a = 0.95 and e = 0.15 were found. Cermet films of Au/Al_2O_3, Ag/Al_2O_3 and Cr/Al_2O_3 were developed by McKenzie [1979] [they were vacuum evaporated with two separate sources] on copper substrates. The evaporation ratios were kept constant by translating the substrate on a carrier so that it passed from a point closer to the metal source to a point closer to the ceramic source. The measured a and e values were given as $\underline{a}$ = 0.89 - 0.93, $\underline{e}(300^{\circ}C)$ = 0.22 - 0.04 for Au/Al_2O_3 and $\underline{a}$ = 0.88, $\underline{e}$ = 0.025 for Ag/Al_2O_3 and $\underline{a}$ = 0.91 with $\underline{e}$ = 0.029 for Cr/Al_2O_3.

Ashcroft et al (1979) prepared a composite of Ni/Al_2O_3 on copper. This surface gave $\underline{a}$ = 0.94 and $\underline{e}(200^{\circ}C)$ = 0.1 and for Pt/Al_2O_3 on copper, it gave $\underline{a}$ = 0.94 and $\underline{e}(200^{\circ}C)$ = 0.1. The latter surface showed stability when heated for 300 hours at 600°C, while the former surface showed stability when heated up to 500°C.

Recently a 'black Mo' prepared by CVD from $Mo(CO_6)$ has been reported by Chain et al (1980). This coating consisted of Mo and MoO_2. The measured values of $\underline{a}$ = 0.74 and $\underline{e}$ = 0.08, after heating to 500°C, were found. The absorptance of this convertor increased to 0.90 after overcoating it with a layer of 75 nm thickness of Si_3N_4.

A summary of the different types of selective surfaces and the different preparation techniques as developed since 1955 is shown in Table 1.1.

Table 1.1 Properties of some selective surfaces for Solar Energy Application

Surface	a	e	Reference
CuO on Al; by spraying dilute $Cu[NO_3]_2$ solution on hot Al plate and baking	0.93	0.11	Hottel and Unger [1959]
CO_3O_4 on Cu; by plating the copper with pure cobalt and then anodizing the surface	0.93	0.24	Gillette [1960]
'Nickel Black'; containing oxides and sulfides of Ni and Zn, on polished Ni	0.91 0.94	0.11	Tabor et al [1961]
'Nickel Black' on galvanized iron [experimental]; commercial process	0.89	0.12 0.16 0.18	Tabor et al [1964]
CO_3O_4 on silver; by deposition and oxidation	0.90	0.27	Kokoropoulos et al [1959]
CuO on Ni; made by electrodeposition of Cu and subsequent oxidation	0.81	0.17	Kokoropoulos et al [1959]
Ebanol C on Cu; commercial Cu-blackening treatment giving coatings largely CuO; commercial process	0.90	0.16	Edwards et al [1962]
'Cu Black' on Cu, by treating Cu with solution of NaOH and $NaClO_2$; commercial process	0.89	0.17	Close [1962]
PbS crystals on Al	0.89	0.2	Williams et al [1963]
Al_2O_3-MO-Al_2O_3-MO-Al_2O_3-Mo-Al_2O_3 interference layers on Mo [e[250°C]	0.91	0.085	Schmidt and Park [1965]
'Cu Black' by Ebanol C or NaOH/$NaClO_2$ and burnished after treatment	0.91	0·16	Mattox and Sowell [1974]

Table 1.1 (cont)

Surface	a	e	Reference
Ebanol S on 1018 steel; forms Fe_3O_4	0.88		-
304 stainless steel black, using Ebanol S.S.; forms Fe_3O_4	0.91		-
W-Dendritic surface; produced by hydrogen reduction of WF_6 on sapphire, polished tungsten and stainless steel	0.98	0.26 at 550°C	Cuomo et al (1975)
$TiO_2/Ag/TiO_2$; by rf sputtering in Ar-atmosphere, TiO_2 target, and Ag target on CG 7059 glass	0.54	0.01	Fan and Bachner (1976)
PbS paint; 10nm - 15 nm particle size sprayed on polished 1018 steel substrate, then cured in air at 150°C for over 2 hours	0.96	0.7 at 300°C	Pettit and Sowell (1976)
'Black Nickel'; by electroplating from the chloride bath on bright nickel electroplated mild steel substrates	0·80-0·88	0·13	Pettit and Sowell (1976)
MgO/Au cermet film; by rf sputtering on Mo-coated stainless steel; stable up to 400°C	0.9	0.1	Fan and Zarracky (1976)
TiNx and ZrNx; by vacuum sputtering of Ti or Zr in partial pressure of nitrogen on silver film on stainless steel	0.88- 0.93	0.04- 0.19	Blickensderfer et al (1977)
'Chrome Black'; on Cu using Chromox on tin free steel	0.87 0.92	0.03 0.08	Driver et al (1977)
MgO-Au, Cr_2O_3-Cr; cermet films, by rf sputtering on MO substrate, stable up to 400°C, on copper; stable up to 200°C and stable up to 300°C if on stainless steel	0.90	0.1	Fan (1978)

Table 1.1 (cont)

Surface	a	e	Reference
Dendritic surface (Ni); by CVD on Al by H_2 reduction for coating of 6 μm thickness	0.95	0.75	Grimmer et al (1978)
of 2 μm thickness	0.95	0.2	
'Black Ge'; by rf sputtering on Corning 2947 microslides	0.90		Gilbert et al (1978)
'Black Chrome' on nickel plated steel	0.94	0.14	Gogna and Chopral (1979)
Ni/Al_2O_3, porous Al_2O_3 films; by dc. anodization in dilute phosphoric acid on Al metal	0.93-0.96	0.1-0.2	Grangvist et al (1979)
TiOx/Ti on pyrex; by reactive evaporation of Ti film in O_2, efficiency reported only and is equal to 75%			Yoshida (1979)
Cermet film; by vacuum evaporation (on copper substrate) from two separate sources			McKenzie (1979)
Gold cermet film - aluminium	0.89-0.93	0.022-0.041	
$Ag-Al_2O_3$	0.88	0.025	
$Cr-Al_2O_3$	0.918	0.029	
Ni/SiO_2 cermet film; by electron beam evaporation	0.90		Okuyama et al (1979)
MgO/Ni cermet film	0.88		
Black Mo; by CVD of $(Mo(CO)_6)$ in presence of oxygen. The substrate temperature is 300°C; the emittance is measured at 500°C	0.74	0.08	
by adding Si_3N_4 (75 nm)	0.90	0.08	Chain et al (1980)
Black Mo; by CVD of $MoClO_2$ in presence of hydrogen, the substrate temperature is 700°C			

Table 1.1 (cont)

Surface	a	e	Reference
'Black Chrome'; commercially electroplated decorative finish on steel	0.868	0.088	McDonald (1975)
Al_2O_3-Mo-Al_2O_3; by vacuum evaporation on Mo substrate; the emittance is measured at 1000°C and is equal to 0.11 at 500°C. Stable up to 400°C	0.85	0.22	Peterson and Ramsey (1975)
NiS-ZnS coating, 'Black Nickel' on plating metal with Ni; produced by electroplating	0.95	0.07	-
Black Nickel (produced by chemical conversion) deposit on galvanized iron, zinc electroplated and zincated aluminium substrates	0.93 0.94 0.90	0.08 0.1 0.14	Gogna and Chopra (1979)

CHAPTER 2

SELECTIVE SURFACES

2.1 DEFINITION AND ADVANTAGES OF SELECTIVE SURFACES

Selective surfaces are surfaces for solar thermal absorbers which reduce re-radiation losses and hence give increased thermal efficiency for collectors.

Recently, the interest in the utilization of solar radiation has increased. Three main collector temperature levels can be identified:

1) Low temperature level, 25°C - 40°C, with application in the heating of swimming pools.

2) Moderate temperature level, 40°C - 150°C, for example, in systems for space and water heating and cooling.

3) High temperature level > 150°C, for the production of steam and for generation of electricity.

For the low temperature level, a simple flat plate collector will receive the total incoming solar radiation. However, for the high temperature level a high optical concentration of solar radiation is needed. For the moderate level both flat plate and low-concentration collectors can be used.

The performance of a collector in a given site essentially depends on its design and the optical and thermal properties of the material of which it is composed. In order to determine the contribution of the absorber surface to the collection and conversion system, we must first examine the energy flow at the converter surface [Seraphin 1979]. The basic principle of photothermal solar energy conversion is shown in Figure 2.1. Some optical device, such as a lens or mirror, may be used to increase the flux per unit area incident on the collector surface. This concentration factor X is the ratio of the area of the collector aperture to that of the absorber that emits thermal radiation at the absorber temperature.

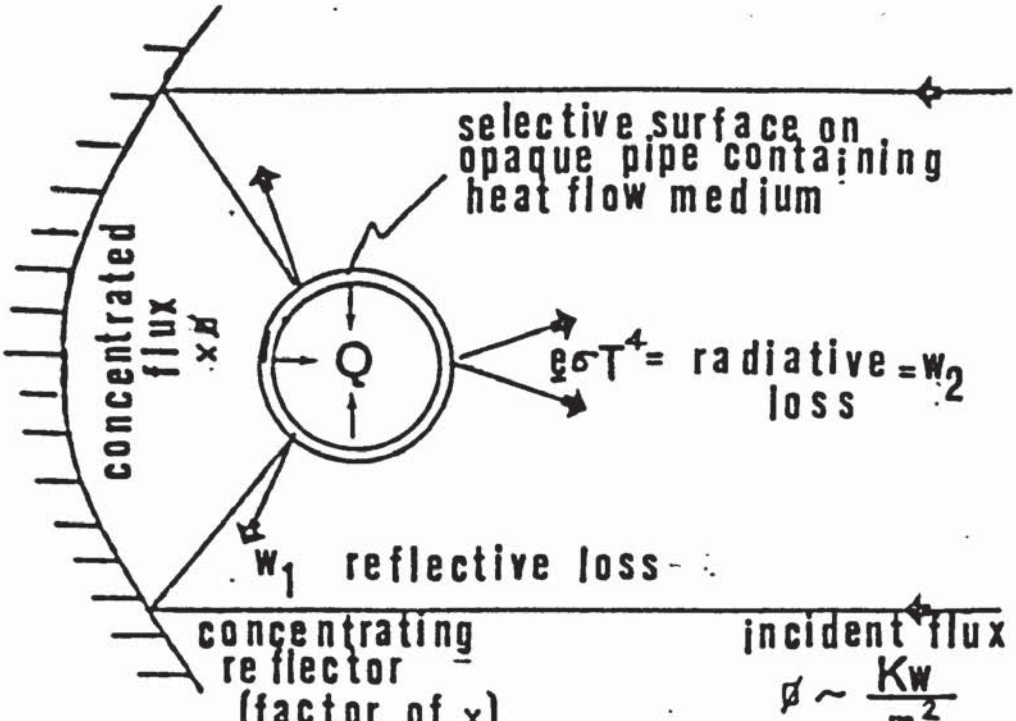

Figure 2.1 Energy balance at the surface of a photothermal conversion unit

The element is shown in Figure 2.1 as a pipe which runs along the focal position of the lens. A heat transfer medium flows through the pipe which is coated on the outside with a selective absorber. The importance of selectivity can be quantified by calculating the conversion efficiency, A_m, as the useful power, Q which is transferred to the heat flow medium in Figure 2.1, divided by the amount of solar power incident on the converter element, $X\emptyset_s$.

The conversion efficiency is determined by first writing a heat balance equation at the surface of the converter in the above figure. The incident power, $X\emptyset_s$, is divided into three components: W_1 which is reflected outright; W_2 which is re-radiated in the thermal infrared according to the radiation laws for a real body at temperature T; Q which is passed on as heat, produces useful work. The simplified heat balance equation is therefore given by the expression:

$$X\emptyset_s \underline{a} = \underline{e}\,\sigma(T^4 - T_o^4) + L_{cc} + Q \qquad (2.1)$$

where, $\emptyset_s$ is the solar flux incident on the collector

$\underline{a}$ is the total absorption coefficient

$\underline{e}$ is the total hemispherical emittance of the absorber at temperature T

L_{cc} is the loss due to convection and conduction and

Q is the useful heat extracted from the system.

In other words, energy absorbed is equal to the sum of the radiative losses, conductive and convection losses, and the energy passed to working fluid.

The nett radiative power is assumed to be the difference between the power radiated from the absorber, at temperature T, and the power radiated to the absorber by the surroundings at temperature T_o. Furthermore, the absorptance of the surface for radiation from the surroundings is taken to be equal to the thermal emittance of the absorber. At high temperatures, conduction and convection losses are negligible compared to radiation losses and the heat balance is then given by

$$X\varnothing_s \underline{a} = \underline{e}\,\sigma T^4 + Q \quad ; \quad T^4 >> T_o^4 \qquad (2.2)$$

The thermal efficiency of the converter can then be defined as

$$A_m = \frac{Q}{X\varnothing_s} = \underline{a} - \frac{\underline{e}\,\sigma T^4}{X\varnothing_s} \qquad (2.3)$$

From equation 2.3 we see that the efficiency at a given temperature T can be increased by increasing $\underline{a}$, decreasing $\underline{e}$ or increasing the flux density $X\varnothing_s$ at the absorber. However, since the sun can be approximated by a black body at 6000 Kelvin and since the conversion temperatures do not exceed 1000 Kelvin for most of the applications, there is a very distinct separation between the spectral distribution of solar radiation and that of the thermal radiation emitted by the absorber as shown in Figure 2.2.

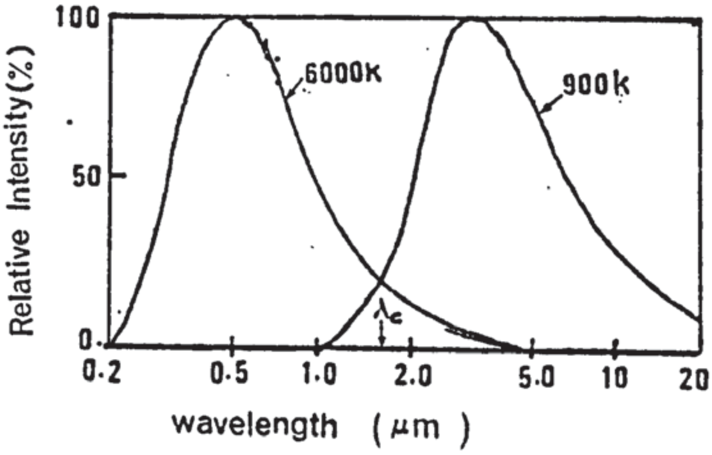

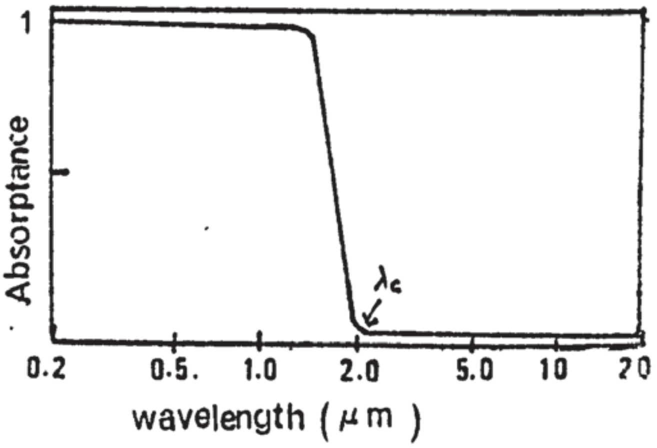

Figure 2.2 Spectra of solar and black body (900 k) radiation

Figure 2.3 Spectral profile of the absorptance for an ideal photothermal converter

From this, it follows that if materials or surfaces can be synthesized so that they differentiate in their absorptance, reflection or transmission characteristics between wavelengths above 2 µm, i.e. in the 'thermal' range and wavelengths below 2 µm, i.e. in the 'solar' range, then it may be possible to trap solar energy, i.e. to collect it by absorption but to prevent or minimize the thermal radiation loss. Such materials or surfaces are called 'selective'. (Although, strictly speaking, any surface whose optical properties vary with wavelength may be termed selective, the term is used in this present context to refer either to band pass filter properties or as a one way value, i.e.

surfaces whose characteristics are substantially constant but different over broad bands of wavelengths). In the ideal case (Figure 2.3) the surface is totally absorbent or 'black' at wavelengths below λ_c (λ_c designates the cut-off wavelength of the two spectral distributions) and is totally reflecting or 'white' for wavelengths above λ_c. It should be noted that the value of λ_c depends on the temperature and the concentration coefficient as shown in Figure 2.4.

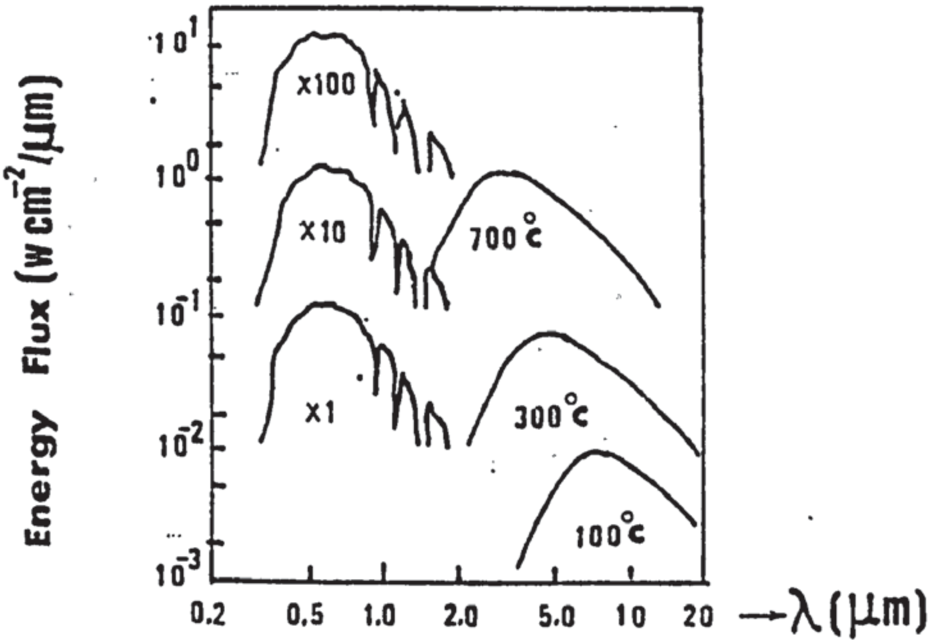

<u>Figure 2.4</u> Spectral profile of the energy flux of solar input for three concentrations, and of reradiative loss at three converter temperatures

Figure 2.5 shows the plot of A_m of a converter exhibiting $\underline{a}$ = 0.95 against the emittance for the x values equal to 100, 250 and 1000 at temperatures of 4oo°C and 500°C.

Assuming the system exhibits maximal absorptance, we see from Figure 2.5 that either high X or low e must be employed to attain the highest A_m. As a result, the solar engineer faces a trade-off between providing a high X value with complex concentration systems and providing low e and high a with spectral selective coatings. The expense of concentrating systems increases with increasing X, increasing from the flat plate with [X = 1], the Winston collector with [X = 10], and the parabolic trough with [X > 10], to the central receiver or power tower with [X > 1000].

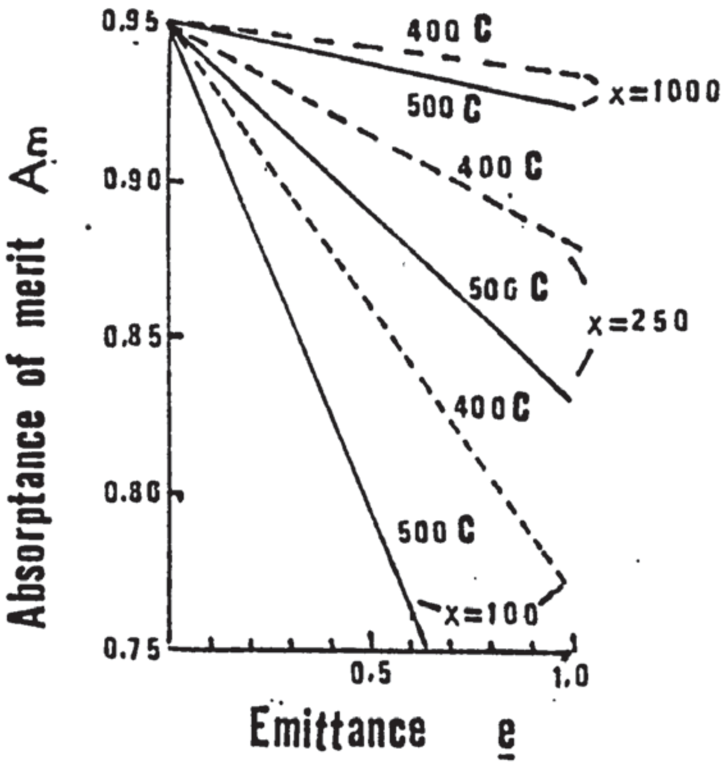

Figure 2.5 Conversion efficiency A_m versus emittance for a converter of a = 0.95 at various concentration ratio, X, and for T = 400°C and 500°C

Figure 2.6 illustrates the four characteristics, characterized by increasing values of X. Masterson [1977] has shown that even systems with X = 500 benefit from using spectral selectivity. Both this fact and the expense of large concentration systems justify extensive research into selective coatings.

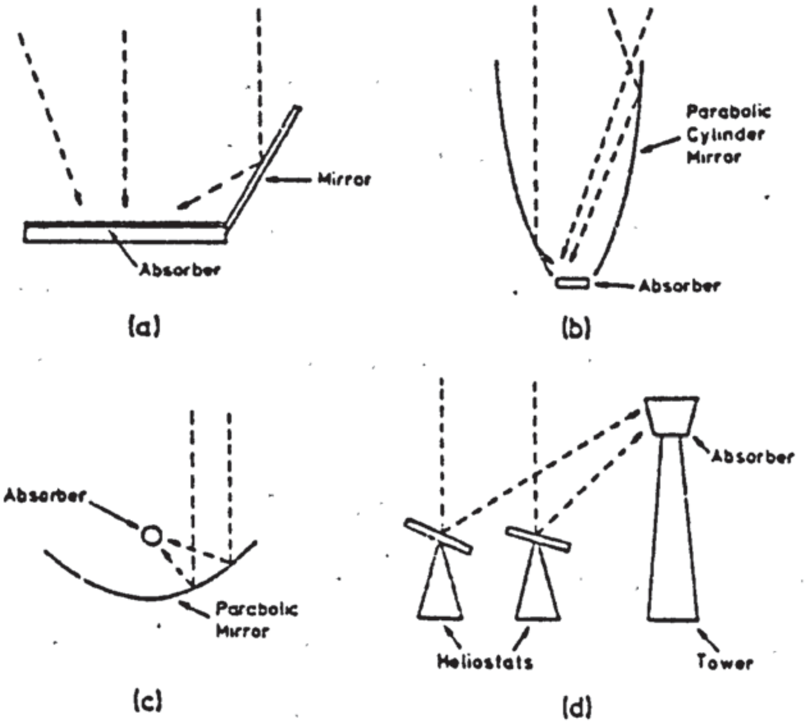

Figure 2.6 Schematic representation of the basic types of nonimaging (a,b) and imaging (c,d) solar collectors: (a) flat plate; (b) Winston parabolic concentrator; (c) parabolic trough; and (d) power tower.

2.2 REQUIREMENTS OF SELECTIVE SURFACES (SS)

The basic requirements for selective surfaces to be used in conjunction with solar radiation can be given as follows:

1. High solar absorptance $\underline{a} = 1$
2. Low thermal emittance $\underline{e}$
3. Long-term stability at the desired operating temperature
4. Stability to or recovering from short-term overheating due to failure to extract energy from the collector
5. Stability against atmosphere corrosion
6. Compatability with given substrate materials
7. Reproducibility
8. Reasonable cost.

2.3 PHYSICS OF SELECTIVE SURFACES [Harrison , 1960]

2.3.1 RADIANT ENERGY

Radiation is electromagnetic energy that is propagated through space at the speed of light. For most solar energy applications, only thermal radiation is important, and is defined as radiant energy emitted by a medium that is due solely to the temperature of the medium. The emitted radiation is usually distributed over a range of wavelengths.

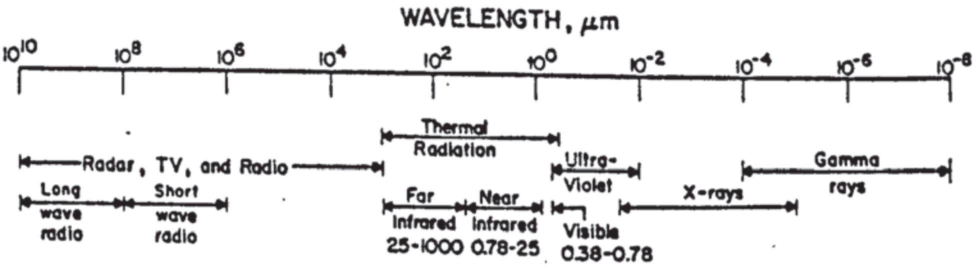

Figure 2.7 Spectrum of electromagnetic radiation

Figure 2.7 illustrates the spectrum range of electromagnetic radiation. The wavelengths of importance in solar energy and its applications are in the ultraviolet to near-infrared range, that is, from 0.2 to about 25 μm. Solar radiation outside the atmosphere has most of its energy in the range of 0.2 to 4 μm, while solar energy received at the ground is substantially in the range of 0.29 to 3.0 μm.

The physics of selective surfaces are governed by four physical laws: those of Stephan-Boltzmann, Kirchhoff, Planck and Wien.

2.3.2 STEPHAN-BOLTZMANN EQUATION

An ideal black surface is one which, when heated to a temperature T, emits thermal radiation W_2 (per unit area) which is given by the expression:

$$W_2 = \sigma T^4 \tag{2.4}$$

where σ is the Stephan-Boltzmann constant 5.6697×10^{-8} watt/m^2k^4, T is the absolute temperature in degrees Kelvin. W_2 is termed the emissive power. No surface can emit more energy at temperature T than this amount. Most surfaces emit less and equation 2.4 for a real surface is written:

$$W_2 = \underline{e}\,\sigma T^4 \tag{2.5}$$

where <u>e</u> is less than unity and is termed the thermal emissivity or emittance (emissivity refers to the property of a material and is numerically equal to the emittance of the sample material that has an optically smooth surface and is sufficiently thick to be opaque.

2.3.3 KIRCHHOFF'S LAW

This is sometimes stated in the form: The emissivity of a body is equal to its absorptivity, or loosely translated: a good absorber is a good emitter: a poor absorber - a poor emitter. This inexact form can lead to difficulties: the correct formulation of Kirchhoff's Law is that the monochromatic emittance and monochromatic absorptance are equal for radiation of any given wavelength λ, i.e.

$$\underline{e}_\lambda = \underline{a}_\lambda \qquad [2.6]$$

where $\underline{a}_\lambda$ is the monochromatic absorptance at wavelength λ and $\underline{e}_\lambda$ is the monochromatic emittance at the same wavelength.

For any surface, the sum of absorptance, $\underline{a}_\lambda$, transmittance, t_λ and reflectance R_λ must be unity. Thus, for a non-transparent material:

$$\underline{a}_\lambda + R_\lambda = 1 \qquad [2.7]$$

where R_λ is the reflectance for radiation of wavelength λ, where equation 2.6 can be written [for a non-transparent material]:

$$\underline{e}_\lambda = \underline{a}_\lambda = 1 - R_\lambda \qquad [2.8]$$

This equation is useful in that it allows $\underline{e}_\lambda$ or $\underline{a}_\lambda$ to be determined by a reflection measurement - in some cases. It is important in computing the interchange of radiation between surfaces.

2.3.4 PLANCK'S LAW

The black emission of equation 2.4 covers a wide range of wavelengths, the spectral distribution of energy governed by Planck's equation:

$$I_B = c_1 \lambda^{-5} [\exp [\frac{c_2}{\lambda T}] - 1]^{-1} \qquad [2.9]$$

where I_B is the Planck black body output at wavelength λ and $c_1 = 3.7415 \times 10^{-16}$ watt/m^2 and $c_2 = 1.43879 \times 10^{-2}$ watt/m^2

are first and second radiation constants. If the body is not black, equation 2.9 becomes:

$$I_B = e_\lambda c_1 \lambda^{-5} [\exp [\frac{c_2}{\lambda T}] - 1]^{-1} \qquad [2.10]$$

Real body emission in the range 0 to $\lambda = \int_0^\lambda I_B[T]\, d\lambda$

2.3.5 WIEN'S LAW

The expression 2.9 is a curve having a peak value at λ_{max} given by Wien's formula:

$$\lambda_{max} = \frac{2898}{T} \qquad [2.11]$$

where λ is in micrometers [μm] and T is in degrees Kelvin. About 25% of the emitted energy is at wavelength below λ_{max} and 75% above. Only 1% of the energy is emitted at wavelengths below 0.5 λ_{max} and a negligible amount below 0.4 λ_{max}.

Solar radiation in outer space corresponds fairly closely to black body radiation at a temperature of about 6000 Kelvin, i.e. the peak intensity is at a wavelength of about 0.5 μm. Allowing for absorption in the atmosphere, the solar radiation is almost entirely confined to the range of wavelength 0.3 to 2.0 μm. Equation 2.11 shows that at 'terrestrial' temperatures, the wavelengths of emitted radiation are much longer than for solar radiation. Thus at a temperature of say, boiling water, i.e. T = 373 Kelvin, the peak wavelength is 7.8 μm. In this case 1% of the radiation energy is below 3.9 μm and a negligible amount is below 3.1 μm.

2.4 FIGURE OF MERIT FOR SELECTIVE SURFACE a/e

The optical properties of selective surfaces are summarised by two quantities: the solar absorptance, a, and the thermal emittance, e.

The ratio of a/e is often sited as a figure of merit for selective surfaces. a/e varies with the temperature and wavelength. A large value of a/e as well as a large value of $a \sim 1$ are necessary for an efficient surface. For example, a surface with either $a = 0.90$ and $e = 0.1$ or $a = 0.45$ and $e = 0.05$ has $a/e = 9.0$. Under equilibrium radiation conditions with no energy extraction, both surfaces would reach the same temperature in space. However, within the purpose is to provide the energy, the first surface would be a better solar absorber because it would absorb twice as much available energy per unit area when operating below its radiation equilibrium temperature. Thus, for efficiency of the overall system, however, it is important to give a and e separately.

2.4.1 ABSORPTANCE, a

This is the percentage of radiant energy of solar origin which is absorbed by the surface. The absorptance can be either spectral or total and either be normal or angular or hemispherical.

THE DIRECTIONAL SPECTRAL ABSORPTANCE

This is a property of a surface and is defined as the absorbed fraction of incident radiation of wavelength λ from the direction θ_i, ϕ_i. Figure 2.8 shows θ_i as the polar angle and ϕ_i as azimuthal angle.

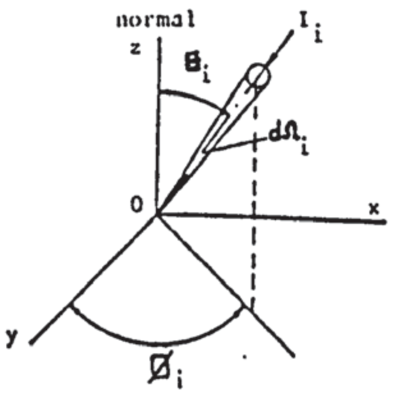

Figure 2.8 Directional absorptance

The equation is

$$\underline{a}\,[\theta_i,\ \phi_i, \lambda] = I_a\,[\theta_i,\ \phi_i, \lambda]/I_i\,[\theta_i,\ \phi_i, \lambda] \qquad [2.12]$$

in which the subscript i relates to the incident radiation and 'a' relates to the absorbed radiation within a wavelength interval $d\lambda$ and a solid angle $d\Omega_i$.

THE DIRECTIONAL TOTAL ABSORPTANCE

This is defined as the factor of all the radiation [i.e. over all wavelengths] from the direction θ_i, ϕ_i that is absorbed by a surface. It is expressed by the following

$$\underline{a}(\theta_i, \phi_i) = \frac{\int_0^\infty \underline{a}(\theta_i, \phi_i, \lambda)\ I_i(\theta_i, \phi_i, \lambda)\ d\lambda}{\int_0^\infty I_i(\theta_i, \phi_i, \lambda)\ d\lambda} \qquad (2.13)$$

THE TOTAL NORMAL ABSORPTANCE

For radiation falling along the normal axis on the surface the total normal absorptance is given by:

$$\underline{a}_n = \frac{\int_0^\infty \underline{a}_n(\lambda)\ I_i\ d\lambda}{\int_0^\infty I_i(\lambda)\ d\lambda} \qquad (2.14)$$

where $\underline{a}_n(\lambda)$ is the normal spectral absorptance.

THE HEMISPHERICAL TOTAL ABSORPTANCE

This is defined as follows

$$a_{Hem} = \frac{\int_0^\infty \int_0^\pi \int_0^{\pi/2} a(\theta_i, \phi_i, \lambda)\ I_i(\theta_i, \phi_i, \lambda) \cos\theta_i \sin\theta_i\, d\theta_i\, d\phi_i\, d\lambda}{\int_0^\infty \int_0^\pi \int_0^{\pi/2} I_i(\theta_i, \phi_i, \lambda) \cos\theta_i \sin\theta_i\, d\theta_i\, d\phi_i\, d\lambda} \qquad (2.15)$$

where the solar radiation is involved, I_i can be replaced by ϕ_s and the term hemispherical solar absorptance. The normal solar absorptance as often used in solar collectors for the wavelength range 0.35 to 2.5 μm:

$$a_n = \frac{\int_{0.35}^{2.5} a_n(\lambda)\ \phi_s(\lambda)\ d\lambda}{\int_{0.35}^{2.5} \phi_s(\lambda)\ d\lambda} \qquad (2.16)$$

2.4.2 EMITTANCE, e

This is the property of a real surface; it is the ratio of the rate of emission of radiant energy from the surface to that emitted from a black body radiator at the same temperature under the same conditions. The emittance can be either normal, angular or hemispherical and they can also be either spectral or total.

THE DIRECTIONAL SPECTRAL EMITTANCE

The directional spectral emittance of a surface with temperature T is defined by

$$\underline{e}\,(\theta_e, \O_e, \lambda\,, T) = I_e\,(\theta_e, \O_e, \lambda,)/I_B\,(\lambda, T)\ dAe \quad (2.17)$$

where

$I_e\,(\theta_e, \O_e, \lambda, T)$ is the emitted spectral radiant intensity (within a wavelength interval $d\lambda$ and solid angle $d\Omega e$), of surface with temperature T in the direction $(\theta_e, \O_e)$ and in which $I_B(\lambda, T)$ is the spectral lan black body output at the same temperature T. dAe is the emitting surface of concern (Figure 2.9). The spectral curves of I_B for different surface temperatures are shown in Figure 2.10.

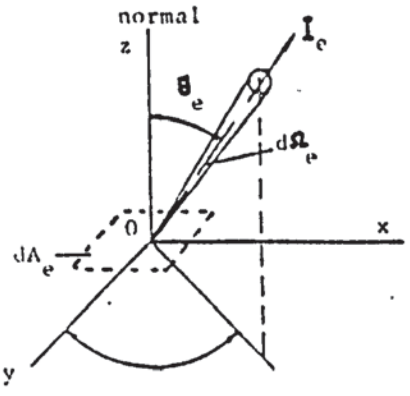

Figure 2.9 Directional emittance

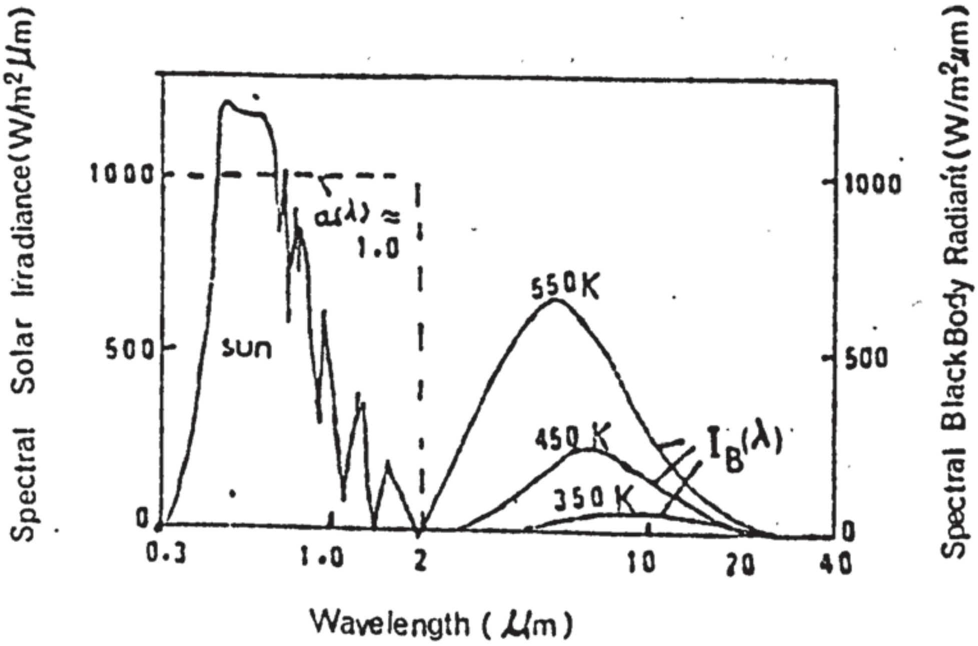

Figure 2.10 Spectral energy distributions (theoretical) of the sun taken from Moon (1940) and of a black body with different surface temperatures

THE DIRECTIONAL TOTAL EMITTANCE

The directional total emittance is given by

$$\underline{e}\ (\theta_e, \emptyset_e, T) = \frac{\underline{e}\ (\theta_e, \emptyset_e, \lambda, T)\ I_B\ (\lambda, T) d\lambda}{I_B\ (\lambda, T)\ d\lambda} \qquad (2.18)$$

For radiation emitted along the normal axis, the normal total emittance is defined as

$$\underline{e}_n(T) = \frac{\int_0^\infty \underline{e}_n(\lambda,T)\ I_B(\lambda,T)\ d\lambda}{\int_0^\infty I_B(\lambda,T)\ d\lambda} \qquad (2.19)$$

in which $\underline{e}_n(\lambda,T)$ is the normal spectral emittance of a surface of temperature T.

THE HEMISPHERICAL TOTAL EMITTANCE

The hemispherical total emittance of a surface with temperature T is in terms of $\underline{e}(\theta_e, \phi_e, T)$ and is given by

$$e_{Hem}(T) = \frac{\int_0^\infty \int_0^{2\pi} \int_0^{\pi/2} \underline{e}(\lambda,T,\theta_e,\phi_e)\ I_B(\lambda,T)\ \sin\theta_e \cos\theta_e\, d\theta_e\, d\phi_e\, d\lambda}{\int_0^\infty \int_0^{2\pi} \int_0^{\pi/2} I_B(\lambda,T)\ \sin\theta_e \cos\theta_e\, d\theta_e\, d\phi_e\, d\lambda} \qquad (2.20)$$

where $\underline{e}(\theta_e, \phi_e, \lambda, T)$ is the spectral-angular emittance.

The above quantities are all functions of surface conditions such as roughness, temperature and cleanliness.

Equations 2.15 and 2.20 are difficult to implement, since information on the directional variation of the spectral absorptance, emittance and solar intensity is generally not available. Basic assumptions are therefore often made:

1. The solar flux is assumed to impinge on the absorber surface at normal incidence such that we can express absorptance as normal absorptance equation (2.16).

2. The normal emittance is often used instead of the hemispherical emittance (equation 2.19).

The second assumption is made when $\underline{e}_n$ is determined by measuring the reflectance of the converter surface. This statement can be explained by demonstrating how the reflectance is related to the emittance by using the statement of the conversion of energy, 2.8, which could be written for the opaque surface as

$$R_{Hem}\ [\theta,\ \emptyset, \lambda, T] + \underline{a}\ [\theta, \emptyset, \lambda, T] = 1 \qquad [2.21]$$

The energy in a beam of light incident from a single direction [θ, Ø] is either absorbed within the converter or scattered into the hemisphere above the converter. If the converter is in thermal equilibrium with its surroundings we can also use Kirchhoff's Law [equation 2.6]:

$$\underline{e}\ [\theta,\ \emptyset, \lambda, T] \ = \ \underline{a}\ [\theta, \emptyset, \lambda, T] \qquad [2.22]$$

Equations 2.21 and 2.22 can then be combined to write

$$\underline{e}\ [\theta, \emptyset, \lambda, T] \ = \ 1 - R_{Hem}\ [\theta, \emptyset, \lambda, T] \qquad [2.23]$$

To find the hemispherical emittance we would then need to measure R_{Hem} $[\theta, \emptyset, \lambda, T]$ to determine $\underline{e}[\theta, \emptyset, \lambda, T]$ from equation 2.23.

One way to determine R_{Hem} $[\theta, \emptyset, \lambda, T]$ is to measure what is known as the directional-hemispherical reflectance at all angles [Siegal and Howell 1972]. In other words, we would need to place a pencil beam on a converter from a direction [θ, Ø], collect all scattered light in the hemisphere and do this for all sets of θ and Ø. The difficulty of this measurement justifies using equation 2.19 with $\underline{e}_n[\lambda,T]$ determined from equation 2.23 [with $\theta \approx 0$] to find the total normal emittance $\underline{e}_n[T]$. We still see, however, that the normal emittance depends on a directional hemispherical reflectance measurement for high temperatures up to 300°C. The fact that $\theta = 0$ is chosen in equation 2.23 for evaluating $\underline{e}\ [\lambda,T]$, as opposed to any other angle, belies the error in assuming that $\underline{e}_n[T]$ can be used to evaluate the radiative loss term in Figure 2.1, i.e. that $\underline{e}_n[T]$ equals $\underline{e}_{Hem}[T]$.

3. The third assumption often used to simplify equations 2.15 and 2.20 is that $\underline{a}$ and $\underline{e}$ are not functions of temperature. This assumption is difficult to justify when one considers the reversible changes in reflectance and absorption that occur for the samples as they are heated and then cooled back to room temperature.

We have discussed assumptions which are made to determine approximations of $\underline{a}$ and $\underline{e}$ so that the absorptance and emittance which we quote in the remainder of this work will be firmly defined, with all these assumptions clarified. In all cases, the following relationships have been used.

$$\underline{a} = \frac{\int_0^\infty [1-R_{Hem}\ [\theta,\lambda,T]\ ]\ \phi_s\ [\lambda]\ d\lambda}{\int_0^\infty \phi_s[\lambda]\ d\lambda} \qquad [2.24]$$

$$\underline{e}_n = \frac{\int_0^\infty [1-R_n\ [\lambda,\overset{\text{[up to 300°]}}{T},\theta = 7°]\ ]\ I_B\ [\lambda,T]d\lambda}{\int_0^\infty I_B\ [\lambda,T]\ d\lambda} \qquad [2.25]$$

where ϕ_s represents the solar flux for Air mass 2*, I_B the Planck black body function for the total radiation normal to the radiating surface of a black body per unit area, per unit solid angle and per unit wavelength, was used in equation 2.25.

The following three comments concern the angles, the type of reflectance (hemispherical or specular) and the temperature used in equations 2.24 and 2.25.

1. θ, in equation 2.24, was set at an off-axis angle of 19°, selecting θ equal to a non-zero value is just another way of simplifying equation 2.15, except that the result is now $\underline{a}_\theta$ instead of the $\underline{a}_n$ of equation 2.16.

---

* Air mass at a given declination of the sun is the path length of the sun's rays through the atmosphere pressure at a point of observation. Mass is used because it is the quantity or mass of air through which the rays pass and not the actual length of the path that determines attenuation. For example,

Air mass (0) will refer to the absence of the atmosphere attenuation.
Air mass (1) will refer to the path length through the atmosphere when the sun is directly above a point of observation at sea level and standard atmospheric pressure.

Similarly, Air mass (2) may be defined as the path length through the atmosphere when the sun is 60° from the vertical on a unit area at sea level. The aerosol scattering parameters $\alpha = 1.3$, $\beta = 0.04$ represent a moderately clean environment where α and β, Angström turbidity coefficients, are related to the size distribution and density of aerosols. A higher value of β corresponds to a more turbid atmosphere. As turbidity increases the transmitted energy decreases. A detailed account of aerosol scattering parameters has been given by Bilton, Flowers, Cormick and Kurfis (1973).

In equation 2.25, θ has always been set at 7°. This value is so close to zero that the average of the S and P polarisation reflectances will be virtually equal to the normal reflectance. The values of $\underline{e}$ from equation 2.25 can, therefore, still be used for $\underline{e}_n$ within the relation $\underline{e}_{Hem} = 1.3\ \underline{e}_n$ to get an estimation of the lower limit of the hemispherical emittance.

2. The R_{Hem} values in equation 2.24 were measured with an integrating sphere reflectometer, as discussed in Chapter 2.

3. Most of the $\underline{a}$ and $\underline{e}$ values mentioned later were determined from reflectance measurements made at room temperature.

To summarise, the $\underline{a}$ values which are quoted in this work can be considered hemispherical quantities; the $\underline{e}$ values must be considered to be appropriate with respect to the temperatures at which the reflectance measurements were taken.

2.4.3 DETERMINING FIGURE OF MERIT $\underline{a}/\underline{e}$

To determine the figure of merit for a selective surface, two methods are generally used to calculate the absorptance, $\underline{a}$, and the emittance, $\underline{e}(t)$.

i) Computed method.

ii) Distorted -graphs method.

i) COMPUTED METHOD

If the directional hemispherical reflectance, R_{Hem}, is known, the total directional-hemispherical absorptance, $\underline{a}_{Hem}$ is computed as $1-R_{Hem}$. The $\underline{a}_{Hem}$ is then computed as the weighted average directional spectral absorptance, with relative solar spectral irradiance $\text{Ø}_s(\lambda)$ as the weighting function, expressed mathematically as

$$\underline{a}_{Hem} = \frac{\int_{\lambda_1}^{\lambda_2} \underline{a}(\lambda)\, \text{Ø}_s(\lambda)\, d\lambda}{\int_{\lambda_1}^{\lambda_2} \text{Ø}_s(\lambda)\, d\lambda} \qquad (2.26)$$

where λ_1 and λ_2 are the extreme limits of integration of the solar range. Most of the terrestrial solar irradiance of 0.35 μm to 2.7 μm normally contains about 99% of this energy.

Since neither $R(\lambda)$ or $\text{Ø}_s(\lambda)$ is known as an algebraic function, the integration must be approximated by a summation. Two methods are generally used:

1. The weighted ordinate method.
2. The selected ordinate method.

WEIGHTED ORDINATE METHOD

Briefly, in this method, values of $\text{Ø}_s(\lambda_i)$ are taken at convenient wavelength intervals, $\Delta\lambda_i$, at which value

$\phi_s [\lambda_i]$ applies, i.e. if λ_1, λ_2, λ_3 are the wavelengths for three successive spectral irradiance values $\phi_s [\lambda_1]$, $\phi_s [\lambda_2]$ and $\phi_s [\lambda_3]$; and $\Delta\lambda_2$ is taken as $[\lambda_3 - \lambda_1]/2$. These values of $\phi_s [\lambda_i]$ are multiplied by $\underline{a}[\lambda] . \Delta\lambda$ and then a summation is made. The sum is divided by the sum of the products of $\phi_s [\lambda_i]$ and $\Delta\lambda_i$ at the same wavelength. Equation 2.26 then becomes:

$$\underline{a}_{Hem} = \frac{\sum_{i=1}^{n} \phi_s [\lambda_i] \, \underline{a} [\lambda_i] \Delta\lambda_i}{\sum_{i=1}^{n} \phi_s [\lambda_i] \, \Delta\lambda_i} \qquad [2.27]$$

where n is the number of wavelengths at which $\phi_s [\lambda]$ is known.

If the wavelength intervals are all equal, then n $\Delta\lambda$'s come outside the summation sign in both numerator and denominator and cancel, and the equation becomes

$$\underline{a}_{Hem} = \frac{\sum_{i=1}^{n} \phi_s [\lambda_i] \, \underline{a}[\lambda_i]}{\sum_{i=1}^{n} \phi_s [\lambda_i]} \qquad [2.28]$$

The above procedure simplifies the computation, but may result in errors if $\Delta\lambda$ is large, because of the several sharp absorption peaks in the terrestrial solar irradiance curve.

Values for use in equation 2.27 are given by Thekaekara [1973, 1974] for different air masses.

Values for use in equation 2.28 are given in the ASTM method E-424-71. This technique is given in a book [ASTM, 1977, pp. 297-303], with $\Delta\lambda$ = 50 nm.

SELECTED ORDINATE METHOD

In this method, the area under the solar insolation profile, $\phi_s(\lambda)$ is divided into n (usually 100) equal areas, A_i by vertical lines. An average λ_i, which divides the energy interval into two equal parts, is assigned for each area A_i. Then $\underline{a}_s$ is computed as $\frac{1}{n}$ times the sum of $\underline{a}_{s,i}$ values at the $n\,\lambda_i$ values, expressed mathematically as

$$\underline{a}_s = \frac{1}{n} \sum_{i=1}^{n} \underline{a}(\lambda_i) \tag{2.29}$$

A computer can be used to calculate the hemispherical absorptance and the emittance by using the above equation, using Kirchhoff's relationship and the corresponding values of the reflectance.

This method has been adopted for the evaluation of the hemispherical absorptance and the emittance in the present study. In the case of the solar absorptance, air mass (2) (AM 2) has been used following Thomas and Richmond (1978). In evaluating the normal emittance, λ_1 and λ_2 have been taken as 2.5 μm and 15 μm respectively and ϕ_s has been replaced by I_B, black body emission at a specified temperature.

The results from this method were compared to those calculated by using a distorted wavelength graph. The results obtained by the two methods generally differed by about 0.5%.

ii) DISTORTED λ GRAPHS METHOD

In the distorted scale-planimeter (Drummeter and Hass, 1964), the spectral reflectance is plotted as a function of wavelength on a special graph paper in which the wavelength scale is distorted so that the selected ordinates referred to above are uniformly spaced and equal areas represent equal amounts of incident energy.

It is necessary to use two distorted λ-graphs for the presentation of selective surfaces, one for estimating solar absorptance and the other for thermal emittance. For computing solar absorptance of the surfaces in this study, a distorted graph paper, Figure 2.11, has been used as supplied by the Optical Sciences Center of Arizona University. This plot is based on the AM 2 solar spectral irradiance curve (Thomas and Richmond, 1978).

For computing the thermal emittance at the desired temperature, for instance at 200°C (473 Kelvin), a distorted λ-graph is constructed and is illustrated in Figure 2.12. This plot is based on the black body, I_B, emission at a temperature of 473 Kelvin. To plot the above graph, a universal black body selected ordinate source, proposed by Pivovonsky and Nagel (1961) has been used. Table 2.1 gives the fraction of radiation contained in the wavelength shorter than λ, for desired temperature distributions, and starts with the ratio, expressed in half percent increments, in the equation

$$D\,\% = \frac{\int_{0}^{\lambda'} I_B \, d\lambda}{\int_{0}^{\infty} I_B \, d\lambda} \qquad [2.30]$$

where the symbol D is designed for this fraction and λ' is the upper limit of the upper integral, which is to be determined. For each percentage, a value of λT is given, which can be divided by an arbitrary temperature for the black body [in degrees Kelvin], to provide the desired value of λ'. This can give a set of wavelengths separated by equal amounts of energy for calculations of the emittance at any desired temperature. The tabulated values are given for both centimetres and microns [the microns data was used in the present case].

The half percent increments have been plotted versus λ [i.e. $\lambda T/T$, where T = 473 Kelvin in this example] on linear graph paper for a wavelength range 3 μm to 15 μm as shown in Figure 2.13. Figure 2.12 is extracted from the above figure, where the abscissa of Figure 2.12 is linear in terms of the fraction of radiation contained in wavelengths shorter than λ_{w}, [top scale] and is thus non-linear in λ . The corresponding λ values [Table 2.1] are listed on the bottom scale and the abscissa is graduated in terms of the λ scale.

For instance, at a wavelength of 10 μm, the corresponding point on the y-axis which is designated by the half percent increments in Figure 2.13 is 0.60. This is located at the top axis specified by the fraction of the black body

%T0 λ T	λT[cm K] $\times\overline{10}^{2}$	λT[µ K]	λ[µ]
.5	13.22	1323	2.797
5	18.83	1883	3.981
10	21.94	2194	4.638
15	24.45	2445	5.169
20	26.75	2675	5.655
25	29.0	2896	6.123
30	31.17	3117	6.590
35	33.43	3344	7.070
40	35.81	3580	7.569
45	38.32	3832	8.101
50	41.05	4105	8.679
55	44.05	4405	9.313
60	47.42	4743	10.027
65	51.29	5130	10.846
70	55.86	5587	11.812
75	61.44	6145	12.992
80	68.52	6860	14.503
85	78.44	7844	16.584
90	93.71	9371	19.812
92	102.92	10293	21.761
94	115.8	11577	24.476
95	124.5	12453	26.328
97	151.9	15194	32.123
98	177.1	17713	37.448
99	293.5	22872	48.355

Table 2.1 Universal Black Body Selected Ordinate Source Table. [Pivovonsky and Nagel, 1961]

emissive power falling below the wavelength λ at 473 Kelvin of Figure 2.12 and so on for the other wavelengths.

In both cases, the values of the reflectance are plotted on the chart at the appropriate λ positions. The area under the curve, and that of the entire graph representing 100%, have been determined with a planimeter. The total reflectance has been taken as the ratio of the area under the curve to that of the entire graph. Assuming the sample to be opaque and Kirchhoff's Law to be valid, the thermal emittance, $\underline{e}(T)$, and the solar absorptance can be determined.

Also, Figures 2.11 and 2.12 show the plots of the spectral reflectance data of the sample corresponding to the INCO surface of 5 mV for a wavelength range from 0.35 μm to 2.7 μm and 2.5 μm to 15 μm respectively. The calculated values of the hemispherical absorptance and the normal emittance are displayed in Table 2.2.

	From Figure 2.11	From Figure 2.12
Area under curve	412	3191.5
Total area of graph	3169.23	2824.04
$\frac{\text{Area under curve}}{\text{Total area of graph}}$	0.13	0.885
Hemispherical absorptance, $\underline{a}_{Hem} = 1-R_{Hem}$	0.87	
Normal emittance, $\underline{e}_n = 1-R_n$	-	0.115

Table 2.2 The calculated values of the absorptance, $\underline{a}_{Hem}$ and the emittance $\underline{e}_n(200^{\circ}C)$ for the 5 mV sample by using distorted -graph plots

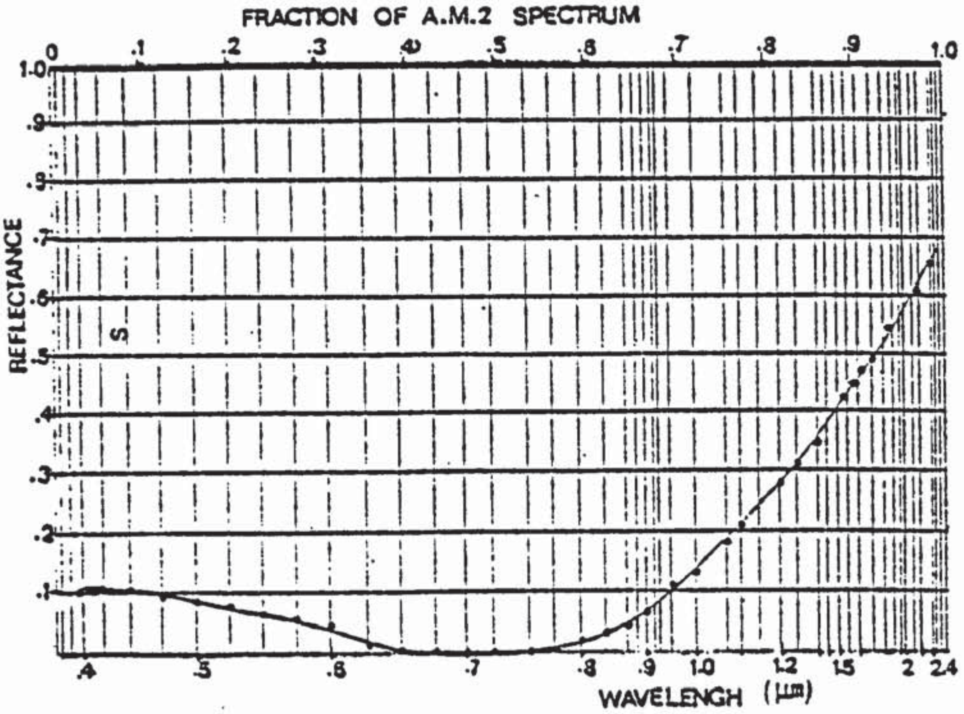

Figure 2.11 Hemispherical reflectance as a function of wavelength for the 5 mV sample plotted in equal fractions of the solar AM^2 spectrum

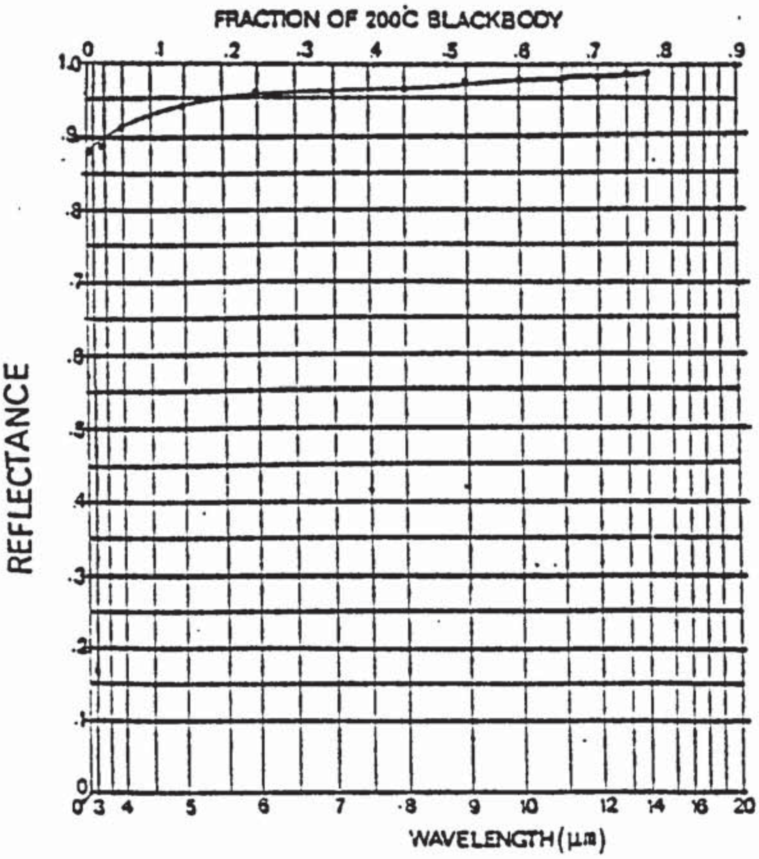

Figure 2.12 Specular reflectance as a function of wavelength for the 5 mV sample, plotted in equal fractions of the 200°C blackbody spectrum

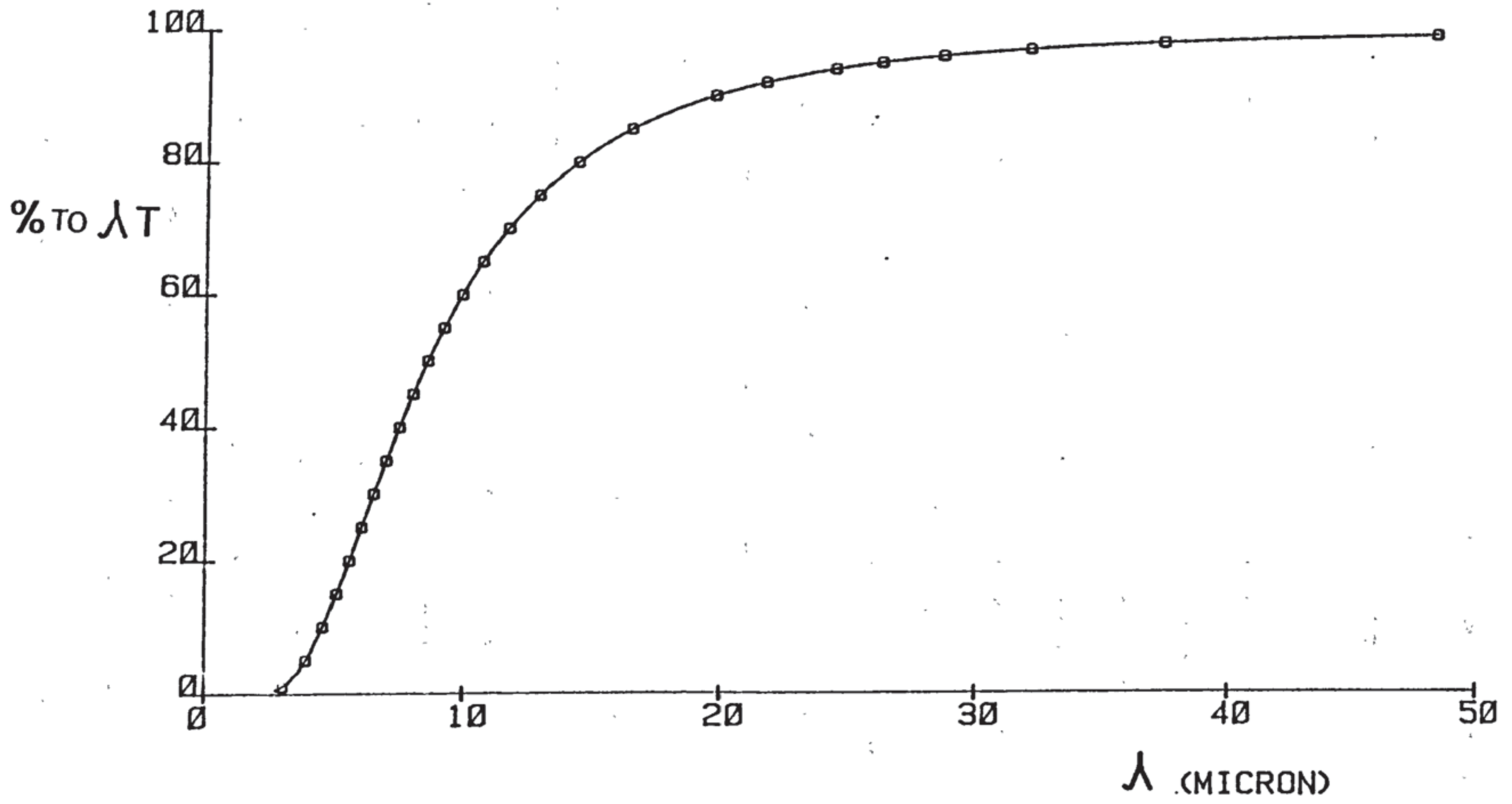

Figure.2.13 Equal fraction of the 200°C Black Body Radiation versus the wavelength

CHAPTER 3

MEASUREMENT PROPERTIES OF SURFACES

3.1 MEASUREMENTS OF OPTICAL CONSTANTS BY USING THE ELLIPSOMETER

Ellipsometry, which may be characterised as reflection polarimetry or polarimetric spectroscopy, involves the measurement of the effect on the state of polarisation of light reflected from a surface. Such measurements may be interpreted to yield the optical constants n and k of the reflecting material which is film free or, when the reflecting material is a film-covered substrate, the thickness and optical constants of the film. For the measurement of optical constants of the substrates, ellipsometry has the advantages over conventional techniques in that it can be applied to strongly absorbing media and because of its relative simplicity of measurement and sample preparation. Ellipsometry can be applied to surface films depending on absorption for a given wavelength throughout the thickness range from partial monoatomic coverage up to layers which are of the order of microns in thickness. Throughout most of this range, n, the refraction of a non-absorbing film is obtained and n and k, for an absorbing film media. Recent developments in computation instrumentation techniques make ellipsometry a more attractive tool for surface examination. Ellipsometry can invariably make a contribution to knowledge either in its own right or as a method which complements other surface techniques, such as Auger Electron Spectroscopy.

Many of the experimental procedures, some of the theory of interpreting the measurements and most of the examples of application of ellipsometry, are reported by McCrackin et al [1963], Heavens [1955, 1960] and Vasicek [1960]. Recently, a review article about ellipsometry and its application has been given by Neal [1979].

The equipment used for the optical studies in this work was a two angle ellipsometer, but in this investigation only one angle of incidence was employed [Figure 3.1]. The wavelength range was in the visible region from 397.1 nm to 576.6 nm.

3.1.1 BASIC EQUATION OF ELLIPSOMETERY

When monochromatic collimated polarised light falls on a surface, the incident light can be resolved in two components parallel [P] and perpendicular [S] to the plane of incidence. If after reflection the P and S components are in phase the resultant wave is plane polarised. A difference in phase, other than 180°, corresponds to elliptical polarisation. In general reflection (waves a change in the relative phase of the P and S curves and a change in the ratio of their amplitudes. The effect of reflection is characterised by the angle Δ, defined as the relative change in phase, and the angle ψ, the arctan

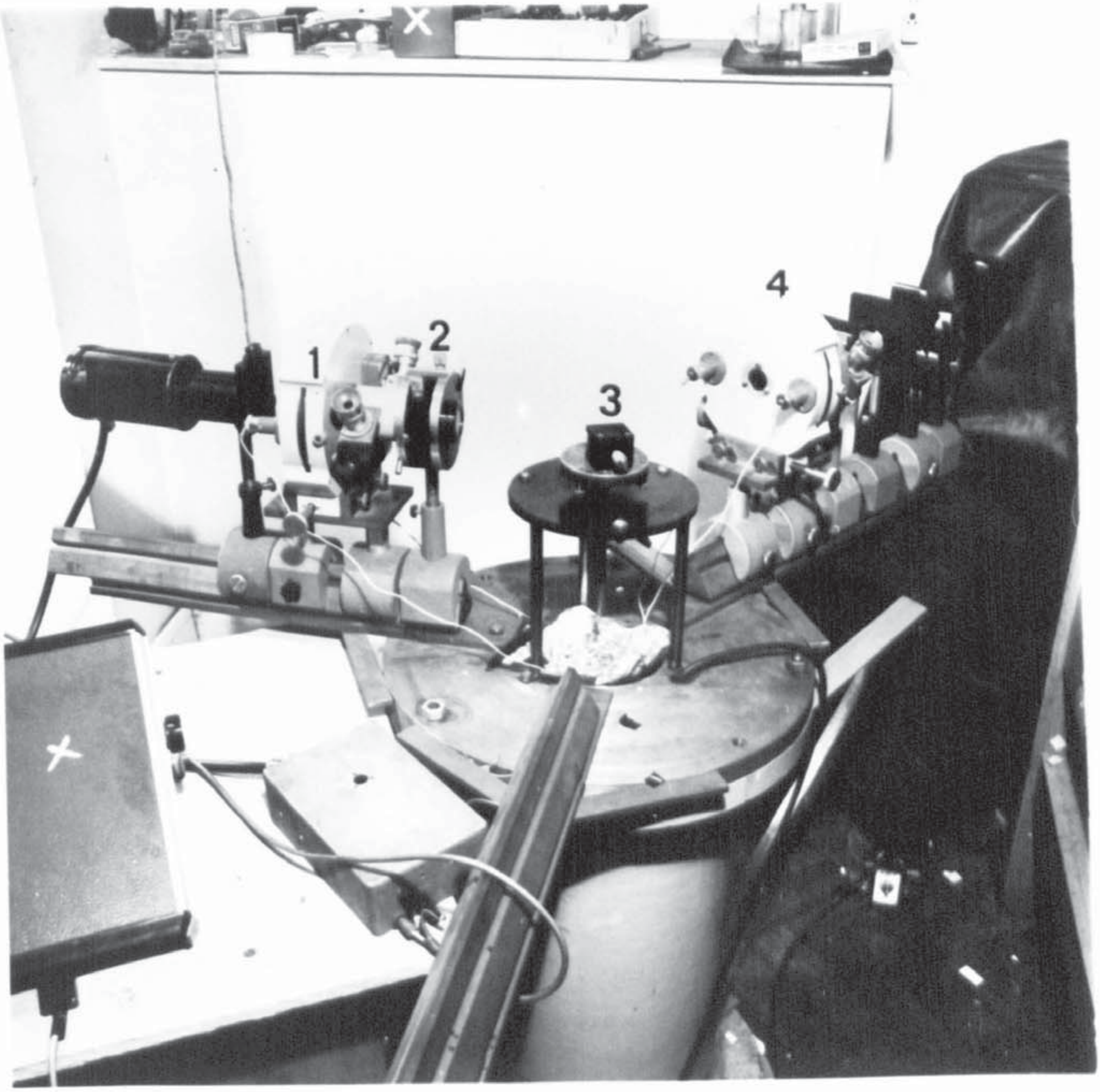

FIGURE (3.1) ELLIPSOMETER

1) Analyser. 2) Compensater

3) Sample Holder 4) Polariser

of factor by which the amplitude ratio changes. If the amplitudes of the incident and reflected beams are designated E_{inc} and E_{ref} respectively, and the phase angles Δ, then

$$\Delta = [\Delta_P - \Delta_S]_{ref} - [\Delta_P - \Delta_S]_{inc} \qquad [3.1]$$

$$\psi = \arctan \left[[\frac{E_P}{E_S}]_{ref} \cdot [\frac{E_S}{E_P}]_{inc} \right] \qquad [3.2]$$

Ellipsometry involves the measurement of Δ and ψ. The relationship between Δ and ψ and the properties of a reflecting system is expressed by the Fresnel reflection coefficients. The Fresnel reflection coefficient, r, of an interface is the ratio of the electric field vector, E'_{ref}, of the reflected wave to that of the incident wave E'_{inc}, i.e.

$$r_{P,S} = \frac{[E'_{ref}]\ P,S}{[E'_{inc}]\ P,S} \qquad [3.3]$$

In terms of the amplitudes of the incident and reflected waves E_{inc} and E_{ref}, respectively, and the phase change Δ , accompanying reflection,

$$r = \frac{E_{ref}}{E_{inc}} \; e^{i\Delta} \qquad [3.4]$$

The coefficient depends upon the orientation of the wave relative to the plane of incidence, and the reflection of a wave of any polarisation is described by the two coefficients r_P and r_S for the component waves. The ratio of these reflection coefficients is

$$\frac{r_P}{r_S} = \frac{[E_{ref}]_P}{[E_{ref}]_S} \cdot \frac{[E_{inc}]_S}{[E_{inc}]_P} \; e^{i[\Delta_P - \Delta_S]} \qquad [3.5]$$

From equations3.1 and3.2 it follows that

$$\frac{r_p}{r_s} = \tan \psi \, e^{i\Delta} \qquad (3.6)$$

This is the basic equation of ellipsometry.

3.1.2 BASIC PRINCIPLES OF REFLECTION OF NON-ABSORBING AND ABSORBING MEDIA

Figure 3.2 illustrates the reflection of a beam of light at an optically clean surface.

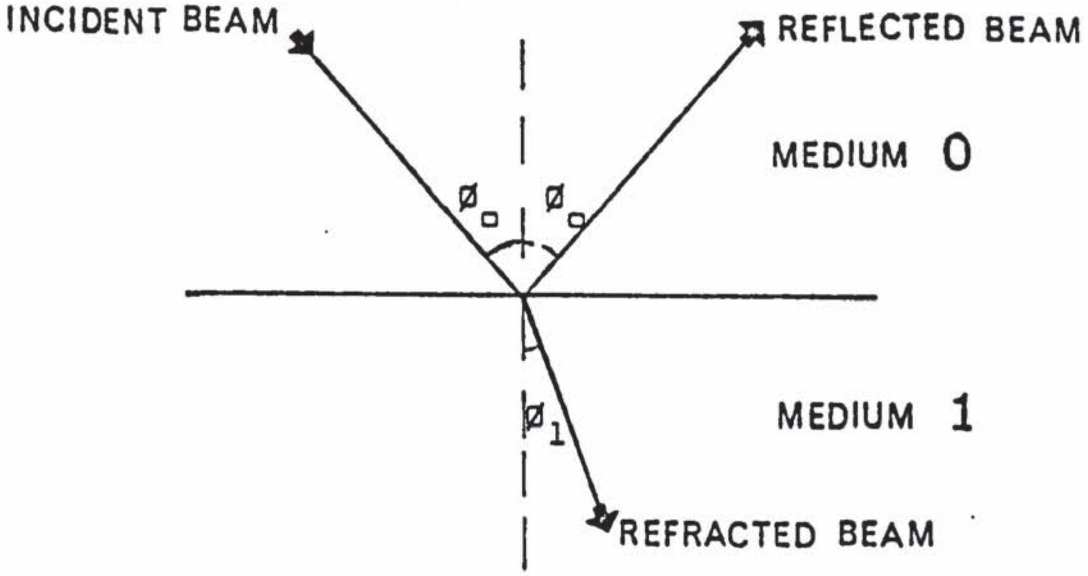

Figure 3.2 Representation of reflection at a film free interface

As sketched in this figure, the subscript 0 and 1 refers to the media bonding the reflecting interface, $\emptyset_o$, is the angle of incidence and $\emptyset_1$, the angle of refraction.

If the refraction indices are n_o and n_1 respectively, then the Fresnel reflection coefficients are (Heavens, 1955)

$$r_{01(P)} = \frac{n_0 \cos \phi_1 - n_1 \cos \phi_0}{n_0 \cos \phi_1 + n_1 \cos \phi_0} \qquad (3.7)$$

$$r_{01(S)} = \frac{n_0 \cos \phi_0 - n_1 \cos \phi_1}{n_0 \cos \phi_0 + n_1 \cos \phi_1} \qquad (3.8)$$

where $(r_{01})_{P,S}$ is the amplitude of reflected light vector/amplitude of incident light vector and P and S refer to vectors parallel and perpendicular to the plane of incidence respectively.

The reflectance at an interface is given by

$$(R)_{P,S} = \frac{\text{Reflected energy}}{\text{Incident energy}} \qquad (3.9)$$

so that

$$(R_{01})_{P,S} = (r_{01})^2_{P,S} \qquad (3.10)$$

For an optically absorbing medium, the refractive index, N, is a complex quantity given by

$$N = n - ik \qquad (3.11)$$

where n and k are referred as the optical constants of an absorbing medium, k, the extinction coefficient, is related to the absorption coefficient α, (units of cm^{-1}) by $k = \alpha\lambda/4\pi$ and λ is the vacuum wavelength.

In this case, the value n_1 in equation 3.7 and equation 3.8 must be replaced by $N_1 = n_1 - k_1$ to evaluate the Fresnel reflection coefficients.

In the case where $\phi_0 = \phi_1 = 0$ (normal incidence), the Fresnel reflection coefficients are the same for both P and S components of polarisation.

The normal reflectance is given by

$$[R_{01}]_P = [R_{01}]_S = \frac{[n_0 - n_1]^2 + k_1^2}{[n_0 + n_1]^2 + k_1^2} \qquad [3.12]$$

3.1.3 OPTICAL PROPERTIES OF THE FILM FREE SURFACES

The formulae for deriving the optical constants from values ψ and Δ which were obtained from instrument readings are derived from equations 6, 7, 8 and 11. The results are given by [Ditchburn, 1955]

$$n^2 - k^2 = \sin^2\phi_0 + \frac{\sin^2\phi_0 \tan^2\phi_0 \, [\cos^2 2\psi - \sin^2 2\psi \sin^2\Delta]}{[1 + \sin 2\psi \cos\Delta]^2} \qquad [3.13]$$

$$2nk = \frac{\sin^2\phi_0 \tan^2\phi_0 \, \sin 4\psi \sin\Delta}{[1 + \sin 2\psi \cos\Delta]^2} \qquad [3.14]$$

Equations 3.13 and 3.14 apply for the case of material in a medium with an index of refraction $n_0 = 1$ in which the angle of incidence is ϕ_0.

The technique used in this work for measuring the optical constant is to determine ψ and Δ either by the compensator method for one radiation wavelength 546.1 nm or the Beattie and Con method for a wavelength range 397.1 - 576.6 nm at a fixed angle of incidence,n and k were calculated using equations 3.13 and 3.14.

3.1.4 OPTICAL PROPERTIES OF SURFACE FILMS ON METAL SUBSTRATES

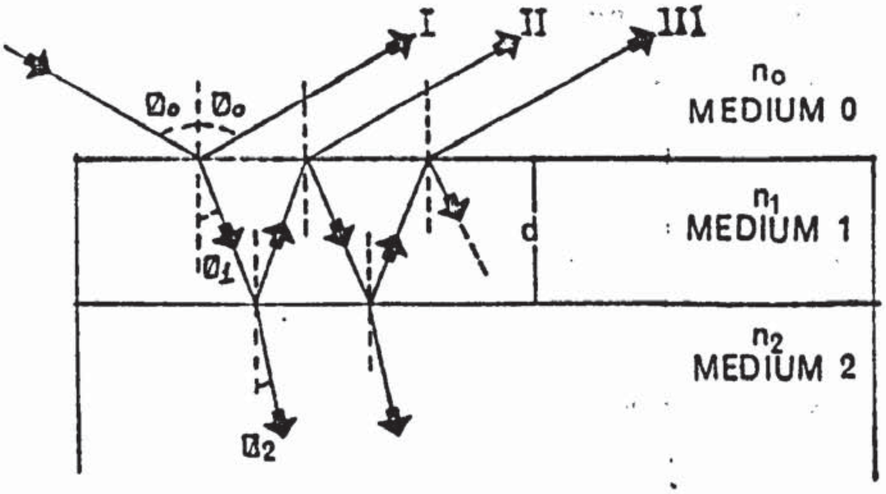

Figure 3.3 Reflection of polarised light from a film covered surface

Figure 3.3 shows a surface layer or film of refractive index n_1 (non-absorbing, $k_1=0$) overlaid on an absorbing substrate of refractive index $(n_2 - ik_2)$.

It has been illustrated that the instrument angles ψ and Δ (for a given angle of incidence) enable the optical constant to be evaluated. Both angles will be modified by the presence of a film, so that values of optical constants n' and k' ignoring the presence of a film will be pseudo constant relating to a composite surface characterised by the angle ψ' and Δ'. The surface film could be absorbing or non-absorbing.

The Fresnel coefficients of such a system can be derived [Heavens 1955] by considering the interference between the multiplicity of beams resulting from reflection in the film. It is assumed that all media are isotropic and homogeneous and that films or layers are of uniform thickness.

The light of unit amplitude of wavelength λ is incident at the interface between a medium (0) and a film medium (1) on a substrate medium (2). There is the possibility of amplitude reflections taking place in the film, as illustrated in Figure 3.3, and the first three of the infinite number of reflected beams are:

Beam I is directly reflected.

Beam II results from transmission through the ambient-film interface, reflection from the film substrate-interface and transmission through the film-ambient interface. Each of these reflections and refractions affect the relative amplitude and phase of the beam, and in addition, a phase change -2D, relative to beam I, results from the double transversal of the film of thickness d where

$$D = \frac{2\pi}{\lambda} n_1 d \cos \emptyset_1 \text{ degrees} \qquad (3.15)$$

$$\text{where } \cos^2 \emptyset_1 = \frac{n_1^2 - \sin^2 \emptyset_0}{n_1^2} \qquad (3.16)$$

Beam III results from reflection twice from the film-substrate interface and from film-ambient interface before being transmitted into the ambient so that there is a phase change $-4D$ relative to beam I caused by the film traversed in addition to the changes that occur at each refraction and reflection. And so on for subsequent beams. The amplitude of the reflected beam can be found by a summation of the amplitudes of successive rays taking into account the relative phases. The Fresnel reflection coefficients for a film covered surface can be written as

$$r_{p,s} = \frac{(r_{01})_{p,s} + (r_{12})_{p,s}\ \mathrm{Exp}\ (-2D)}{1 + (r_{01})_{p,s}\ (r_{12})_{p,s}\ \mathrm{Exp}\ (-2D)} \qquad (3.17)$$

$(r_{01})_{p,s}$ and $(r_{12})_{p,s}$ can be evaluated by substituting the relevant values $n(0, 1, 2)$ and $\emptyset\ (0, 1, 2)$ into equations 3.7 and 3.8.

For an absorbing layer film with a complex refractive index $n_1 - ik_1$, the coefficients become complex and the value of D in equation 3.15 becomes D' where

$$D' = \frac{2\pi}{\lambda}\ N_1\ d\ \cos \emptyset_1 \qquad (3.18)$$

By analogy with equation 6, the resulting fundamental equation of ellipsometry is

$$\tan \psi\ e^{i\Delta} = \frac{(r_{01})_p + (r_{12})_p\ \ e^{-2iD}}{1 + (r_{01})_p\ (r_{12})_p e^{-2iD}} \cdot \frac{1 + (r_{01})_s\ (r_{12})_s e^{-2iD}}{(r_{01})_s + (r_{12})_s e^{-2iD}} \qquad (3.19)$$

The above equation gives ψ and Δ as a function of the angle of incidence, the vacuum wavelength of light, the optical constants of the film and the substrate and the thickness of the film.

The separation of equation 3.19 into real and imaginary parts yields one equation for Δ and one for ψ. The equations are extremely complicated and their solution and use for interpreting ellipsometric data requires electronic computation.

A basic program which has been written to calculate the values of optical properties of the surface layer film is given in Appendix 1-a. The computer yields tables of Δ and ψ as a function of film thickness for any value for the optical constants n, k, of the film inserted in the program. The fixed constants used in the evaluation are: the angle of incidence, the radiation wavelength and the optical constants n_2 and k_2 of the substrate.

In summary, film growth on a surface changes the values of both ψ and Δ. The magnitude of the changes depends on film thickness, the optical constants of the substrate and film material and radiation wavelength.

Winterbottom [1946, 1948] drew attention to the fact that a polar diagram plot of tan ψ versus Δ, for film growth on a surface, produced a loop for non-absorbing films but the curve for an absorbing layer film was not closed.

In this work plots of tan ψ versus Δ for different thermal oxide layers on titanium have been compared with computer generated values using assumed optical constants for the oxide and the measured optical constants for the titanium substrates. A knowledge of the optical constant of the surface film is required to estimate the effect of surface films on the reflectance of metals.

For the case of normal incidence, the reflectance is given by (Heavens 1964)

$$R = \frac{P_2^2 e^z + 2P_2 P_1 \cos (B_2 - B_1 + Y) + P_1^2 e^{-z}}{e^z + 2P_2 P_1 \cos (B_2 + B_1 - Y) + P_2^2 P_1^2 e^{-z}} \quad (3.20)$$

where

$$P_1^2 = g_1^2 + h_1^2 , \quad P_2^2 = g_2^2 + h_2^2$$

$$B_1 = \arctan h_1/g_1, \quad B_2 = \arctan h_2/g_2$$

$$g_1 = \frac{(n_o^2 - n_1^2) + (k_o^2 - k_1^2)}{(n_o + n_1)^2 + (k_o + k_1)^2}$$

$$h_1 = \frac{2(n_o k_1 - n_1 k_o)}{(n_o + n_1)^2 + (k_o + k_1)^2}$$

$$g_2 = \frac{n_1^2 - n_2^2 + k_1^2}{(n_1 + n_2)^2 + k_1^2}$$

$$h_2 = \frac{-2 n_2 k_1}{(n_1 + n_2)^2 + k_1^2}$$

$$z = \frac{4\pi k_1 d}{\lambda} , \quad Y = \frac{4\pi n_1 d}{\lambda}$$

A basic program which has been written to calculate the values of reflectance as a function of film thickness is given in Appendix 1-b.

3.1.5 THE BASIC INSTRUMENT

Figure 3.1 shows one possible arrangement of instruments components. The basic instrument can be comparatively simple and inexpensive with good resolution perpendicular to the plane of the sample.

The ellipsometer employed in the present work consisted of the following components.

1. The light source which was a 24 volt, 150 watt projector lamp, type A_1/212.

2. A collimatar and filter.

3. Two of the modified polariser heads were used interchangeably as a polariser or analyser. Each head carried a modified calcite Glan Thomson prism giving a high degree of precision of polarisation. A single index line actuated by a micrometer screw divided drum was incorporated into the head, enabling the 1/4 degree division on the scale to be subdivided directly to 0.01 degrees. It also carried two scale readings with telescopes to provide readings at 180 degrees a part to eliminate any centering errors. The scale illumination was provided by low voltage bulbs supplied from a 6 volt transformer, placed inside the ellipsometer base.

4. The phase compensator or quarter wave plate [$\lambda/4$]; the compensator can be constructed of a birefringent material [for example mica]. The optical properties of a mica quarter waveplate may be characterised as follows. There are two mutually perpendicular axes in the plane of the plate. As indicated by the designations fast and slow for the axes, the index of refraction of the plate depends upon the axis with which the electric field vector of the light coincides. During transmission through the plate, the beam is considered to be resolved into plane wave components [the ordinary and extraordinary beams] with electric vectors that coincide respectively with the slow and fast axes. Then, since the components travel at different speeds, their transmission by the plate results in a phase shift between them. The phase shift, called relative retardation of the plate ς, depends upon the thickness of the plate, t, the wavelength of the light , and the difference between the indices of refraction [$n_{or} - n_{ex}$]:

$$\varsigma = \frac{2\pi}{\lambda} [n_{or} - n_{ex}]t \qquad [3.21]$$

For an exact quarter waveplate ς equals $\frac{\pi}{2}$ determined by

$$t = \frac{\lambda}{4} \Big/ [n_{or} - n_{ex}] \qquad [3.22]$$

This gives the thickness of plate [t] to introduce a phase difference of $\frac{\pi}{2}$ corresponding to a quarter wave [$\lambda/4$] between the two perpendicular vibrations. Plates can have thicknesses of odd multiples of $\frac{\lambda}{4}$. Since the compensator is cut as to introduce a phase difference of odd multiples of $\lambda/4$, it is often referred to as quarter waveplate. That means a different compensator is required. It is therefore necessary to calibrate the compensator to ensure that the actual phase difference falls within the required limits.

5. The detector used was a type 6094B photomultiplier tube supplied by EMI Electronics Limited and was employed in conjunction with a stabilised power supply type 532/D from ISOTPE Developments Limited. A solartron digital voltmeter type A203 which had a sensitivity of 1 microvolt was utilised for observing the voltage drop across a standard 1000 ohms resistance, enabling currents of less than 10^{-9} ampers to be detected.

The three triangular optical benches shown in Figure 3.1 were set to make angles of approximately 90°, 120° and 150° to one another. The light source, collimater, filter and polariser were mounted on the fixed bench. The compensator (when the compensator method was being used), analyser and the detector were mounted on one of the other two arms, which were set at an angle of about 120°. This arm could be moved to $\pm 5^{\circ}$ about the centre positions and permitted the angle of incidence to vary between 55° and 75°.

3.1.6 MODES OF OPERATION

There are two methods of analysis which have been used in this work:

i) The compensator method for fixed wavelength of 546.1 nm

ii) The method due to Beattie and Conn (1955).

i) THE COMPENSATOR METHOD

The procedure is schematically illustrated in Figure 3.4. Plane polarised light produced by the polariser, P, is incident on the sample surface with azimuth ψ, i.e. its transmission axis is inclined at an angle ψ to the plane of incidence. On reflection from the surface the difference in phase change and in amplitude reduction between parallel (P) and perpendicular (S) components gives rise to reflected light which is, in general, elliptically polarised. This elliptically polarised light then passes through the compensator. If the fast axis of the compensator is arranged to be parallel to the major axis of the reflected ellipse, the vibrations along the major and minor axes of the ellipse (for which a phase difference of 90° exists) are again brought into phase, and plane polarised light results. Then the light passes through the analyser, which may be rotated until its transmission axis is perpendicular to the electric vector. In this condition the light intensity received by the photomultiplier detector is zero.

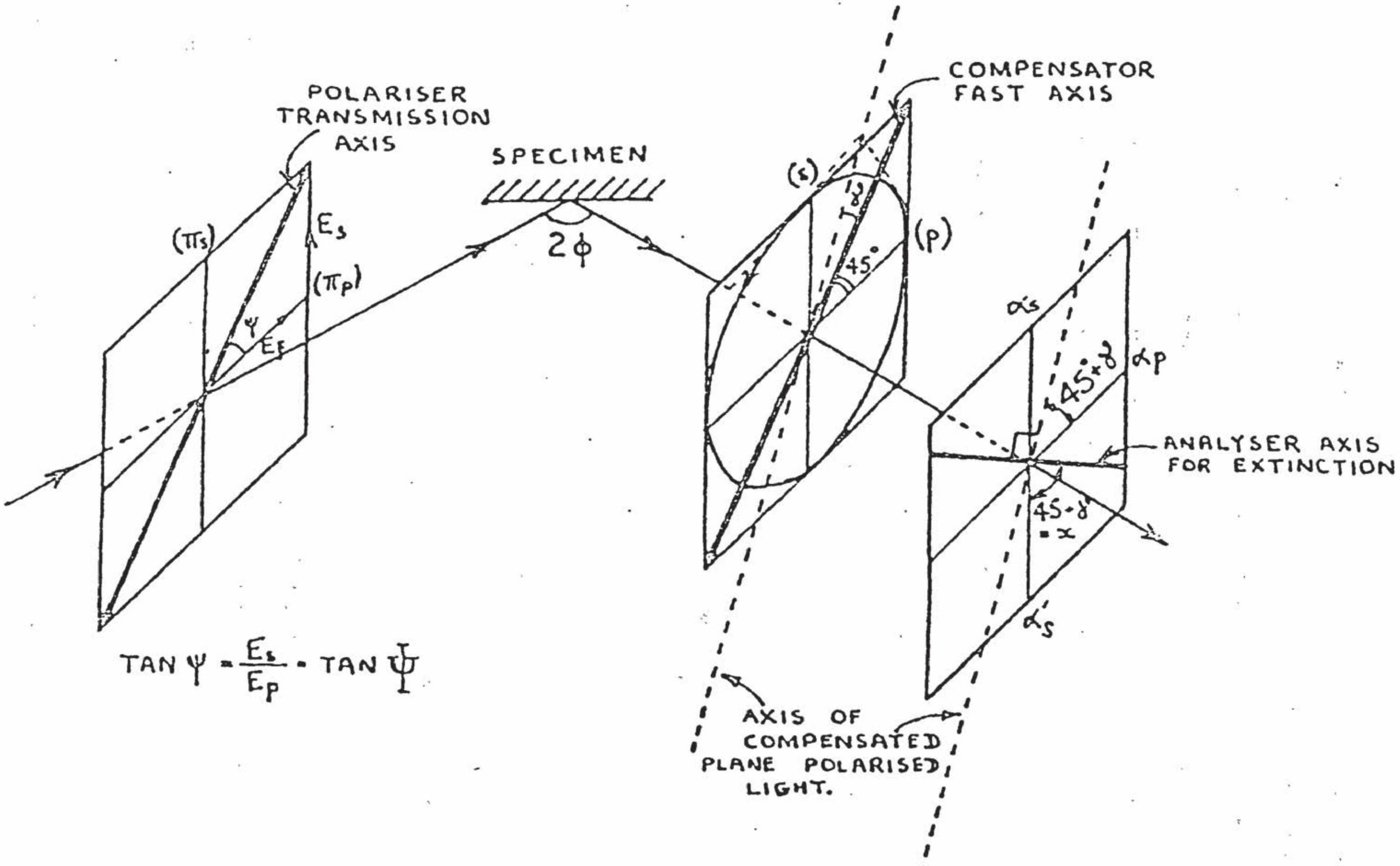

Figure 3.4 Basis of the Compensator Method of Ellipsometry

According to the experimental procedure, the compensator was first locked with its fast axis at exactly 45° to the plane of incidence. The polariser and the analyser were then adjusted so that the detected beam is extinguished. The situation then corresponds to that shown in Figure 3.4. The azimuth of the reflected ellipse is always 45°, or in other words, the amplitudes of the reflected (P) and (S) components are equal, i.e. $(E_P)_{ref} = (E_S)_{ref}$.

The azimuth of the polariser (ψ) is then equal to the parameter Ψ mentioned in Figure 3.4, from this figure

$$\tan \psi = (E_S/E_P)_{inc} \qquad (3.23)$$

but $\tan \Psi = (\frac{E_P}{E_S})_{ref} / (\frac{E_P}{E_S})_{inc}$

and since from above $(\frac{E_P}{E_S})_{ref} = 1.00$

$$\text{thus } \tan \Psi = \frac{1}{(\frac{E_P}{E_S})_{inc}} = (\frac{E_S}{E_P})_{inc} \qquad (3.24)$$

By analogy with equation 3.23, the values of ψ must equal Ψ.

The ellipticity γ (indicated in Figure 3.4) is related to the phase difference Δ between (P) and (S) components. In general, it may be shown that

$$\tan \Delta = \frac{\tan 2\gamma}{\tan 2x} \qquad (3.25)$$

since from $x = 45^\circ$, $\sin 2x = 1.00$ and thus $\Delta = 2\gamma$ (3.26)

The ellipticity γ and hence the phase difference Δ was determined from the analyser azimuth, as shown in Figure 3.4. The azimuth of the compensated light was $45^\circ + \gamma$, so that the azimuth of the analyser in its extinction position will be $45 + \gamma$. The azimuth of the analyser in its extinction position would be $45 + \gamma$ with respect to α'_s [α_s- reference azimuth in which plane polarised light with its electric vector parallel to the plane of the incidence could not pass through], the perpendicular to the plane of incidence. It was this quantity, marked x, which was measured experimentally. Since $x = 45 + \gamma = 45 + \Delta/2$

$$\text{then } \Delta = 2x - 90 \text{ degrees} \qquad [3.27]$$

In general, pairs of polariser and analyser azimuths for extinction occur which fall into four zones. MacCrackin [1963] gives a detailed explanation of the effect, although it should be noted that in his paper, the names of 'polariser' and 'analyser' are interchanged with those in this work, because his experimental arrangement has the compensator placed in the incident beam before the reflection.

ii] THE BEATTIE AND CONN METHOD

For this method the compensator is removed. The method involves the measurement of the absolute intensity of light transmitted by the system; polariser, sample surface-analyser for four different settings.

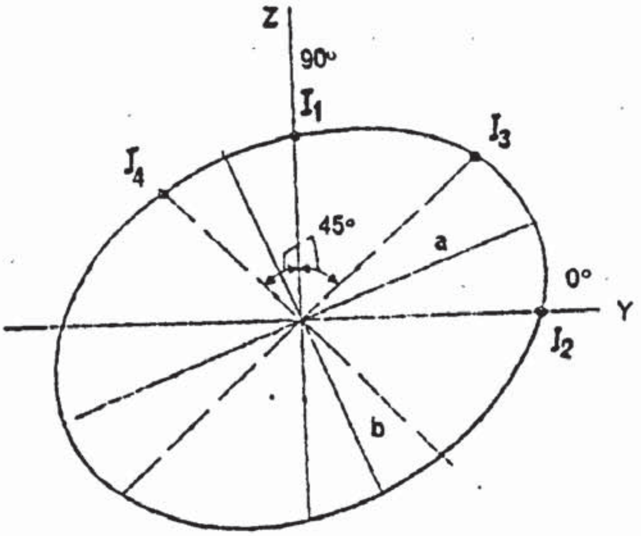

Figure 3.5 Intensity measurements to determine ψ and Δ (Beattie and Conn Method)

Figure 3.5 illustrates the principle of the method. The two parameters ψ and Δ can be measured in two ways:

1. Setting the polariser at 45 degrees with respect to an azimuth position and measuring the light intensity at four analyser settings.

2. Setting the analyser at 45 degrees from an azimuthal position and measuring the light intensity at four polariser settings.

Method 1 was adopted in this work and the light intensities I_1, I_2 I_3, and I_4 were measured at analyser settings of 90°, 0°, 45° and -45° with respect to an azimuth. Thus $I_1(+\pi/4, +\pi/2)$ indicates the light intensity with the polariser at $\pi/4$ (polariser azimuth, P) and the analyser at $\pi/2$ with respect to an azimuth. A similar notation has been adopted for other intensity values. The intensity measured may be expressed as:

$$I(P,A) = I_0\,(\sin^2 P \sin^2 A) + \rho^2 \cos^2 P \cos^2 A + \tfrac{1}{2}\rho \sin 2P \sin 2A \cos \Delta) \qquad (3.28)$$

where $\rho = \tan\psi$

From equation 3.28 the four intensities are:

$$I_1\,(+\tfrac{\pi}{4}, \tfrac{\pi}{2}) = \tfrac{1}{2} I_0 \qquad (3.29)$$

$$I_2\,(+\tfrac{\pi}{4}, 0) = \tfrac{1}{2} I_0 \rho^2 \qquad (3.30)$$

$$I_3\,(+\tfrac{\pi}{4}, \tfrac{\pi}{4}) = \tfrac{1}{4} I_0\,(1 + \rho^2 + 2\rho \cos\Delta) \qquad (3.31)$$

$$I_4\,(+\tfrac{\pi}{4}, -\tfrac{\pi}{4}) = \tfrac{1}{4} I_0\,(1 + \rho^2 - 2\rho \cos\Delta) \qquad (3.32)$$

Values of ψ and Δ can then be evaluated using

$$\rho = \tan\psi = \sqrt{\frac{I_2}{I_1}} \qquad (3.33)$$

and $$\cos\Delta = \tfrac{1}{2}(\rho + \tfrac{1}{\rho})\,\left(\frac{I_3 - I_4}{I_3 + I_4}\right) \qquad (3.34)$$

A simple check which is found to be true to within 0.5% to 1.0% is that:

$$I_1 + I_2 = I_3 + I_4 \qquad (3.35)$$

and errors due to incorrect reference azimuth can be reduced by measuring the four corresponding intensities on the opposite sides of the reference azimuth and taking an average of the results.

3.1.7 EXPERIMENTAL PROCEDURE

i) DETERMINATION OF REFERENCE AZIMUTH FOR THE POLARISER AND THE ANALYSER

The readings on the divided circles of the polariser and analyser that correspond to the transmission axis of the polaroids being parallel and perpendicular to the plane of incidence are known as the reference azimuths. In the two methods of ellipsometry undertaken, the experimental azimuths are expressed relative to the plane of incidence.

Approximate values can be quickly obtained by arranging the light beam to be reflected at a dielectric surface at the Brewster angle of incidence; the intensity of the - compensator beam is zero. Briefly, each polaroid in turn is rotated until minimum light is visible through; the transmission axis is then approximately vertical. The polariser is rotated 90 degrees so that the transmission axis is horizontal and the analyser is kept with its transmission axis perpendicular to the plane of incidence.

To find the exact azimuths for the polariser and the analyser, the compensator was removed and light was reflected from a metal surface in which the following procedure was used: The extinction setting for the polariser is determined by measuring polariser settings that give equal intensities on each side of the minimum intensity. The exact minimum, π_p, is the average of the two settings.

The polariser is then set at π_p and the analyser extinction setting α_s, is the average of the two settings that gives equal intensities on each side of the minimum. Both polariser and analyser are then rotated 90 degrees and the entire procedure repeated. These alternative positions correspond to azimuth π_s and α_p and there are non-significant positions at 180 degrees to each of the scale readings and these are represented by a dash ['].

ii) DETERMINATION OF REFERENCE AZIMUTH FOR THE COMPENSATOR

A reference position for the compensator [when used] is obtained by setting the polariser and the analyser to a pair of related reference positions and then rotating the compensator until a position of minimum transmission is obtained. Again, the exact reference position is the average of the two settings that give equal intensities on each side of the minimum. The position corresponds to either the fast axis or slow axis of the compensator being parallel to the plane of incidence.

The procedure is repeated for the alternative compensator position which is 90 degrees from the first position for a correctly aligned apparatus.

There are non-significant positions at 180 degrees to both the above positions. The results for the azimuths of the polariser, analyser and the compensator used in this work are displayed in Table 3.1.

λ = 546.1 nm		
Polariser Azimuth (degrees)	Analyser Azimuth (degrees)	Compensator Azimuth
π_p = 141.28	α_s = 132.42	74° 40'
$\pi_{p'}$ = 321.28	$\alpha_{s'}$ = 312.41	164° 40'
π_s = 51.69	α_p = 42.32	254° 39'
$\pi_{s'}$ = 231.69	$\alpha_{p'}$ = 222.27	344° 39'

Table 3.1 Results for the reference azimuth for the polariser, analyser and the compensator

iii) PROCEDURE FOR DETERMINATION OF ψ AND Δ FOR SPECIMEN USING COMPENSATOR METHOD FOR λ = 546.1 nm

The compensator was set with its axis at 45 degrees to a reference position, so that the axes of the compensator coincided with the axes of the reflected ellipse. Light of any ellipticity is then compensated, i.e. converted to plane polarised light and can be characterised by the angles ψ and Δ. After locking the $\lambda/4$ plate, the polariser and analyser are successively turned to give minimum light intensity. The polariser extinction position, say P_1, is then found by 'bracketing' the minimum position. With the polariser then set at its extinction position, the analyser extinction position, say A_1, is likewise found by 'bracketing'. P_2 and

A_2 are found by the same procedure for a polariser azimuth in another quadrant. In general, the polariser settings are symmetrically placed about π_p, i.e. $P_1 - \pi_p$ should equal $\pi_p - P_2$, then the average is

$$\psi = \frac{[P_1 - \pi_p] + [\pi_p - P_2]}{2} \qquad [3.35]$$

It is found that P_3 and P_4 at 180 degrees to P_1 and P_2 respectively. A_3 and A_4 are also 180 degrees to A_1 and A_2 respectively, and sequentially also P_3 and P_4 are symmetrically placed about π_p', i.e.

$$[P_3 - \pi_p'] = \pi_p' - P_4$$

and $$\psi = \frac{[P_3 - \pi_p'] + [\pi_p' - P_4]}{2}$$

Tan ψ is relative amplitude reduction between the [P] and [S] components produced by reflection from the specimen. The analyser readings A_1 and A_2 are always separated by approximately 90 degrees, $\alpha_s - A_1$ should equal $\alpha_p - A_2$. In general the average = x, i.e.

$$x = \frac{[\alpha_s - A_1]\ [\alpha_p - A_2]}{2} \qquad [3.36]$$

where the angle 2x - 90 = Δ [the relative phase retardation between [P] and [S] components].

Results taken on bulk titanium [Ti] will be used to demonstrate the procedure adopted throughout these investigations.

The compensator was taken $+\frac{\pi}{4}$, i.e. at 299° 40' and the following values were found:

$P_1 = 173.88^\circ \quad A_1 = 66.02^\circ \quad A_1 - \alpha_s' = x$

$P_2 = 108.64^\circ \quad A_2 = 336.08^\circ \quad A_2 - \alpha_p' = x$

$P_3 = 353.90^\circ \quad A_3 = 246.30^\circ \quad A_3 - \alpha_s = x$

$P_4 = 288.66^\circ \quad A_4 = 156.20^\circ \quad A_4 - \alpha_p = x$

The compensator was then locked at $\frac{\pi}{4}$, i.e. 29° 40' and the following values were found:

$P_1 = 108.76^\circ \quad A_1 = 18.37^\circ \quad \alpha_s - A_1 = x$

$P_2 = 173.94^\circ \quad A_2 = 288.28^\circ \quad \alpha_p - A_2 = x$

$P_3 = 288.67^\circ \quad A_3 = 198.52^\circ \quad \alpha_s' - A_3 = x$

$P_4 = 353.90^\circ \quad A_4 = 108.40^\circ \quad \alpha_p' - A_4 = x$

ψ_{av} = 32.62 degrees

x_{av} = 113.88 degrees

Δ_{av} = 137.76 degrees

iv) PROCEDURE FOR DETERMINATION OF ψ AND Δ FOR A SPECIMEN USING THE BEATTIE AND CONN METHOD

As mentioned earlier, the absolute intensities of the light transmitted by the system of the polariser-specimen-analyser is measured for eight pairs of settings of polariser and analyser and are given as follows:

Polariser: Analyser:

$\pi_p + 45 = 186.28$ degrees $\alpha_s = 132.42^\circ = I_1$

$\alpha_p = 42.32^\circ = I_2$

$\alpha_p - 45 = 357.32^\circ = I_3$

$\alpha_p + 45 = 87.32^\circ = I_4$

Polariser: Analyser:

$\pi_p - 45 = 96.28$ degrees $\alpha_s' = 312.41^\circ = I_1'$

$\alpha_p' = 222.27^\circ = I_2'$

$\alpha_p' + 45 = 267.27^\circ = I_3'$

$\alpha_p' + 45 = 177.27^\circ = I_4'$

The parameters ψ and Δ are then calculated from the formulae 3.33 and 3.34.

The same specimen, Titanium (bulk) was used to prove the procedure and to check the results taken by $\lambda/4$ method and these are given below:

$I_1 = 9.44$ $I_1' = 8.76$

$I_2 = 3.75$ $I_2' = 3.78$

$I_3 = 10.64$ $I_3' = 10.80$

$I_4 = 2.09$ $I_4' = 2.20$

for checking $I_1 + I_2 = I_3 + I_4$; $12.745 = 12.865$

$\psi_{av} = 32.79^\circ$ and

$\Delta_{av} = 137.05^\circ$.

The results of ψ and Δ agreed with above one for the same sample and at the same wavelength 546.1 nm.

v) ERROR ANALYSIS

The scale readings for the polariser (P) and the analyser (A) could be measured to 0.01 degrees and the angle of incidence was measured to within ± 0.5 degrees.

Several readings were taken immediately following each other by the bracketing method as described in Section 3.1.7. The calculated standard deviation of the reading was about 0.09 degrees for the analyser and 0.06 degrees for the polariser.

Thus the error arising from the ellipsometry's parameters (angle of incidence, $\emptyset_0$; polariser reading, P, and the analyser reading, A,) cause the alternate error in the optical constants n and k.

The following method has been used to estimate the error in n and k from the errors associated with the above parameters.

n and k have been calculated as a function of the angle of incidence using fixed values of P and A, fixed values of A and angle of incidence by varying P, etc. Figure 3.6 shows the variations of the calculated values of n and k by uncertainties of the experimental parameters for the titanium for the wavelength 546.1 nm. This figure suggests that:

1. An error of ± 1 degree in the angle of incidence changes the value of n by about + 12% and of k by about ± 17%.

2. An error in Δ of ± 0.1 degrees changes the n value by about ± 0.7% and k by about ± 0.4%.

3. An error in ψ of ± 0.1 degrees changes the n value by about ± 0.1%.

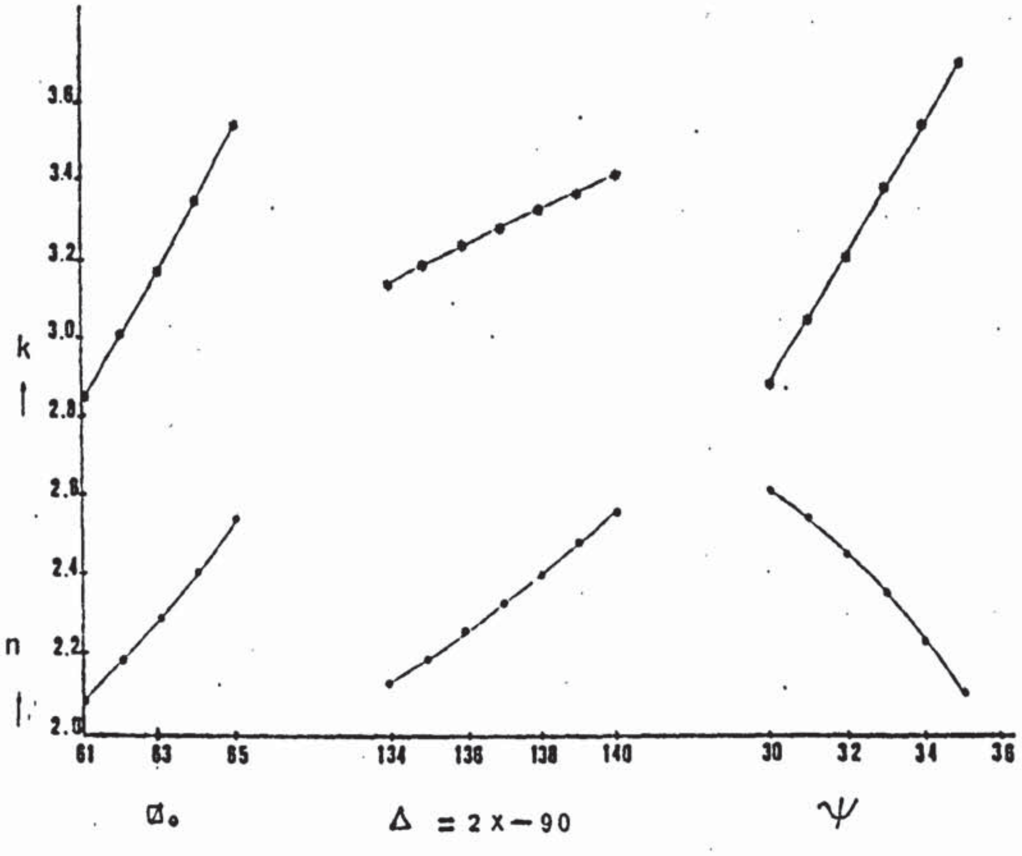

Figure 3.6 Errors of n and k caused by slight deviation of the angle of incidence, Δ and ψ from the correct values

3.2 MEASUREMENT OF REFLECTANCE

The following types of spectrophotometers have been used to measure the reflectance in the study.

i) A Perkin-Elmer 450 spectrophotometer, Figure 3.7, was used to measure normal specular reflectance over a range of wavelengths from 0.35 μm to 2.7 μm of the electromagnetic spectrum. The following process has been adopted:

1. A reference sample with freshly evaporated aluminium is seated in the reflectance holder attachment and housed in the lower reference compartment box, which is below the testing compartment box. These boxes are located to the right of the PE 450 housing. The testing box will be empty from the reflectance attachment of the sample holder for this step. After closing these boxes, the instrument is set so that the scanning over the desired range of wavelengths, i.e. the visible (VIS) or near infrared (NIR) occurs by putting the corresponding chart in the proper place and setting the scale knob and pen to approximately '80%' on full scale knob.

2. The sample to be investigated is placed in the testing compartment box and seated in the reflectance holder attachment and a second scanning follows. The surfaces of the reference film and that of the sample should face the beam front, i.e. away from the operator.

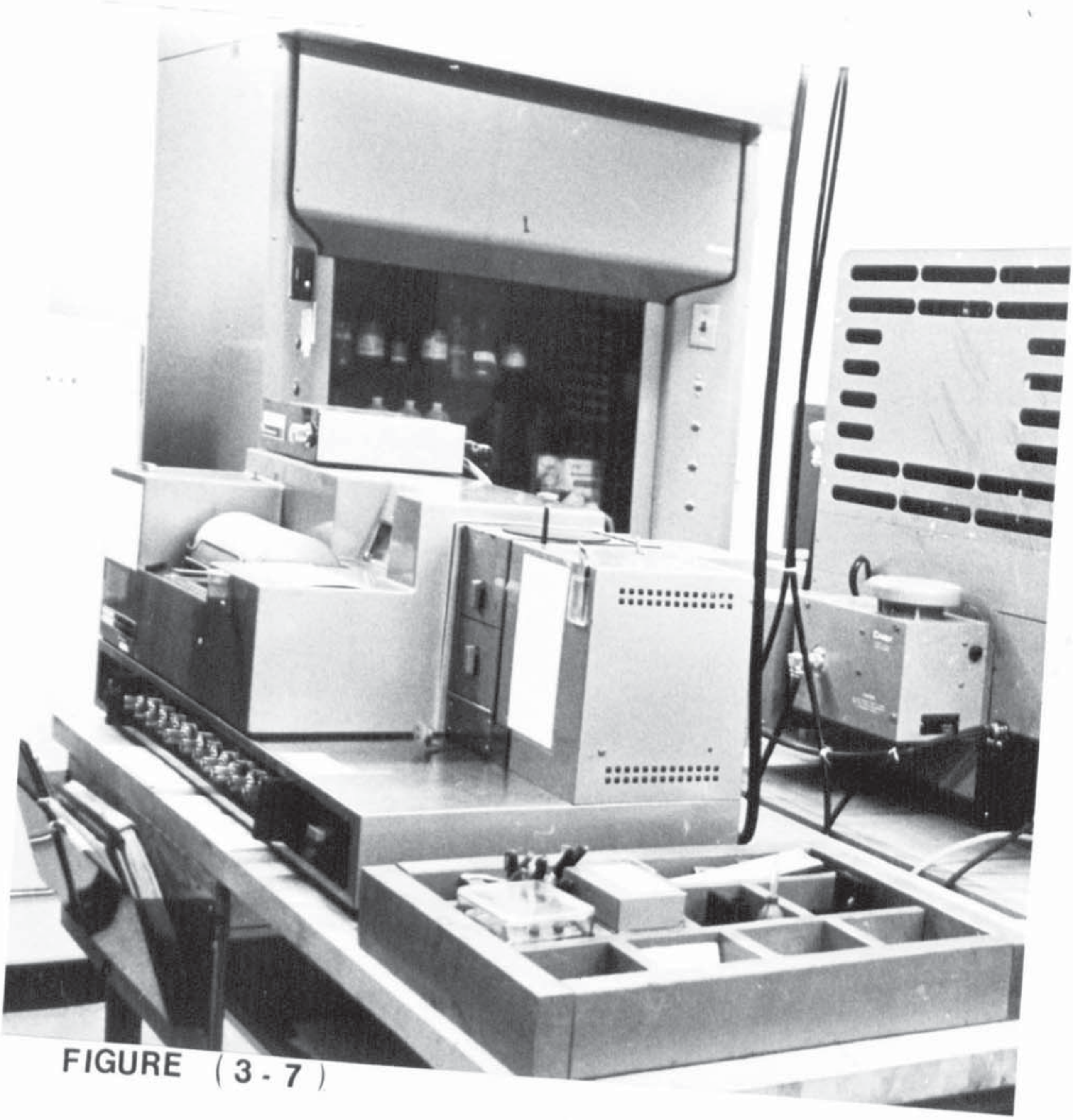

FIGURE (3-7)

PERKIN-ELMER 450 SPECTROPHOTOMETER
WAVELENGTH RANGE : 0-6 to 2-7 μm

Figure 3.8 displays one example of the output corresponding to the sample of 5 mV.

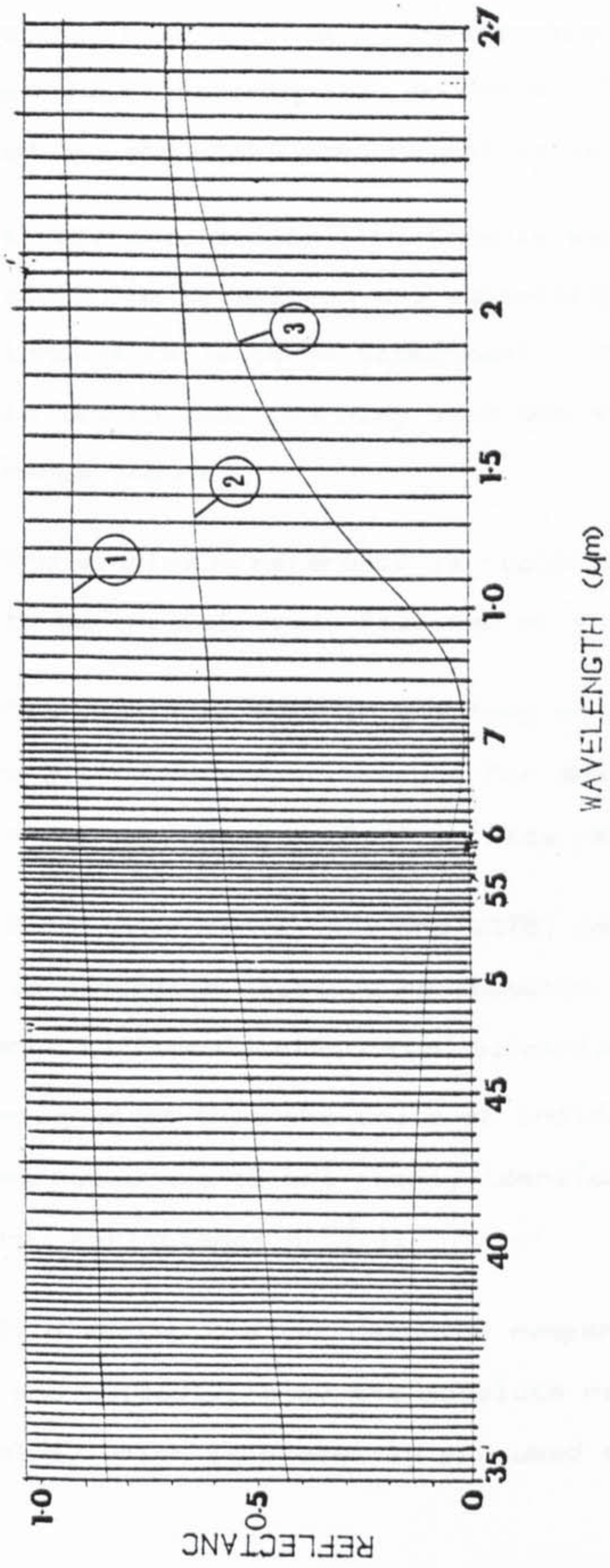

Fig. 3.8 Example of chart records of 450 spectrophotometer

(1) the aluminium reference run
(2) the uncoated 304 stainless steel (INCO) run and
(3) the 5 mV sample run

ii) A Perkin-Elmer Model 1378 infrared spectrophotometer, Figure 3.9, was used to measure the normal specular reflectance over a range of wavelengths from 2.5 μm to 15 μm of the electromagnetic spectrum. The procedure adopted for the above measurement is as follows:

1. A reference sample with freshly evaporated aluminium is laid on the supporting plate of the inhouse reflectance attachment. The instrument is set so that scanning over the whole wavelength range occurs.

2. The aluminium reference is replaced by the sample to be investigated, followed by a second scanning.

The data output is in the form of a chart recording. Figure 3.10 displays an example for the output of the sample corresponding to INCO surface of 5 mV process.

Both instruments, 450 and 1378, operate in double beam mode to determine relative reflectance of a surface as compared to freshly evaporated aluminium. These instruments are designed so that the angle of incidence is 7 degrees and the measurements are nearly identical to the normal spectral reflectance $R_n(\lambda)$.

By dividing the two detector responses from either chart and multiplying by the absolute reflectance of aluminium, which is presently presumed to be equal to the

FIGURE (3-9)

PERKIN- ELMER 137 SPECTROPHOTOMETER

WAVELENGTH RANGE : 2.5 to 15μm

published data on absolute reflectance of laboratory aged aluminium films, Table 3.2, we obtain the normal specular reflectance of the sample, which is $R_n(\lambda)$. The normal specular reflectance result over the infrared region of the spectrum, allows for an evaluation of the normal emittance as has been discussed in Chapter 2.

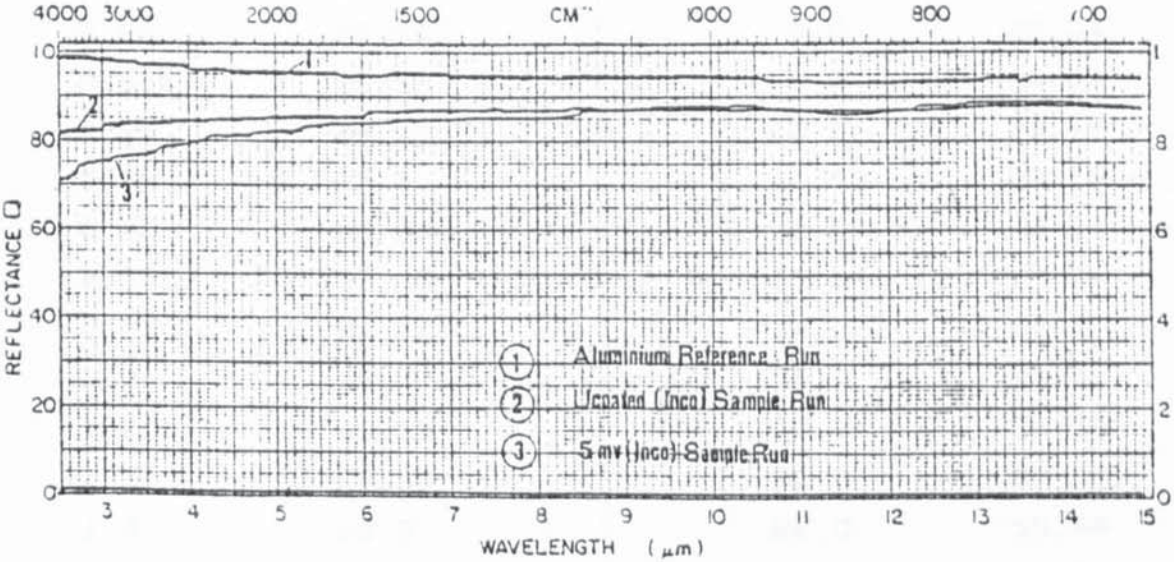

Fig. 3.10 Example of chart record for 137B spectrophotometer.
(1) the aluminium reference run
(2) the uncoated 304 stainless steel (INCO) run and
(3) the 5 mV sample run.

λ [μm]	R [hv. aged] %	λ [μm]	R [hv. aged] %
0.4	90.76	2.1	97.1
0.45	90.61	2.2	97.2
0.50	90.34	2.4	97.3
0.55	90.32	3.0	97.36
0.60	90.27	3.5	97.5
0.65	89.76	4.0	97.58
0.70	88.86	5.0	97.7
0.75	87.61	6.0	97.84
0.775	86.78	7.0	97.94
0.80	85.96	8.0	98.04
0.825	85.56	9.0	98.07
0.85	85.96	10.0	98.12
0.875	87.3	11.0	98.16
0.90	88.94	12.0	98.21
0.925	90.30	13.0	98.26
0.95	91.54	14.0	98.3
1.0	93.2	16.0	98.38
1.2	95.85	18.0	98.15
1.3	96.58	20.0	98.52
1.4	96.5	22.0	98.56
1.5	96.6	24.0	98.61
1.55	96.7	26.0	98.64
1.60	96.7	28.0	98.67
1.65	96.8	30.0	98.7
1.70	96.8	32.0	98.72
1.75	96.9		
1.80	96.9		
2.00	96.99		

Table 3.2 Reflectance of evaporated aluminium films produced from Bennett et al, 1963

iii) INTEGRATING SPHERE REFLECTOMETER (ISR): the reflectance of radiation falling on a rough surface consists of specular and diffuse components. Scattering from such a surface can cause an error by neglecting the diffuse component of the reflectance for the spectrophotometers measuring reflectance at near normal incidence. To detect the total reflected radiation, a so-called integrating sphere reflectometer, ISR, can be used. An ISR can be operated in one of two modes: direct or indirect. In the direct mode, the sample is irradiated directly and the detector views an area on the sphere wall. A similar reading is then taken on a comparison reference of known reflectance under the same conditions. The measured directional hemispherical reflectance factor $R'(\theta, 2\pi)$ is then the ratio of the sample reading to the reference reading times the known reflectance of the reference.

In the indirect mode, the beam from the source is first incident on the sphere wall, and the sample is irradiated uniformly over a hemisphere. The detector views the sample directly. A similar comparison reading is then taken on a reference of known reflectance under the same conditions. The measured hemispherical directional reflectance factor $R'(2\pi, \theta)$ is then the ratio of the sample reading to the reference reading times the known reflectance of the reference. The measured reflectance factors $R'(\theta, 2\pi)$ and $R'(2\pi, \theta)$ are each equal to the directional hemispherical reflectance R_{Hem} [illegible]) and are frequently reported as such. This equality has also been used in this work.

The ISR instrument developed by Jacobson and Lamoreaux [1979] at the Optical Sciences Center, Arizona University, operates in hemispherical directional mode. This instrument is illustrated in Figure 3.11. The Tungsten Halogen source is mounted at a side port [1] of an integrating sphere. The sphere of this instrument is shown in Figure 3.12. It is made up of two hemispherical aluminium caps which are coated inside with a barium sulphite coating, a material which maintains a diffuse reflectance of above 70% up to wavelengths of the order of 3 μm. If a radiation beam is coming into the sphere and hits the wall, the individual rays will be diffusely reflected by this wall coating and this results in a uniform radiation density inside the sphere, and uniform brightness over the surface of the sphere. The sample is placed in the centre of the sphere and is illuminated hemispherically. It is supported by a shaft which can be rotated by a knob outside a second sphere port; this enables one to measure the directional reflectance at various angles. There are three apertures in the sphere, one for the incident beam, one for the detector and one for the sample holder. The sample is irradiated with a source through port 1 and the detector is located at port 3. The monochromator is located between the sphere and the detector. The detector used covers 96% of the air mass 2 [Thomas and Richmond 1978].

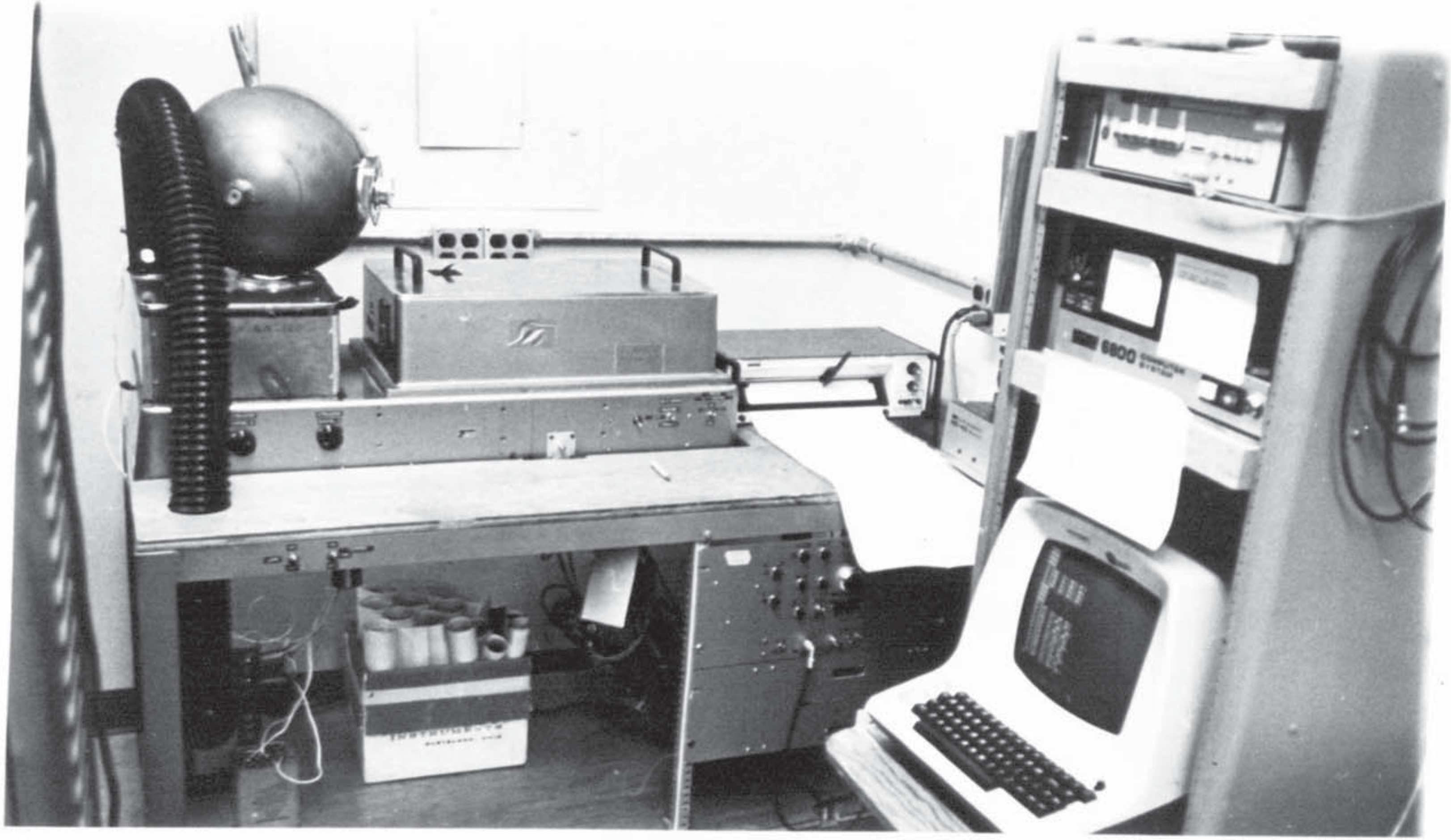

FIGURE (3-11) INTEGRATING SPHERE REFLECTOMETER

WAVELENGTH RANGE : 0.40 to 2.7 μm

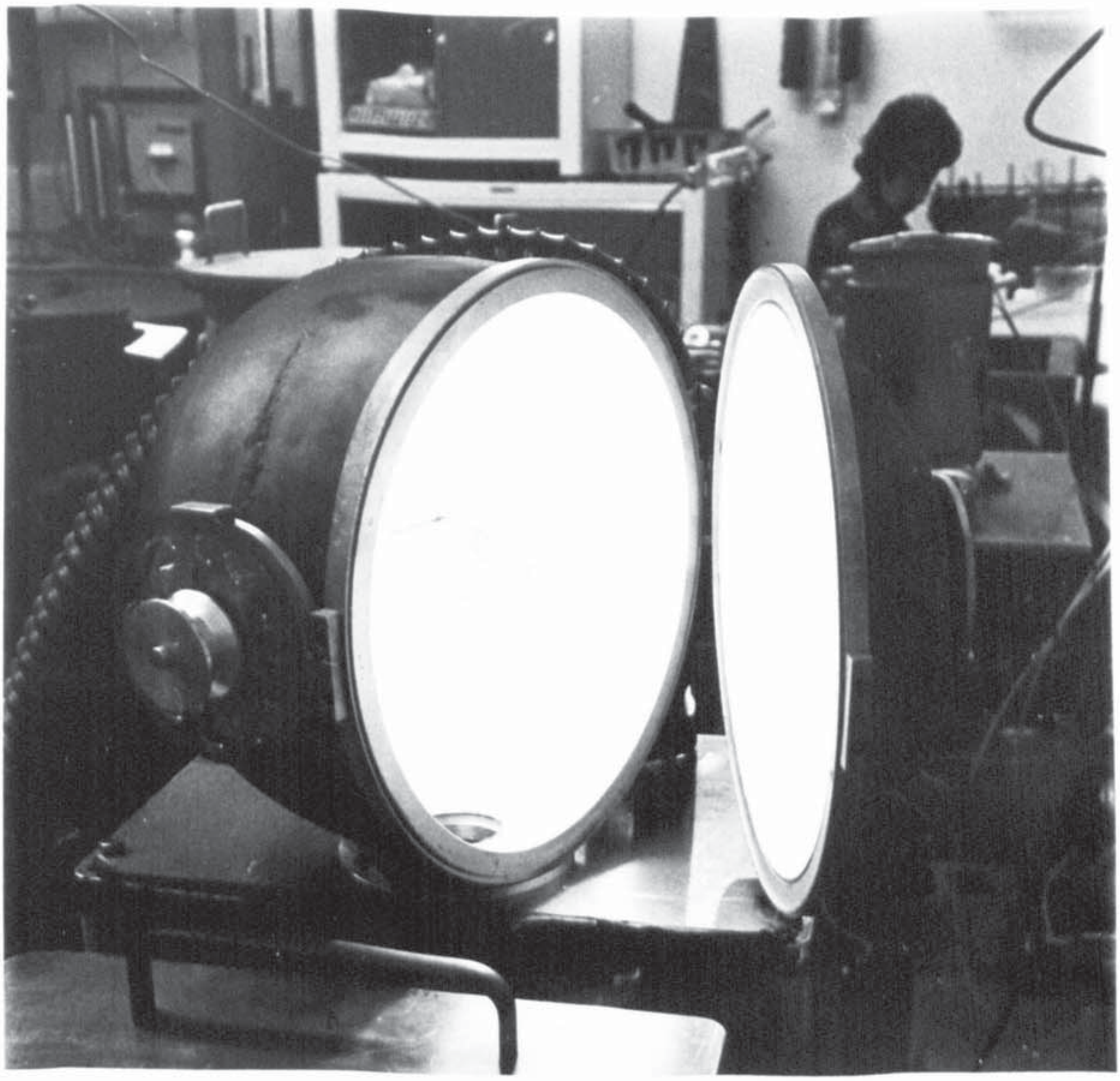

FIGURE (3-12) INTEGRATING SPERE

[300 mm Diameter Alumihium Sphere
Coated With Kodak White Reflectance
Coating]

The procedure adopted for surface analysis by this instrument is as follows:

1. A reference sample with freshly evaporated aluminium is placed on the holder and the surface film faces the detector port. Scanning takes place over the whole range of wavelengths (0.4 to 2.7 μm) and measurements are made.

2. The reference is removed and replaced by the black glass and followed by a second scan, under the same conditions. This step allows for the correction against the white sphere background for the aluminium reference and the sample to be investigated.

The results of step 1 and step 2 are measured and stored in a computer memory.

3. The black glass is then removed and replaced by the sample and followed by a third scan.

This procedure provides corrected reflectance factors for both the sample and for the aluminium reference. The former is divided by the latter, causing the sphere wall's reflectance to cancel. The last step is the multiplication of this ratio by the absolute reflectance of laboratory aged aluminium film. Figure 3.13 shows a strip chart output as an example for this type of analysis.

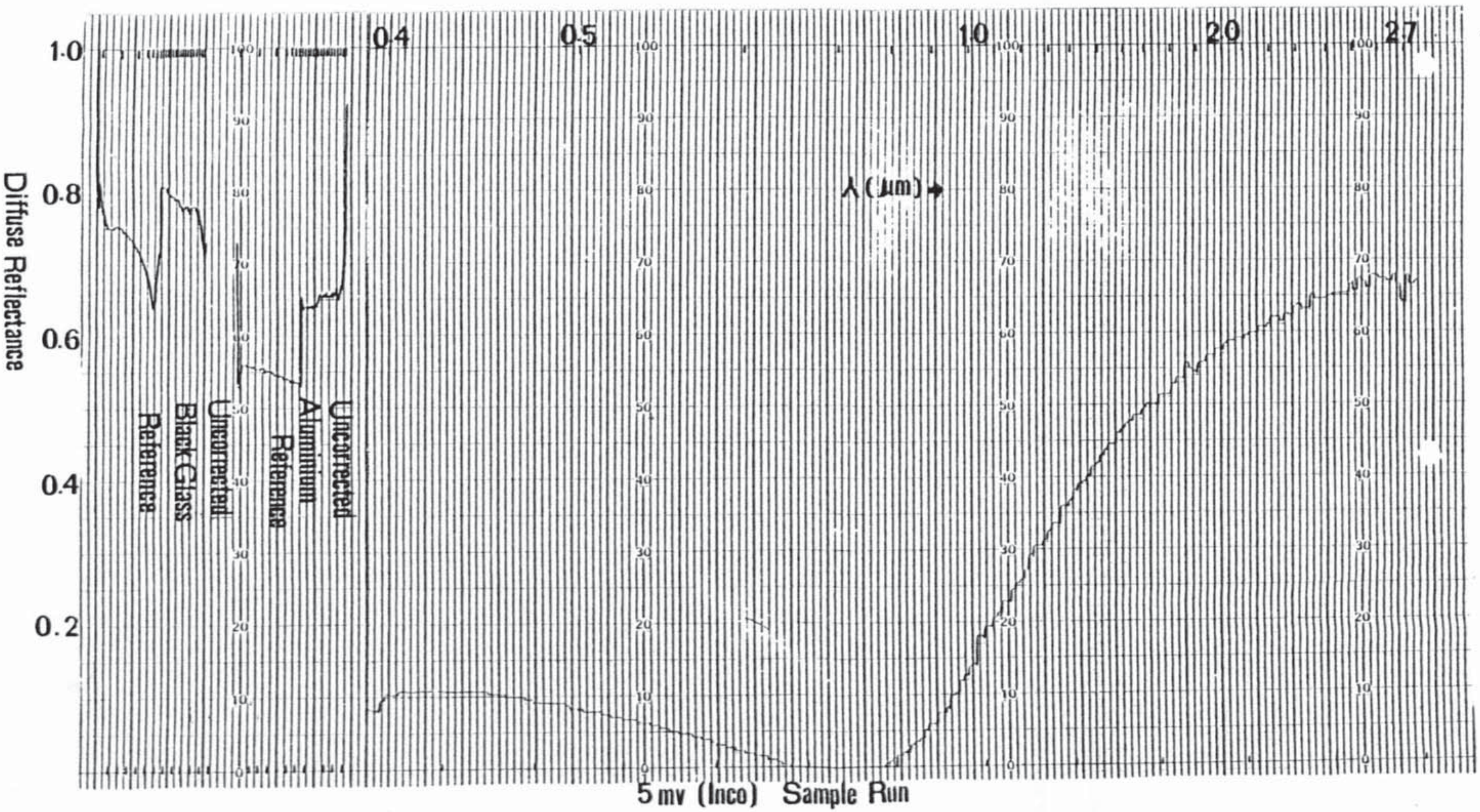

<u>Figure 3.13</u> Example of Strip Chart Record for ISR.
The aluminium, the black glass and 5 mV sample runs are indicated on the figure. Wavelength range for each run is 0.4 to 2.7 μm.

The ISR allowed for a calculation of hemispherical solar absorptance as has been discussed in Chapter 2. All instruments mentioned above, the 450, 137B and ISR determine relative values of reflectance which are accurate to ± 1%.

The reflectance measurements by the above instruments were done in the Measurement Laboratory, Optical Sciences Center, Arizona University, Touson, USA.

3.3 MEASUREMENT TECHNIQUES FOR LIFE TESTING

Figure 3.14 represents the tube furnaces used in such tests. These furnaces can expose spectrally selective surfaces to extreme conditions, open to the atmosphere or in a controlled atmosphere over temperatures ranging from 25°C to 1200°C. The controllers used were: Lindberg Solid State Digital Controllers.

The above furnaces have been used in the current investigation for life testing in air and for thermally oxide growth on bulk titanium and for stainless steel and one is able to hold the temperature to ± 5°C.

Figure 3.15 represents the life cycle furnaces. The twin furnaces simulate thermal transients due to cloud passage and the diurnal cycle, experience by solar receivers. Testing has been carried out for nickel black and INCO surfaces in air and in soft vacuum, 0.1 Torr.

Their temperatures ranged from 25°C to 1200°C.

Furnaces used: Paragon 011P units on air-operated stages.

The cycling was programmable.

The life testing was carried out in the Optical Sciences Center, Arizona University, Touson, USA.

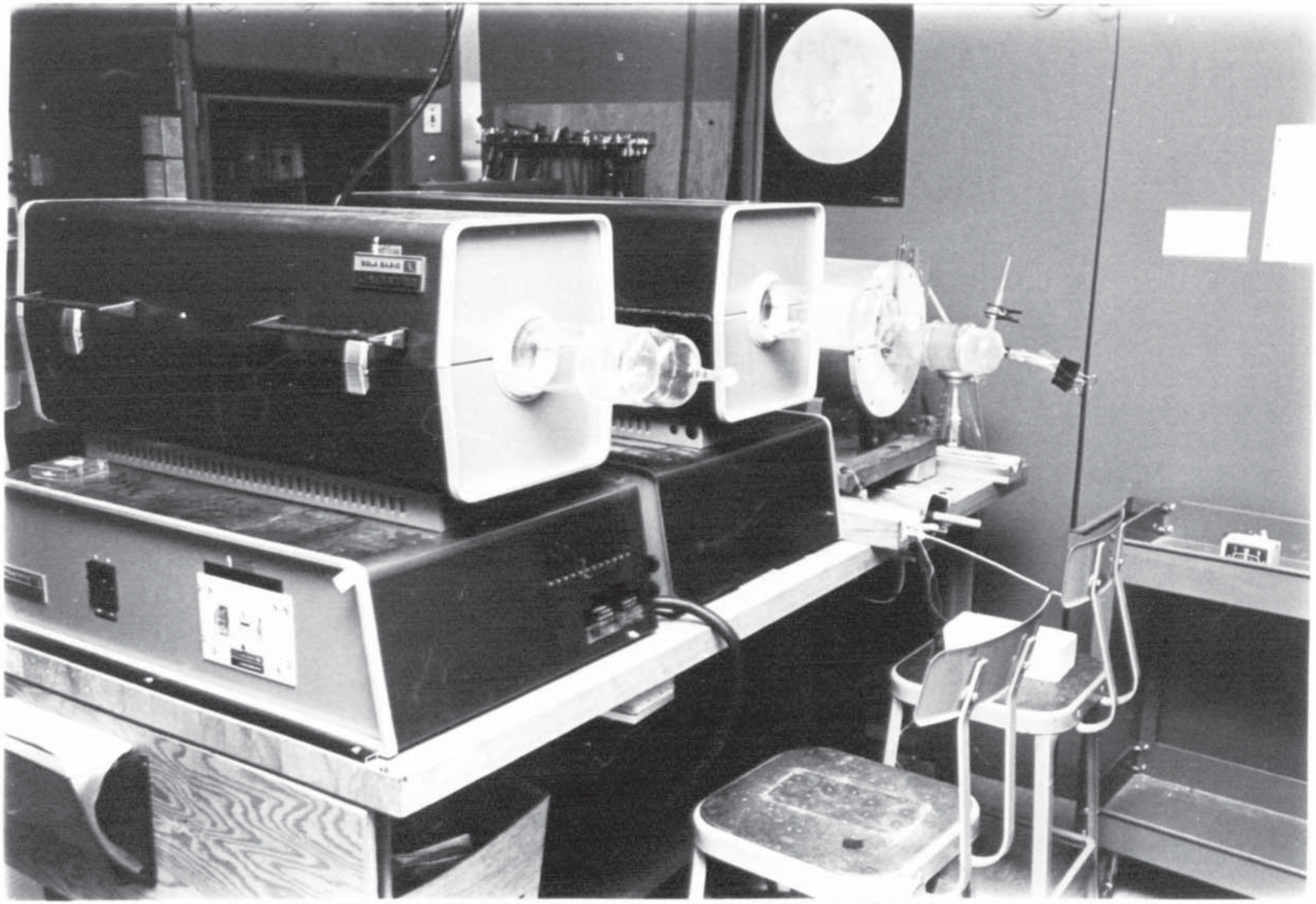

FIGURE (3.14) TUBE FURNACES, LINDBERG FURNACE

TEMPERATURE RANGE : 25 Deg.C. to 1200 Deg.C.

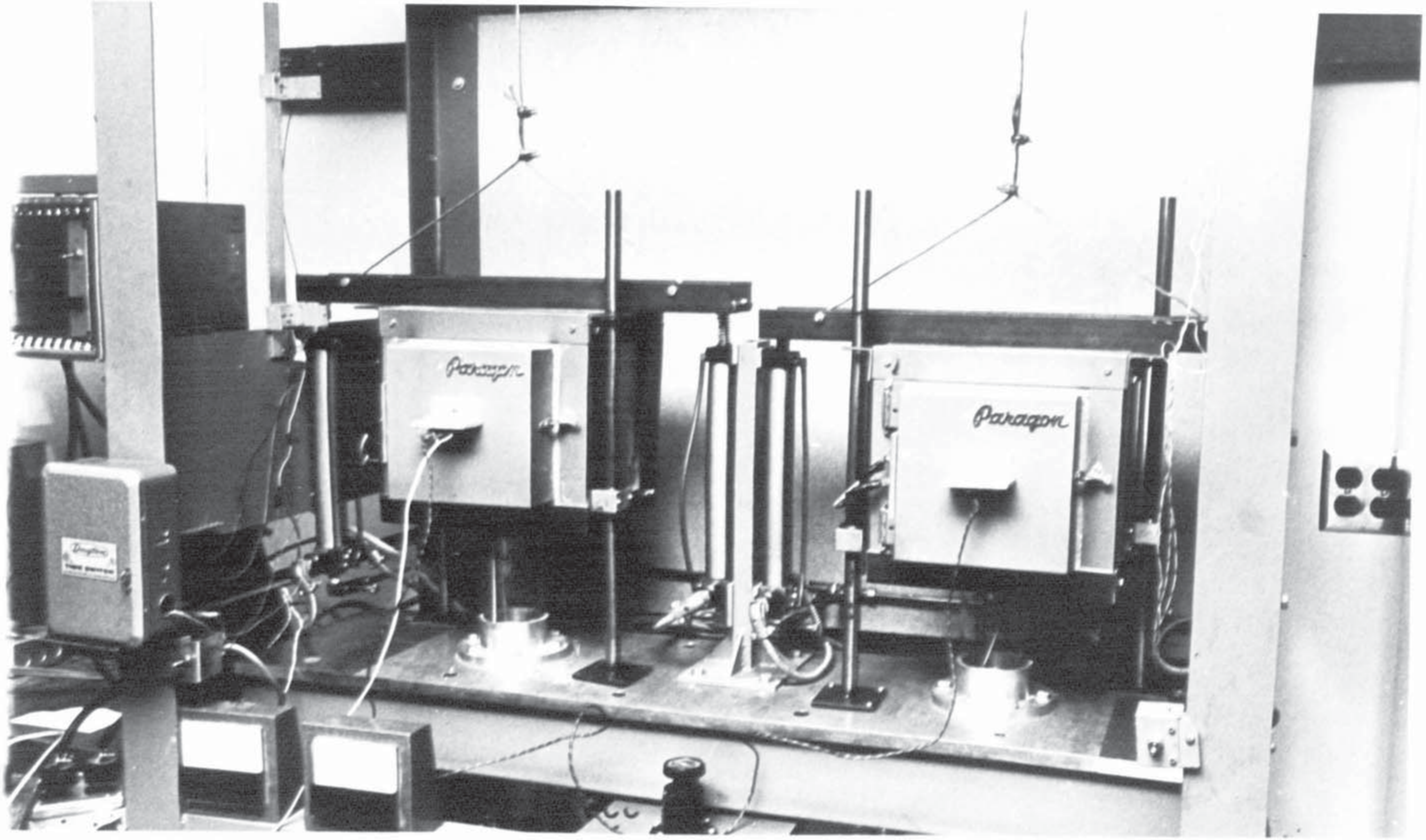

FIGURE (3-15) LIFE CYCLE FURNACES

TEMPERARATURE RANGE : 25 DEG. C. to 1200 DEG. C.

3.4 MEASUREMENT OF THE CHEMICAL COMPOSITION

Two techniques have been used to investigate the chemical composition of the selective surfaces which have been supplied by INCO. Birmingham: Auger spectroscopy for the samples corresponds to 5 mV and 9 mV [unheated] and the electron microprobe for the black nickel foil.

The principle of Auger electron spectroscopy can be summarised as follows: A beam of 1.5 KeV electrons, 1 μA, bombards the surface of the sample which then emits secondary electrons from within a very thin surface layer [5 Angstrom to 20 Angstrom]. Some of these electrons, called Auger electrons, are characteristic of the emitted atoms. Since the energy of the emitted Auger electrons are, in fact, dependent on the atom they come from, the energies of the Auger electrons can be used to determine the composition of a film. The following formula represents a first order method of deriving atomic percents from the quantity of detected Auger electrons.

$$\text{Atomic \%} = C_x = \frac{I_x/I_x^H}{\sum_i I_i/I_i^H} \qquad [3.37]$$

I_x is the measured Auger signal

I_x^H is the peak to peak of the Auger signal as measured from an elemental standard, taken from the handbook of Auger electron spectroscopy, Palmberg et al [1972].

In the microprobe technique, the electron microprobe bombards the sample with electrons and detects X-rays. An Applied Research Laboratories Scanning Electron Microscope Quantometer, housed in the University of Arizona's Space Sciences Center, was used to analyse the nickel black foil before and after heat treatment. However, we could not use the above technique for the coloured samples of stainless steel (INCO surfaces) because the oxide layer is thin.

CHAPTER 4

EXPERIMENTAL RESULTS

The purpose of this chapter is to present the experimental data which relate to the Ellipsometric, Reflectance, composition and life testing measurements, which have been made on the surfaces to be investigated.

The figure below shows the sequence of experiments used to characterise and evaluate the surfaces.

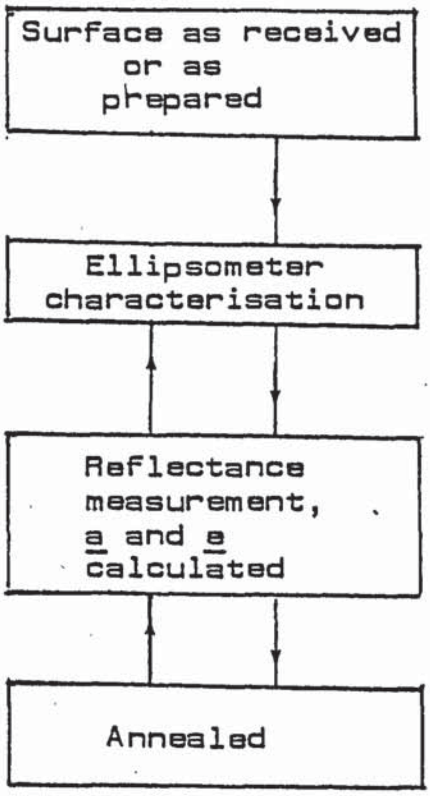

4.1 TITANIUM OXIDE/TITANIUM

There has been a growing interest in the oxide films of titanium as energy converters of solar radiation energy. Fujishima and Honda [1972] decomposed water photo-electrochemically using a TiO_2 electrode. Recently Stalder and Augustyrski [1979] reported the application of titanium dioxide in process of photo-reduction of water to produce hydrogen. The use of oxide films of titanium as transparent antireflectory coating has been reported by Fan and Buchner [1976] and as antireflecting coating on metal for selective solar absorbers by Yoshida [1979], who deposited titanium oxide films on titanium by reactive evaporation in oxygen of 99.99% purity using an electron beam gun.

The work reported here relates to optical properties of thermally grown oxide films on mechanically polished titanium. The refractive index and the extinction coefficient of the growth of an oxide film on bulk titanium in air at 750°K as well as for the bulk titanium are determined over a wavelength range from 347.1 nm to 576.1 nm by using ellipsometry. The spectral reflectivity of the above system which consists of a metal and its derivative oxides layer produced at 750°K for various firing times were measured over a wavelength range from 0.375 μm to 15 μm.

4.1.1 ELLIPSOMETRIC STUDIES

TITANIUM SUBSTRATE SAMPLE PREPARATION

The titanium (99.9% purity) used as substrates for the film growth tests was supplied by the Koch-Light Laboratories Ltd. The manufacturers quoted the following known impurities to be present: iron, nitrogen, hydrogen and traces of carbon. Samples 12 mm by 27 mm were cut from 1.25 mm sheet. The samples were mechanically polished with abrasive papers (numbers 400-600) in running water and then polished with medium grade alumina on a cloth. During this process the samples were washed several times with water to ensure that particles removed from the surface of the samples could not cause further scratching of the surface. Gamma alumina on a cloth was used to complete the last polishing stage. Finally samples were cleaned in distilled water and in boiling isopropyl alcohol and dried by removing through the alcohol vapour.

OPTICAL CHARACTERISATION OF TITANIUM SUBSTRATES

The titanium substrates were examined optically prior to the growth of oxide films and were characterised by the instrument angle settings ψ and Δ as previously mentioned. The values were measured for light radiation of five wavelengths in the range 397.1 nm to 576.6 nm. Because of the wavelength spread the Beattie-Conn method was employed as opposed to the use of the compensator method. The values obtained are given in Table 4.1 together with the corresponding optical constants n and k for the clean substrate.

λ [nm]	Ψ degrees	Δ degrees	n_2	k_2
576.6	32.48	139.29	2.52	3.36
546.1	32.62	137.76	2.36	3.28
499.7	33.65	134.29	2.01	3.26
454.1	32.60	131.08	1.94	2.96

Table 4.1 Optical constants of titanium substrate:

Figure 4.1 shows plots of computed values of Ψ against n and Δ against n for values of k ranging from 3.22 to 3.28. Experimentally determined values of Ψ and Δ at a given wavelength for the surface of a clean titanium substrate are shown as horizontal lines. The points of intersection giving the same value of n and k are the values taken to characterise the substrate prior to oxide growth. Two methods were used to check the values of Ψ and Δ at 546.1 nm: by compensation and by that due to Beattie and Conn. For wavelengths other than 546.1 nm the latter method was adopted since a phase compensation plate would have been required for each wavelength if the former method had been adopted throughout.

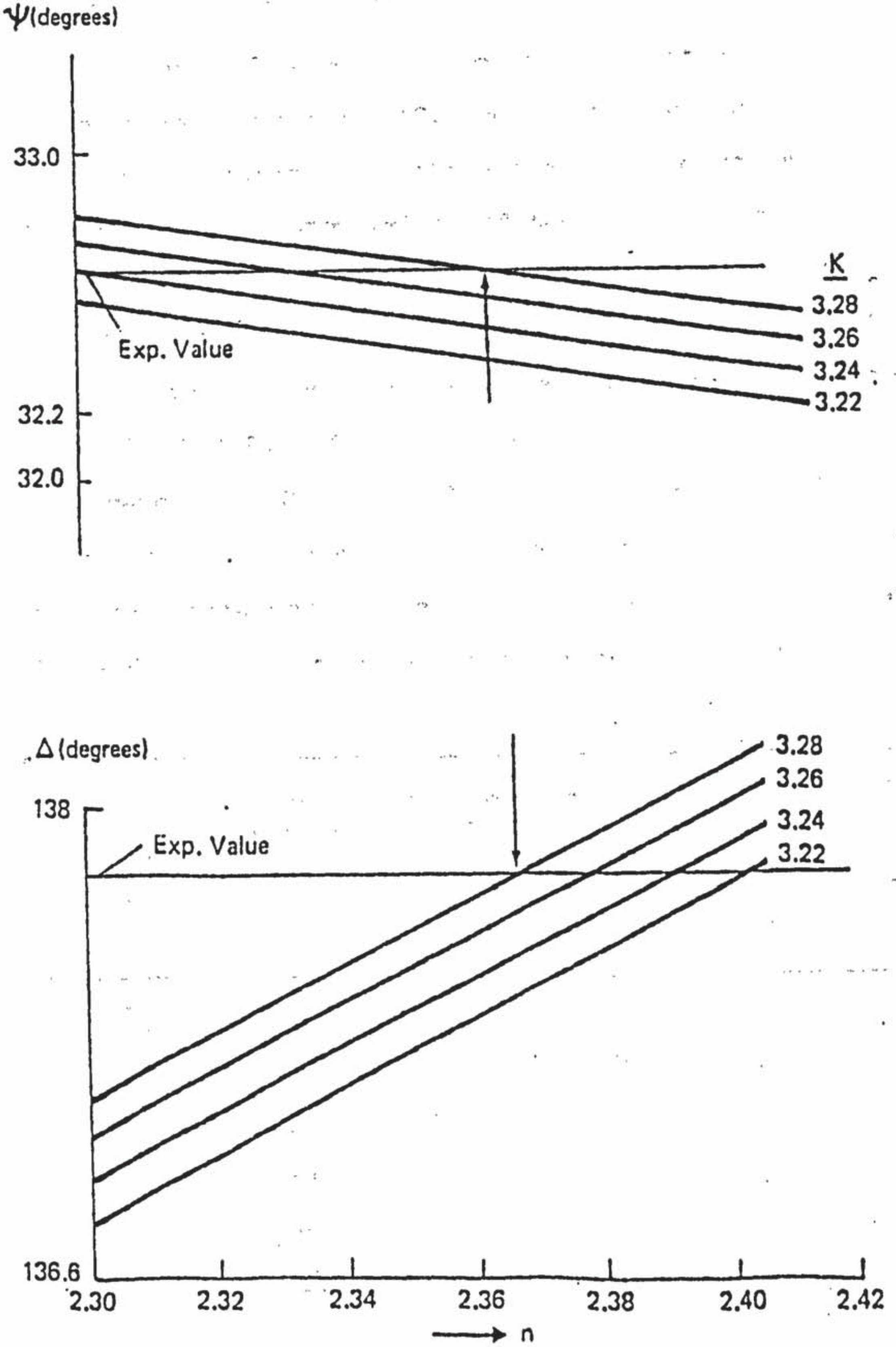

Figure 4.1 Angles ψ and Δ versus n for differing values of k

RESULTS OF OXIDE GROWTH EXPERIMENTS

Figure 4.2 shows an example of a plot of tan ψ against Δ at a wavelength of 546.1 nm for the growth of an oxide film on bulk titanium in the air at 750K at stages during the growth. Computed values of tan ψ and Δ are also shown for films of different thickness on a substrate with optical constants determined experimentally. In the example shown the computed values were generated using optical constants n = 2.40, k = 0.24 for the titanium oxide on a titanium substrate n = 2.36, k = 3.28 (from Figure 4.1). The values of n and k were determined as indicated above and the optical constants obtained at the various wavelengths are given in Table 4.2, together with substrate reflectances.

Wavelength nm	Optical constant of substrate (Ti)		Optical constant of titanium oxide film		Substrate reflectance
	n_2	k_2	n_1	k_1	%R
576.6	2.52	3.36	2.45	0.23	57.4
546.1	2.36	3.28	2.40	0.25	57.1
499.7	2.01	3.26	2.39	0.25	59.2
454.1	1.94	2.96	2.38	0.24	55.9
397.1	1.76	2.78	2.38	0.23	54.1

Table 4.2 The optical constant of titanium substrate, titanium oxide and the calculated reflectances

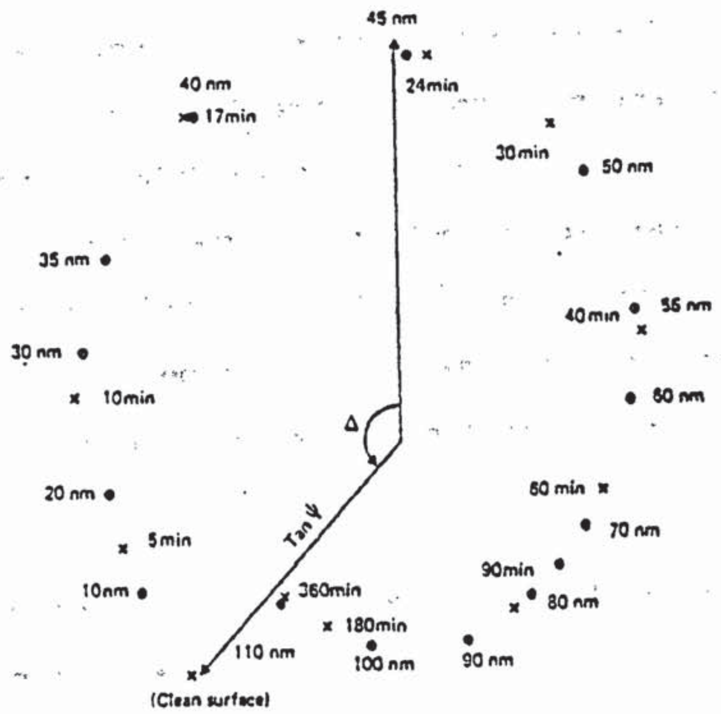

Figure 4.2 A plot of tan ψ versus Δ for (titanium oxide-titanium system)

× experimental values

. computed values for assumed optical constant of titanium oxide (2.40-0.24i) on titanium (2.36-3.28i)
ϕ = 63.8°, λ = 546.1 (nm)

The reflectance of the titanium oxide/titanium system was calculated from the expression as given by Heavens [1964] for an absorbing surface covered by an absorbing layer. Figures 4.3A and 4.3B show reflectance against wavelength for differing thickness of oxide on titanium and reflectances against oxide thickness for the two extreme wavelengths respectively. Table 4.3 shows the variation in ψ and Δ with time obtained at various wavelengths for oxide film grown at 750K and indicate the large changes observed at this temperature.

Figure 4.4 shows plots of the ellipsometer angle Δ against time at a wavelength of 546.1 nm for oxide growth on bulk titanium at different temperatures. In the cases of films grown at 420K, 490K and 560K the film thicknesses are small and $\delta\Delta$ is proportional to thickness. This assumption is not applicable when thick films are grown as has already been mentioned. A film thickness of 15 nm was produced in 30 minutes when the substrate temperature was maintained at 660K and in 5 minutes at 750K. The corresponding shift in Δ was in the region of 20 degrees of rotation on the analyser. At a given temperature the relationship between oxide thickness (t) and the time (T) followed a relationship as proposed by Vermilyea (1958) for the formation of oxide film on tantalum:

$$t = A + B \log T$$

where A and B are constants.

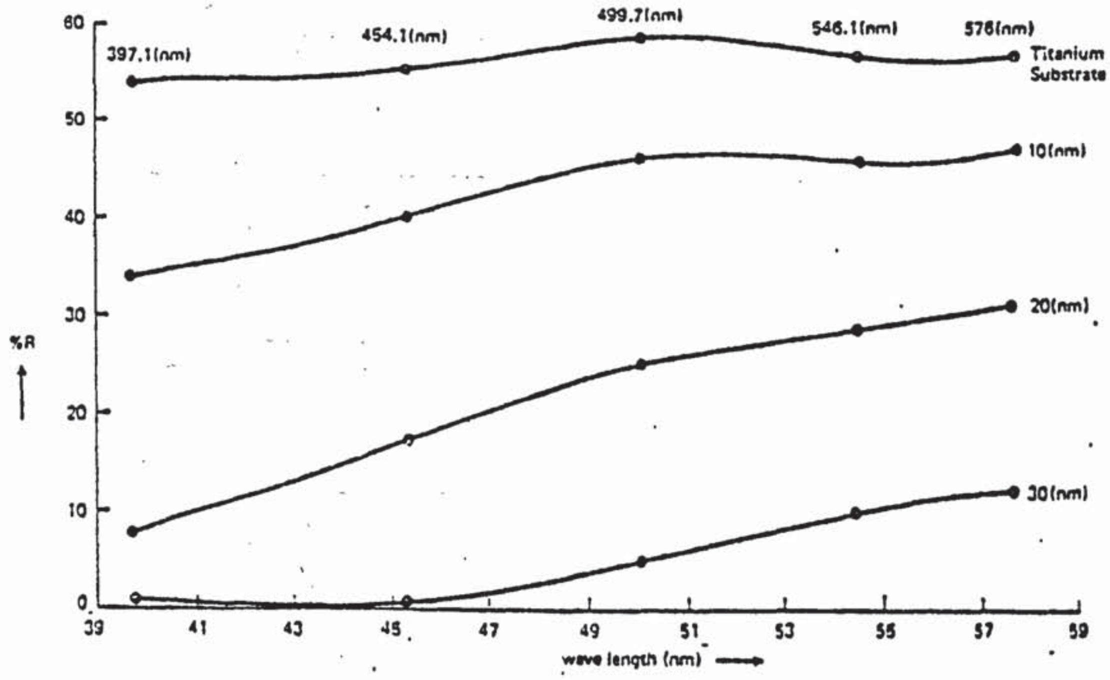

Figure 4.3A Reflectance against wavelength for differing thickness of titanium oxide on titanium

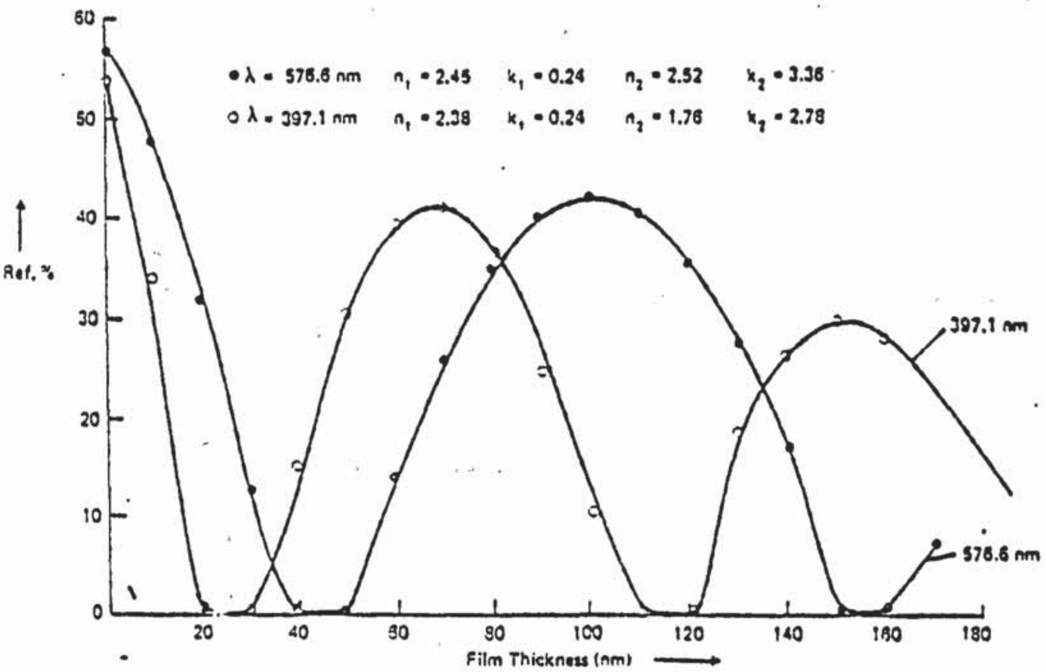

Figure 4.3B Reflectance curves for (titanium oxide-titanium) system

Time of oxidation (minutes)	λ = 576.6 nm		λ = 546.1 nm		λ = 499.7 nm		λ = 454.1 nm		λ = 397.1 nm	
	ψ ±.01 (Deg)	Δ±.01 (Deg)	ψ±.01 (Deg)	Δ±.01 (Deg)	ψ±.01 (Deg)	Δ±.01 (Deg)	ψ±.01 (Deg)	Δ±.01 (Deg)	ψ±.01 (Deg)	Δ±.01 (Deg)
0	32.48	139.29	32.62	137.76	33.65	134.29	32.60	131.08	32.46	127.34
5	31.74	111.69	31.38	110.19	32.61	100.16	31.38	89.0	32.62	76.14
10	31.80	87.3	32.22	81.76	34.22	75.99	37.23	53.88	37.6	46.34
15	37.6	59.1	36.5	53.76	39.35	55.49	40.36	26.58	39.69	18.14
17	37.95	39.2	37.66	31.7	42.30	27.99	40.7	12.58	41.35	359.04
24	40.03	3.19	39.01	355.24	41.9	344.89	40.03	333.08	36.13	321.3
30	37.6	339.13	36.13	335.76	39.35	322.69	32.62	312.08	30.95	297.84
40	31.38	303.09	28.8	295.76	30.54	287.79	27.92	281.58	27.47	267.54
60	24.70	263.19	23.27	257.7	23.75	249.59	21.8	241.88	23.37	231.04
90	22.09	220.79	22.29	214.0	22.78	207.89	22.29	200.1	22.78	191.54
180	22.78	158.60	21.80	157.66	22.29	140.29	21.31	131.58	20.81	128.74
360	23.27	145.8	21.8	143.0	-	-	-	-	-	-

Table 4.3 The variation of ψ and Δ with the time for oxide films grown at 750 K.

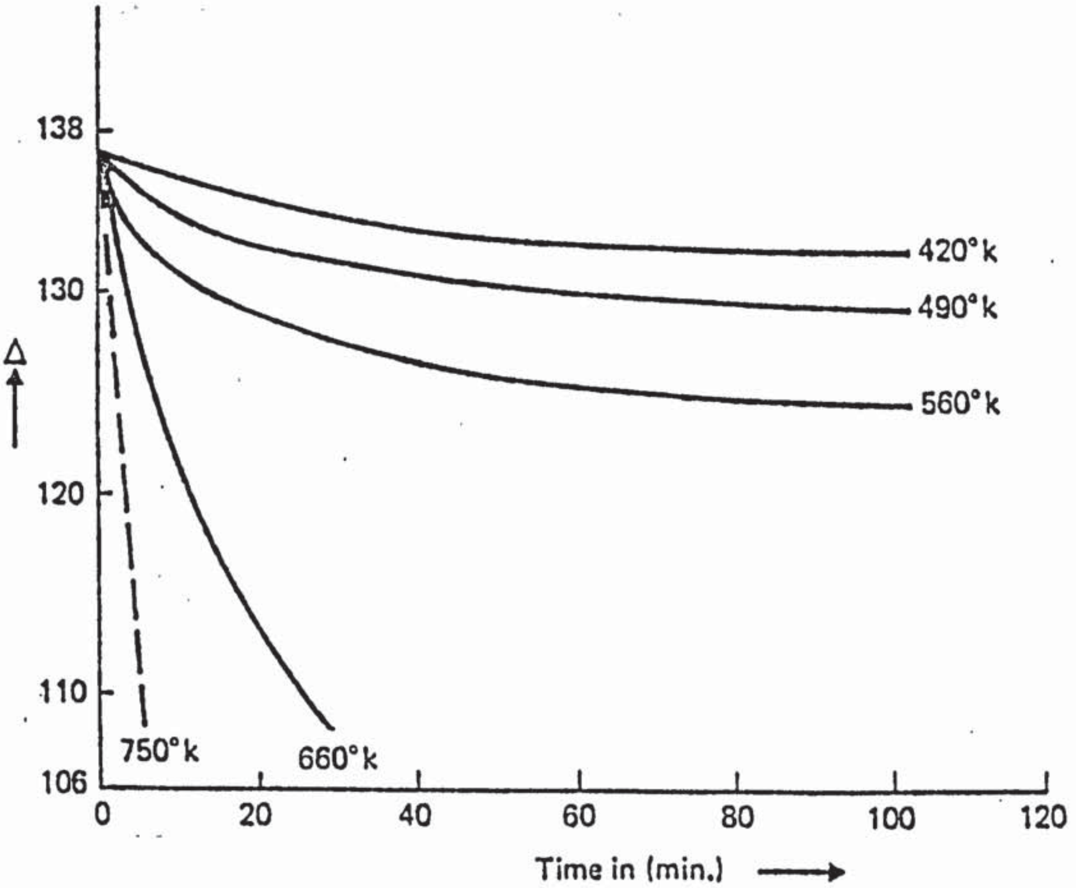

Figure 4.4 Δ against time during oxidation of bulk titanium in air at various temperatures for λ = 546.1 nm

4.1.2 REFLECTANCE RESULTS

Thermal oxidation in air of bulk titanium produced a range of coloured interference films. The surface first appeared yellow, gold, purple, dark blue, bright light blue and dull light grey. These coloured films were produced at a temperature of 750K and the colours could be produced at other furnace temperatures. Investigation of oxidation at high temperatures (for example 1198 Kelvin) has been attempted, but the rate of oxidation was too rapid to be effectively controlled.

The room temperature reflectance curves for bulk titanium thermally oxidised at a temperature of 750 Kelvin are displayed in Figure (4.5).

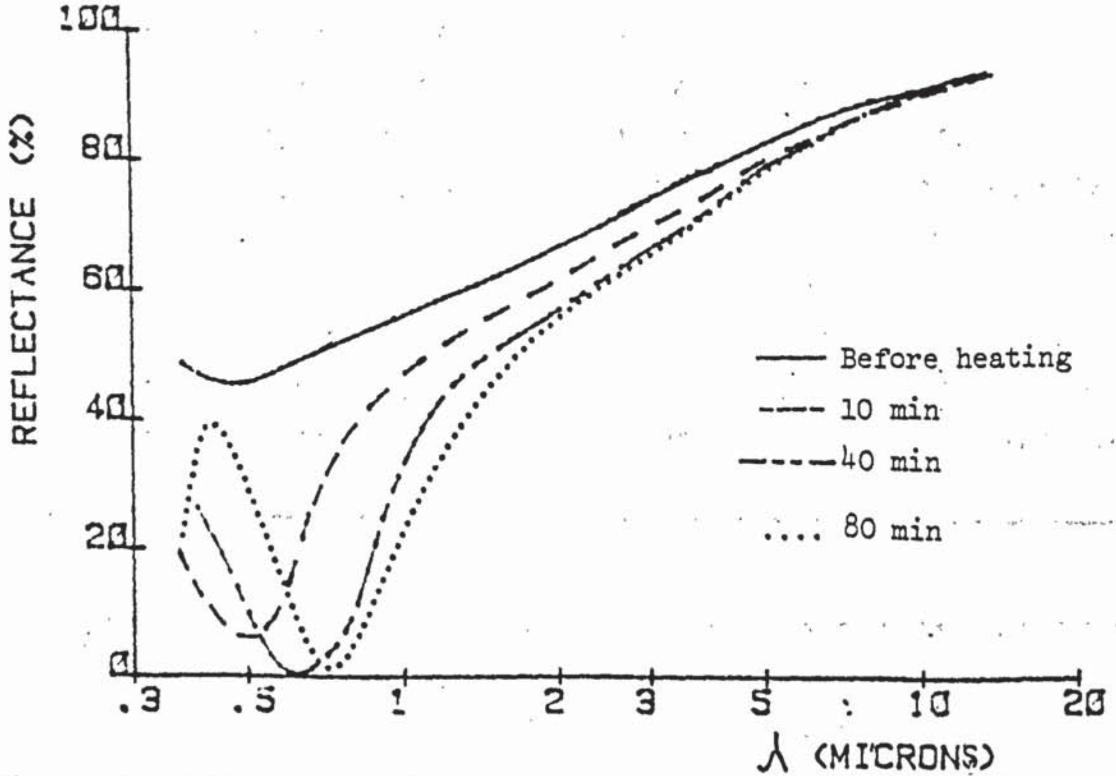

Fig. 4.5 Specular reflectance versus wavelengths for polished titanium and after heat treating in air at temperature 750 K.

The reflectances for wavelengths longer than 8μm are the same and approach the reflectance of a polished bulk titanium. During heating at 750 Kelvin, the shift of the reflectance showed the same pattern for the sample at different sintering times, but it causes the fringes to shift towards longer wavelengths with increased time of heating, i.e. increasing the oxide thickness.

The values for solar absorptance, $\underline{a}$, and the thermal emittance, $\underline{e}$(t) at temperatures of 25°C, 100°C, 150°C, 200°C, 250°C and 300°C were obtained and the results are shown in Table 4.4.

Heating time min.	Absorptance $\underline{a}$ %	Emittance %						Colour
		$\underline{e}$ (25°C)	$\underline{e}$ (100°C)	$\underline{e}$ (150°C)	$\underline{e}$ (200°C)	$\underline{e}$ (250°C)	$\underline{e}$ (300°C)	
0	46.79	6.06	7.52	8.25	9.23	10.34	11.15	silver
5	54.23	7.1	8.52	9.40	10.64	11.72	13.1	yellow
10	67.3	8.01	9.78	10.56	11.74	13.11	14.04	gold
15	76.3	8.84	10.73	11.45	12.83	14.17	15.34	purple
25	77.0	9.71	11.70	12.92	14.17	15.43	16.56	dark blue
40	79.0	10.41	12.49	13.59	14.86	16.37	17.31	dark blue
80	77.5	11.37	13.04	14.13	15.47	16.48	17.76	dark blue
180	78.0	13.03	14.71	15.84	16.79	18.04	19.37	light blue
234	77.7	13.03	14.71	15.84	16.79	18.04	19.37	dull grey

Table 4.4 Optical properties of titanium and titanium oxide for various heating times at a temperature of 750 degrees Kelvin

4.2 TITANIUM OXIDE/ALUMINIUM

In this part of the work, aluminium has been used as the underlayer material instead of titanium. The samples were prepared by vacuum evaporation of pure titanium (99.97%) on an anodized aluminium plate (polished, supplied by Alcan). The thickness of the deposits of titanium was altered by the mass evaporated from 0.055 gm to 0.09 gm with a source-substrate separation of 24.5 cm under a pressure of 4×10^{-5} Torr.

The spectral reflectivity was determined before and after heat treatment for different periods of time at 670° Kelvin in air and the results are shown in Figure 4.6.

Figure 4.7 shows the reflectance spectra during oxidation of the deposited titanium film on a previously heated aluminium substrate in air for three hours at 670° Kelvin.

Table 4.5 displays the calculated values of the absorptance, $\underline{a}$, and the emittance, $\underline{e}(t)$, at temperatures of 100°C, 150°C, 200°C and 300°C for the samples corresponding to 0.055 gm and 0.09 gm respectively.

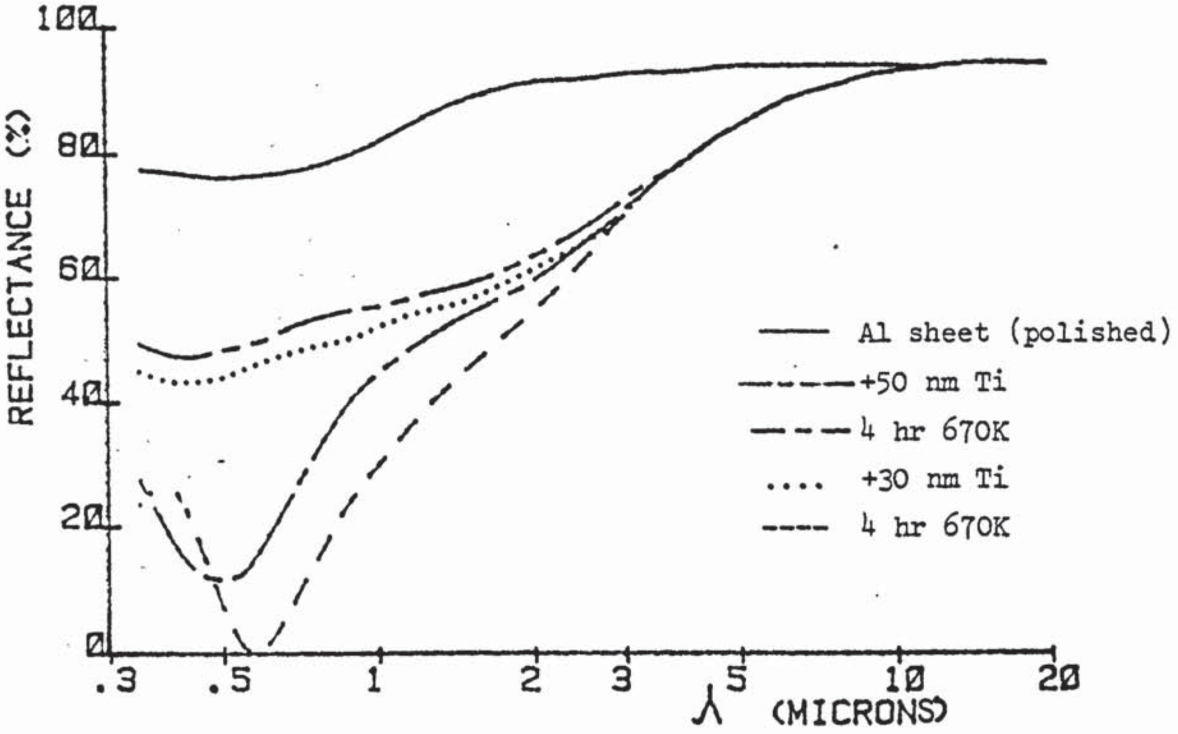

Fig. 4.6 Specular reflectance versus wavelength for titanium film deposited on aluminium sheet and after heat treating in air.

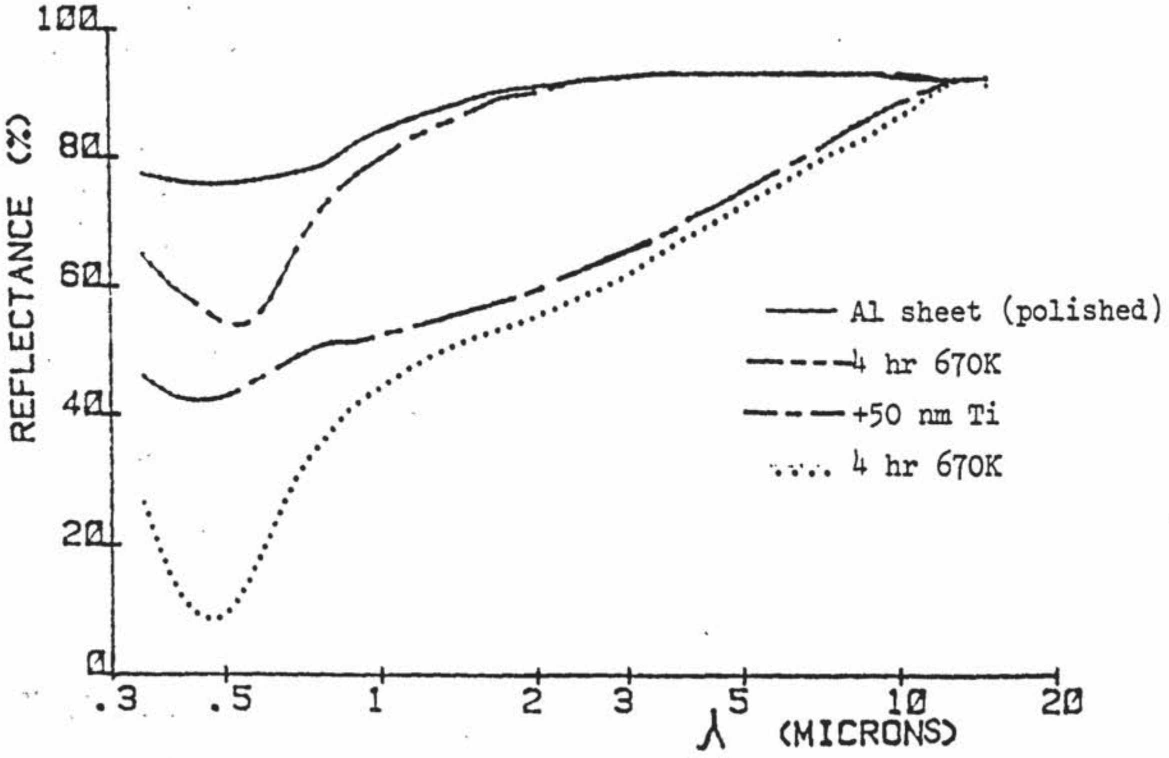

Fig. 4.7 Specular reflectance versus wavelength for titanium film deposited on heated aluminium sheet and after heat treating in air.

Sample treatment	Absorptance $\underline{a}$ %	Emittance %				
		$\underline{e}$ (100°C)	$\underline{e}$ (150°C)	$\underline{e}$ (200°C)	$\underline{e}$ (300°C)	Colour
Al-sheet (polished) supplied by Alcan	21.0					silver
+ 55 mg Ti	50.0	8.31	9.27	10.48	12.76	
Heated 4 hr (670 K)	80.0	8.42	9.64	10.8	12.96	dark blue
Al-sheet (polished) plus 90mg Ti	47 .0	10.99	12.90	14.06	15.27	
Heated 4 hr (670K)	68.6	12.99	14.09	15.96	17.41	dark blue
+ heated 1 hr (670K)	70.6	13.40	14.4	15.5	15.13	blue
+ heated 1 hr (670K)	72.3	14.4	16.66	19.23	19.23	indigo colour
Al-sheet (polished) heated 3 hr (670K) plus 90 mg Ti	51.0	14.38	15.81	17.34	20.71	
Heated 4 hr (670K)	70.0	16.38	17.99	19.28	21.88	goldish brown
+ heated 1 hr (670K)	70.0	16.99	18.57	20.12	22.98	dark violet

Table 4.5 Optical properties of thermally oxide titanium film on unheated and heated aluminium sheet at various testing times at a temperature of 670 Kelvin

4.3 CHEMICALLY COLOURED STAINLESS STEEL (INCO SURFACES)

Among surface treatment techniques now in practical use, the chemical conversion reaction method has been utilized for a long time because of its simplicity and suitability from mass treatment. Previously, the colouring of steel was intended for decorative purposes. The fabrication of solar absorber coatings on stainless steel substrates has recently received wide spread study. Edwards et al (1962) reported selective finishes on stainless steel formed by both chemical oxidation using Ebanol salts and thermal oxidation in air at elevated temperatures. Evans et al (1973) have reported a process of colouring stainless steel by immersion in a hot mixture of chromium and sulphuric acid. The film has excellent adhesion, abrasion resistance and selectivity properties. The thickness of oxide film increases in proportion to the duration of immersion and various colours appear as the thickness changes.

Five samples of different colour on 304 stainless steel were obtained directly from International Nickel Company (INCO) for the present observations. These samples are referred to as 1.5 mV, 3 mV, 5 mV, 7 mV and 9 mV samples and were produced by the above process. The voltage relates to the preparation conditions. A higher voltage gives increased layer thickness and such a range of colours is achieved.

We report here a study of the following colours, brown, violet, blue, light grey and dark grey corresponding to 1.5 mV, 3 mV, 5 mV, 7 mV and 9 mV respectively. The room temperature specular reflectance of the above samples were measured over a wavelength range 0.35 μm to 15 μm. Absorptance and the emittance values were calculated for every sample. The effect of temperature ageing in air and in a vacuum was also investigated by calculating the absorptance and emittance before and after heating.

It was possible to stabilize the sample corresponding to 5 mV and to increase the absorptance of the 1.5 mV and 3 mV samples and to stabilize them at higher temperature by coating the samples with a thin film of Si_3N_4.

Ellipsometer studies have also been carried out on the various INCO prepared samples of stainless steel.

The composition of unheated samples corresponding to 5 mV and 9 mV was measured by Auger Analysis.

4.3.1 ELLIPSOMETER RESULTS

INCO SURFACES (COLOURED STAINLESS STEEL)

Measurements were made by an ellipsometer on the uncoated (polished) stainless steel 304 type and on five different coloured surfaces corresponding to 1.5 mV, 3 mV, 5 mV, 7 mV and 9 mV. The above surfaces were obtained from INCO, Birmingham, England in a sheet form. Samples measuring 25 x 25 mm were used in both the ellipsometry and reflectance measurements, and were cut from the same sheet.

OPTICAL CHARACTERISATION OF 304 STAINLESS STEEL*

This type of stainless steel was supplied in the form of polished, specular sheet 0.93 mm thick. The sample to be investigated was cleaned in distilled water and boiling isopropyl alcohol and dried by removing through the alcohol vapour.

The sample was characterised by the ellipsometer angle settings ψ and Δ as previously mentioned. The values were measured for one radiation wavelength of 546.1 nm. The

---

* The base material for the coloured oxide INCO finishes was 304 stainless steel.
This contained the following elements with the corresponding percentage of composition.
17.8% Cr, 8.7% Ni, 0.08% C, 0.52% SI, 1.29% Mn, 0.56% Mo, less than 0.05% Ti, the remainder being Fe.

compensator method was used in this series of experimental studies. The values obtained for the angles ψ and Δ are 35.57 degrees and 138.43 degrees. Since the stainless steel surfaces which have not received heat treatment contain chromium oxide, the published figures, Hill and Weaver (1958) for the optical constants of chromium oxide ($n = 2.42$, $k = 0$), together with the above measurements for the substrate, were used to compute $\delta\Delta$ and $\delta\psi$ for various oxide thicknesses up to 5 nm. This approach was adopted for stainless steel by Fane et al (1973). Calculations show that in such a case the computed thickness of oxide on the supplied sample could be $\sim$ 30 nm corresponding to $\Delta = 138.43$ and $\psi = 35.57$, and $\Delta = 144.03$ and $\psi = 35.41$ corresponding to zero thickness of chromium oxide. By using these values for the substrate surface, together with equation (3.13) and equation (3.14), the optical constants n_2 and k_2 of the substrate were found to be 2.28 and 3.70 respectively.

RESULTS OF THE FIVE COLOURED SURFACES OF 304 STAINLESS STEEL (INCO)

The measurement of ψ and Δ for the five coloured stainless steel corresponding to 1.5 mV, 3 mV, 5 mV, 7 mV and 9 mV were obtained before and after heat treatments and are shown in Table 4.6, for one light radiation of wavelength 546.1 nm. Figure 4.8 shows plots of ψ and Δ for the above samples before and after heat treatments. The figure 4.8 indicates that the 5 mV sample has the lowest values of ψ and

Δ . It keeps this property up to heating for 192 hours at 210°C and for 160 minutes at 300°C. However, the Δ values of all the above samples decreased. After heating to 300°C for 192 hours, only the Δ values of 5 mV sample increased by ~80 degrees and the sample corresponding to 3 mV has the lowest values of Ψ and Δ .

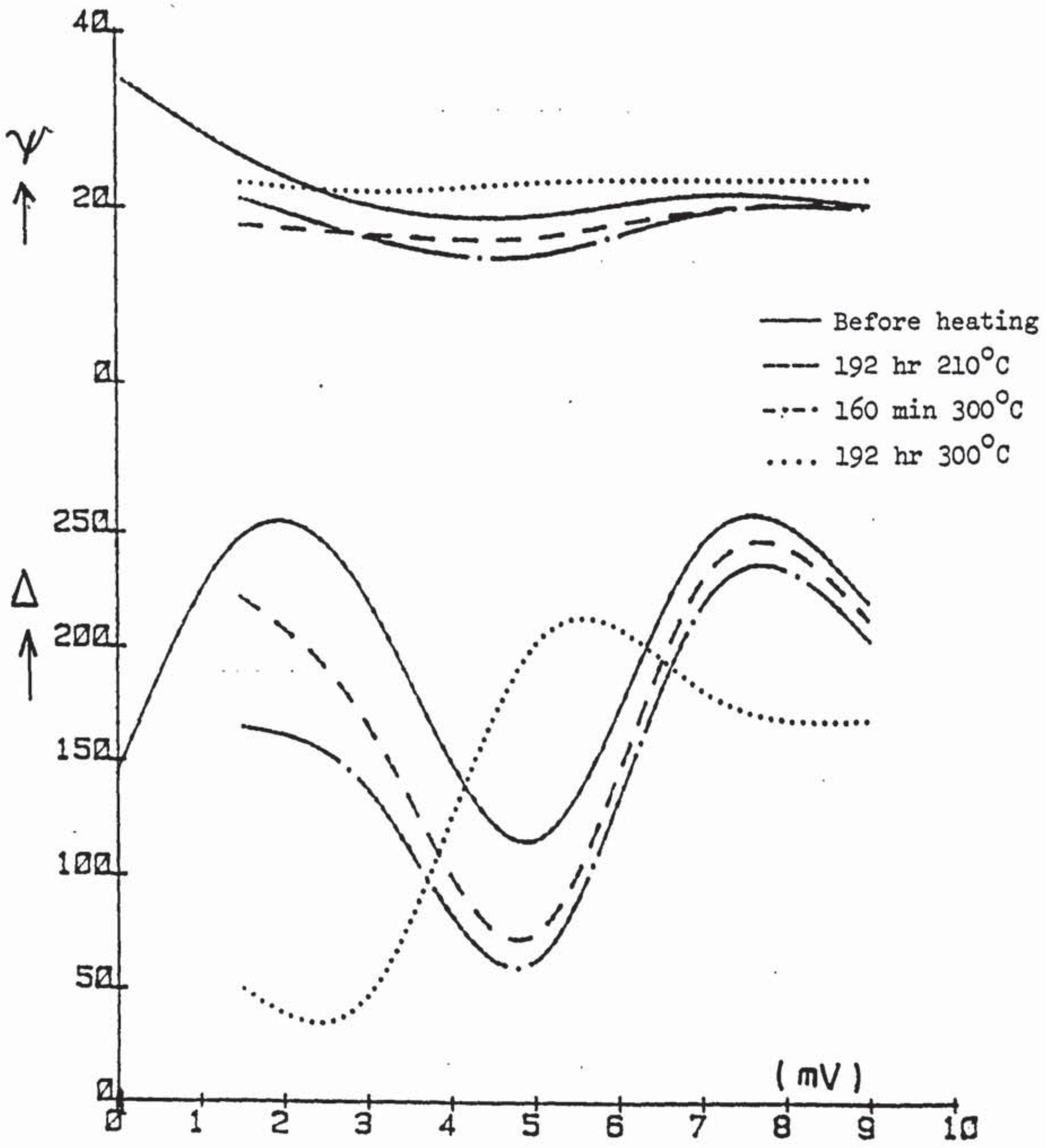

Fig. 4.8 Plots of Ψ and Δ for the 1.5, 3, 5, 7 and 9 mV samples and after heat treating in air.

λ = 546.1 nm ø = 61.22 deg	The base material is 304 stainless steel			ψ = 35.1° Δ = 143.68°			n_2 = 2.28 k_2 = 3.70			
INCO samples	1.5 mV		3 mV		5 mV		7 mV		9 mV	
	ψ degrees	Δ degrees	ψ degrees	Δ degrees	ψ degrees	Δ degrees	ψ degrees	Δ degrees	ψ degrees	Δ degrees
unheated	26.01	247.88	20.98	221.89	19.0	114.89	21.38	244.31	20.18	219.41
heated 192 hr. (210°C)	17.99	221.91	16.85	167.11	16.53	74.57	19.65	228.05	20.18	212.16
heated 160 min (300°C)	21.11	161.95	16.53	133.77	14.45	60.11	19.32	214.75	19.76	199.52
heated 192 hr. (300°C)	22.91	46.97	21.73	44.70	22.78	197.54	23.11	177.84	23.11	165.19

Table 4.6 Experimental values of the two angles ψ and Δ for the five coloured INCO surfaces. [Base material 2.28 - 3.7i].

4.3.2 REFLECTANCE RESULTS

The room temperature specular reflectance (R.T.S.R.) was measured for the five different coloured samples and the uncoated one over a wavelength range extending from 0.35 μm to 15 μm. The results are shown in Figure 4.9.

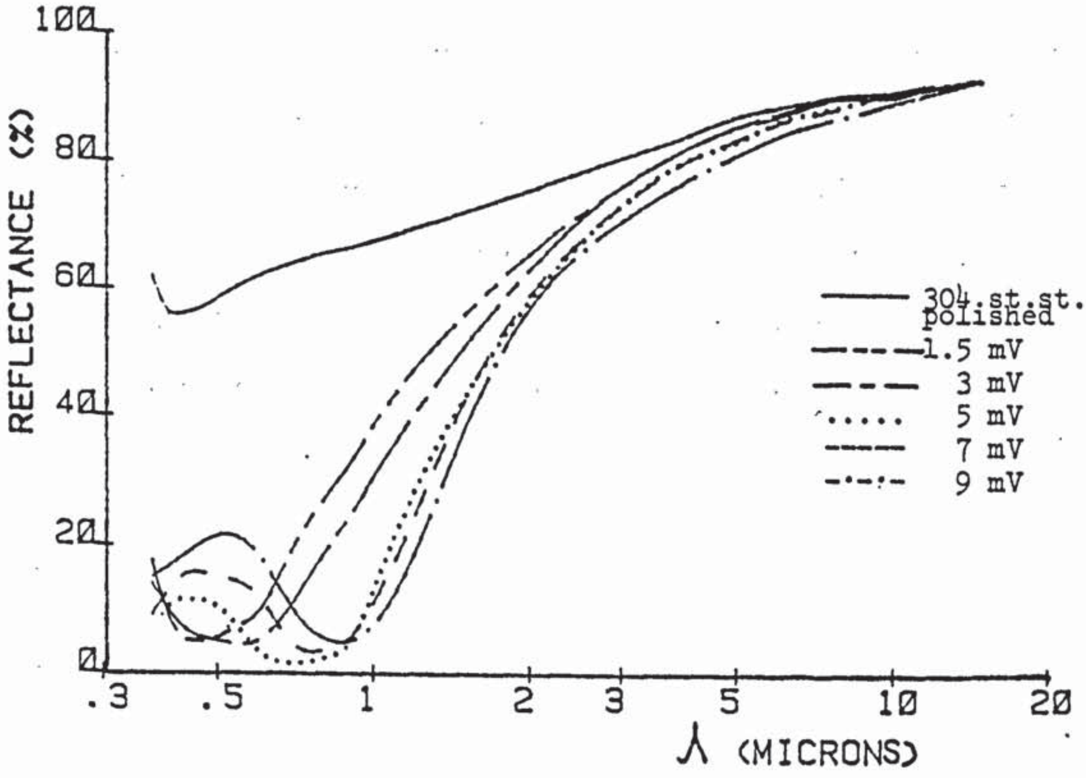

Fig. 4.9 Specular reflectance versus wavelength for polished 304 stainless steel and INCO samples.

This figure shows that the sample corresponding to 5 mV (blue in colour) is of the most favourable optical properties; it shows the lowest reflectance in the solar region, although the interference fringes look similar (gently wavey) for all the five samples in the above region. The reflectance for wavelengths longer than 8 μm is the same for the five samples and shows the same reflectance as for a polished (uncoated) sample of 304 stainless steel. This figure shows that clearly and in all different coloured samples, there is a major step from low to high reflectance in the wavelength 1 - 5 μm.

Values of the absorptance, a, and the emittance, e, for the uncoated and the five different coloured samples were determined, the emittance was calculated at 100°C, 200°C and 300°C. These data are tabulated in Table 4.7. Figure 4.10 illustrates the plots of the absorptance of the INCO surfaces (unheated). This figure suggests the blue colour sample, corresponding to 5 mV, had the highest absorptivity.

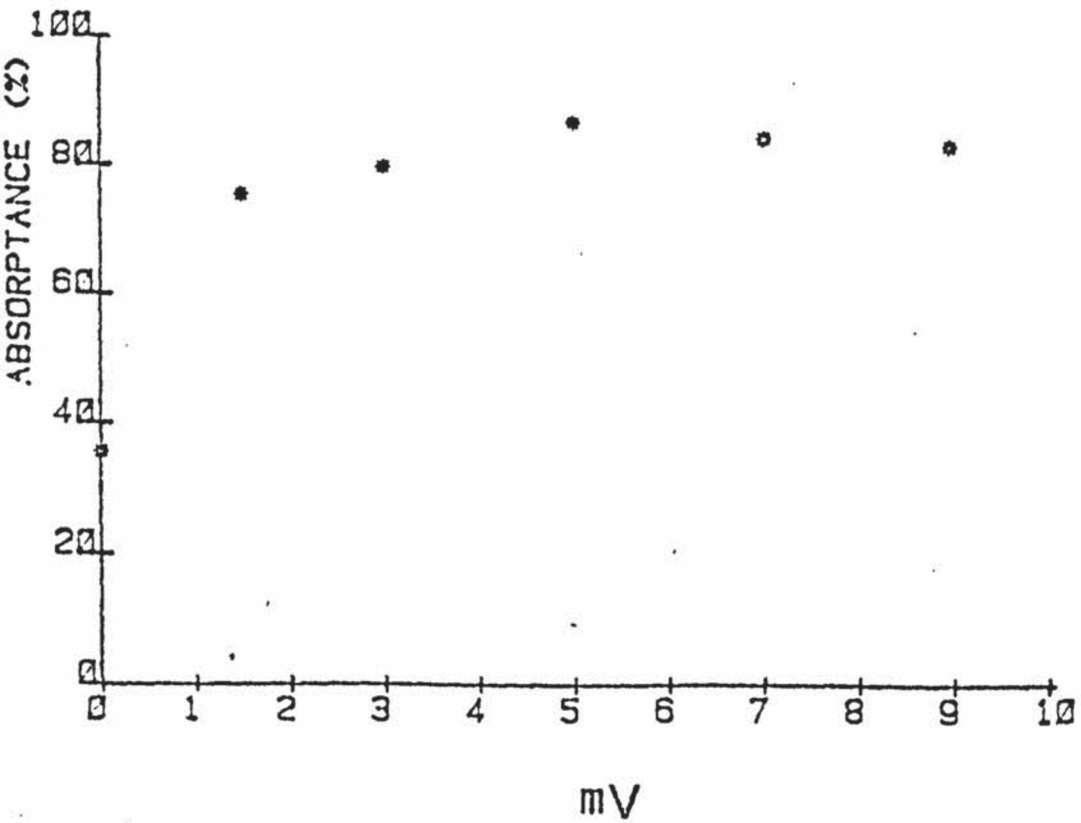

Fig. 4.10 A plot of absorptance for the INCO samples corresponding to 0, 1.5,3,5,7 and 9 mV process.

4.3.3 ABSORPTANCE VERSUS THE OFF-AXIS ANGLE

To investigate the dependence of the absorptance of the above surfaces on the angle of incidence, the spectral hemispherical directional reflectance of two different coloured samples 1.5 mV and 5 mV) have been measured as a function of the off-axis angle up to 50 degrees. Then the absorptances have been determined and are recorded in Table 4.8.

Figure 4.11 shows the plots of a-values versus the off-axis angle.

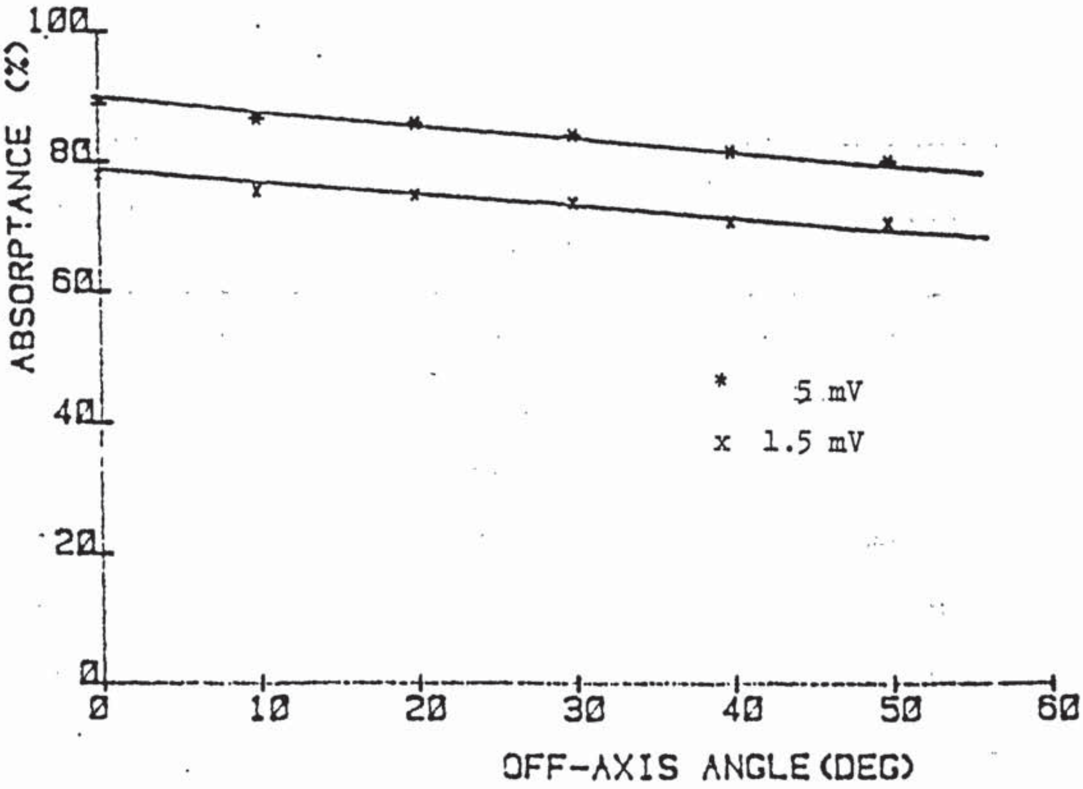

Fig. 4.11 Absorptance versus the off-axis angle for 1.5 mV and 5 mV samples

Sample	Absorptance a%	Emittance %		
		e(100°C)	e(200°C)	e(300°C)
uncoated 304 s.s.	35.00	9.1	10.0	11.3
1.5 mV	74.90	9.8	11.1	12.40
3 mV	79.60	10.10	11.10	12.60
5 mV	86.50	10.10	11.10	13.50
7 mV	83.90	10.10	11.30	13.40
9 mV	82.30	10.65	11.50	13.40

Table 4.7 Optical properties of INCO surfaces (unheated)

Off-axis angle (degrees)	Absorptance %	
	1.5 mV	5 mV
10	77.9	88.9
15	75.5	86.8
20	74.8	86.0
30	73.4	84.0
40	70.7	81.5
50	70.5	80.0

Table 4.8 The absorptance as a function of the off-axis angle for the 1.5 mV and 5 mV samples

4.3.4 LIFE TESTING

(i) CONTINUOUS ANNEALING IN AIR

The INCO coated coloured stainless steel surfaces have been annealed in air at temperatures between 110°C - 300°C, by using a Lindberg Oven, Figure 3.15. The temperature stability was tested by subjecting one set of samples (1.5 mV - 9 mV) to successively increasing temperatures. Figures 4.12 to 4.16 show the results of the above tests. Figure 4.17 shows the reflectance spectra of 5 mV sample before and after heating for 60, 160 minutes and 192 hours at 300°C. The values of the absorptance, $\bar{\underline{a}}$, and the emittance, $\underline{e}$(100°C, 200°C and 300°C) are determined for each test and recorded in Table 4.9.

(ii) CYCLING ANNEALING IN AIR

Three sets of INCO samples were processed. The first two cycled for 48 hours at the rate of 4 cycles/hr between 50°C and 110°C in one case and 50°C and 210°C in the other and the third for 192 hours at the rate of 2 cycles/hr between 50°C and 210°C. Figures 4.18 to 4.22 show the above test.

(iii) ANNEALING IN SOFT VACUUM (0.1 Torr)

A set of 1.5 mV to 9 mV samples has been annealed in a soft vacuum (0.1 Torr) at 300°C for 96 hours. The values of the absorptance and emittance are calculated and recorded in Table 4.9. E.g., the reflectance spectrum for 5 mV sample is shown in Fig.4.23. The cycling tests and of the soft vacuum have been carried out using the life cycling furnaces Figure 3.16.

4.3.5 STABILIZATION OF INCO SURFACES BY Si_3N_4

Carver et al [1978] have proposed and successfully used Chemical Vapour Deposition [CVD] method to passivate molybdenum oxidation by coating the surface with a film of either $Cr_2O_3.SiO_2$ or Si_3N_4.

It was decided to cover INCO coloured stainless steel samples with Si_3N_4. The first attempt was to coat them such that the first fringe was located ~ 2-3 μm. The thickness of Si_3N_4 film was 250 nm.

The results of the specular reflectance at room temperature were plotted in curves 4.24 to 4.28. The values of the absorptance and the emittance for the above test are also recorded in Table 4.9.

The successful attempt was one in which the first fringe was located ~ 0.9 - 1.8 μm. This was with a film of 125 nm thickness of Si_3N_4. The reflectance spectrum of this attempt is illustrated in the above figures. The values of absorptance and emittance of the samples after coating with 125 nm thickness of Si_3N_4 are recorded in Table 4.9.

The coated samples with 125 nm thickness of Si_3N_4 were annealed in air for 192 hours at 250°C, and for 3½ hours at 300°C. The calculated values of the absorptance and the emittance are also tabulated in Table 4.9.

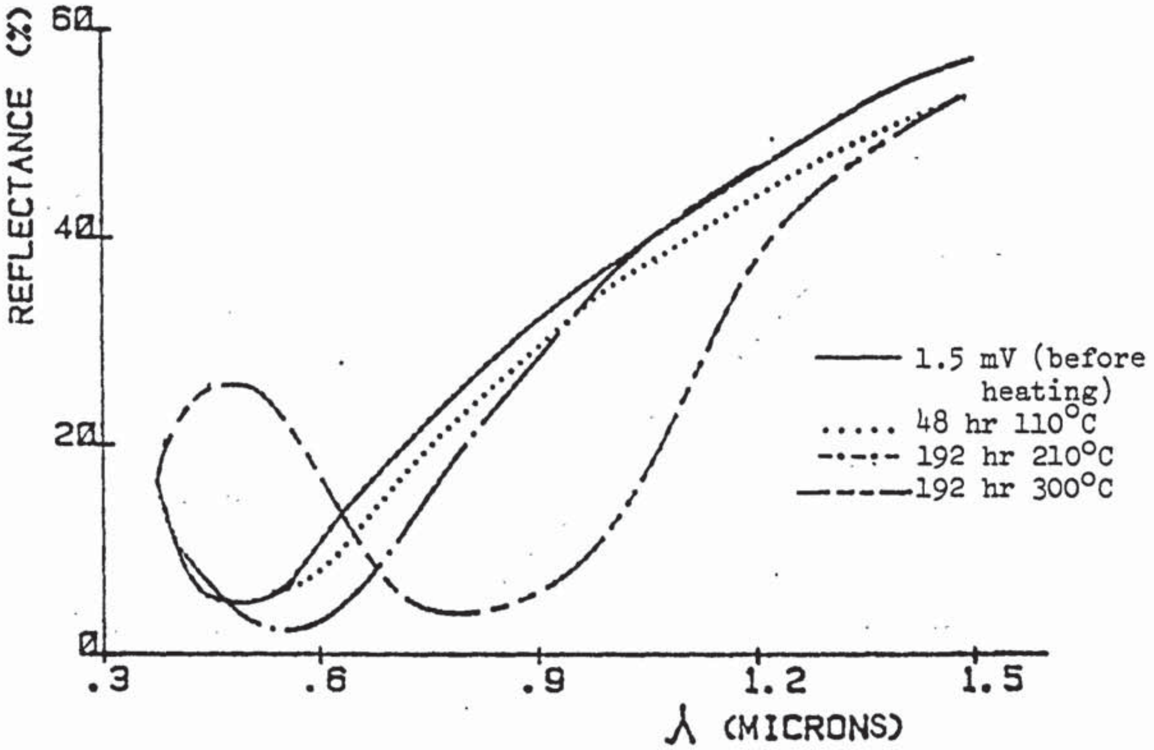

Figure 4.12 Specular reflectance versus wavelength of 1.5 mV sample and after heat treating in air.

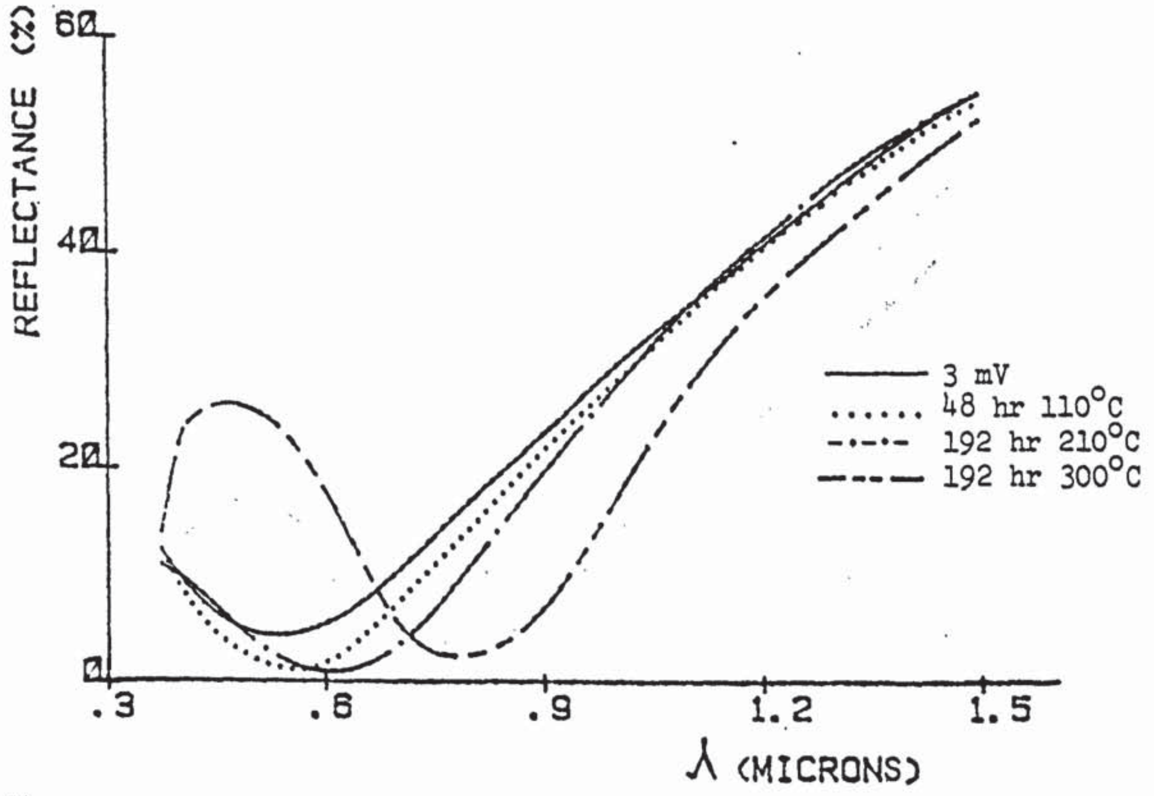

Figure 4.13 Specular reflectance versus wavelength for 3 mV sample and after heat treating in air.

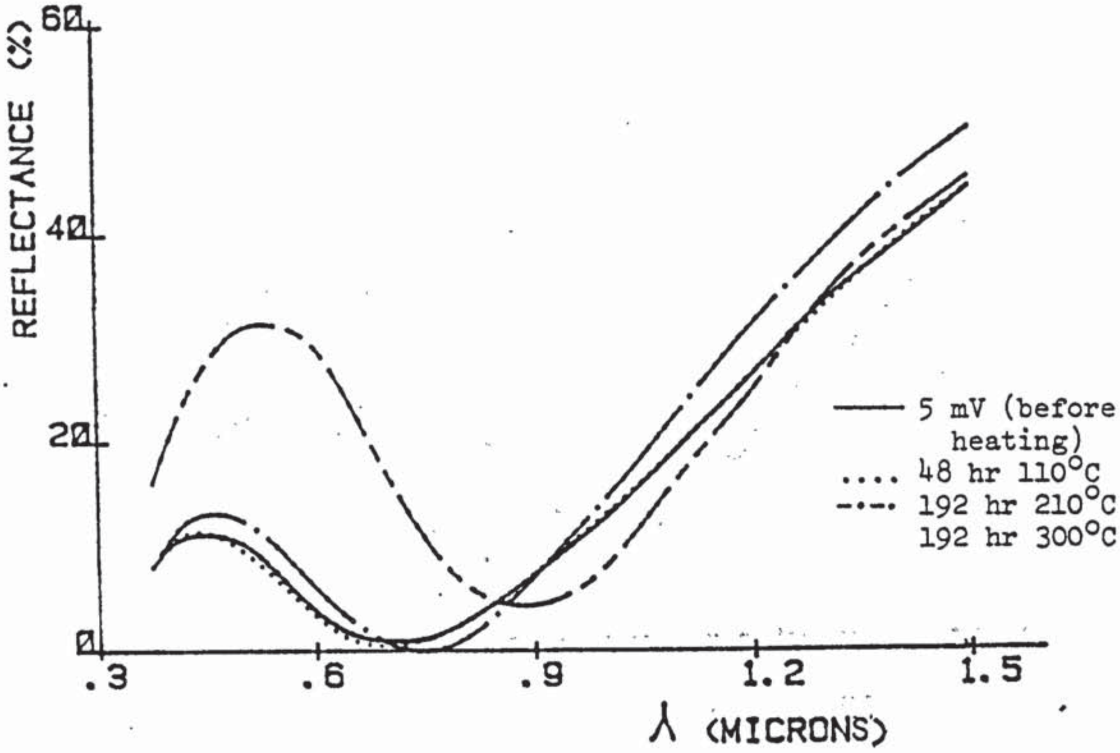

Fig. 4.14 Specular reflectance versus wavelength for 5 mV sample and after heat treating in air.

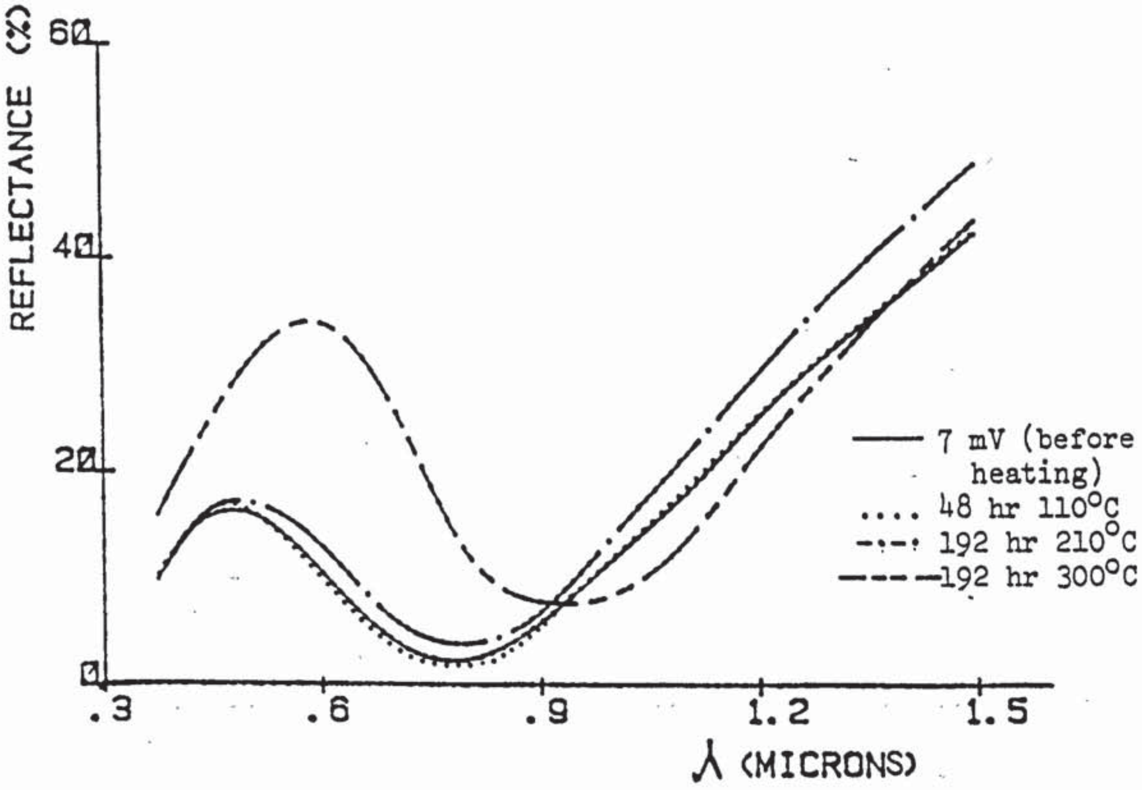

Fig. 4.15 Specular reflectance versus wavelength for 7 mV sample and after heat treating in air.

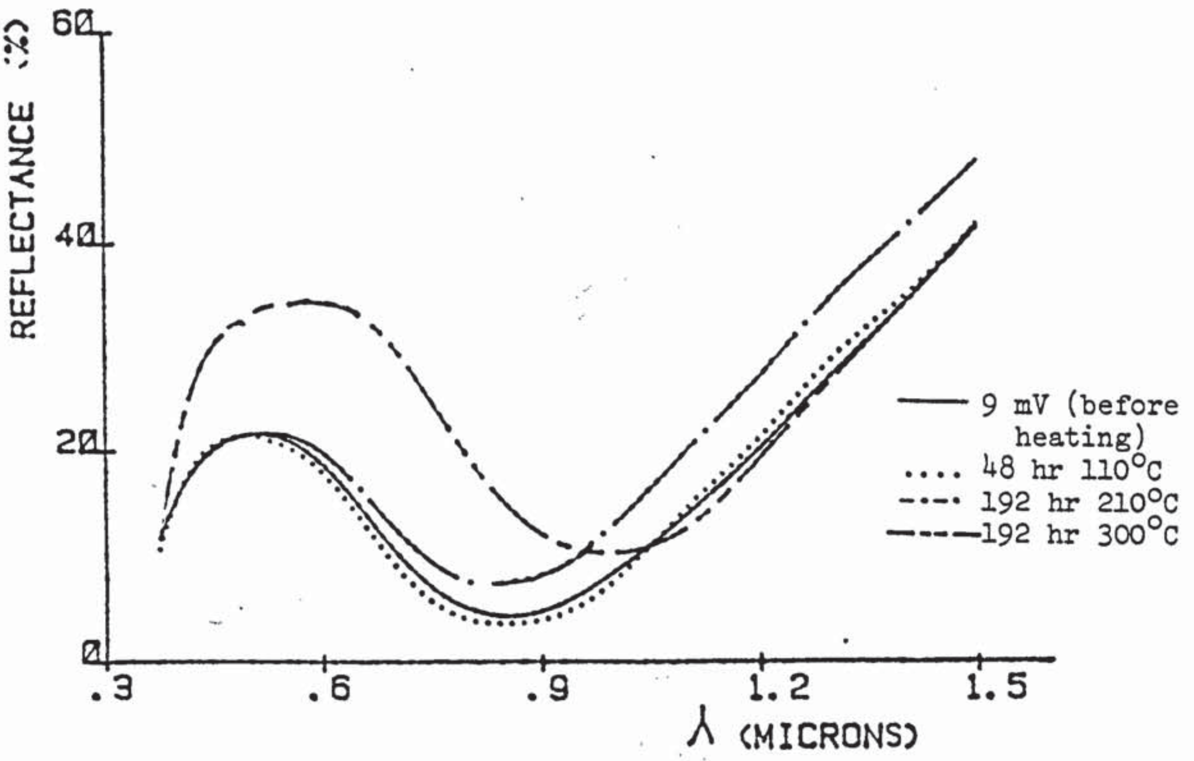

Fig. 4.16 Specular reflectance versus wavelength for 9 mV sample during annealing in air.

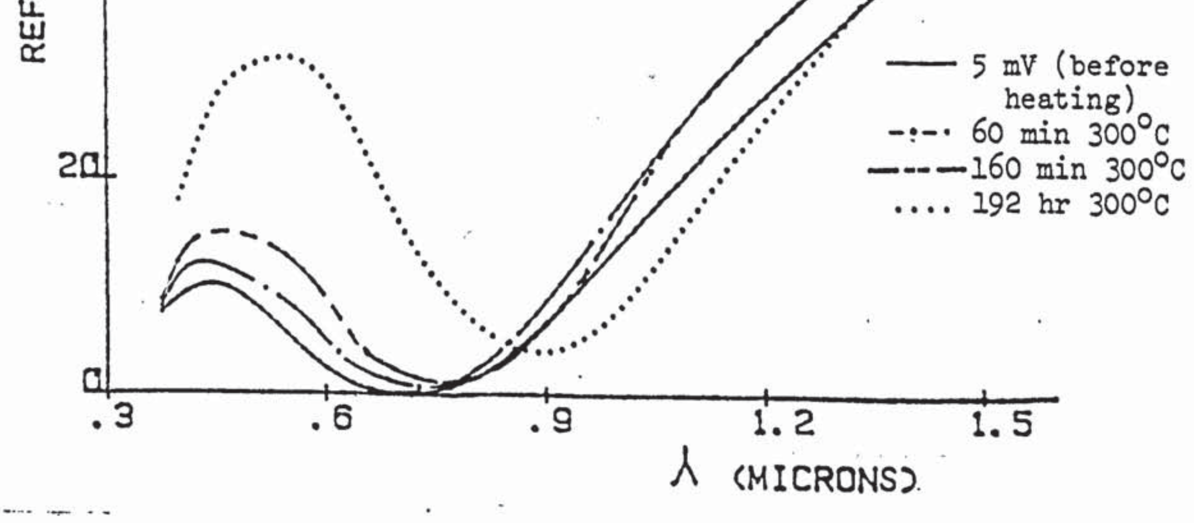

Fig. 4.17 Specular reflectance versus wavelength for 5 mV sample during annealing in air.

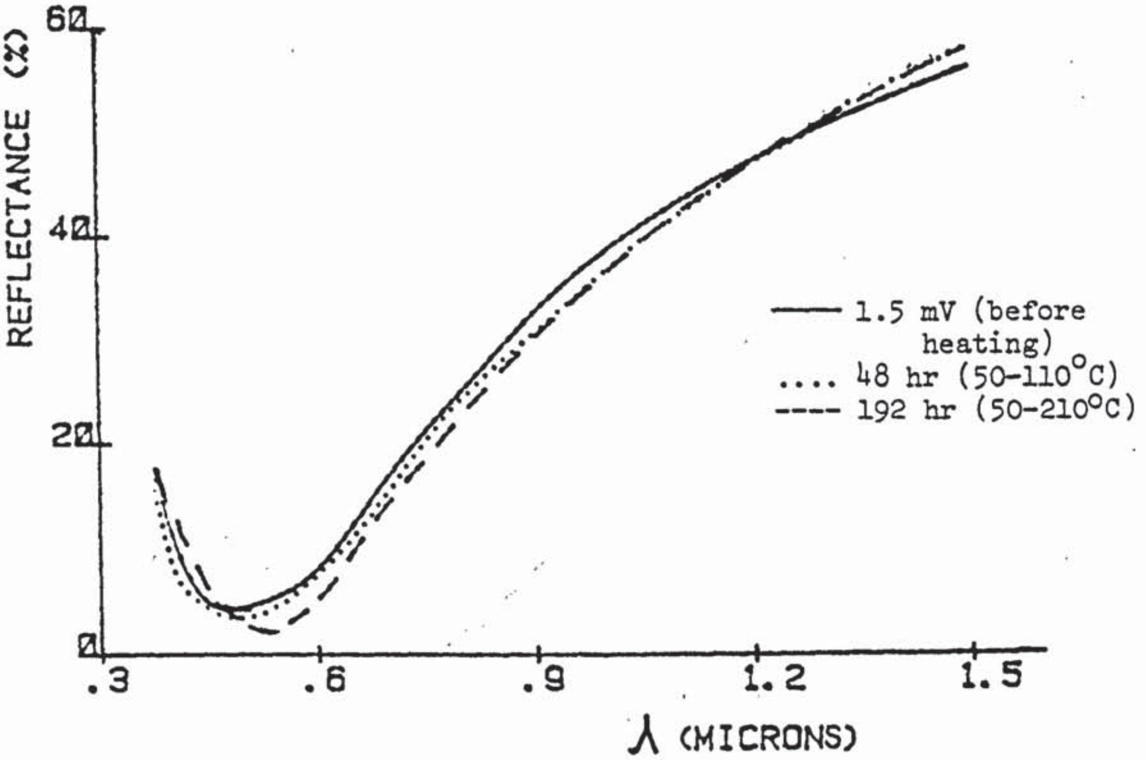

Fig. 4.18 Spectral hemispherical reflectance for 1.5 mV sample and after cycling in air.

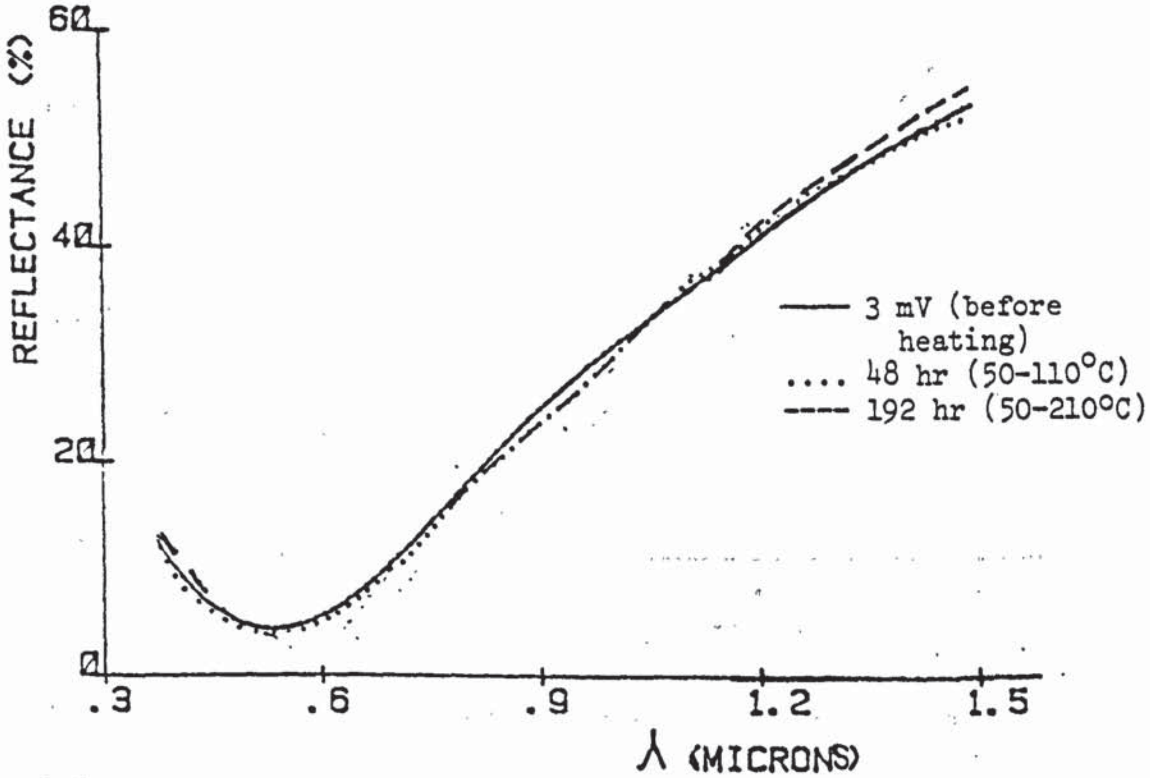

Fig. 4.19 Spectral hemispherical reflectance for 3 mV sample and after cycling in air.

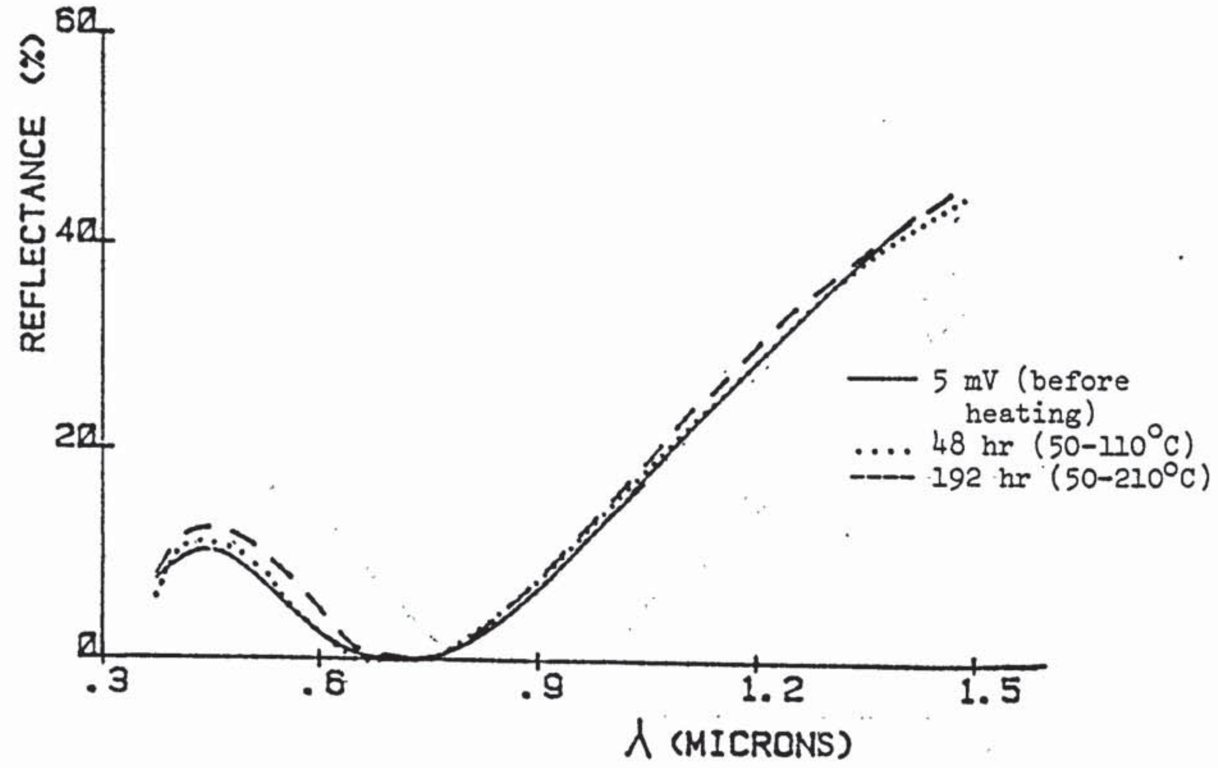

Fig. 4.20 Spectral hemispherical reflectance versus wavelength for 5 mV sample and after cycling in air.

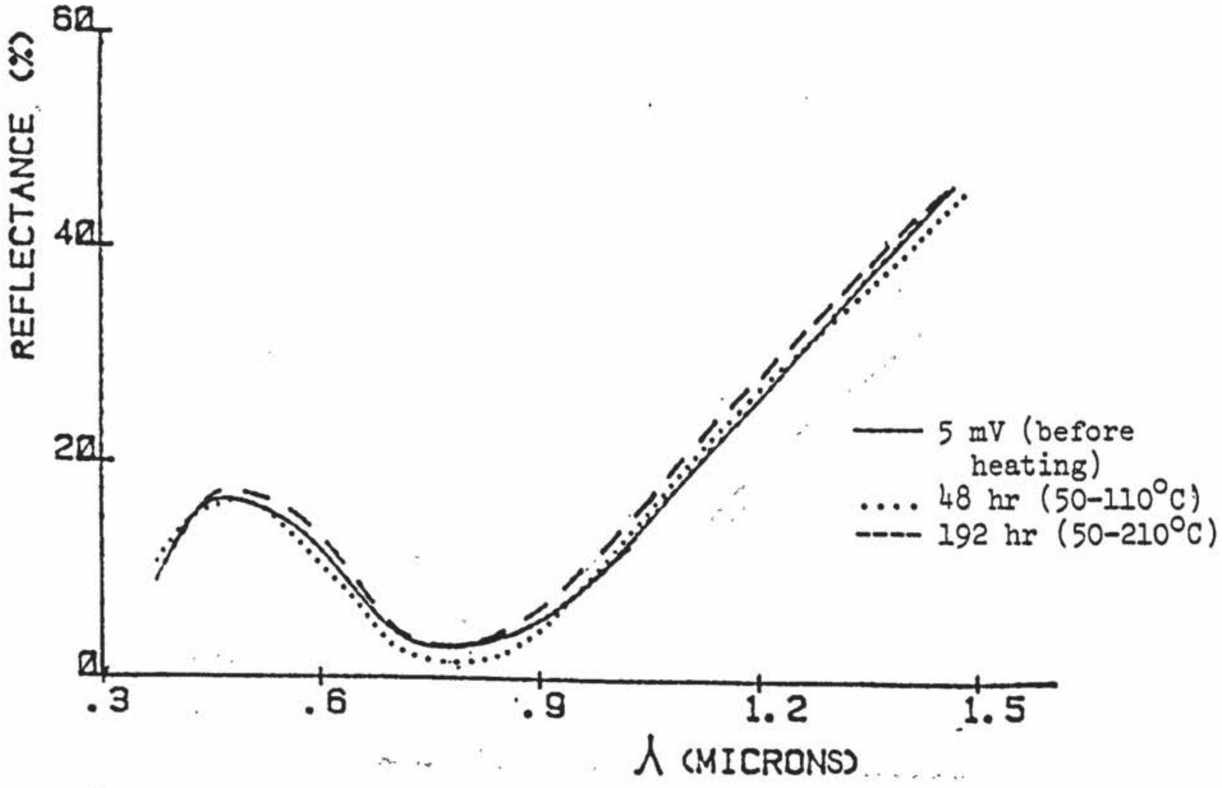

Fig. 4.21 Spectral hemispherical reflectance versus wavelength for 7 mV sample and after cycling in air.

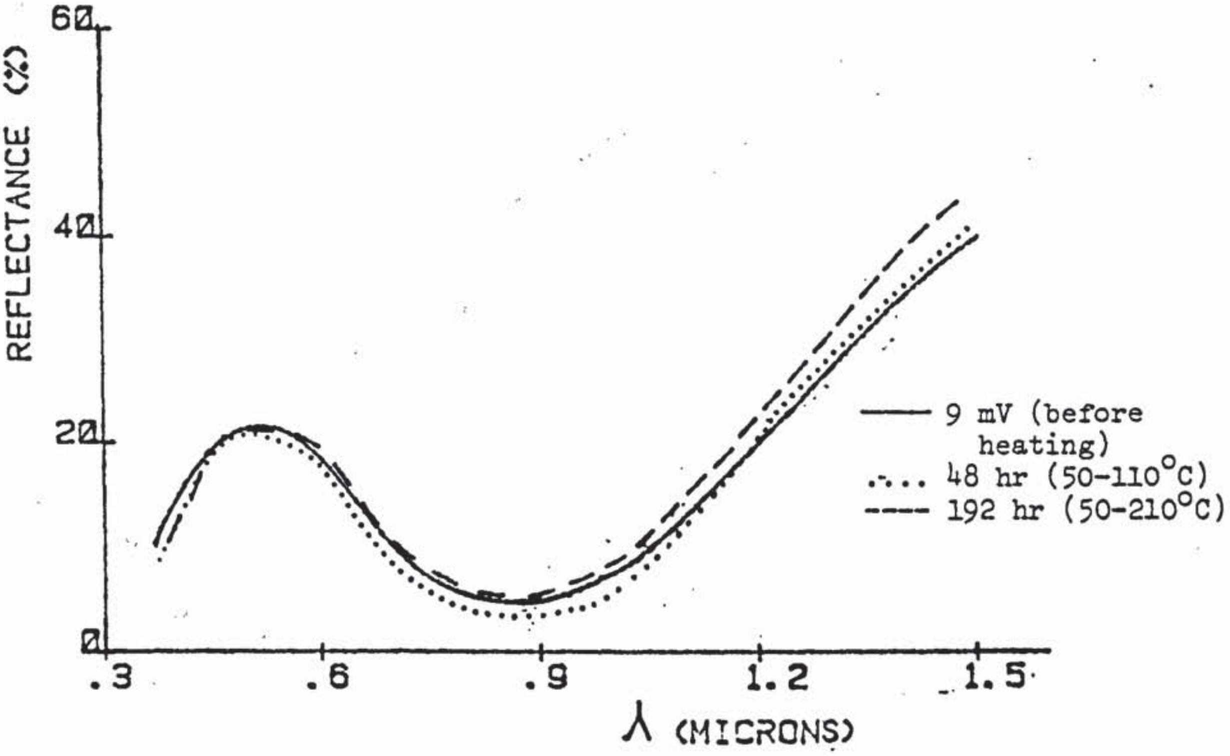

Fig. 4.22 Specular hemispherical reflectance versus wavelength for 9 mV sample and after cycling in air.

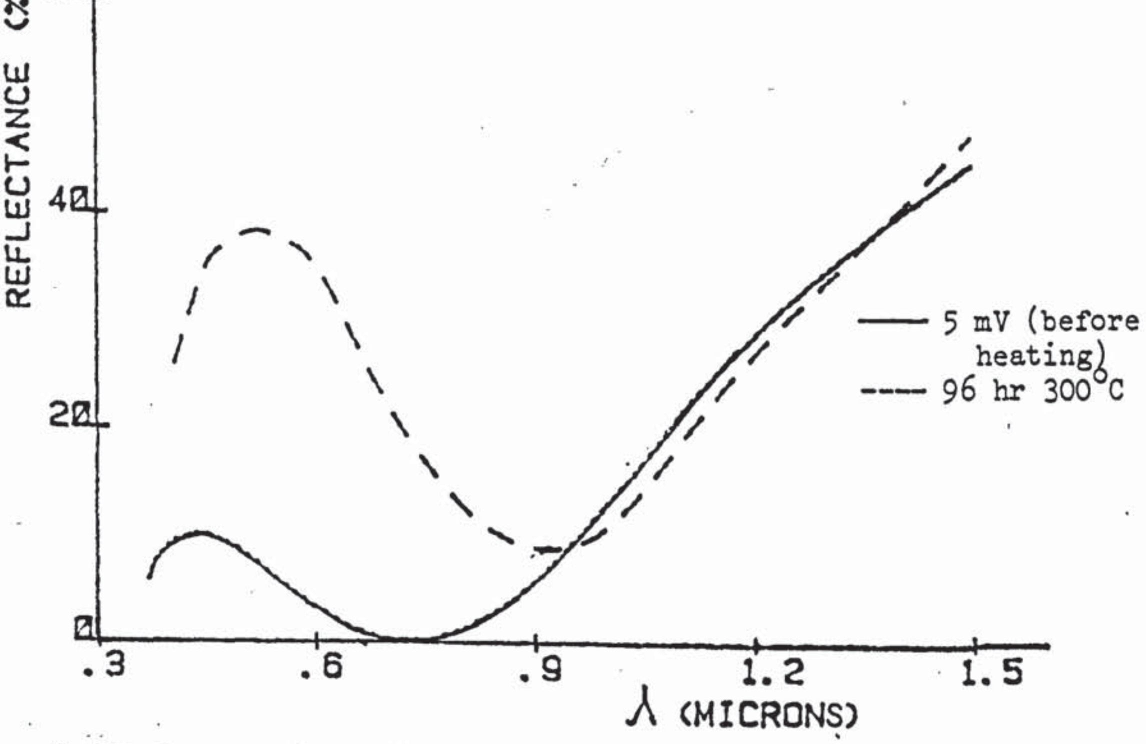

Fig. 4.23 Spectral hemispherical reflectance versus wavelength for 5 mV sample and after heating in soft vacuum [0.1 Torr].

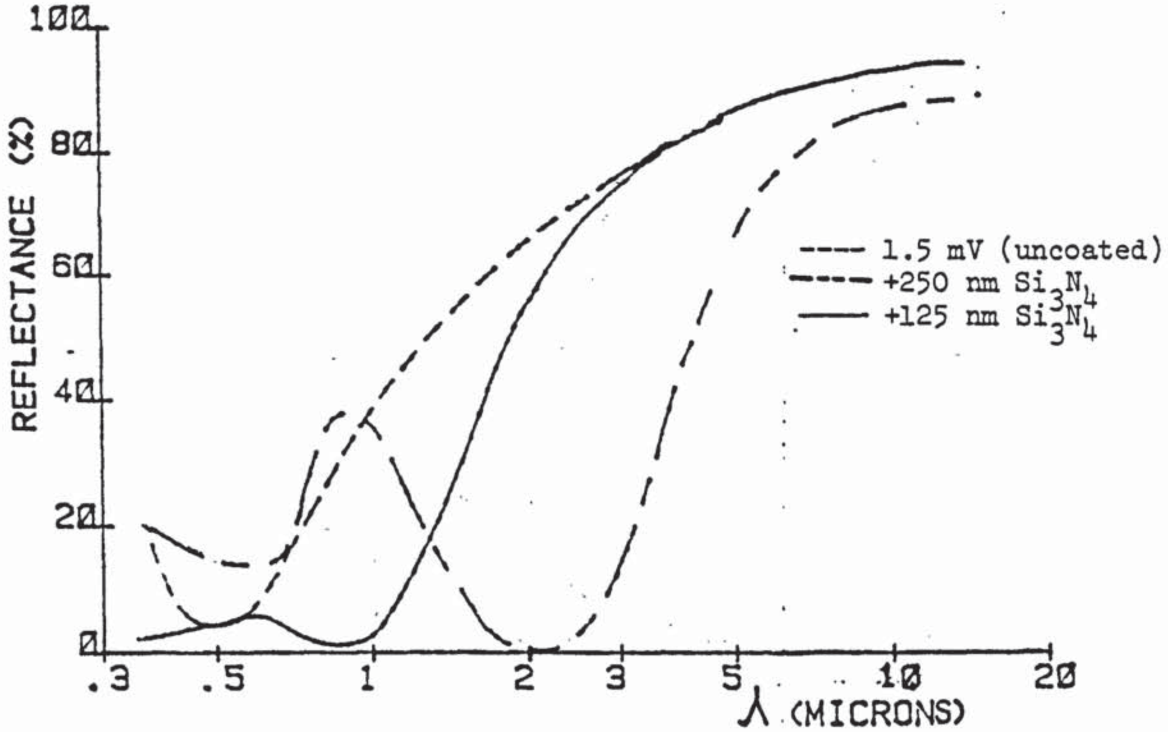

Fig. 4.24 Specular reflectance versus wavelength of Si_3N_4 coated 1.5 mV sample in comparison with that of an uncoated one.

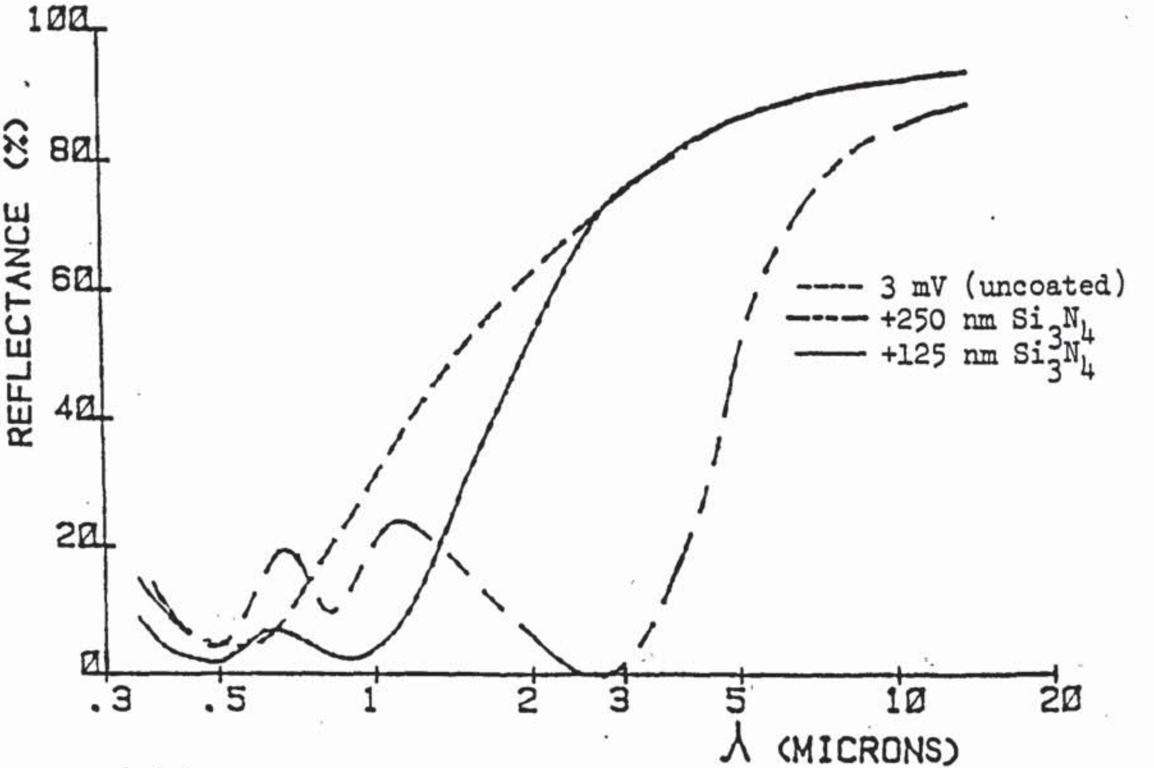

Fig. 4.25 Specular reflectance versus wavelength of Si_3N_4 coated 3 mV sample in comparison with that of an uncoated one.

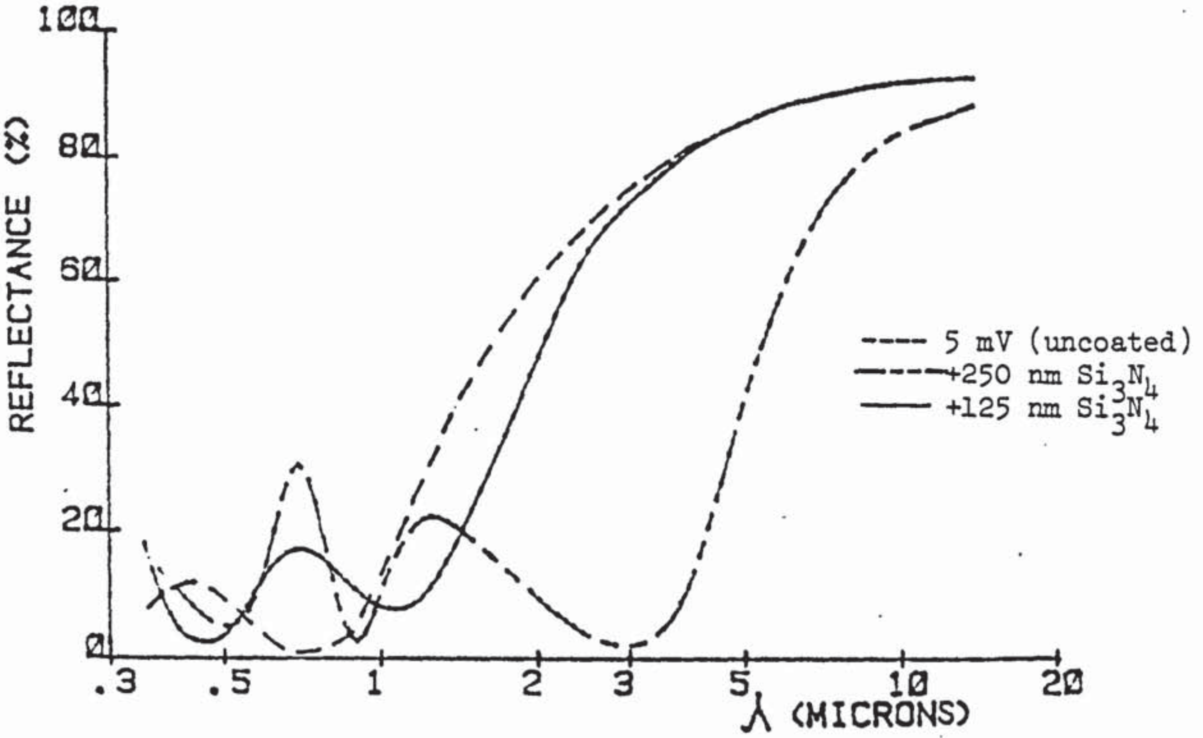

Fig. 4.26 Specular reflectance versus wavelength of Si_3N_4 coated 5 mV sample in comparison with that of an uncoated one.

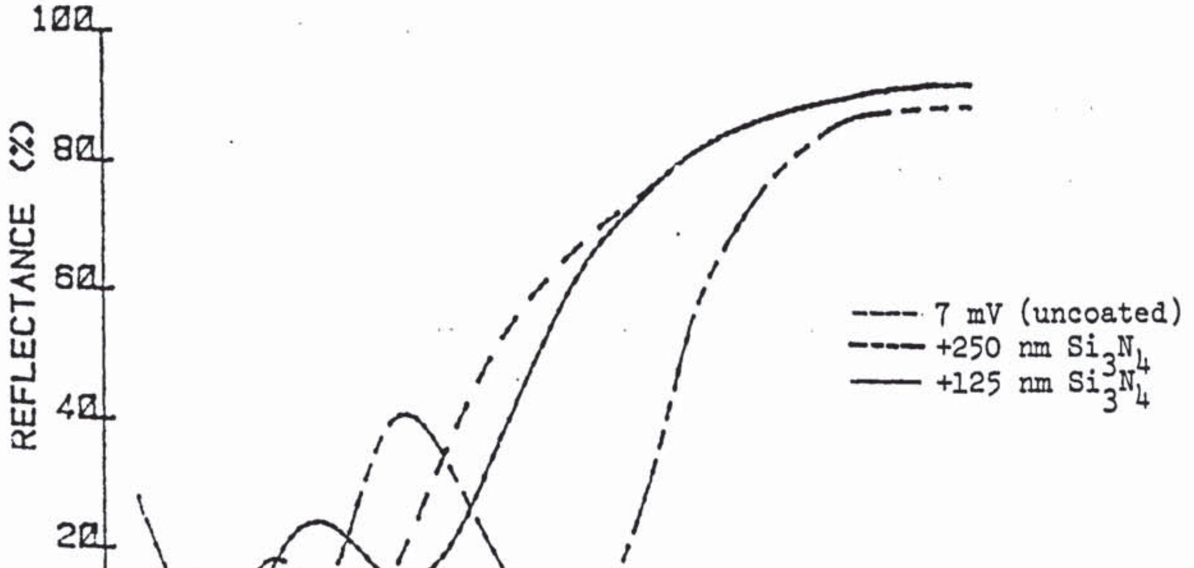

Fig. 4.27 Specular reflectance versus wavelength of Si_3N_4 coated 7 mV sample in comparison with that of an uncoated one.

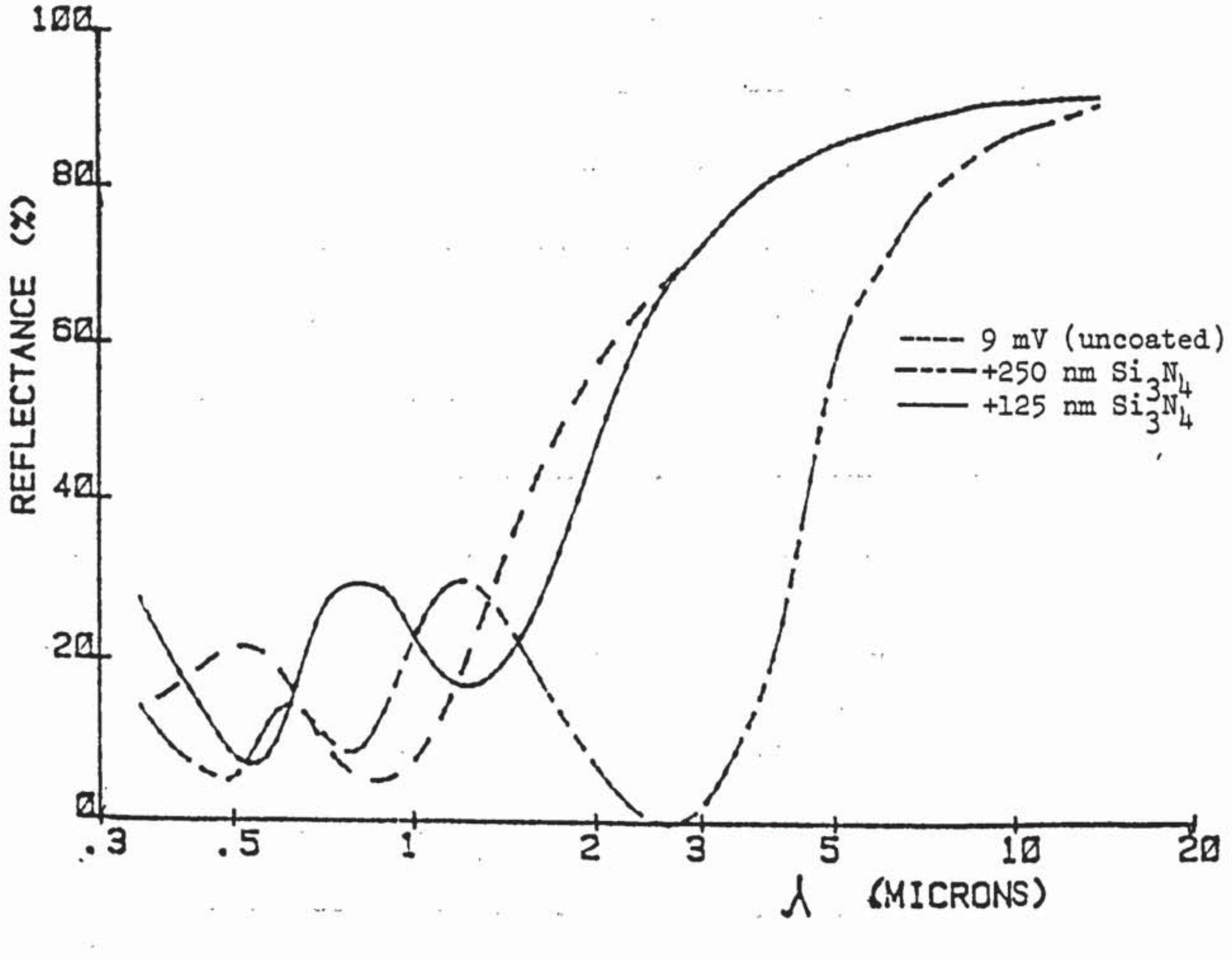

<u>Fig. 4.28</u> Specular reflectance versus wavelength of Si_3N_4 coated 9 mV sample in comparison with that of an uncoated one.

Sample treatment	1.5 mV				3.0 mV				5.0 mV				7.0 mV				9.0 mV			
	Abs	Emittance %			Abs.	Emittance %			Abs.	Emittance %			Abs.	Emittance %			Abs.	Emittance %		
	a%	e (100°C)	e (200°C)	e (300°C)	a%	e (100°C)	e (200°C)	e (300°C)	a%	e (100°C)	e (200°C)	e (300°C)	a%	e (100°C)	e (200°C)	e (300°C)	a%	e (100°C)	e (200°C)	e (300°C)
Unheated	73.00	9.80	11.11	12.4	79.60	10.10	11.10	12.60	86.50	10.10	11.10	13.5	83.90	10.10	11.30	13.40	82.30	10.65	11.60	13.40
H. 48 h. (110°C)	75.80	9.80	11.69	12.78	81.30	10.10	11.10	12.60	86.48	10.10	11.10	13.5	83.40	10.10	11.30	13.40	81.70	10.66	11.51	13.40
H. 192 h. (210°C)	77.20	9.68	10.62	12.26	81.06	9.68	10.62	12.25	86.49	9.68	10.92	12.25	83.00	9.79	11.39	12.88	78.30	9.79	11.39	12.88
H. 192 h. (250°C)	78.00	9.14	10.59	11.14	81.13	9.01	10.51	11.14	80.74	9.20	10.39	11.14	78.47	8.57	10.12	11.14	77.30	9.78	11.40	12.90
H. 5 min. (300°C)	74.70	9.80	11.11	12.40	79.58	9.82	11.14	12.13	84.48	10.10	11.10	13.50	82.20	10.10	11.30	13.40	80.39	10.65	11.50	13.41
H. 60 min. (300°C)	79.40	9.86	11.20	12.49	79.76	9.82	10.80	12.50	83.94	9.79	11.10	13.50	81.31	9.66	11.42	12.62	79.39	9.78	11.29	12.62
H. 160 min. (300°C)	79.00	9.64	11.62	12.09	81.4	9.64	10.63	12.09	82.66	9.47	10.89	12.26	79.77	9.47	10.89	12.26	78.39	9.47	10.89	12.26
H. 192 h. (300°C)	75.9	8.57	10.12	11.27	77.63	9.26	10.72	11.98	75.20	9.20	10.39	11.76	73.01	8.57	10.12	11.27	72.96	9.26	10.72	11.98
H.C. 48 h. (50-110°C)	75.00	10.51	11.69	12.78	80.11	8.58	9.54	11.66	86.48	8.92	10.60	12.21	83.00	8.85	10.48	12.01	81.60	8.85	10.48	12.01
H.C. 48 h. (50-210°C)	75.30	10.40	11.65	12.50	80.23	9.82	11.13	11.98	86.47	9.70	11.10	12.45	83.10	8.84	10.46	12.01	81.71	8.84	10.48	12.0
H.C. 192 h. (50-210°C)	75.50	10.45	11.61	12.30	80.28	9.80	10.10	12.33	85.2	9.73	11.15	12.65	81.69	9.93	11.44	12.31	79.19	9.73	11.17	12.2
H.V. 96 h. (300°C)	73.8	10.10	11.11	12.38	73.60	10.10	11.12	12.38	70.7	5.92	6.06	7.13	73.70	5.08	6.06	7.13	69.03	5.15	6.06	7.59
Unheated + 125nm(Si_3N_4)	89.66	8.41	9.77	11.41	89.90	8.70	10.23	11.72	85.8	9.35	10.54	12.17	81.77	9.35	10.53	12.30	78.89	9.35	10.53	12.37
H. 192 h. (250°C)	89.64	9.38	10.61	11.98	89.91	8.61	9.71	11.61	86.2	9.73	10.92	12.33	81.70	10.23	11.31	12.57	78.10	9.77	11.23	12.31
H. 3½ h. (300°C)	89.60	9.69	10.78	11.52	89.97	9.03	10.85	11.92	85.7	9.83	10.19	12.61	82.17	9.83	10.99	12.71	78.00	10.42	11.80	12.42

Table 4.9 Optical properties of INCO samples before and after heat treatment

H.	designated for continuous heating
H.C.	designated for cycling heating and
H.V.	designated for heating in a 0.1 Torr vacuum

4.3.6 RESULTS OF THE COMPOSITION ANALYSIS

The surfaces of the two samples corresponding to 5 mV and 9 mV (unheated) have been examined using Auger analysis. The variation of element concentration with the depth below the surface for the above samples have been investigated by successively removing layers by argon bombardment of energy 2 KV and beam current density of $1 \mu A\ cm^{-2}$, the sputtering speed being 0.2 nm/minute.

Figures 4.29 and 4.30 respectively represent the Auger spectrograms for the above samples before and after sputtering for different periods of time. These traces show the presence of chlorine, sulphur, carbon, chromium, and oxygen on the surface at zero time of sputtering.

Figures 4.31 and 4.32 show the argon bombarded depth profiles of the samples 5 mV and 9 mV respectively. The elemental concentration has been calculated for every element by using the equation 3.37 in chapter three.

Tables 4.10 and 4.11 respectively display the calculated elemental concentrations for different periods of sputtering time and are plotted in Figures 4.33 and 4.34 for the 5 mV and 9 mV samples.

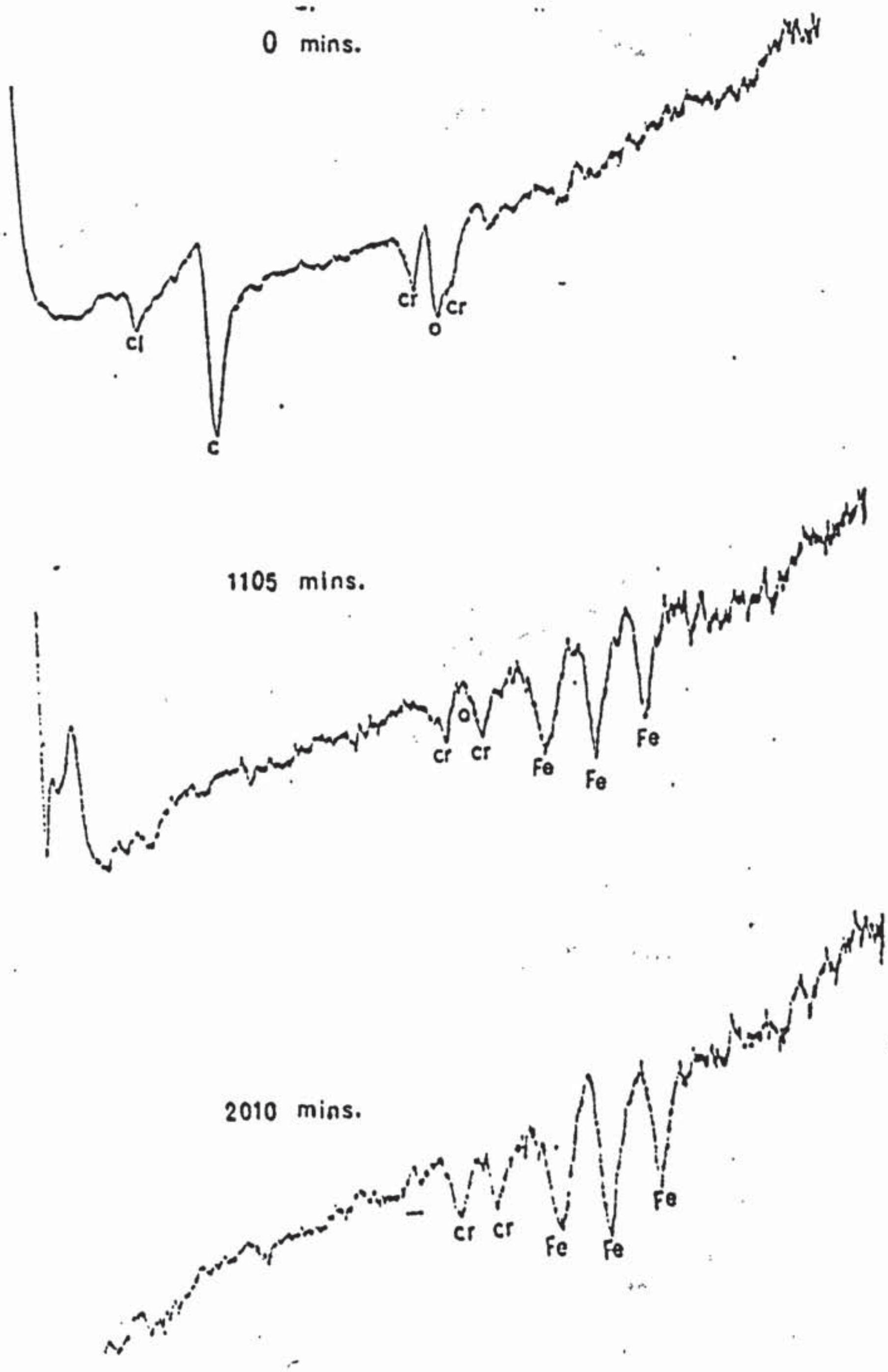

Fig. 4.29 AES after various sputter times for 5 mV sample.

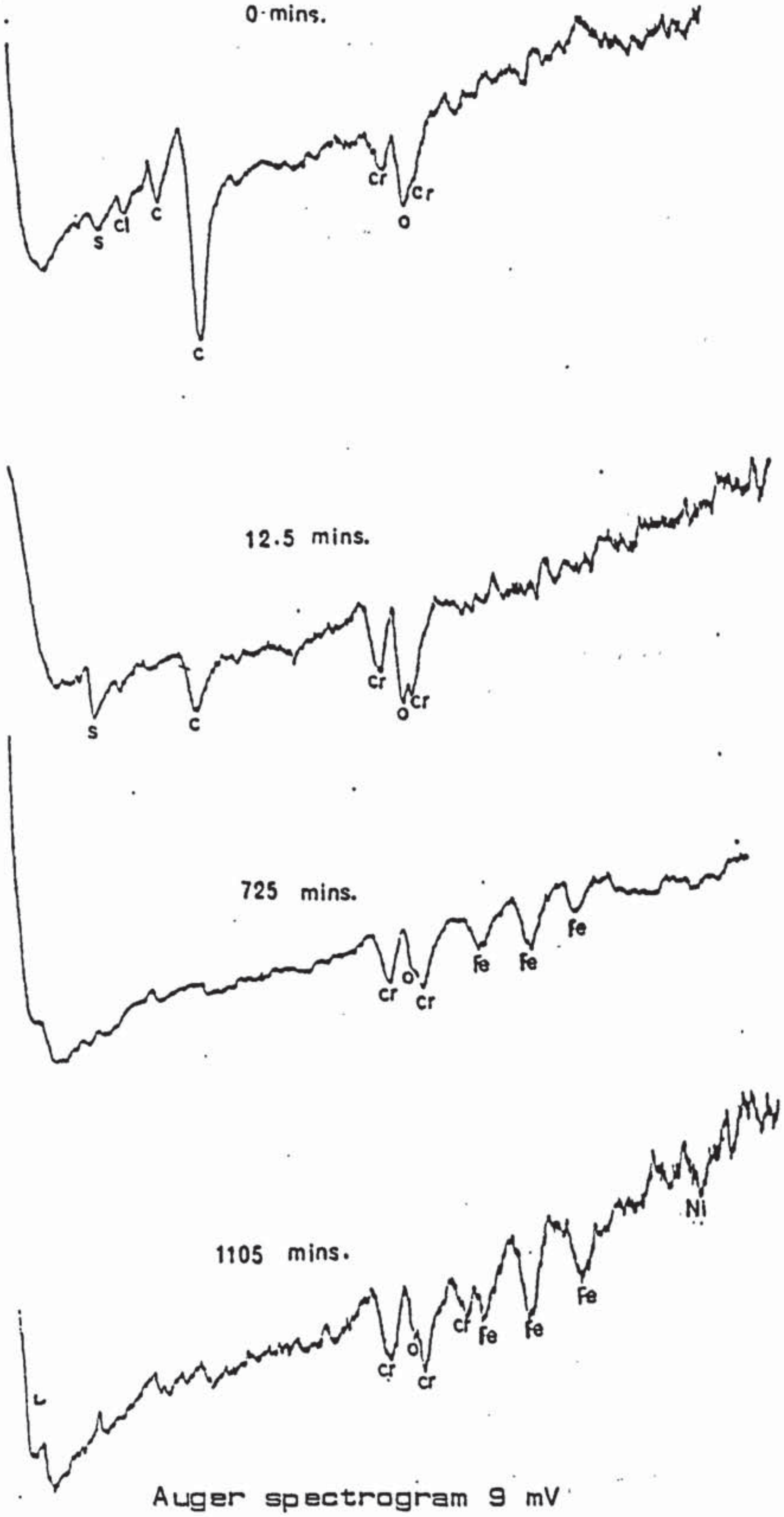

Fig. 4.30 AES after various sputter times for 9 mV sample.

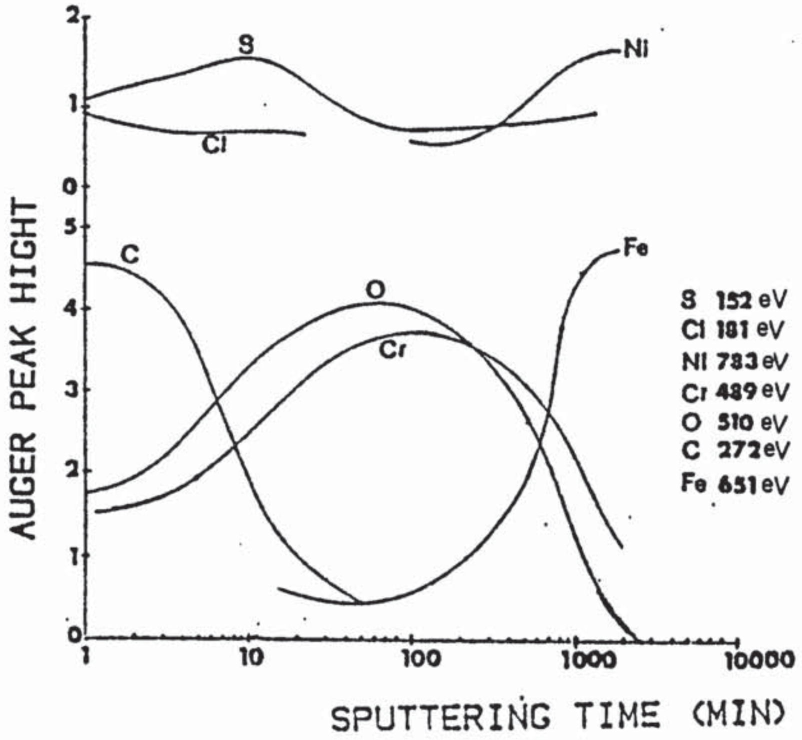

Fig. 4.31 Auger peak to peak height as a function of sputtering time for 5 mV sample.

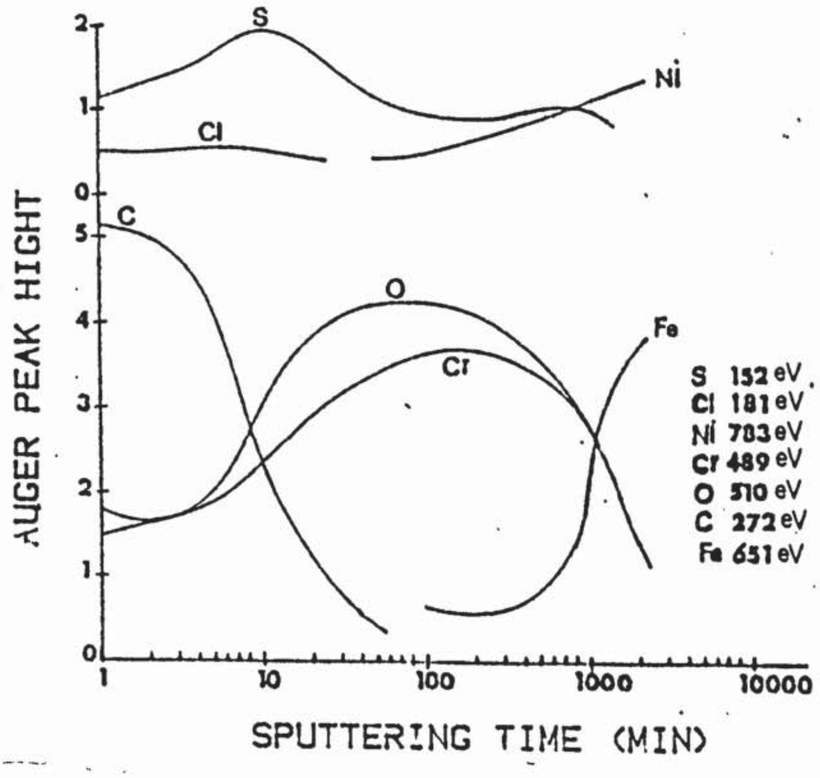

Fig. 4.32 Auger peak to peak height as a function of sputtering time for the 9 mV sample.

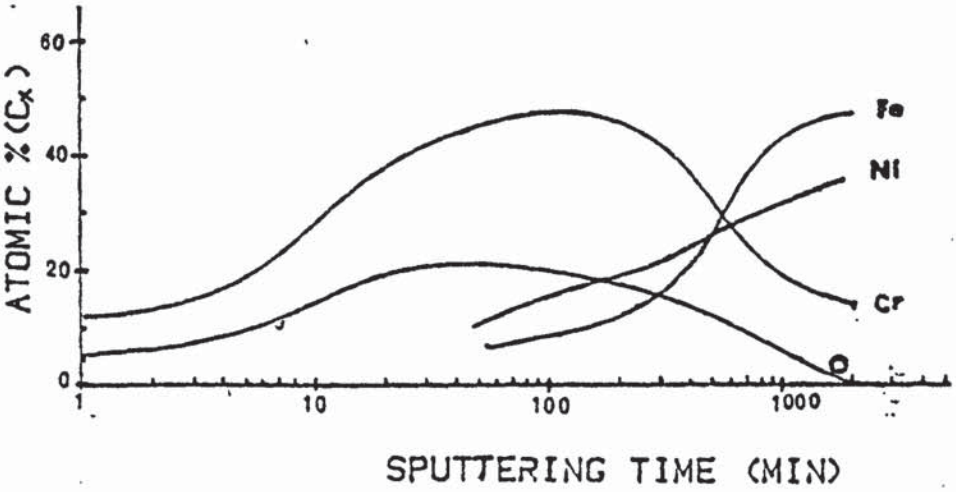

Fig. 4.33 Depth profile of the 5 mV sample.

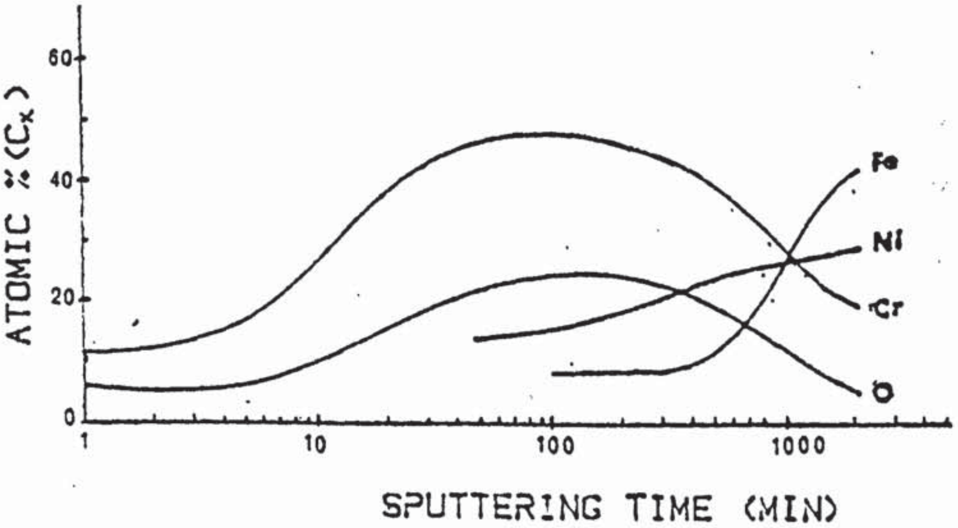

Fig. 4.34 Depth profile of the 9 mV sample.

Time min.	Atomic % (C_X)						
	SULPHUR	CHLORINE	NICKEL	CARBON	OXYGEN	CHROMIUM	IRON
1	3.40	6.26	0.0	72.12	6.21	12.02	0.0
2	3.44	4.99	0.0	72.06	6.97	12.55	0.0
4	4.23	5.49	0.0	65.04	9.20	16.04	0.0
6	5.96	6.18	0.0	56.16	11.65	20.06	0.0
8	5.75	6.96	0.0	48.68	13.2	25.4	0.0
10	6.19	7.49	0.0	41.01	15.68	29.62	0.0
20	5.19	7.85	0.0	25.47	21.37	40.12	0.0
50	3.78	0.0	10.76	11.12	21.53	44.49	8.31
100	4.00	0.0	17.55	0.0	20.28	47.75	10.43
200	3.93	0.0	17.22	0.0	18.86	45.66	14.33
300	3.74	0.0	20.19	0.0	16.21	42.32	17.55
500	2.85	0.0	27.40	0.0	12.64	33.58	23.53
800	2.20	0.0	28.18	0.0	7.66	20.23	41.73
1000	2.49	0.0	32.92	0.0	3.16	16.85	44.57
2000	2.66	0.0	35.07	0.0	0.0	13.93	48.34

Table 4.10 Atomic percentage composition of the 5 mV sample (unheated)

Time Min.	Atomic % [C_X]						
	SULPHUR	CHLORINE	NICKEL	CARBON	OXYGEN	CHROMIUM	IRON
1	3.11	3.14	0.0	76.38	5.91	11.46	0.0
2	3.07	3.10	0.0	76.82	5.35	11.67	0.0
4	4.15	3.35	0.0	71.74	6.49	14.27	0.0
6	5.50	4.57	0.0	62.97	9.39	17.60	0.0
8	6.58	4.61	0.0	55.05	11.84	21.92	0.0
10	7.10	4.52	0.0	48.41	14.67	25.30	0.0
20	7.41	6.53	0.0	25.13	21.91	39.02	0.0
50	5.26	0.0	14.66	10.78	23.48	45.82	0.0
100	4.18	0.0	15.52	0.0	23.43	46.68	10.18
200	4.09	0.0	17.94	0.0	22.37	45.65	9.95
500	4.72	0.0	24.98	0.0	19.75	41.07	9.48
600	4.07	0.0	24.85	0.0	18.18	38.82	14.08
800	3.69	0.0	26.06	0.0	13.58	35.92	20.75
1000	3.44	0.0	25.53	0.0	12.62	30.92	27.50
1100	3.18	0.0	26.08	0.0	11.65	28.13	30.96
1350	3.06	0.0	27.28	0.0	9.92	22.06	37.67
2000	3.01	0.0	30.02	0.0	5.30	19.70	41.97

Table 4.11 Atomic percentage composition of the 9 mV sample (unheated)

4.4 THERMALLY OXIDIZED STAINLESS STEEL TYPES 304 AND 316*

The section reported here deals with the optical properties of thermally grown oxide films on polished stainless steel of the two types, 304 and 316 heated in air at atmospheric pressure at temperatures of 773° Kelvin, 823° Kelvin, 973° Kelvin and 1198° Kelvin over a range of exposure times.

4.4.1 ELLIPSOMETER RESULTS

SUBSTRATE SAMPLE PREPARATION

The sample 25 x 25 mm was cut from 316 stainless steel sheet ; the 316 stainless steel type sample was polished to a mirror finish by initial grinding, followed successively by 6, 1 and ¼ diamond paste polishes. The sample was then ultrasonically cleaned to remove loosely bound polishing particles, and then finally boiled in isopropyl alcohol and removed through the vapour to eliminate all traces of grease. The other type [304 stainless steel] was received from INCO as a polished and specular surface in the form of a sheet.

OPTICAL CHARACTERIZATION OF STAINLESS STEEL SUBSTRATE

The optical characterization of 304 stainless steel has been reported in Section 4.3.1, and the same procedure was adopted for the 316 stainless steel type. The measurement ...

---

* The stainless steel type 316 contains 17.5% Cr, 0·08 Ni, 3% Mo, 0.5% Mn, 1.2% V and 0.3% Si.

values obtained for the angles Ψ and Δ are 35.08 degrees and 137.63 degrees respectively. The computed values of Ψ and Δ showed that the measurement values corresponded to a chromium oxide thickness of ~35 nm and the values corresponding to zero oxide thickness were found to be 35.37 degrees and 144.18 degrees respectively. By using these values for the substrate, together with equations 3.13 and 3.14, the optical constants n_2 and k_2 were found to be 2.30 and 3.70 respectively.

RESULTS OF OXIDE GROWTH ON 304 STAINLESS STEEL AND 316 STAINLESS STEEL IN AIR

The 304 type sample was exposed in air and at atmospheric pressure to 823 Kelvin from 60 seconds to one hour. The sample was removed from the furnace and allowed to cool to room temperature naturally. This sample showed a range of coloured interference films, depending on the heating period. The surface appeared gold, yellow, and then progressed to purple, dark blue and finally, after extending the exposure time, it turns to matt light grey. Values of Ψ and Δ at a wavelength of 546.1 nm for the growth of an oxide film on the substrate were measured at each stage. The same procedure has been used with another set of 304 stainless steel samples but the sintering temperature was 973 Kelvin. By the same way Ψ and Δ values for 316 stainless steel type were measured for the above ranges of temperatures. The results of the above measurements are tabulated in Table 4.12. Figure 4.35 shows plots of the angle Δ versus time of sintering at a wavelength 546.1 nm for oxide growth on bulk stainless steel of two types at temperatures of 823 Kelvin and 973 Kelvin.

λ = 546.1 nm
ϕ_o = 62.22°

Sample treatment	Heating temp (Kelvin)	Heating time (min)	ψ (degrees)	Δ (degrees)	n_2	k_2	Colour
304 s.s. type (polished)	unheated	-	35.41	144.03	2.28	3.70	silver
	823	2	31.00	95.50			yellow
		4	17.90	79.80			gold
		8	19.60	44.42			brown
		16	19.80	29.13			dark blue
	973	1	30.76	95.90			yellow
		2	18.18	60.46			gold
		3	20.10	30.13			brown
		5-6	21.80	10.70			dark brown
316 s.s. type (polished)	unheated	-	35.37	144.18	2.30	3.70	silver
	823	5	17.28	78.78			gold
		10	18.00	46.80			light brown
		16	19.91	30.49			purple
	973	2	24.72	63.17			yellow
		5	19.90	30.42			violet
		10	20.86	20.12			dark violet

Table 4.12 The variation of ψ and Δ with the time for oxide film grown on the 304 and 316 stainless steel types

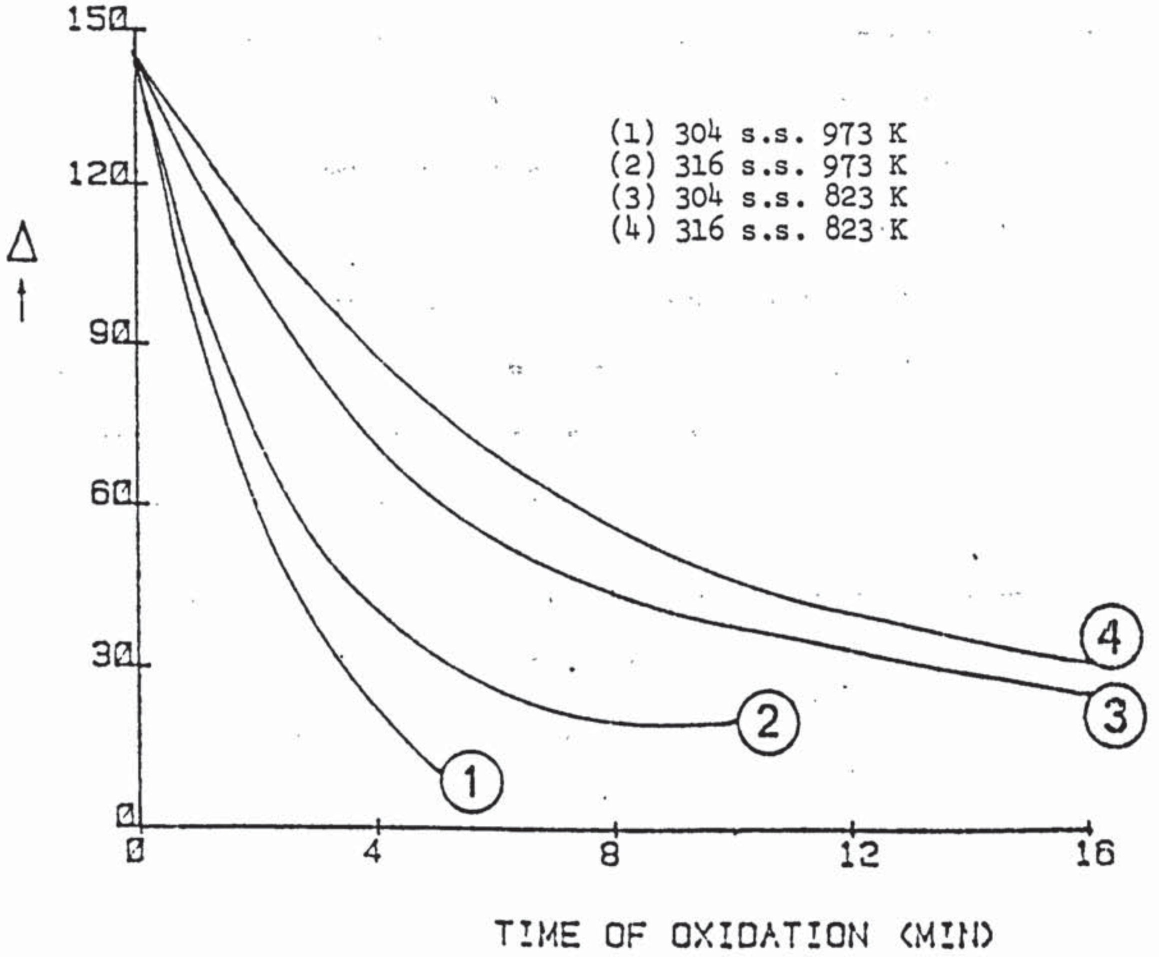

Fig. 4.35 Δ against time during oxidation of bulk stainless steel of types 304 and 316 in air for λ = 546.1 nm.

4.4.2 REFLECTANCE RESULTS

The room temperature specular reflectance was measured for the samples of stainless steel of the two types unheated and heated in air over a range of furnace temperatures (823 Kelvin, 973 Kelvin and 1198 Kelvin) for a number of different exposure times extending from 60 seconds to one hour. (The above samples were allowed to cool to room temperature naturally outside the oven). The results of the spectral reflectance of 304 stainless steel and 316 stainless steel unheated and heated for a temperature of 973 Kelvin are illustrated in Figures 4.36 and 4.37.

The values of the absorptance and the emittance at different temperatures (100°C, 200°C and 300°C) were calculated and are given in Table 4.13.

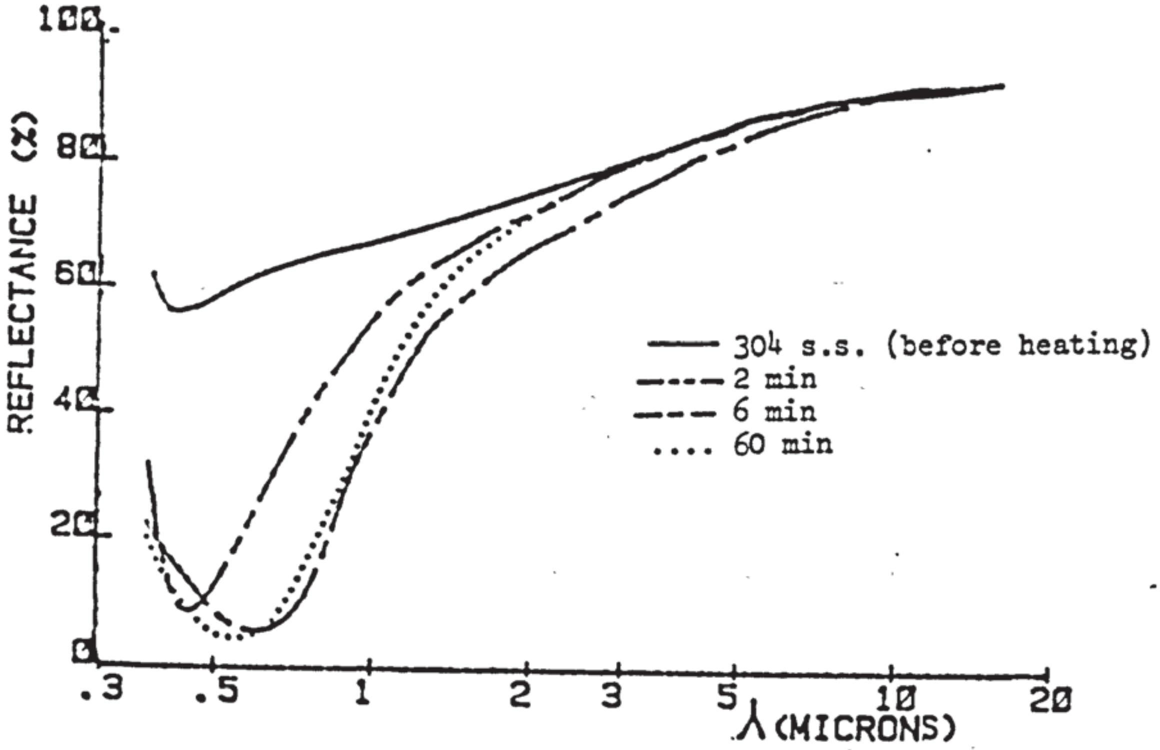

Fig. 4.36 Specular reflectance versus wavelength for 304 stainless steel (polished) and after heat treating in air at 973 K.

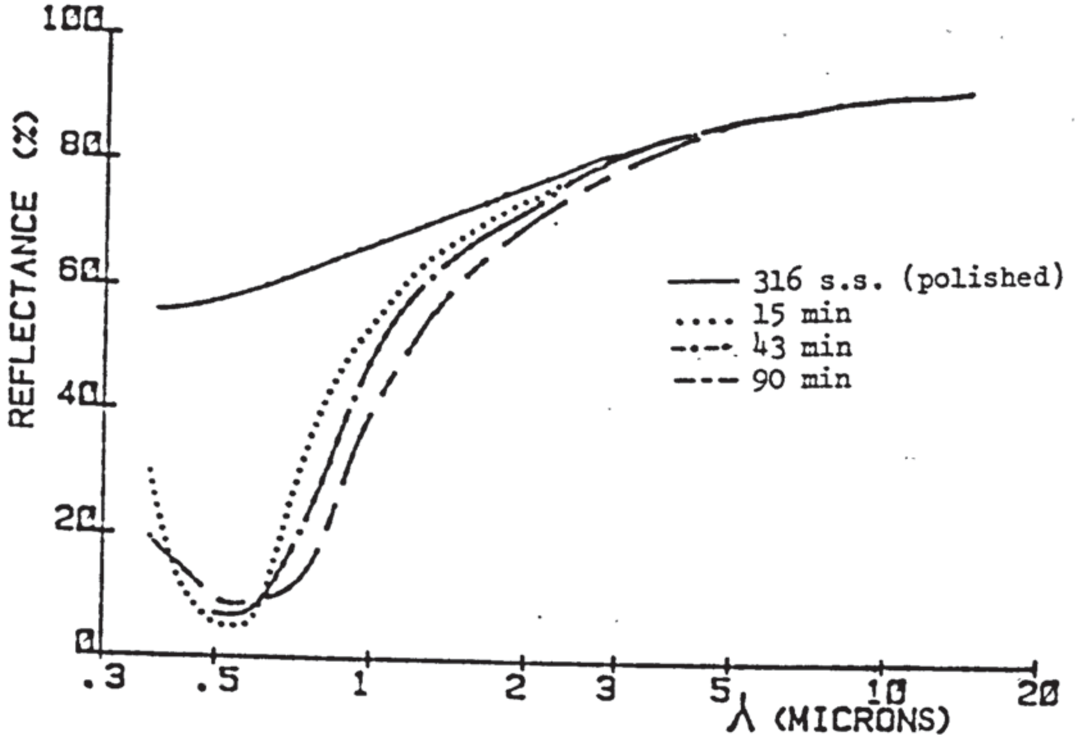

Fig. 4.37 Specular reflectance versus wavelength for 316 stainless steel (polished) and after heat treating in air at 973 K.

Sample treatment	Heating temp. (K)	Heating time (min)	Absorptance a%	Emittance %			Colour
				e(100°C)	e(200°C)	e(300°C)	
304 s.s. type (polished)	unheated	-	35.00	9.10	10.00	11.30	silver
	973	1	45.00	8.99	9.94	10.01	yellow
		2	60.00	9.23	10.13	11.01	gold
		3	62.00	9.23	10.18	11.01	brown
		6	75.00	9.46	11.10	11.49	dark blue
		8	71.0	9.44	11.10	11.40	-
		60	75.0	10.10	11.05	11.50	dark blue
	1198	2	66.4	8.66	9.50	11.20	brown
		3	71.0	8.44	10.12	11.06	dark blue
		5	75.0	8.48	10.20	11.12	dark blue
		32	73.5	9.10	10.62	11.86	dark grey
316 s.s. type (polished)	unheated	-	35.2	9.43	9.77	11.07	silver
	823	5	51.6	9.48	9.93	11.40	gold
		10	54.1	9.53	10.40	11.19	light brown
		15	58.0	9.72	10.45	11.34	purple
		23	62.0	9.88	10.95	12.15	light violet
		40	64.0	9.46	10.53	11.64	violet
	973	2	44.3	9.63	10.51	11.56	yellow
		5	62.0	9.56	10.48	11.63	violet
		10	63.0	9.92	10.82	11.73	dark violet
		15	65.0	9.60	10.65	11.53	purple
		25	67.0	9.65	10.63	11.58	blue
		43	71.0	9.75	10.66	11.78	dark blue
		90	74.0	9.80	11.26	12.34	dark blue
	1198	3	59.0	11.30	12.42	13.11	dark brown
		10	74.0	11.33	12.68	13.48	dark blue
		25	73.0	11.7	13.2	14.01	dark grey

Table 4.13 Optical properties for 304 s.s. and 316 s.s. before and after oxidation at various temperatures for differing periods of time

4.5 BLACK NICKEL FOIL (MARKETED NAME MAXORB)

(produced by MPD Ltd., Wiggen Street,
Birmingham B16 0AJ, England)

In this section, results are presented on tests made on commercial samples of the black nickel foil coated with DC 282 pressure sensitive adhesive on the under surface.

The objective has been to demonstrate its effectiveness, stability in air, vacuum and high humidity environments.

4.5.1 REFLECTANCE RESULTS

The spectral reflectance values for radiation from 0.35 μm to 15 μm for the uncoated and coated black nickel foil sample attached to the aluminium substrate of 25 x 25 mm^2 have been measured and are shown in Figure 4.38.

It can be seen that the total reflectance is effectively constant (~ 2%) over a range of the solar spectrum up to 1.2 μ m. The reflectances at wavelengths greater than 8 μm are the same as uncoated nickel black. The absorptance and the emittance at 100°C, 150°C and 200°C were calculated and tabulated in Table 4.14.

Sample treatment	Absorptance $\underline{a}$ %	Emittance %		
		$\underline{e}$(100°C)	$\underline{e}$(150°C)	$\underline{e}$(200°C)
uncoated nickel foil (as supplied)	33.43	14.10	14.21	14.99
black nickel foil (unheated)	98.60	13.66	14.82	16.91
H.48 hrs 110°C	98.60	13.65	14.81	16.91
H.48 hrs 210°C	98.50	13.66	14.82	16.90
H.192 hrs 210°C	98.40	13.55	14.82	16.91
H.192 hrs 250°C	98.30	13.55	14.67	16.52
H.5 min. 300°C	98.00	15.95	17.57	19.19
H.60 min. 300°C	97.60	15.94	17.57	19.19
H.160 min. 300°C	97.60	17.36	18.65	20.17
H.C. 48 hrs (50-110°C)	98.60	13.65	14.78	16.92
H.C. 48 hrs (40-210°C)	98.74	13.65	14.75	16.91
H.C. 192 hrs (40-210°C)	98.74	15.51	17.32	19.35
H.V. 48 hrs 110°C	98.50	13.66	14.80	16.90
H.V.192 hrs 210°C	98.50	13.64	14.81	16.91
H.V.192 hrs 210°C	98.30	13.55	14.67	15.51
H. 72 hrs (R. humidity 98% Temperature 67°C)	98.66	13.98	15.65	17.72
H. 192 hrs (R. humidity 98% Temperature 67°C)	98.44	14.35	15.90	17.59

Table 4.14 Optical properties of black nickel foil before and after heat treatment H. designated for continuous heating, H.C. designated for cycling heating and H.V. designated for heating in a 0.1 Torr vacuum

4.5.2 ABSORPTANCE VERSUS THE OFF-AXIS ANGLE

To investigate the dependence of the absorptance of the black nickel foil on the angle of incidence, the spectral hemispherical direction reflectance of a set of samples has been measured as a function of the off-axis angle up to 50 degrees. The absorptances have been computed and are recorded in Table 4.15.

Figure 4.39 shows the plots of absorptance versus the off-axis angle.

Off-axis angle (Degrees)	Absorptance a %
10	98.70
20	98.60
30	98.0
40	97.50
50	97.00
60	96.00

Table 4.15 Absorptance of black nickel foil versus off-axis angle

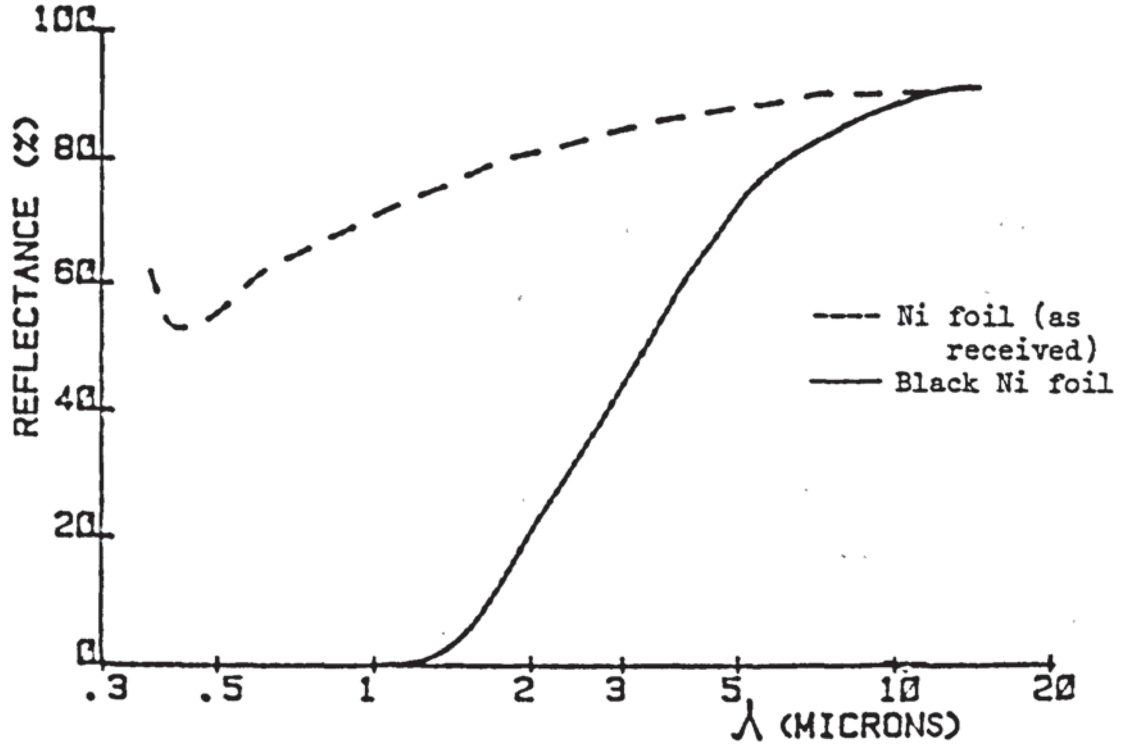

Fig. 4.38 Specular reflectance versus-wavelength for nickel foil (as received) and the black nickel foil sample.

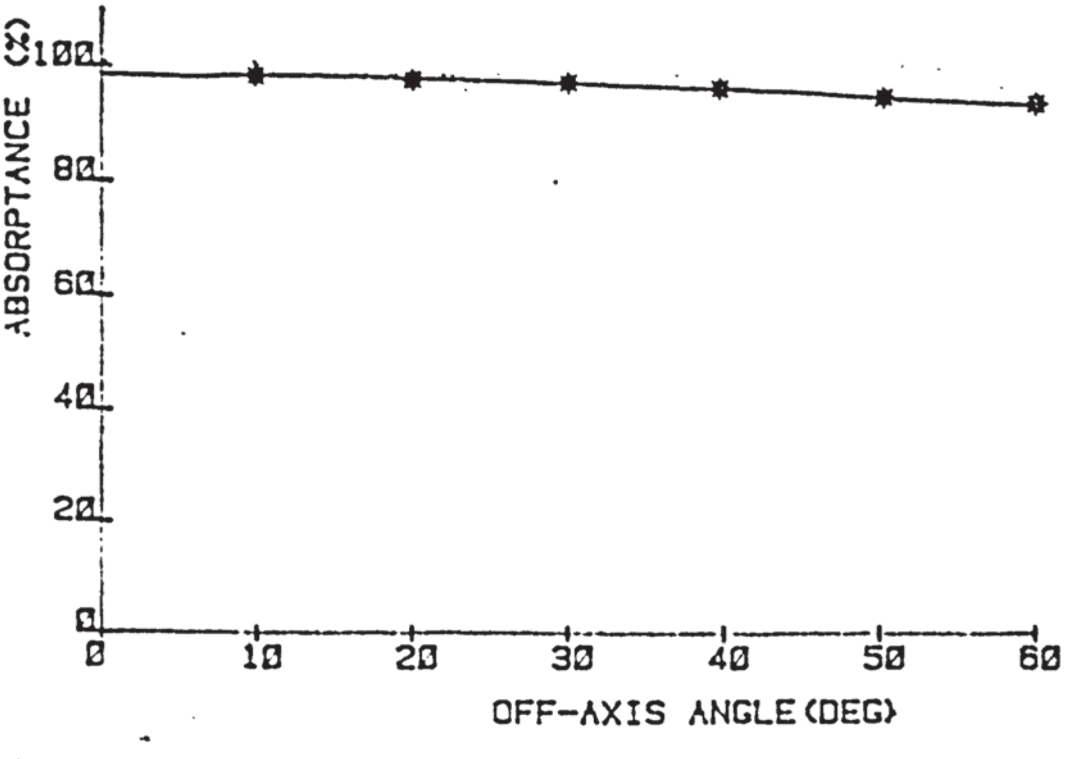

Fig. 4.39 A plot of absorptance versus the off-axis angle for the black nickel foil.

4.5.3 LIFE TESTING

A set of black nickel foil samples have been annealed in air at atmospheric pressure as well as in a vacuum (0.1 Torr), at temperatures of 110°C, 210°C, 250°C and 300°C for periods up to 484 hours. The temperature stability was also tested by subjecting a set of samples to successively increasing temperatures between 110°C and 250°C for a total time of 480 hours with frequent measurements. This is illustrated in Figure 4.40.

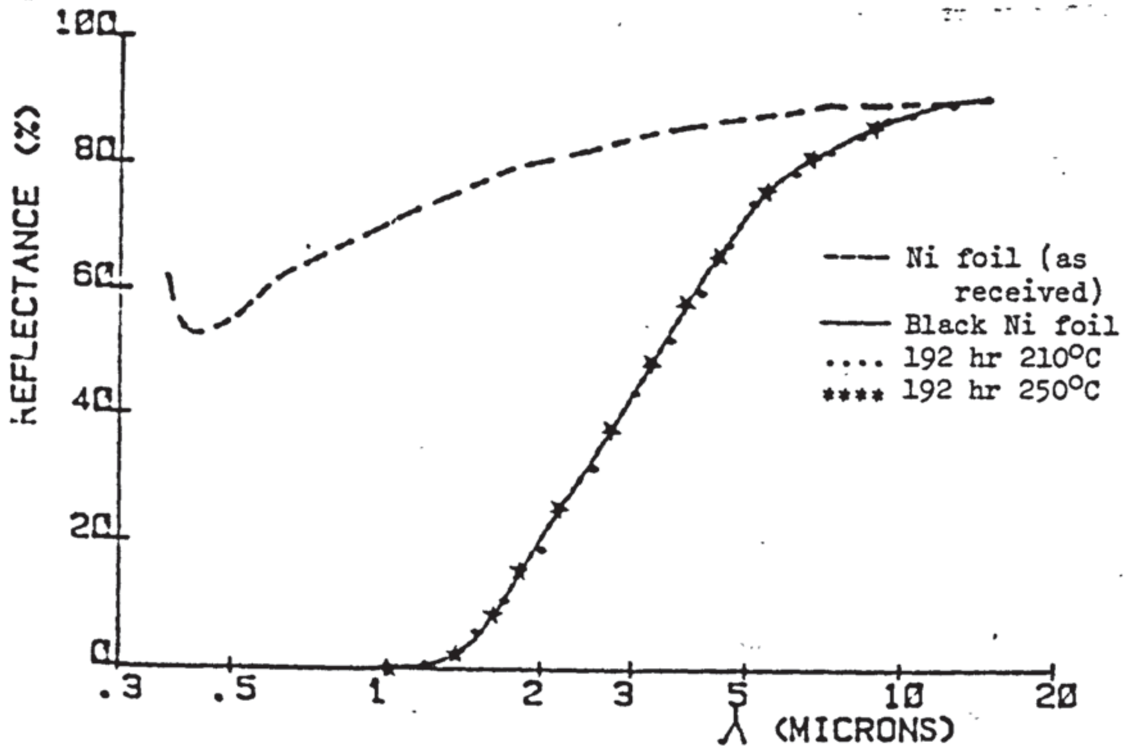

Fig. 4.40 Specular reflectance versus wavelength for black nickel foil and after heat treating in air.

Another set of the samples was subjected to heat cycling over a range of temperatures extending from 40°C to 110°C every fifteen minutes for 48 hours and over a temperature range of 40°C to 220°C every thirty minutes for 192 hours.

The calculated average values of the absorptance and the emittance before and after heating tests are also given in Table 4.14. This table indicates that the absorptance , a, remains nearly constant after heating in air up to 250°C as well as in a vacuum. But for 300°C the adhesive on the under surface broke down after only five minutes of heating.

4.5.4 HUMIDITY TEST

The black nickel foil has been tested in air at a constant temperature of 67°C and 97% relative humidity for the periods of 72 hours and for 192 hours. The calculated average values of the absorptance and the emittance of the samples are tabulated also in Table 4.14.

4.5.5 RESULTS OF THE COMPOSITION ANALYSIS

The surfaces of a sample of unheated black nickel foil and a sample after 8 days of heating at 210°C were measured with a scanning electron microscope quantometer, which was housed in the Space Sciences Center of the University of Arizona. Figure 4.4 shows the micrographs of the above sample. This technique has been used to detect the composition in the black nickel foil with incident electrons at 5 KeV. The microscope sees about 300 nm into the black foil and can detect the presence of 100 ppM of nickel and 500 ppM for either oxygen or carbon. The results of this analysis for the unheated and heated black nickel foil samples are given in Table 4.16.

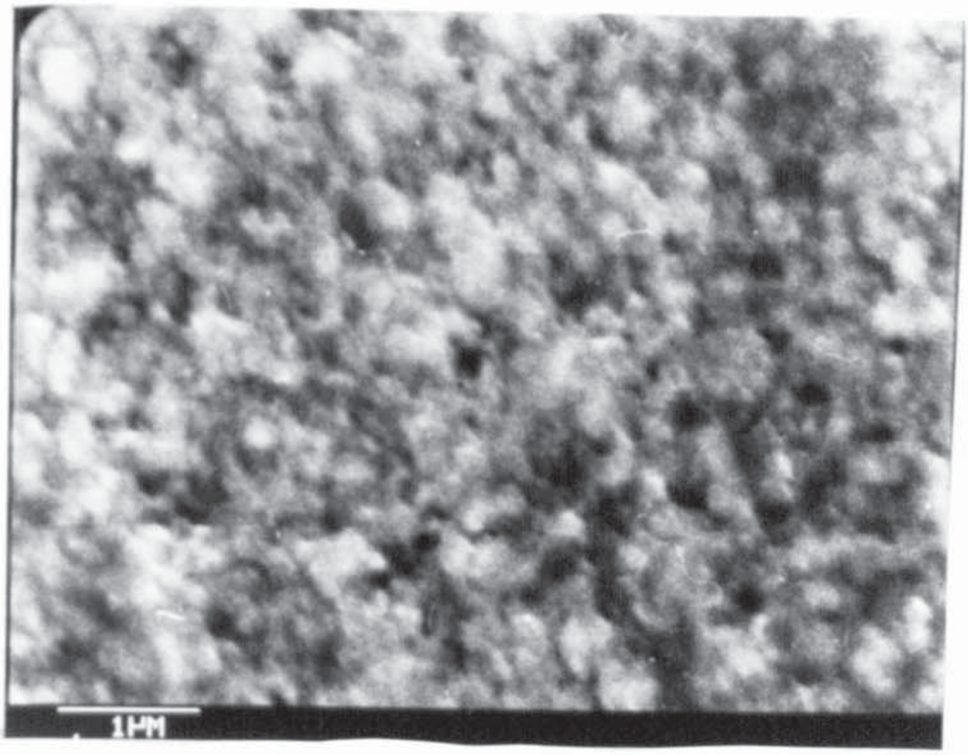

Figure 4.41 Scanning Micrograph of the Black Nickel Surface

Element present	Atomic %	
	Unheated black nickel foil	Heated for 192 hr at 220°C
Ni	55.26	47.19
O	38.64	48.31
C	6.1	9.46
Cr	0.35	-

Table 4.16 Atomic percentage of black nickel foil before and after heat treatment

CHAPTER 5

DIRECT MEASUREMENT OF TOTAL HEMISPHERICAL EMITTANCE

One of the objectives of this project was to develop an instrument capable of measuring the total hemispherical emittance directly for the standard laboratory samples.

This chapter gives a brief discussion of a number of abailable measurement techniques; the technique adopted for the present purpose. It also describes the apparatus designed and error analysis conducted.

Total hemispherical emittance values of Quartz, stainless steel (polished), pure nickel foil (as supplied), black nickel foil, INCO surface corresponding to 5 mV process and 3M-Nextel black paint have also been presented and compared with the computed normal emittance carried out in the earlier section of this study.

5.1 EMITTANCE MEASUREMENT TECHNIQUES

A summary of the techniques available for emittance measurement is tabulated in Table 5.1. One could divide the techniques mentioned in this table which are used for emittance measurements into two categories:

1. Calorimetric Techniques and
2. Reflectance Techniques.

For a calorimetric measurement, a sample of known radiating surface area is placed in an environment where heat loss or gain is by radiant heat transfer only. The emittance is then computed from a knowledge of the amount of power (usually supplied by an internal electrical heater) required to maintain the sample at a measured equilibrium temperature. This is called the 'steady state technique'. With a knowledge of heat capacity of the specimen, the emittance can also be computed from a measurement of the rate of temperature change of the sample, which may be called the 'transient technique'. For details see Fussell et al (1963). In either case, the total hemispherical emittance is measured directly.

The advantages of the calorimetric techniques are: it is simple, requiring only measurements of temperature and electric power; it is direct and requires no integration of directional or spectral data.

Reflectance techniques do not determine the total hemispherical emittance directly. They determine the emittance as a function of wavelength and incident angle. By integrating these data over the appropriate black body spectrum and angles, the total hemispherical emittance is obtained. Kirchhoff's Law forms the basis for the determination of the emittance by reflectance techniques.

Reflectance techniques have the following advantages: they give fast acquisition of spectral reflectance data;

sample geometry and mounting becomes easy and they give spectral and angular emittance data.

A more detailed comparison of these emittance measurement techniques has been reported by Millard and Streed (1969).

Table 5.1 Measurement techniques for emittance

Technique	Wave-length (μ	Angle range degrees	Temp. range Kelvin	Major features	References
1 Calorimetric					
1. Total hemi-spherical (steady state method)	ALL	$0,2\pi$		heat balance in cooled evacuated chamber, long time consuming, uncertainties in temp. measurement	Tanaka (1979); Meinel & Mienel (1976); Pettit (1975)
2. Total hemi-spherical (trans-ient method)	ALL	$0,2\pi$		temperature decay in vacuum, requires cold wall, coating the sample on both sides, uncertainties in heat leak, temperature gradients, and decay curve slope	Verst & Ramanathan (1978); Willrath & Gammon (1978); Roger et al (1979)
2 Reflectance					
1. Heated cavity	2-35	$0,2\pi$	R.T. - 900	A versatile infrared instrument; in widespread use, platinum reference surface	Gier et al (1954)

<u>Table 5.1</u> (cont)

Technique	Wave-length (μ)	Angle range degrees	Temp. range Kelvin	Major features	References
2. Integrating Mirrors					
(i) paraboloidal	2-100	0,2π	R.T.	2π steradian illumination, chopped uniform source, gold reference, exit port error, difficult for angular use, physically large components, suitable for surfaces of arbitrary reflection distribution function	Dunkle (1960); Neher & Edwards (1965)
(ii) ellipsoidal	1-15	0,2π	R.T. - 400	2π illumination, absolute method, vacuum, or inert gas operation, initial high cost, abberations are reduced by using an ellipsoidal mirror with true focal points instead of a hemispherical mirror	Dunn et al (1966)
3 <u>Soecular</u>	2.5-50	10°	R.T.	relative method, uses commercial attachment with front surfaced aluminized mirror references susceptible to scattering from sample	Millard & Streed (1969)

Table 5.1 (cont)

Technique	Wave-length (μ	Angle range degrees	Temp. range Kelvin	Major features	References
4 Integrating sphere suptituation or comparative type	0.3-2.6	0,2π	R.T.	sample mounted at centre of the sphere or at the sphere surface; technique used in many commercial spectrophotometers, may be sensitive to sample texture	Goebel (1967); Jacquez & Kuppenheim (1954)
Absolute	0.2-2.6	0,2π	R.T.	sample mounted at sphere centre suitable for samples of arbitrary reflection distribution function	Edwards et al (1961)
Laser source	0.63-1.15	0,2π	R.T.-2500	laser used as conventional source	Kneissl & Richmond (1968)
5 Multiple reflection					
Strong technique	0.3-35	0	R.T.	for specular reflectors only	Fowler (1960); Gates et al (1958); Strong (1938)
Bennett-reflectometer	0.2-0.35	0	R.T.	errors minimized by unique optical design; accuracy: state of the art ±0.001 unit	Bennett & Koehler (1960)

5.2 THE TECHNIQUE ADOPTED

The method for measuring directly the total hemispherical emittance in this project is a 'calorimetric technique-steady state method'. It is based on the measurement of heat flow by determining the differential temperature across a slice of material of known thermal conductivity used as heat flow sensor.

5.2.1 DESCRIPTION OF THE CALORIMETRIC EMITTANCE TECHNIQUE

The instrument is shown in Figure 5.1. It has the following components:

1. The vacuum system
2. Vacuum chamber
3. Heat sink [sample holder]
4. Sensor.

The vacuum system has an ultimate vacuum of approximately 10^{-5} Torr. The initial rough pumping of the vacuum chamber was done by means of an Edwards single stage rotary pump, followed by an oil diffusion pump. A liquid nitrogen trap was interposed between the pump and chamber to prevent backstreaming of oil vapour from the diffusion pump and rotary pump into the vacuum chamber.

The vacuum chamber was made of brass and measured 210 mm in height by 150 mm in diameter. The inner walls were grit blasted and coated with 3M Nextel black paint [of emittance 0.97]. The high emittance inside wall surface results in

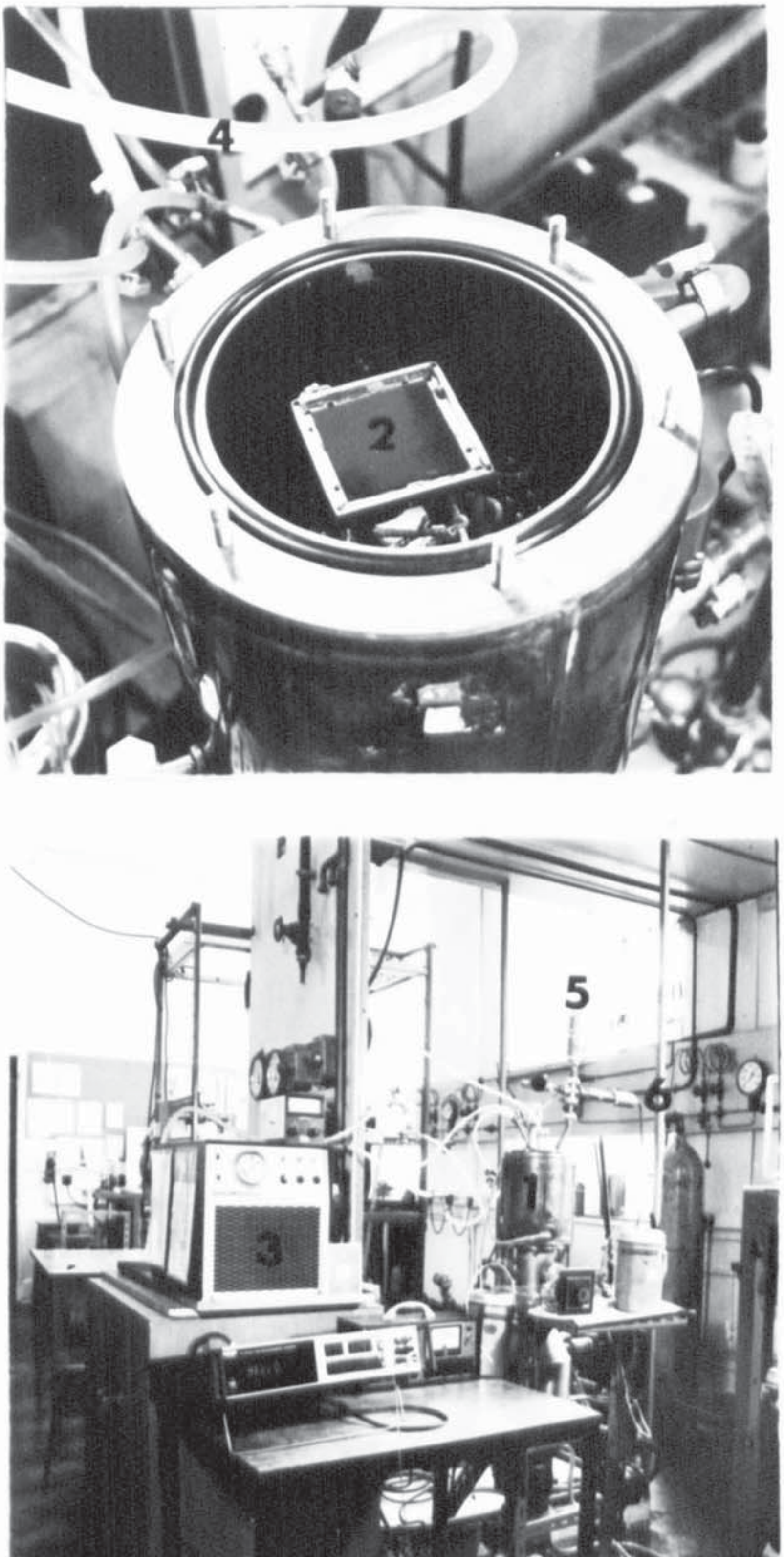

FIGURE (5-1) CALORIMETRIC INSTRUMENT

1) Vacuum Chamber 2) Sample

3) Closed Circuit System 4) Water Tube

5) Penning Gauge 6) Pirani Gauge

negligible reflected radiation from the chamber walls to the specimen. The vacuum chamber was surrounded by a copper jacket of a diameter of 160 mm, leaving a gap between the outer wall of the vacuum chamber and the inner wall of the copper jacket. The temperature of the vacuum chamber wall was regulated by circulating water through the gap with a controlled temperature by a closed circuit system, so that effective radiation can take place.

The temperature of the walls surrounding the sample was monitored by four pairs of Alumel-chromel wires of 0.125 mm each. Two mounted at the upper part of the inside wall facing each other, and the other two were mounted at the mid-way point on the inside wall opposite each other by using high temperature cement (AP*).

The heat sink was a block of copper with dimensions of 20 × 50 × 50 mm. This holder was equipped with two electric heaters (9 × 37 mm; 50 watt; 120 volt). Power to the heater was supplied by a power supply. The heat sink was mounted on a pointed glass support as shown in Figure 5.2.

---

* AP cement is a high thermal conductivity compound and is recommended when upper temperatures will not exceed 250°C for application. It is available from Omega Engineering Inc., (USA)

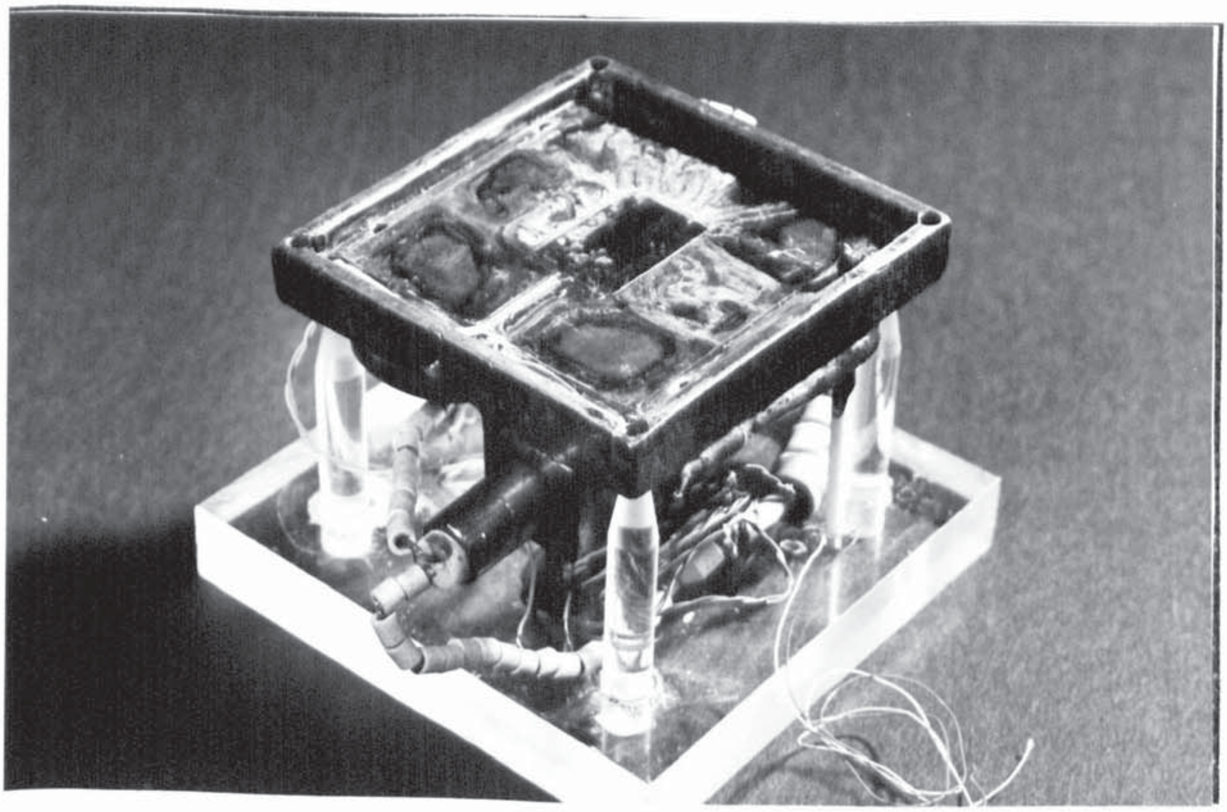

Figure 5.2 Photograph showing the heat sink and the sensor embedded in AP cement

The sensor is available from RdF Corporation (Hudson, USA) as RdF micro-foil, ie a heat flow sensor. Its function is to measure heat flow to and from an object.

The operating theory of the sensor is as follows: it is represented electrically and schematically as a multi-junction thermopile as shown in Figure 5.3.

The RdF microfoil is fabricated with homogeneous thermoelectric alloys in each leg between junctions. Also, each leg is made from 0.0002" foil, which greatly reduces thermal losses due to lead conduction. Thermoelectric junctions are

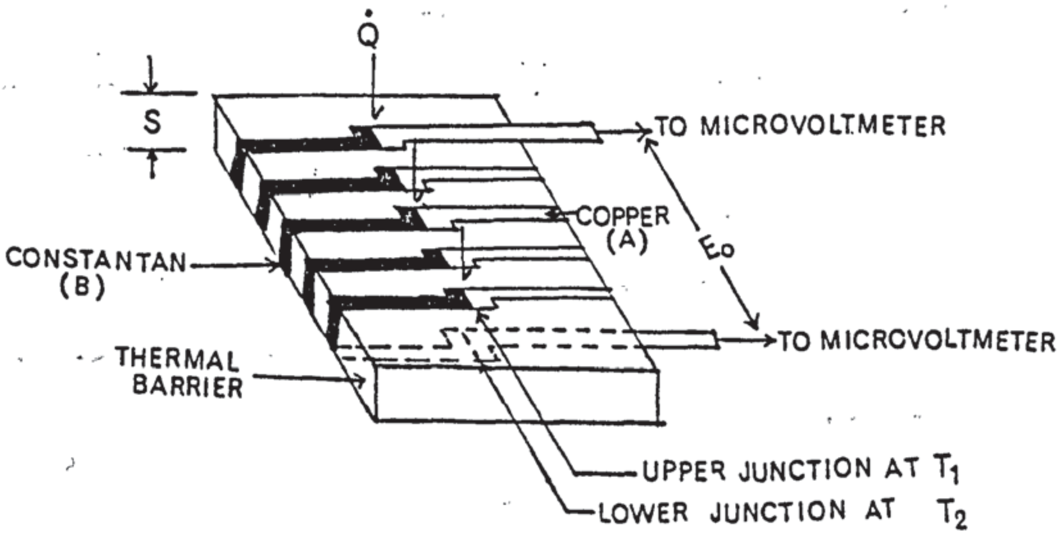

Figure 5.3 Sensor construction

formed from materials (A) and (B) on the upper surface of the barrier. In series with these are corresponding junctions on the lower surface. This construction results in an equal number of junctions on the upper and lower surfaces. The two output leads, therefore, are of the same material, with one coming from the first junction on the upper surface and the other from the last junction on the lower surface. Multiple pairs of junctions are used to generate a larger signal. The output signal is derived as follows:

The heat flow sensor is placed in contact with the surface for which heat transfer rates are desired. Therefore, the same energy must pass through the sensor as through the surface to which it is attached. Whenever thermal energy passes through the thermal barrier, a temperature difference ΔT is generated. This difference is directly proportional to the magnitude of the thermal transfer/sec., i.e. the heat transfer rate. Likewise, each pair of thermoelectric junctions forms a completed thermocouple circuit whose voltage output is proportional to the temperature difference ΔT. The factors which affect the magnitude of ΔT are the heat transfer rate, the thickness of the thermal barrier and the thermal conductivity of the barrier material. The following expression shows the relationship between these factors

$$T_1 - T_2 = \Delta T = \dot{Q} \frac{S}{K_b} \qquad [5.1]$$

where T_1 is the temperature of the upper junction

T_2 is the temperature of the lower junction

$\dot{Q}$ is the heat transfer rate/m^2.

S is the thickness of thermal barrier and

K_b is the thermal conductivity of the barrier.

For a more detailed treatment, one is referred to the article 'Thin Foil Heat Meter', by Hager [1965].

The following properties of the sensor have been used in the present design:

output at $21^{\circ}C$ difference = 3.15 W/m^2

response time: 0.4 seconds

lead polarity: (For heat flow into surface)
white = positive (+)
red = negative (-)

dimension = 20 × 15 × 0.3 mm, which is cemented into a 50 mm square Kepton Insulator.

temperature range: up to 250°C.

To compensate the flowmeter reading for the temperature dependent sensitivity of the sensor, a calibration chart provided by RdF Corporation has been used. This calibration chart is shown in Figure 5.4.

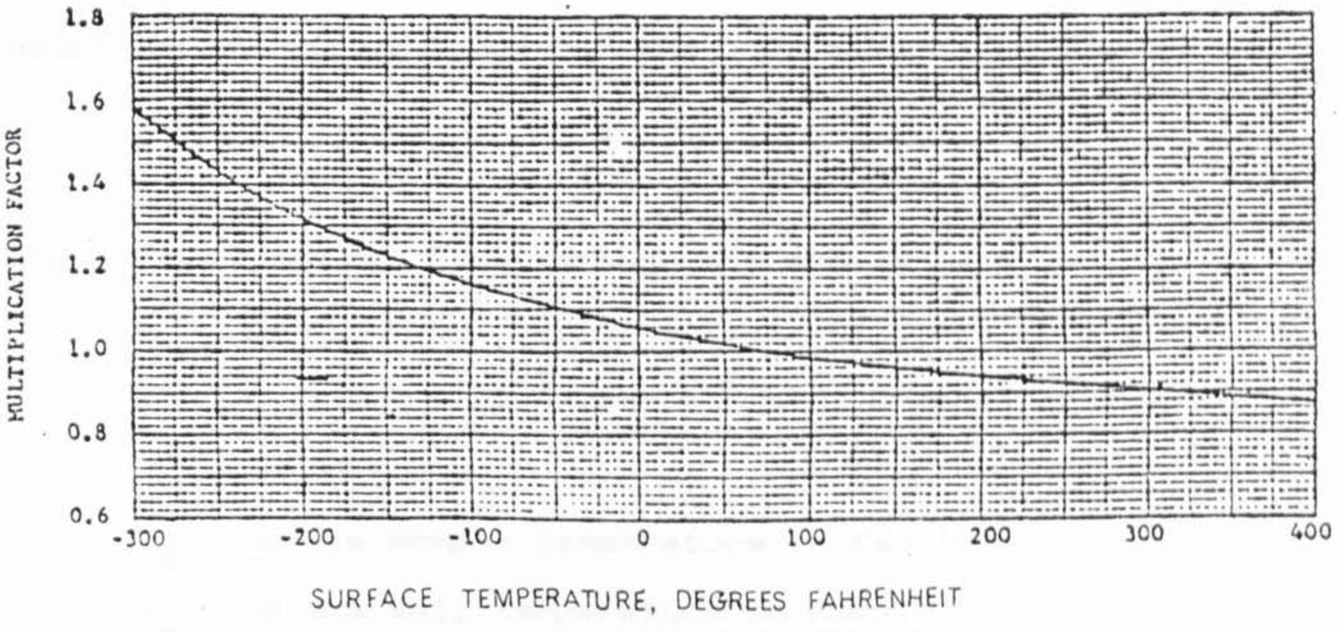

Fig. 5.4 Microheat flow sensor output multiplication factor versus receiving surface temperature (70°F Base).

5.3 BASE LINE EMITTANCE MEASUREMENT

The size of the sample used was 50 × 50 mm. The sensor is placed between the sample to be measured and a heat sink. AP cement is used to maintain good thermal contact between the sink, the sensor, and the sample. The entire assembly, as shown in Figure 5.2, is placed in a vacuum to minimize conduction through the residual gas.

One chromel-alumel thermocouple was sandwiched under the sample to determine the temperatures of the sample. The walls of the vacuum chamber were cooled by the flowing water. The sample was heated to a higher temperature than the walls. At equilibrium, the equation for the heat balance of the system is

$$F = e_{Hem}\sigma [T_S^4 - T_W^4] + K[T_S - T_W] \qquad [5.2]$$

where F is the heat flow through the sample [W/m^2]

e_{Hem} is the total hemispherical emittance of the sample

σ = 5.668×10^{-8} watt m^{-2} k^{-4}, Stephan-Boltzmann constant

T_S is the sample temperature in Kelvin

T_W is the wall temperature in Kelvin

and $K[T_S - T_0]$ is the heat losses, i.e. non-radiat[illegible] losses in watt m^{-2}.

From the equation above, it is readily seen that knowing the heat flow to the sample, the ambient temperature, and the value of the conductance loss from the surface, the total hemispherical emittance can be determined.

5.4 CALIBRATION OF THE CALIROMETER

Calibration of the calorimeter means evaluating the conductance term, i.e. $K(T_S - T_0)$.

The conductance term is evaluated by applying Mienal et al method (1976). According to this method, the calorimetric data of a known emittance sample is fitted to the equation 5.2 in the form

$$F = X\,(T_S^4 - T_W^4) + Y\,(T_S - T_W)^n \qquad (5.3)$$

using a least square fit to the coefficients X and Y. This fit was done for unit power for the conductance term (n = 1). The resulting values are the hemispherical emittance e_{Hem} and the conductance term, K.

Generally, the two most likely powers for the conductance term are n = 1 and n = 1.25. Since the measurement in this work was carried out in a vacuum of order of 3×10^{-5} Torr-10^{-5} Torr, the unity power for the conductance term was used; the fluid is in a stationary or stagnation condition, transferring heat by conductionm just as solids do. In this case, a parallel layer of stationary fluid of thickness L and having the temperature T_S on one face and $T_W < T_S$ on the other face, the heat flux, H_L, across the layer is simply

$$H_L = \frac{K}{L}\,(T_S - T_0) \qquad (5.4)$$

where K is the thermal conductivity of the fluid.

According to our instrument, the least square fit result gave the value of K divided by L. Thus by multiplying the least square fit result corresponding to the K value by the width of the layer from the top surface of the sample, the thermal conductivity of the reduced gas pressure inside the chamber can be evaluated.

5.5 TOTAL HEMISPHERICAL EMITTANCE AND CONDUCTANCE TERM DETERMINATION

Emittance testing for the sample to be investigated began when a pressure of 5×10^{-5} Torr had been attained and pumping continued throughout the test to maintain the lowest possible pressure, i.e. 10^{-5} Torr.

The sample under investigation was heated electrically to the desired test temperature.The reading was taken when the power and temperature stabilized. The temperature of the wall had been set at 293 Kelvin. After steady state conditions had been attained, the test continued at the steady state with the necessary measurements being made to determine the average temperature of the inside wall chamber, T_W, and the input heat flow to the sample, F. The observation continued at intervals of not less than 10 minutes, until three successive sets of observations gave values corresponding to T_S, T_W and F, differing by not more than 1-2%. The same method was also adopted for other sample temperatures.

By fitting the heat flow data for at least twelve temperatures to the equation 5.3 and using least square fit as mentioned previously in Section 5.5, the resulting values of e_{Hem} and K for quartz, pure nickel (as supplied, INCO) and 3M-Nextel black paint have been determined and tabulated in Table 5.2.

Sample	e_{Hem} %	K	n
Quartz	81.03	0.81	1
Pure nickel (INCO)	18.3	0.83	1
3M-Nextel black paint	96.23	0.80	1

Table 5.2 Values of e_{Hem} and K in equation 5.3 as determined by least square fit to heat flow data, F(T) for quartz, pure nickel and 3M-Nextel black paint

The result obtained on the above samples fits the flow equation given below:

$$F = e_{Hem} \sigma (T_S^4 - T_W^4) + 0.82 (T_S - T_W) \qquad (5.5)$$

and are shown in Figure 5.5.

Calorimetric measurements data of F(T) for the supplied polished 304 stainless steel, 5 mV (blue colour) and black nickel samples were also taken.

The value of the hemispherical emittance for each of the above samples was calculated from four to five of the heat flow data, F(T) around temperature T = 373 Kelvin and 473 Kelvin by using the equation 5.5. The results are tabulated in Table 5.3.

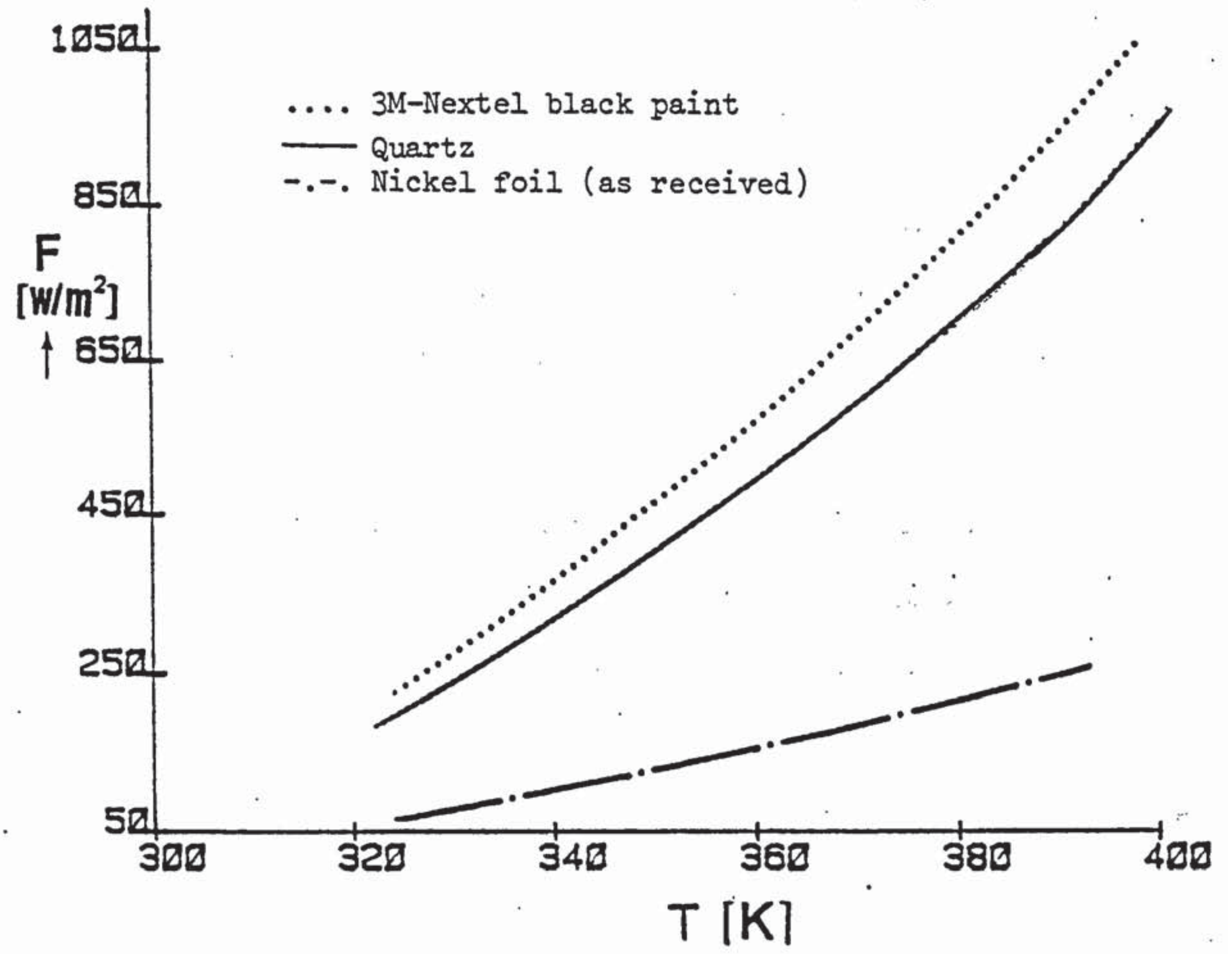

Figure 5.5 Least square fit of the flow equation 5.5 to data Flow F[T] versus temperature for quartz, nickel [as supplied] and 3M-Nextel black paint

Sample	Total hemispherical emittance % [measured]		Near normal emittance % [calculated]	
	e_{Hem} [100°C]	e_{Hem} [200°C]	e_n [100°C]	e_n [200°C]
304 s.s. [polished] as supplied by INCO	12.1	13.03	9.1	10.01
5 mV [blue colour, INCO surface]	11.0	13.12	10.0	11.1
Black nickel foil		20.24	13.7	16.91

Table 5.3 The measured total hemispherical and the computed near normal emittance values of 304 s.s., 5 mV and black nickel samples at 373 Kelvin and 473 Kelvin

5.6 DISCUSSION OF THE RESULTS

The thermal conductance of air as reported in the American Society of Heating and Refrigeration Engineers (ASHRE) Handbook of Fundamentals is 0.024 watt/m°c. This value is for atmospheric pressure.

In equation 5.5 the quantity K is the thermal conductance divided by an effective separation between the walls and the sample. For our instrument this separation is about 2 cm, so that the value of the conductance is K = 0.82 × 0.02 = 0.016 W/m°c. This value is reasonable and lower than 0.024 because our measurements were done in a vacuum of the order of (4-1) × 10^{-5} Torr.

Table 5.3 suggests that the values of total hemispherical emittance measured by this instrument for the 304 stainless steel, 5 mV and black nickel foil samples were found to be higher than the computed values of the normal emittance from the measured room temperature spectral reflectance. This leads to the conclusion that the total hemispherical emittance is always significantly above the normal emittance for such surfaces. This is in agreement with the conclusion drawn by Hutchins (1979) in his study of selective surfaces. However, Mienel et al (1975) reports conflicting conclusions in their study.

Because the emittance is a surface dependent property, there are at present no emittance standards that can be used for absolute calibration purposes. However, the values of emittance obtained for the same sample on the separate runs show only a marginal variance of 2% to 5% emittance units. Also, the results obtained on polished stainless steel (304 type), quartz, and 3M-Nextel black paint reasonably agree with those previously reported in published literature (see Table 5.4 below).

Sample	Hemispherical Emittance e_{Hem} %		References
	present work	published work	
304 s.s. type	12.2	11.15	Roger et al (1979)
Quartz	82.03	67.0 - 94.0	Optical Engineering Handbook, J.A.Mauro, Ed; General Electric Co., Publishers
		84.0	Bacha et al (1962)
		84.0	Mienel et al (1975)
3M-Nextel black paint	96.23	80.0 - 97.0	ASHRE Handbook of fundamentals, American Society of Heating, Refrigeration and Air-conditioning Engineers, New York, N.Y.

Table 5.4 Comparison of measured hemispherical emittance and the published values for 304 stainless steel, quartz and 3M-Nextel black paint.

5.7 ERROR ANALYSIS

It is difficult to determine the exact measurement of the errors inherent in this measurement technique. However, it is possible to give a qualitative estimation of errors resulting from the following:

(i) RADIATION LOSSES FROM THE SAMPLE EDGE

To achieve the desired accuracy in measuring the emittance, it was necessary to have the edges of the sample carefully surrounded by the copper heat sink. The sample size should be the same size of the sensor to avoid a large radiation loss from the sample edge to the cold wall.

(ii) CHAMBER WALL REFLECTIONS

Equation 5.2 is based upon the assumption that all radiation emitted from the sample under investigation is absorbed by the inner surface of the wall chamber. In reality, some of the radiation emitted by the sample can be reflected from the chamber wall surface back onto the sample. To minimize this effect, the inner surface was coated with 3M-Nextel black paint to provide a highly absorbing surface.

(iii) STATISTICAL ERRORS

The statistical errors could be caused by temperature measurement and conduction from test section. We tried to minimize this factor by:

(a) the use of the thermocouple wire of diameter 0.13 mm and of minimum size;

(b) the attachment of the wires of the thermocouple by spot welding;

and (c) the use of four pairs of thermocouples to measure the temperature of the walls in order to provide a representative average.

(iv) <u>HANDLING THE SAMPLE</u>

Handling the sample by hand can result in the contamination of the surface of the sample and this could result in an error in measurement. We tried to avoid doing that.

CHAPTER 6

CONCLUSIONS

In the preceeding chapters we discussed briefly the results of experiments on various surfaces, namely, titanium oxide/titanium, titanium oxide/aluminium, five different coloured INCO surfaces, thermally oxidized stainless steel types 304 and 316 and the black nickel foil, leading to the design of a calorimetric instrument for measuring the hemispherical emittance directly. In this concluding chapter, we shall discuss in detail the performance of these surfaces as measured by the techniques used in this study.

6.1 TITANIUM OXIDE / TITANIUM

6.1.1 OPTICAL CONSTANTS

The present work clearly shows a slight absorption for titanium oxide over the visible region of the spectrum. Table 6.1 gives the values of optical constants obtained by other workers for titanium films and bulk titanium and can be compared with the present values given in Table 4.1. In the region of 580 nm the present values lie between those of Hass (1955) for films deposited in U.H.V. and those of Minard (1962) for mechanically polished material. At a wavelength of 540 - 550 nm published values of n lie between 1.78 and 2.08 for mechanically polished surfaces in air to 3.09 for bulk material polished in U.H.V., Hass and Bradford (1957); Carrol and Melmed (1974);

Mash and Motulevich [1973]; Smith [1972] and Kivillova and Charikev [1963]. The highest value of n for films deposited in U.H.V. is 3.03. It can be assumed in general that the cleaner the surface the higher will be both the n and k values. Published values for k over the same wavelength region vary from 3.73 for films prepared in U.H.V. to 2.46 for mechanically polished bulk. The optical constants of n = 2.36 and k = 3.28 at a wavelength of 546.1 nm found in this work are lower than the best values reported for U.H.V. films but higher than for bulk samples polished in air, thus indicating a good quality substrate for the oxide growth in this work.

Hass and Bradford [1957] reported k = 0 for the oxide, and obtained a value of n = 2.7 at a wavelength of 546 nm on evaporated titanium film. Minard [1962] gave values of n = 2.4 and k = 0.17 in the wavelength range 588.9 nm for titanium oxide thermally grown in oxygen at 755 degrees Kelvin. The values for air grown titanium oxide obtained in the present work show only a small variation in n from 2.45 to 2.38 over the wavelength range 576.6 nm to 397.1 nm. This result agreed with Yoshida [1979], who reported that TiOx [$x < 2$] is a slightly absorbing film and has a range of values of the extinction coefficient k, in the spectrum range [wavelength 0.2 μm to 2.4 μm] with a peak value of k = 0.50 at 1.1 μm.

The difference between the results for the optical constants of titanium and titanium oxide reported here and those reported in the literature [Table 6.1] is many times the

the estimated error of measurement. It is of great importance to obtain and demonstrate surface cleanliness to obtain accurate values for the optical constants. However, if care in measurement of the angle of incidence is neglected large errors of n and k can result, as shown in Section 3.1.7.

6.1.2 SELECTIVITY

Titanium, oxidized, by heating in air, gives rise to a moderate selectivity from the antireflection oxide film. Its derivative oxide film produces a value of a = 0.77 and e(100°C) = 11.7% for 25 minutes heating at 750 Kelvin, which gives an a/e value of 6.6.

However, the spectral characteristics of oxidized titanium in Figures 4.3b and 4.5 suggest an interference effect. Figure 4.5 also shows that the reflectance of this system in the infrared (IR) is low. This is because the reflectance of the stack in the IR is influenced by the reflectance of metal underlayers. Since titanium has lower reflectance than aluminium in the IR region, the low reflectance of the above system in this region is caused by poor reflectance of the titanium underlayers.

Edwards et al (1962) reported a/e ≈ 3 for as received titanium sheet and after heat treatment in air for 100 hr at 698 degrees Kelvin compared with 6.6 for this work. The low value of 3 could be attributed to the effect of the finishes of the layer underneath the surface film, again indicating the importance of surface preparation.

λ	n	k	R%	Sample	References
436.0	2.40	2.85	51.3	Ti-film prepared in UHV	Hass and Bradford (1957)
546.1	2.53	3.33	57.0	Ti-Film prepared in UHV	Hass and Bradford (1957)
546.1	3.03	3.73	59.8	Ti-film prepared in UHV	Carroll and Melmed (1974)
578.0	2.64	3.42	57.6	Ti-film prepared in UHV	Hass and Bradford (1957)
650.0	3.03	3.65	58.5	Ti-Film prepared in UHV	Hass and Bradford (1957)
540.0	1.78	2.46	48.2	Ti (bulk 0001), air mech.polished	Carroll and Melmed (1974)
540.0	2.03	3.09	56.6	Ti (Bulk) air mech. polished	Carroll and Melmed (1974)
540.0	2.22	2.91	52.8	Ti (Bulk) air elec. polished	Mash and Motulevich (1973)
546.1	2.96	3.70	59.7	Ti (Bulk 0001) cleaned in UHV	Smith (1972)
546.1	3.09	3.40	56.6	Ti (Bulk-polycrystalline) cleaned in UHV	Smith (1972)
550.0	1.85	3.15	58.9	Ti (Bulk) air polished	Kirillova and Charikov (1963)
588.9-589.5	2.41	3.24	-	Ti (Bulk) mech. polished	Menard (1962)

Table 6.1 Titanium optical constants

6.2 TITANIUM OXIDE/ALUMINIUM

The spectral reflectance curves for titanium oxide films on aluminium sheet are given in Figure 4.6 with the results tabulated in Table 4.5. These suggest that the sample with an evaporated mass of titanium of 0.05 gm [producing a film of about 30 nm thickness] on aluminium after four hours heating at 670 degrees Kelvin is more selective than the sample with 0.09 gm of titanium evaporated [producing a film of thickness of about 50 nm.] Figure 4.6 also indicates that a 50 nm deposit layer of titanium shows a rapid rise in reflectance [about $\lambda = 2\ \mu m$] from low reflectance in the visible to high reflectance in the infrared as required for a selective surface.

The selectivity $\underline{a}/\underline{e}[100^{\circ}C]$ of this system is equal to 9.5 and the colour is dark blue. This colour changes to light blue and the emittance starts to increase after prolonged heating at the above temperature.

By using the supplied polished aluminium sheet as the underlayer material, monitoring the thickness of deposited titanium film and then oxidizing it in air, a tandem stack is produced. This tandem leads to an increase in the selectivity by the order of about 3 compared with the previous tandem stack system of titanium oxide on titanium.

An attempt was made to deposit the same amount, for example 50 nm, of titanium on previously heated aluminium sheet [3 hours at 670 degrees Kelvin]. The same result for the absorptance was obtained but an increase in the emittance from 10.99% to 14.38% at 100°C was observed. This is because of the lowering of the reflectance of the underneath layer, i.e. aluminium sheet as a result of previous heating, as shown in Figure 4.7.

The absorptance for the titanium oxide/titanium and the titanium oxide/aluminium (unheated) systems were in the range of 0.78 to 0.80, with the emittance of 8.4% respectively. The low numbers of the absorptance were due to a combination of the narrowness and the non-flatness of the reflectance minima over the visible region.

6.3 CHEMICALLY COLOURED STAINLESS STEEL [INCO SURFACES]

6.3.1 ELLIPSOMETER RESULTS

[i] BASE METAL

Characterization of the base metal, i.e. 304 stainless steel, is reported in Section 6.4.1.

[ii] FIVE DIFFERENT COLOURED INCO SURFACES

Figure 4.8 shows plots of ψ and Δ for the five different coloured samples before and after heat treatments. This figure, together with the results of the spectral reflectance curves shown in Figure 4.10, suggest that the lowest values of ψ and Δ correspond to the best selective surface, which is the sample corresponding to 5 mV [for unheated samples]. Figure 4.8 also shows the effect of oxidation for different time periods. The values of ψ and Δ decreased for all the samples after 192 hours at 210°C and for 160 minutes at 300°C, i.e. the thickness of the oxide layer increased. However, the value of Δ corresponding to 5 mV is still the lowest, while the value of the absorptivity, after this heat treatment, is highest for this sample, i.e. it still has the best selectivity. Although after 160 minutes heating the samples at 300°C causes a decrease in the absorptance of the samples of 5 mV, 7 mV and 9 mV, while for the 1.5 mV and 3 mV samples heating for 160 minutes at 300°C also increases the oxide thickness but their absorptance also increases.

Figure 4.8 also shows the effect of oxidation on these two parameters ψ and Δ for the above samples for prolonged heat treatment, i.e. 192 hours at 300°C. It indicates that only the Δ value of the 5 mV sample increased by $\sim$ 80 degrees and the sample corresponding to 3 mV has the lowest values of ψ and Δ after heating for 192 hours at 300°C.

Table 4.9 shows that the absorptivity of the samples which have sustained prolonged heating at 300°C is lower than that of the corresponding unheated samples. However, the absorptivity of 3 mV sample was found to be higher than that of the others after prolonged heating, whereas it still gives the lowest Δ value after prolonged heating, as shown in Figure 4.8.

These observations suggext that there is a correlation between low Δ value for a sample or set of samples and better selectivity.

We tried to explain the fluctuation in results of ψ and Δ values of the five different coloured INCO samples by investigating whether it is due to the stress or anisotropy in the oxide layer of the above samples, by using the ellipsometer. The following tests were designed for the above purpose for three samples corresponding to 5 mV (unheated).

1. The values of ψ and Δ have been measured for each sample. Two samples were taken out of the oven after heating for 3½ hours at 573 degrees Kelvin. One was left to cool down

to room temperature slowly in air and the other one quenched in the ice bath straight away. The third sample was left to cool to room temperature inside the oven, which had been switched off. The measurement of ψ and Δ after the above processes are given in Table 6.2.

2. The above three samples were then heated for a further 2½ hours at 300°C; the values of ψ and Δ for each sample were also measured and tabulated in Table 6.2. This table suggests that the quenched process suppresses the oxidation because nearly the same values of Δ were obtained before and after heating for 2½ hours at 300°C. For the sample which was left inside the oven to cool down to room temperature, this table shows that the oxidation continued during the heating for the 2½ hours at 300°C, ie the Δ value increased by 10 degrees, but it showed a change of 3 degrees in Δ value after heating for 2½ hours at 300°C for the sample which was taken out of the oven to cool down to room temperature, i.e. the rate of oxidation for this sample was lower than that of the previous one. In summary, this test indicates that no stress could be detected.

For the purpose of anisotropy test, the sample corresponding to 5 mV has been rotated through 90 degrees, 180 and 270 degrees and the two angles ψ and Δ have been measured in each case. The result was found to be the same as that of the unrotated sample. This means that there is no possibility of anisotropy being detected in the film.

These tests suggest that since there was no detectable stress or anisotropy, the actual changes in ψ and Δ of the stainless steel samples could not be attributed to either of these possibilities, but could possibly be attributed to the structure.

The optical constant could not be determined for the coloured stainless steel samples supplied by [INCO] as has been done for thermally grown oxides of titanium. Further studies are needed for every sample using various parameters of deposition and taking the measurements by ellipsometry and direct measurement of the reflectance during the process of deposition. The implication here is that the optical constants of the film could be changing with the thickness.

5 mV Samples		ψ Degrees	Δ Degrees
Sample [1]	unheated	19.0	114.89
	heated 3½ hr [320°C] then quenched in ice bath	22.73	21.77
	+ 2 hr heating 320°C	23.25	20.93
Sample [2]	heated 3½ hr [320°C] then cooled outside the oven to room temperature	19.85	35.30
	+ 2 hr heating 320°C	21.16	28.87
Sample [3]	heated 3½ hr [320°C] then the sample cooled to room temperature inside the oven	22.74	27.22
	+ 2 hr heating 320°C	22.95	24.20

Table 6.2 The experimental values of the sample corresponding to 5 mV process exposed to different conditions after heating for 3½ hours at 320°C.

6.3.2 SELECTIVITY

The reflectance spectra of the five coloured stainless steel samples illustrated in Figure 4.9 and the calculated absorptances of the above samples which are illustrated in Figure 4.10, suggested that the greater selectivity was exhibited by the blue coloured sample of the 5 mV process, where $\underline{a}$ = 0.865 with $\underline{e}(100^{\circ}C)$ = 0.10 were found. Although the reflectance spectra for the above samples, as shown in Figure 4.9, demonstrates gentle wavey fringes occurring in the solar region towards the shorter wavelength, the absorption in the film decreases the fringe amplitude.

This could probably be due to the interference phenomena occurring between the two surfaces of the film.

Figure 4.11 suggests that the absorptivity of these films decreases with the increase of the off-axis angle. This dependence decreases the collector efficiency when the solar beam is projected obliquely with respect to the collector. It is, however, preferable to decrease such an effect by producing a diffuse reflection film. In order to absorb the radiation at all angles, the need for tracking will be minimized and the diffused radiation will be absorbed.

It is also found that the coloured INCO stainless steel samples were insensitive to dirt and could be cleaned by swabbing with detergent solution without changing their optical properties, i.e. the calculated absorptance and the emittance values were the same before and after the cleaning process.

6.3.3 LIFE TESTING

The tests of continuous annealing in air at temperatures of 110°C and 300°C for the five different coloured stainless steel INCO samples are given in Figures 4.12 to 4.16. They show a slow shift of interference fringes to longer wavelength for all the samples for a short heating period, i.e. for 48 hours up to a temperature of 110°C. This shift is seen to be rapid when both the period of heating is extended to 192 hours and the temperature increased to 210°C, and is more rapid at a higher temperature. For example see the curves for each sample.

During the annealing at 110°C for 48 hours, the reflectance of 1.5 mV and 3 mV samples decreased over the solar range extending from 0.4 μm to 1.5 μm, corresponding to an increase in the a values of about 2.8% and 2% respectively, as shown in Table 4.9, while a slight shift change in the reflectances occurred over the above range of wavelengths for the 5 mV, 7 mV and 9 mV samples. These results gave nearly the same values of a and e as those for unheated ones.

After 192 hours of heating at 210°C, the reflectance of the 1.5 mV and 3 mV samples over the solar range of 0.40 μm to 1 μm decreased, corresponding to an increase in the a value of about 4% and 2% respectively, while the slight increase in the reflectance which occurred for the 5 mV sample gave no subsequent changes in the corresponding a value, but the increase in the reflectance which occurred for the samples of 7 mV and 9 mV caused a decrease in the a value of about 1% and 4% respectively, as shown in Table 4.9.

A set of coloured samples were subjected to heat treatment at 300°C for different time periods of 5 minutes, 60 minutes, 160 minutes and 192 hours. All the samples showed the same pattern of the reflectance spectrum as in the case of the 5 mV sample [see Figure 4.17]. This figure illustrates the rapid movement of the interference fringe with the time of heating at 300°C and toward the long wavelength. The changes in the reflectance spectrum over the solar range for the 1.5 mV and 3 mV samples gave an increase in the a value of about 4% for up to 60 minutes heating. For 5 mV, 7 mV and 9 mV samples a decrease in the a values of about 3% respectively was shown. However, the a value of 3 mV sample remained unchanged.

After 192 hours of heating at 300°C the reflectance of all the INCO samples increased over a wavelength range 0.4 μm to 0.6 m. The interference fringe shifted rapidly towards the longer wavelength, as shown in Figures 4.12 to 4.16, corresponding to a decrease in a values from those carried out for the 160 minute test at the same temperature (300°C). These decreases were 3% for the 1.5 mV; 5% for the 3 mV; 8% for the 5 mV; 5% for the 7 mV and 5% for the 9 mV sample. These results have been tabulated in Table 4.9, i.e. the absorptance values of the samples decreased at this temperature even after 60 minutes heating and the colours changed too.

This effect occurred even at 250°C when the samples were heated for 48 hours.

The result of the cycling test in air for the three sets of INCO samples were found as follows:

(i) After cycling between temperatures of 50°C and 110°C at a rate of 4 cycles/hr up to 48 hours, the 1.5 mV sample gave an increase in the a value of about 2%. The 3 mV, 5 mV, 7 mV and 9 mV samples showed stability during the above test.

(ii) After cycling between temperatures of 50°C and 210°C at a rate of 4 cycles/hr up to 48 hours, the 1.5 mV sample gave an increase in a value of about 2% and gave nearly the same value of a as that of the unheated 3 mV sample. The 5 mV, 7 mV and 9 mV samples showed stability during the above test.

(iii) After cycling between temperatures of 40°C and 210°C at a rate of 2 cycles/hr up to 192 hours, the 1.5 mV sample gave an increase in a value of about 2%. The 3 mV sample gave nearly the same value of a as that of the unheated sample. The 5 mV, 7 mV and 9 mV samples showed a decrease in the absorptance value of about 2%, 2% and 3% respectively.

Summarizing the results of the life test, we saw that the effect of annealing on the spectral profile is limited to wavelengths smaller than 2 μ m. In the higher reflectance range, the reflectance is nearly constant.

The blue coloured 5 mV INCO sample displayed the highest selectivity of all other samples. It was also found to be stable up to 210°C heating and for short periods of cycling at this temperature, i.e. between 50°C and 210°C. However, it started to deteriorate after longer periods of cycling at the above temperature, although the 1.5 mV and 3 mV samples showed an increase in selectivity upon heating up to 300°C for short periods. The highest value still remained lower than that of the 5 mV sample (unheated). The 7 mV and 9 mV samples displayed a decrease in selectivity on heating even for short periods at 300°C.

Karlsson and Ribbing (1978) reported that the water content for their green coloured stainless steel sample was one of the two mechanisms which caused the deterioration of selectivity, and they could detect this mechanism by the movement of the interference fringe towards the short wavelength region as the water leaves the film.

Since the water release before the oxidation commences in the vacuum environment, the results of the spectral reflectance of this test at 300°C and in a soft vacuum, as shown in Figure 4.23, followed the same pattern as that of the continuous heating.

Since there was no such movement of the interference fringe towards the shorter wavelength during the heating, either in air or vacuum, we conclude that the oxidation mechanism was responsible for the deterioration of the INCO coloured stainless steel at high temperatures above 210°C; further heating and oxidation increases the optical thickness of the film and moves the fringes to longer wavelengths. This pattern was detected in the life test while heating either in air or vacuum for low temperatures and for high temperatures up to 300°C and for different periods of time.

6.3.4 STABILIZATION OF THE OXIDE LAYER

Figures 4.24 to 4.28 illustrate the spectral reflectance curves obtained when a layer of Si_3N_4 (250 nm) was coated on the coloured stainless steel samples. These figures showed that the first fringe was located at about 2.5 μm to 3 μm. This location causes the decrease of reflectance in thermal region which in turn increases the emittance.

The above figures also include the curves of the coloured stainless steel set with a 125 nm thickness of Si_3N_4. The fringe was located between 0.9 to 1 μm for the samples corresponding to 1.5 mV and 3 mV. This causes an increase in the absorptance of the above samples to 0.897 and 0.899 respectively, while the location of the fringe for the 5 mV sample was slightly beyond 1 μm. The absorptance of the sample corresponding to 5 mV was found to be the same as that of the uncoated sample with Si_3N_4, but the absorptance of the 7 mV and 9 mV samples coated with 125 nm Si_3N_4 decreased, corresponding to the high reflectance in the solar range (see Table 4.9).

The coated Si_3N_4 (125 nm thickness) coloured stainless steel samples showed thermal stability for 3½ hours heating at $300^{o}C$, i.e. the calculated values of the absorptance and the emittance were found to be the same before and after heat treatment (see Table 4.9).

The promising result in the case of the Si_3N_4 (125 nm thickness) coated coloured INCO samples needs further investigation in order to stabilize them against deterioration at higher temperatures.

Summarizing the stability test, we can state that the absorptance of the samples corresponding to 1.5 mV and 3 mV, coated with 125 nm thickness of Si_3N_4 increased from 0.75 to 0.896 and from 0.796 to 0.899 respectively, and were stable after heating for 192 hours at $250^{o}C$ and for 3½ hours at $300^{o}C$. There is an overall improvement in the selectivity characteristics due to the addition of a layer of Si_3N_4, 125 nm thick.

6.3.5 COMPOSITION ANALYSIS

The results from Figures 4.31 and 4.32 suggest that the chlorine, carbon and sulphur were concentrated at the air/oxide boundary but persist throughout the bulk of the surface films. This is probably due to the handling of the sample and to the acidic path treatment. However, the chlorine disappeared after 20 minutes of sputtering.

Figures 4.33 and 4.34 demonstrate that the chromium content of the oxide film exceeds that of the substrate because of the deposition from the acidic solutions (chromic acid).

The iron content decreases gradually toward the film surface. The nickel content follows the same pattern. The metallic chromium content increases rapidly through the oxide film up to 200 minutes of sputtering, after which it starts decreasing with the decrease of the oxide layer thickness.

The oxygen content increases gradually from the surface oxide film and after 50 minutes of sputtering reaches a peak value of concentration ~ 20% for the 5 mV sample and 24% for the 9 mV sample after 150 minutes of sputtering time. The oxygen content then starts decreasing with a decrease in the oxide layer thickness.

The boundary between the oxide layer and the metal substrate corresponds to the point where the concentration of the iron deviates from the horizontal portion, as shown in Figures 4.33 and 4.34. Thus, the thickness of oxide on the 5 mV sample is about 100 nm and that of the 9 mV sample is about 200 nm. The above results suggest that the surface oxide films corresponding to the 5 mV and 9 mV samples were rich in chromium with smaller quantities of iron and nickel present.

Figure 6.1 shows the comparison of the iron, chromium and nickel concentrations with the sputtering time from 100 to 2000 minutes for the 5 mV and 9 mV samples. This figure indicates that the iron concentration increased linearly for the 5 mV sample up to 500 minutes of sputtering time, while the curve of the 9 mV sample shows a flat portion at 100 to

500 minutes of sputtering time. The chromium concentration of both samples decreased linearly. The nickel concentration for both samples was found to be equal up to 500 minutes of sputtering time.

In summary, the composition of the oxide corresponding to the 5 mV sample and the metal in the film changes linearly.

The chromium to oxygen ratio within the film up to 500 minutes of sputtering time is slightly greater for a surface film obtained from a 5 mV process than from that of a 9 mV process.

Finally, the 5 mV sample with the oxide layer thickness of about 100 nm appeared to confer a favourable selective surface among the other INCO surfaces, i.e. 1.5 mV, 3 mV, 7 mV and 9 mV samples.

We believe that further composition analyses are needed for each sample before and after heat treatment in order to investigate the optimum oxide composition which gives the favourable optical properties. To predict the thermal ageing mechanisms, further studies are needed in respect of each colour of the INCO surfaces in order to determine how the structure and composition change upon thermal ageing.

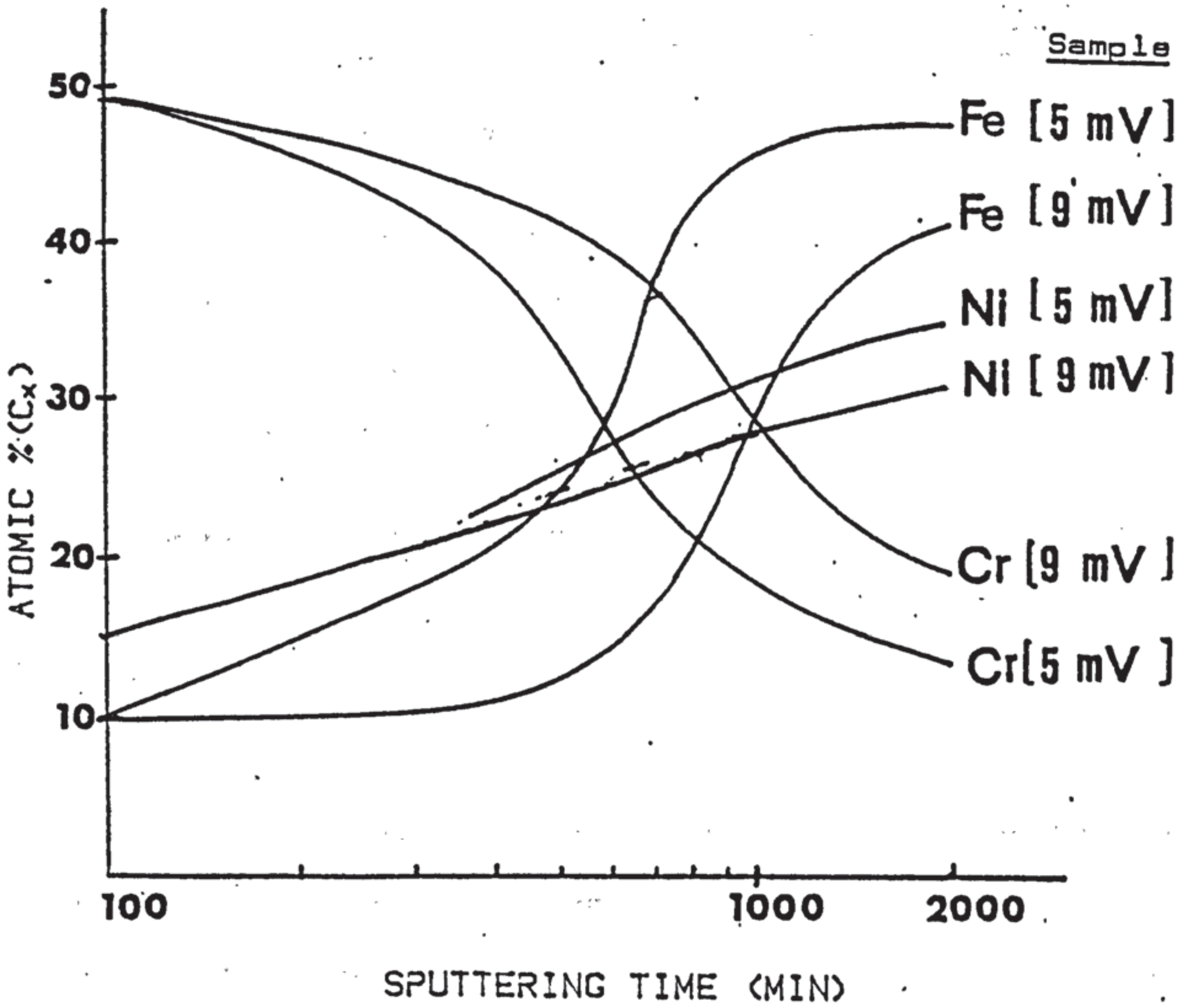

Fig. 6.1 Comparison of the depth profile for the 5 mV and 9 mV samples.

6.4 THERMALLY OXIDIZED STAINLESS STEEL TYPES 304 & 316

6.4.1 ELLIPSOMETER RESULTS

The optical constants of the stainless steel polished surface of the two types as determined by ellipsometer at the wavelength of light radiation 546.1 nm, were 2.28 - 3.7i for 304 stainless steel and 2.30 - 3.70i for 316 stainless steel.

These results show agreement with those of Fane et al (1973), i.e. 2.28 - 3.77i and Latham and Brah (1977), i.e. 2.35 - 3.70i.

The oxidation rate was found to be temperature dependent and it was higher for the 304 stainless steel type than for that of the 316 type at the same temperature (see Figure 4.35).

The diffuse surface which results from the thermal oxidation process made the investigation of the optical constants of thermally oxidized film more difficult and only a limited number of readings of ψ and Δ were possible.

6.4.2 SELECTIVITY

Stainless steel oxidized by heating in air gives rise to a moderate improvement in selectivity from the value for the metal substrate with its original oxide layer. The best optical properties of the surface films were found with 304 and 316 stainless steel types when heated at 973 Kelvin for

6 and 90 minutes respectively, see Figure 6.2. The value of absorptance for both was found to be 0.75. It could not be improved, even by heating for longer periods at this or higher temperatures. On the other hand, the value of the absorptance decreased but the emittance increased when the sample was heated for longer periods. Moreover, the colour of the sample also changed from dark blue to grey (see Table 4.13).

Figures 4.36 and 4.37 show that the value of reflectances for the wavelengths longer than 8 μm remain constant and approach the reflectance of polished bulk stainless steel. During heating either at 823 or 973 Kelvin, the shift of the reflectance showed the same pattern for the sample at different sintering times at either temperature, but with an increased time of heating, the fringe shifted towards longer wavelengths, indicating an increase in the oxide thickness. These fringes suggested that the moderate selectivity of this simple method is obtained by interference between the two surfaces, the substrate and its derivative oxide. Investigations of oxidation at higher temperatures, for example 1198 Kelvin, was carried out, but the rate of oxidation was too rapid to be effectively controlled. Our results here show a marked contrast to those of Sharma and Hutchin (1979) for stainless steel. . Table 6.3 gives details of the comparison.

Figure 6.2 also includes the specular reflectance curve for the INCO surface corresponding to 5 mV sample. This figure indicates that the INCO process shows more selectivity than the simple heating process, i.e. the reflectance for the INCO surface over the solar range from 0.35 μ m to 2 μ m is lower than that of 304 and 316 types of stainless steel at 973 Kelvin.

Sample	Heating temp. Kelvin	Heating time [min]	Present work			Reported work*		
			$\underline{a}$%	e_n [100°C]	colour	$\underline{a}$%	e_n [100°C]	colour
316 s.s.	823	25				77.0	20.0	-
316 s.s.	973	90	74.0	11.3	dark blue	-	-	-
316 s.s.	1198	10	74.0	9.8	dark blue	-	-	-
304 s.s.	1043	45				70.0	5.0	purple
304 s.s.	973	6	75.0	9.5	dark blue	-	-	-
304 s.s.	1198	5	75.0	8.5	dark blue	-	-	-

Table 6.3 Comparison of the calculated optical properties of thermally oxidized stainless steel with the published data.

---

* Sharma and Hutchin [1979]

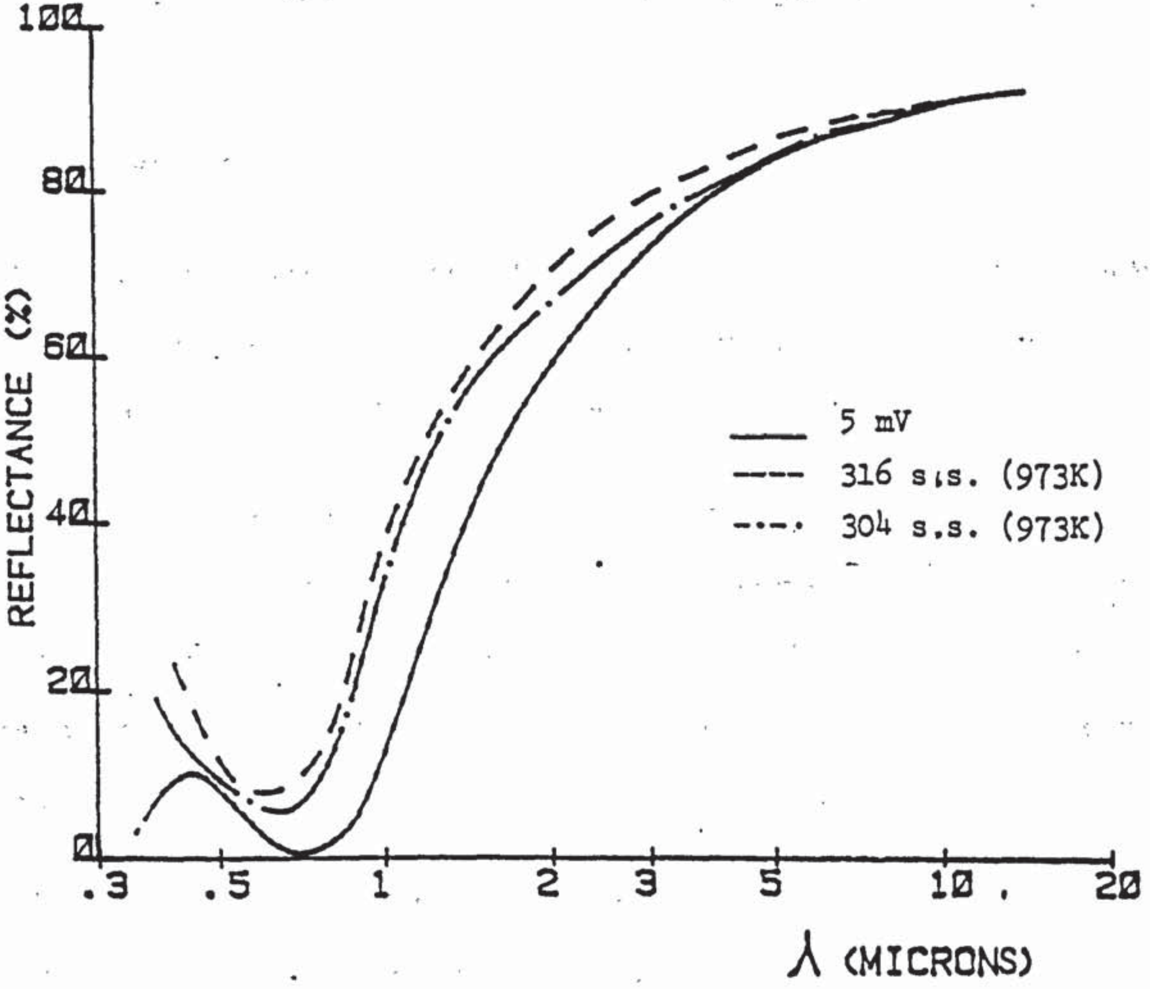

Fig. 6.2 Comparison of specular reflectance for 6 mV and thermally oxidized stainless steel types 304 and 316 samples.

6.5 BLACK NICKEL FOIL

The application of black nickel foil [bonded] on to either stainless steel or aluminium was found to be equally feasible.

6.5.1 SELECTIVITY

The absorptance and emittance values of a set of black nickel foil samples were calculated. The average values found were $\underline{a} = 0.986$ and $\underline{e}(100^{\circ}C) = 0.136$.

The actual manner in which the reflection of the surface varies over the visible spectrum can be seen for the unheated and heated sample from Figures 4.38 and 4.40. It indicates that heating has no effect on the reflectance at short wavelengths.

The general appearance of the surface is velvet black. The blackness of this surface is caused by the topography of the surface. The scanning micrograph in Figure 4.41 suggests that the surface is not smooth, it is rough. Thus the high absorptivity is caused by multiple reflection of light within the surface structure. At the same time the surface appears smooth at a longer wavelength. In addition the black nickel foil provides a very slight gradual decrease in $\underline{a}$ value as a function of the off-axis angle which is an advantage for flat plate collection application, as shown in Figure 4.39.

The results of the spectral measurements of reflectance for black paint [3M-NEXTEL] and black nickel foil obtained in the present work can be compared with the results of McDonald [1975] for black chrome and that of Peterson and Ramsey [1975] for two layers of black nickel, see Figure 6.3. It is clear that in the visible spectrum both the double layer black nickel and the black chrome have minimum-maximum reflectance characteristics, probably due to the index of refraction-layer thickness combinations producing interference effects. There is a displacement of about 0.25 μm between the maximum-minimum points on the black chrome curve and the corresponding points on the double layer of black nickel. However, the reflectance of black nickel foil is independent of the visible spectrum up to 1.2 μm. The reflectance increases more rapidly with wavelength in the infrared region for the double layer of black nickel than for the black chrome and the latter more rapidly than the black nickel. At a wavelength of 10 μm the black nickel foil has the lowest reflectance. It is 4% lower than the reflectance of black chrome and 8% lower than for the double layer of black nickel. This leads the emissivity of the black nickel foil surface to be higher than the other surfaces mentioned [*e* = 0.088 black chrome; *e* = 0.07 double layer; while *e* = 0.13 - 0.14 for the black nickel bonded foil.

The *a*/*e* values reported in the literature for black chrome and double layer black nickel are 9.8 and 13.8 respectively, and the

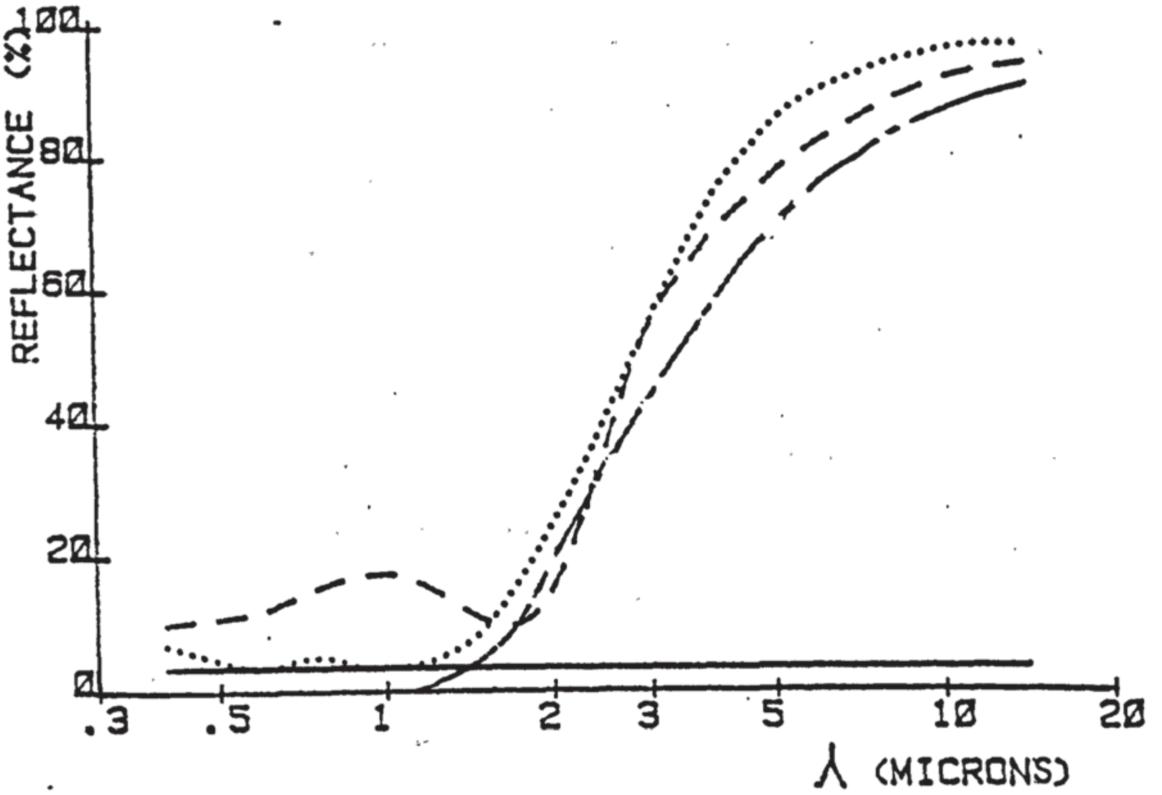

Fig. 6.3 Comparison of the specular reflectance for the black nickel foil [---], with that of double layer black nickel [...], black chrome [-–] and 3M-Nextel black paint [——].

determined values from this work for black paint and the black nickel foil were 1 and 7.3 respectively. The result obtained in this work for $\bar{a}/\bar{e}$ for the black nickel foil, i.e. 7.3 is lower than the value of 8.1 reported by Wright and Mason (1978) for the black nickel foil (without adhesive). This could possibly be due to two factors; firstly the technique of attaching the adhesive foil to the substrate. On heating it was clearly demonstrated that the changes in the surface flatness leads to reflectance changes from one sample to another, thus giving different values of the emittance. So the values given in Table 4.14 are the average of a set of samples for each test. Secondly, the absorptance calculated in this work was from total hemispherical directional reflectance, i.e. a_θ, while those of Wright and Mason were quoted from specular reflectance, i.e. a_n.

6.5.2 LIFE TESTING

The maximum temperature stability of the black nickel adhesive foil has been found to be in the range 220°C - 250°C in air and in a vacuum of 10 mTorr. Above this temperature range the adhesive will break down.

The cycling test between 40°C and 110°C and between 40°C and 210°C up to 48 hours at a rate of 4 cycle/hr showed no effect on the absorptance and the emittance values. However, only the emittance value increased by 2% after cycling between 40°C and 210°C at a rate of 2 cycles/hr up to 192 hours.

Black nickel foil passed the test at a constant temperature of 67°C and 97% relative humidity for 72 hours and 192 hours, i.e. the a and e values did not change under this test, as shown in Table 4.14.

6.5.3 COMPOSITION ANALYSIS

The elemental compositions on the surface of the unheated black nickel foil were found to be rich in nickel and poor in chromium and oxygen. After heating for 192 hours at 210°C the oxygen content increased from 38% to 48% with a reduction in concentration of the nickel, i.e. the nickel oxide increased in depth. This increased layer of the oxide appeared to have no effect on the selectivity of the black nickel foil.

6.5.4 LIMITATIONS

Since black nickel foil with an adhesive underneath has a flat surface, it should be rolled and attached to the substrate carefully such that no air pockets, creases or folds can be seen. This will keep emittance low and hence the surface will have higher selectivity.

6.6 SUMMARY OF CONCLUSION

There appears to be a correlation between low ψ and Δ values and good selectivity for a given sample after treatment or for a group of samples of the same material. This suggests the possibility of using the ellipsometer as a guide to selectivity.

Computation analysis as carried out for the grown titanium oxide case did not produce a model to explain changes in ψ and Δ relating to a varied oxide growth for the INCO stainless steel samples.

Table 6.4 illustrates the optical properties of the surfaces under study before and after heat treatment. This table also gives the efficiency of every surface considered. It is defined as

$$\frac{\text{absorbed flux - emitted flux}}{\text{solar insolation}}$$

The efficiency in this work was calculated at a temperature of 100°C with an insolation of 800 watt m^{-2}.

The absorbed flux is then equal to 800 $\underline{a}$. The emitted flux is $\underline{e}\,\sigma\,[T_S^{\,4} - T_W^{\,4}]$, where $\underline{a}$ is the absorptance and $\underline{e}$ is the emittance at temperature 373 Kelvin and the Stefan Boltzmann constant $\sigma = 5.668 \times 10^{-8}$ watt $m^{-2}\ k^{-4}$.

Table 6.4 suggests that the best candidate for a selective sample surface is the 'black nickel foil'. It is of highest efficiency of about 88% even after heating at 210°C for 192 hours. It is of lower cost than the other surfaces.

The second candidate is the INCO stainless steel surface corresponding to 5 mV with an efficiency about 79% up to 192 hours heating at 210°C.

The advantages of the stainless steel over the black nickel is that it has a good appearance, a good wear resistance, a high corrosion resistance and it has no problem of flatness limitation. However, its disadvantage is that it has a higher cost.

The efficiency of the 1.5 mV and 3 mV surface samples increases by about 10% when they have been coated with Si_3N_4 125 nm thick layer.

The values of the total hemispherical emittance obtained by using the calorimetric [steady state] method were significantly higher than that obtained by reflectance technique for the selective and non-selective surfaces.

Surface treatment	$\underline{a}/\underline{e}_n$(100°C)						Efficiency %					
	Not coated with Si_3N_4			Coated with 125 nm Si_3N_4			Not coated with Si_3N_4			Coated with Si_3N_4		
	Before heating	Heating 192 hr 210°C	Heat. 160 min 300°C	Before heating	Heating 192 hr 250°C	Heating 3½ hr 300°C	Before heating	Heating 192 hr 210°C	Heat. 160 min 300°C	Before heating	Heating 192 hr 250°C	Heating 3½ hr 300°C
1.5mV INCO surface	0.73/ 0.10	0.77/ 0.10	0.79/ 0.10	0.90/ 0.09	0.90/ 0.09	0.90/ 0.10	65	69	71	83	82	82
3.0mV INCO surface	0.80/ 0.10	0.81/ 0.10	0.81/ 0.10	0.90/ 0.09	0.90/ 0.09	0.90/ 0.09	72	73	73	83	83	83
5.0mV INCO surface	0.87/ 0.10	0.87/ 0.10	0.83/ 0.09	0.86/ 0.09	0.86/ 0.10	0.86/ 0.10	78	79	76	78	78	78
7.0mV INCO surface	0.84/ 0.10	0.83/ 0.10	0.80/ 0.09	0.82/ 0.09	0.82 0.10	0.82/ 0.10	76	75	73	75	74	74
9.0mV INCO surface	0.82/ 0.11	0.78/ 0.10	0.78/ 0.09	0.79/ 0.09	0.78/ 0.10	0.78/ 0.10	73	70	71	72	70	70
Black nickel foil INCO	0.99/ 0.14	0.99/ 0.14	0.98/ 0.17	-	-	-	88	88	84	-	-	-
304 s.s. uncoated (polished)	0.35/ 0.09	-	-	-	-	-	28	-	-	-	-	-
304 s.s. heated 6 min (973K)	0.75/ 0.10	-	-	-	-	-	67	-	-	-	-	-
316 s.s. unheated (polished)	0.35/ 0.09	-	-	-	-	-	28	-	-	-	-	-
316 s.s. heated 90 min (polished)	0.74/ 0.10	-	-	-	-	-	66	-	-	-	-	-
Titanium (unheated)(polished)	0.47/ 0.06	-	-	-	-	-	71	-	-	-	-	-
Thermally grown oxide on titan. sheet heat. 40 min (670K) in ai	0.79/ 0.10	-	-	-	-	-	74	-	-	-	-	-
Titanium oxide (30nm) on Al sheet. Heated 4 hr (770K)	0.80/ 0.08	-	-	-	-	-	59	-	-	-	-	-
Titanium oxide (50nm) on Al sheet. Heated 4 hr (770K)	0.69/ 0.13	-	-	-	-	-	57	-	-	-	-	-
Titanium oxide (50nm) on pre heated Al sheet Heat. 4hr (770K)	0.70/ 0.16	-	-	-	-	-		-	-	-	-	-

Table 6.4 Efficiency and the optical properties before and after heating for the surfaces under study in this work

APPENDIX 1.a

Ellipsometer program

The program sets out to calculate the values of ellipsometer parameters   and   for a set of assumed values of n_2,k_2 and thickness for the film.

```
100 REM === ELLIPSOMETER PROGRAM =====
110 REM == THE PROGRAM SETS OUT TO CALCULATE
120 REM == THE VALUES OF ELLIPSOMETER PARAMETERS
130 REM ==        AND        FOR A SET OF ASSUMED
140 REM == VALUES OF N2,K2 AND THICKNESS FOR THE FILM
150 PRINT"▚"
160 PRINT"▚PROGRAM IS RUNNING":PRINT
170 PRINT"▚SCREEN OR ▚PRINTER":PRINT
180 GET A$:IFA$=""THEN180
190 IF A$="S"THENOPEN4,3:GOTO220
200 IF A$="P"THENOPEN4,4:GOTO220
210 GOTO 180
220 PRINT#4,"           PSI DEL"
230 PRINT#4,"====================================="
240 PRINT#4,
250 DIMA(14),B(14),K(3),N(13),R(5),X(5),Y(5)
260 READN(2),K(2),N(3),K(3),T,L,D0,D9,S0
270 PRINT#4,"N2="N(2)SPC(5)"K2="K(2)
280 PRINT#4,"N3="N(3)SPC(5)"K3="K(3):PRINT#4
290 PRINT#4,"WAVELENGTH="L:PRINT#4
300 PRINT#4,"ANGLE (RAD)="T:PRINT#4
310 PRINT#4,TAB(1);"THICKNESS"TAB(10);"DELTA";
320 PRINT#4,TAB(10);"PSI";TAB(14);"REAL DEL"
330 PRINT#4,TAB(1);"========="TAB(10);"=====";
340 PRINT#4,TAB(9);"======";TAB(12);"======
350 FOR D=D0TOD9 STEPS0
360 I=0:X0=K(2+I)*K(2+I):T4=T:X(4)=SIN(T4)
370 X(4)=X(4)*X(4):N(4+I)=N(2+I)*N(2+I)
380 X(2+I)=N(4+I)-X0-X(4)
390 Y(2+I)=2*N(2+I)*K(2+I):X(4+I)=X(2+I)*X(2+I)
400 Y(4+I)=Y(2+I)*Y(2+I):R0=SQR(X(4+I)+Y(4+I))
410 A0=SQR((R0+X(2+I))/2)
420 A(4+I)=N(2+I)*A0:A(7+I)=SQR(ABS((R0-X(2+I))/2))
430 A(9+I)=A(7+I)*K(2+I)+A(4+I):A(4+I)=X0+N(4+I)
440 A(2+I)=A(9+I)/A(4+I):B0=K(2+I)*A0:B(4+I)=N(2+I)*A(7+I)
450 B(2+I)=(B0-B(4+I))/A(4+I):IFA(2+I)>0THEN610
460 A(2+I)=-A(2+I):B(2+I)=-B(2+I)
470 GOTO610
480 X(I)=K(2+I)*K(2+I)
490 T4=T
500 X(4)=SIN(T4):X(4)=X(4)*X(4):N(4+I)=N(2+I)*N(2+I)
510 X(2+I)=N(4+I)-X(I)-X(4):Y(2+I)=2*N(2+I)*K(2+I)
520 X(4+I)=X(2+I)*X(2+I):Y(4+I)=Y(2+I)*Y(2+I)
530 R(I)=SQR(X(4+I)+Y(4+I))
540 A(I)=SQR((R(I)+X(2+I))/2):A(4+I)=N(2+I)*A(I)
550 A(7+I)=SQR((R(I)-X(2+I))/2):A(9+I)=A(7+I)*K(2+I)+A(4+I)
```

APPENDIX 1.a[cont]

```
560 A(7+I)=SQR((R(I)-X(2+I))/2):A(9+I)=A(7+I)*K(2+I)+A(4+I)
570 A(4+I)=X(I)+N(4+I):A(2+I)=A(9+I)/A(4+I)
580 B(I)=K(2+I)*A(I):B(4+I)=N(2+I)*A(7+I)
590 B(2+I)=(B(I)-B(4+I))/A(4+I):IFA(2+I)>0THEN610
600 A(2+I)=-A(2+I):B(2+I)=-B(2+I)
610 I=I+1
620 IFI=1THEN480
630 C=COS(T4):C1=N(2)*C:C2=A(2)-C1
640 E2=C1+A(2):D1=K(2)*C:D2=D1+B(2)
650 F2=B(2)-D1:E=C2*E2:E1=D2*F2
660 G2=E+E1:G=E2*E2:G1=F2*F2:G=G+G1
670 G2=G2/G:F=C2*F2:F1=D2*E2:H2=(F1-F)/G
680 H=N(3)*A(2):H1=K(3)*B(2):H4=N(2)*A(3)
690 H5=K(2)*B(3):C3=H4+H5-H-H1
700 H8=N(3)*B(2):H9=K(3)*A(2):H6=K(2)*A(3)
710 H7=N(2)*B(3):D3=H9-H8+H7-H6
720 E3=H+H1+H4+H5:F3=H8+H7-H9-H6:G4=C3*E3
730 G5=D3*F3:G6=E3*E3:G7=F3*F3+G6
740 G3=(G4+G5)/G7:F4=C3*F3
750 H3=(D3*E3-F4)/G7:P=N(2)*A(2)
760 P1=K(2)*B(2):P2=C-P-P1:P4=N(2)*B(2)
770 P5=K(2)*A(2):S2=C+P+P1:Q2=P4-P5
780 T2=P5-P4:U=P2*S2
790 U1=Q2*T2:U4=S2*S2:U5=U4+T2*T2
800 U2=(U+U1)/U5:U7=Q2*S2:U6=P2*T2-U7
810 V2=U6/U5:Q=N(3)*A(3):Q1=K(3)*B(3)
820 P3=P+P1-Q-Q1:Q4=B(3)*N(3):Q5=K(3)*A(3)
830 Q3=P5-P4+Q4-Q5:S3=P+P1+Q+Q1:T3=P5-P4-Q4+Q5
840 V=P3*S3:V1=Q3*T3:V4=S3*S3
850 V5=V4+T3*T3:U3=(V+V1)/V5
860 V6=P3*T3:V7=Q3*S3:V3=(V6-V7)/V5
870 M1=P+P1:M=6.283185*D/L:M1=M1*M
880 L1=(P4-P5)*M:M3=EXP(2*L1):M=2*M1
890 M2=M3*COS(M):L2=M3*SIN(M):L4=G3*M2
900 L5=H3*L2:A(11)=G2+L4+L5:L6=H3*M2
910 L7=G3*L2:B(11)=H2+L6-L7:S4=U2*U3*M2
920 S5=V2*V3*M2:S6=L2*V3*U2:S7=L2*V2*U3
930 A(12)=1+S4-S5+S6+S7:S8=V2*U3*M2
940 S9=U2*M2*V3:J=U2*U3*L2:J1=V2*V3*L2
950 B(12)=S8+S9-J+J1:Q6=G2*G3*M2
960 Q7=H2*H3*M2:Q8=H2*L2*G3:Q9=H3*L2*G2
970 A(13)=1+Q6-Q7+Q8+Q9:P6=H2*G3*M2
980 P7=H3*G2*M2:P8=L2*G2*G3:P9=H2*H3*L2
990 B(13)=P6+P7-P8+P9:T5=U3*M2
1000 T6=V3*L2:A(14)=U2+T5+T6:T7=M2*V3
1010 T8=U3*L2:B(14)=V2+T7-T8
```

APPENDIX 1.a (cont)

```
 1020 R(2)=A(11)*A(12):J2=R(2)-B(11)*B(12)
 1030 R(3)=B(11)*A(12):J3=A(11)*B(12)+R(3)
 1040 R(4)=A(13)*A(14):J4=R(4)-B(13)*B(14)
 1050 R(5)=B(13)*A(14):J5=A(13)*B(14)+R(5)
 1060 W1=J2*J4:W2=J3*J5:W3=J4*J4:W4=W3+J5*J5
 1070 W=(W1+W2)/W4:Z1=J4*J3
 1080 Z2=J2*J5:Z=(Z1-Z2)/W4:Z3=180*ATN(Z/W)/(4*ATN(1))
 1090 Y1=Z3
 1100 Z3=180+Z3
 1110 Z4=W*W
 1120 Z5=180*ATN(SQR(Z4+Z*Z))/(4*ATN(1))
 1130 PRINT#4,TAB(3);D;TAB(8);Z3;TAB(3);
 1140 PRINT#4,Z5;TAB(1),Y1:NEXT
 1150 END
 1160 REM=========== DATA ==============
 1170 REM DATA N(2),K(2)=FILM& N(3),K(3)= SUBS
 1180 REM T=INC.ANG(RAD)& L=WAVLENGTH(ANG)
 1190 REM DATA D0,D9=MIN & MAX
 1200 REM DATA S0=STEP IN FILM THICKNESS
 1210 REM===============================
 1220 DATA 2.42,0,2.28,3.70,1.07,5461,0,50,5
READY.
```

APPENDIX 1.b

Reflectance versus film thickness program

The program sets out to calculate the values of the spectral reflectance for a system of absorbing film of index $(n_f - ik_f)$ on an absorbing substrate of index $(n_s - ik_s)$.

```
100 REM===THIS PROGRAM IS SET OUT TO
200 REM==CALCULATE THE VALUES OF THE
300 REM==SPECTRAL REFLECTANCE FOR A
400 REM==SYSTEM OF AN ABSORBING FILM
500 REM==OF (NF-IKF) ON AN ABSORBING
600 REM==SUBSTRATE OF (NS-IKS)
610 PRINT#4,
700 READ NF,KF,NS,KS
800 READ W1,W2,SW,T1,T2,TS
900 A=(1-NF↑2+KF↑2)/((1+NF)↑2+KF↑2)
 1000 B=(2*KF)/((1+NF)↑2+KF↑2)
 1100 C1=NF↑2-NS↑2-KS↑2+KF↑2
 1200 C2=(NF+NS)↑2+(KS+KF)↑2
 1300 C=C1/C2
 1400 D1=2*NF*KS+2*NS*KF
 1500 D=D1/C2:OPEN1,4
 1600 PRINT#1,"NF=";NF:PRINT#1,KF=";KF
 1700 PRINT#1,"NS=";NS:PRINT#1,KS=";KS
 1800 PRINT#1,"-----R--------------T----------W"
 1900 PRINT#1,"---------------------------------":PRINT#1
 2000 FOR W=W1 TO W2 STEP SW
 2100 FOR T=T1 TO T2 STEP TS
 2200 E=EXP(-4**T*KF/W)*COS(4**T*NF/W)
 2300 F=EXP(-4**T*KF/W)*SIN(4**T*NF/W)
 2400 G=A+C*E+D*F
 2500 H=B-C*F+D*E
 2600 K=1+A*C*E-B*D*E+F*A*D+F*B*C
 2700 L=E*A*D+B*C*E-F*A*C+F*B*D
 2800 R=((G*K+H*L)↑2-(K*H-G*L)↑2)/((K*K+L*L)↑2)
 2900 PRINT#1,R,T,W
 3000 NEXT:NEXT:CLSE1
 3100 REM === DATA =====
 3200 REM === DATA NF ,KF , NS , KS ==
 3300 REM === DATA W1 ,W2 ,SW ,T1 ,T2 ,TS
 3400 DATA 2.4,.25,2.36,3.28
 3500 DATA 5461,5561,100,100,700,50
READY.
```

PUBLICATION

Optical Properties of Bulk Titanium and Thermally Grown Oxide Films on Titanium Using Ellipsometer.

Accepted for publication in Surface Technology [1980].

REFERENCES

Ashcroft, N.W., Buhrman, R.A., Craighead, H.G., Lamb, W., Sievers, A.J., Smalley, R., Trotter, D.M., Wilkins, J.W., Wojcik, L. and Wood, D.M., 1979. Proceedings second annual conference on absorber surfaces for solar receivers. Jan. 24 & 25, 77-86.
A Study of Metal/Insulator Composite Media and Metal Surfaces for Use in Selective Absorber Systems.

ASHRE Handbook of Fundamentals, American Society of Heating, Refrigeration and Air Conditioning Engineers, New York, N.Y.

ASTM Book of Standards 1977, Pt 46, 297-303.
Standards Methods of Test for Solar Energy Transmittance and Reflectance [Terrestrial] of Sheet Materials.

Bacha, C.P., Honea, F.I., and Watanabe, D. 1962 SID 62-335 AD 606250.
Temperature Control Systems for Space Vehicles.

Beattie, J.R. and Conn, G.K.T. 1955 Philos. Mag. 46, 222-234.
Optical Constants of Metals in the Infrared Principles of Measurement.

Bennett, H.E. and Koehler, W.F. 1960 J. Opt. Soc. Am. 50, 1-6.
Precision Measurement of Absolute Specular Reflectance with Minimized Systematic Errors.

Bennett, H.E., Silver, M. and Ashley, E.J. 1963 J. Opt. Soc. Am. 53, 1089-1903.
Infrared Reflectance of Aluminium Evaporated in Ultra-High Vacuum.

Bilton, T., Flowers, E.C., McCormik, R.A. and Kurfis, K.R. 1973 Report and Recommendations of the Solar Energy Data Workshop, Nov.29-30. Charles Turner, Editor, NOAA, Environmental Research Laboratories, Air Resources Laboratories, Silver Springs, Md.

Blattner, R.J., Evans, C.A. and Braundmeier 1977 J. Vac. Sci. Technol., 14, 1132-1138.
Mechanism of High-Temperature Instability of CuO-Ag Thin Film Absorber.

Blickensderfer, R., Deardorff, D.K. and Lincoln, R.L. 1977 Solar Energy 19, 429-432.
Spectral Reflectance of TiNx and ZrNx Films as Selective Solar Absorbers.

Carrol, J.J. and Melmed, A.J. 1974 J. Opt. Soc. Am. 64, 514-515.
Optical Constants of Titanium.

Carver, G.E., Gurev, H.S. and Seraphin, B.O. 1978 J. Electrochem. Soc. 125, 1138-1140.
Passivating CVD Molybdenum Films Against Infrared Reflection Losses Caused by Oxidation.

Chain, E.E., Carver, G.E. and Seraphin, B.O. 1980. Presented at International Conf. On Metallurgical Coatings, San Diego, CA. April 21-25. Thin Solid Films [to be published].

Close, D.J. 1962 Report E.D.7 Engr. Sect. Commonwealth Scientific and Industrial Research Organization Melbourne, Australia.
Flat Plate Solar Absorber: The Production and Testing of Selective Surfaces for Copper Absorber Plates.

Close, D.J. 1963 Solar Energy 7, 117-124.
For Low and Moderate Temperature Applications.

Cuomo, J.J., Ziegler, J.F. and Woodall, J.M. 1975 Applied Physics 26, 557-559.
A New Concept for Solar Energy Thermal Conversion.

Czanderna, A.W., Prince, E.T. and Helbig, H.F. 1979 Proceedings 2nd Annual Conf. on Absorber Surfaces for Solar Receivers 42-47, SERI/TP-49-182.

Distefano, T.H., Pettit, G.D., Woodall,J.M. and Cuomo, J.J. 1978 Appl. Phys. Lett. 32, 676-679.
Conformal Antireflective Coatings on a Textured Tungsten Surface.

Ditchburn, R.W. 1955 J. Opt.Soc. Am. 45, 743-748.
Some New Formula For Determining the Optical Constants from Measurements.

Donnadieu, A., and Seraphin, B.O., 1978 J. Opt. Soc. Am. 68, 292-297.
Optical Performance of Absorber-Reflector Combinations Photothermal Solar Energy.

Driver, P.M., Jones, R.W., Riddiford, C.L. and Simpson, R.J. 1977 Solar Energy 19, 301-306.
A New Chrome Black Selective Absorbing Surface.

Drummeter, L.F. and Hass, G. 1964 Phys. Thin Films 2, 304-361.
Solar Absorptance and Thermal Emittance of Evaporated Coatings.

Dunkle, R.V. 1960 Surface Effect on Spacecraft Materials 117-137. F.J. Clauss, Ed. Willey, New York.

Dunn, S.T., Richmond, J.C. and Wiebelt, J.A. 1966 J. Res. Natl. Bur. Stand., C70, 75.
Ellipsoidal Mirror.

Edwards, D.K., Gier, J.T., Nelson, K.E. and Roddik, R.D. 1961 J. Opt. Soc. Am. 51, 1279-1288.
Integrating Sphere for Imperfectly Diffuse Samples.

Edwards, D.K., Gier, J.T., Nelson, K.E. and Roddik, R.D. 1962 Solar Energy 1, 1-8.
Spectral and Directional Thermal Radiation Characteristics of Selective Surfaces for Energy Collectors.

Evans, T.E., Hart, A.C. and Skedgell, A.N. 1973 Trans. Inst. Met. Fin. 51, 108-112.
The Nature of the Film on Coloured Stainless Steel.

Fan, J.C.C. 1976 Proceedings of the Society of Photo-optical Instrumentation Engineers 85, 35-46.
Wavelength-Selective Surfaces for Solar Energy Utilization.

Fan, J.C.C. 1978 Thin Solid Films 54, 139-148.
Selective-Black Absorbers Using Sputtered Cermet Films.

Fan, J.C.C. and Bachner, F.J. 1976 Appl. Optics 15, 1012-1017.
Transparent Heat Mirrors for Solar-Energy Applications.

Fan, J.C.C. and Zavracky, P.M. 1976 Appl. Phys. Lett. 29, 478-480.
Selective Black Absorbers Using MgO/Au Cermet Films.

Fane, R.W., Neal, W.E.J. and Latham, R.V. 1973 Appl. Phys. 44, 740-743.
Ellipsometric Observations of an Electron-Bombarded Stainless Steel Surface.

Fujishima, A. and Honda, K. 1972 Nature 238, 37-38.
Electrochemical Photolysis of Water at a Semiconductor Electrode.

Fussell, W.S., Triolo, J.J. and Henninger, J.H. 1963 NASA *TN D-1716*.
A Dynamic Thermal *Vacuum Technique for Measuring the* Solar Absorptance and Thermal Emittance of Space Craft Coatings.

Fowler, P. 1960 National Technical Information Services, U.S. Government AD 418456.
Far Infrared Absorptance of Gold.

Gates, D.M., Shaw, C.C. and Beaumont, D. 1958 J. Opt. Soc. Am. 48, 88-92.
Infrared Reflectance of Evaporated Metal Films.

Gier, J.T., Dunkle, R.V. and Bevans, J.T. 1954 J. Opt. Soc. Am. 44, 558-562.
Measurement of Absolute Spectral Reflectivity from 1.0 to 15 Microns.

Gilbert, L.R., Messier, R. and Roy, R. 1978 Thin Solid Films 54, 149-157.
Black Germanium Solar Selective Absorber Surfaces.

Gillette, R.B. 1960 Solar Energy 4, 24-32.
Cobalt Oxide and a Chrome-Nickel-Vanadium Alloy Plate.

Goebel, D.G. 1967 Appl. Optics 6, 125-128.
Generalized Integrating-Sphere Theory.

Gogna, P.K. and Chopra, K.L. 1979 Solar Energy 23, 405-408.
Selective Black Nickel Coatings on Zinc Surfaces by Chemical Conversion.

Gogna, P.K. and Chopra, K.L. 1979 Thin Solid Films 63,183-187.
Optical and Topographical Properties of Selective Black Chrome.

Granqvist, C.G., Andersson, A., and Hunderi, O. 1979 Appl. Phys. Lett. 35, 268-270.
Spectrally Selective Surfaces of Ni-pigmented Anodic Al_2O_3.

Grimmer, D.P., Herr, K.C. and McCreary 1978 J. Va. Sci. Technol. 15, 59-64.
Possible Selective Solar Photothermal Absorber: Ni Dendrites Formed on Al Surfaces by the CVD of $Ni(CO)_4$.

Hager, N.E. 1965 The Review of Scientific Instruments 36, 1564-1570.
Thin Foil Heat Meter.

Hass, G. 1955 J. Opt. Soc. Am. 45, 945-952.
Filmed Surfaces for Reflecting Optics.

Hass, G. and Bradford, A.P. 1957 J. Opt. Soc. Am. 47, 125-129.
Optical Properties and Oxidation of Evaporated Titanium Film.

Heavens, O.S. 1955 Optical Properties of Thin Solid Films (Dover, New York).

Heavens, O.S. 1960 Reports on Progress in Physics, ed. by A.C. Strickland, 23, p. 1, The Physical Society, London.
Optical Properties of Thin Films.

Heavens, O.S. 1964 Physics of Thin Films, 2, 193-237.
Measurement of Optical Constants of Thin Films.

Hill, R. and Weaver, C. 1958 Trans. Faraday Soc. 54,1140-1146.
The Optical Properties of Chromium.

Hollands, K.G.T. 1963 Solar Energy 7, 108-117.
Directional Selectivity, Emittance, and Absorptance Properties of Vee Corrugated Specular Surfaces.

Horwitz, C.M. 1974 Optics Communications, 11, 210-212.
A New Solar Selective Surface.

Hutchins, M.G. 1979 Proceedings of IEE Conf. Future Energy Concepts, London, 249-252.
Thin-Film Coatings in Solar Water Heating Systems.

Hottle, H.C. and Unger, T.A. 1959 Solar Energy 3, 10-15.
Properties of a Copper Oxide-Aluminium Selective Black Surface Absorber of Solar Energy.

Jacobson, M.R. and Lamoreaux, R.D. 1979 Proceedings of the 2nd Annual Conf. on Absorber Surfaces for Solar Receivers, 151-160, SERI/TP-49-182.
Instrumentation for the Evaluation of Selective Surfaces at the University of Arizona.

Jacquez, J.A. and Kuppenheim, H.F. 1955 J. Opt. Soc. Am. 45, 460-47-.
Theory of Integrating Sphere.

Kadryashova, M.D. 1969 Applied Solar Energy 5, 82-88.
New Selective Coatings for Collector Surfaces of Solar Plants.

Karlsson, B. and Ribbing, C.G. 1978 Proceedings of the Society of Photo-Optical Instrumentation Engineers Vol. 161/IV. Optics Applied to Solar Energy.
Coloured Stainless Steel: A New Type of Selective Absorber.

Kirillova, M.M. and Charikov, B.A. 1963 Phys. Metals, Metallog. USSR 15, 138-139.
Optical Properties of Titanium in the Quantum Transition Range.

Kneissl, G.T. and Richmond, J.C. 1968 NBS Technical Note 439, National Bureau of Standards, Washington, D.C.

Kokoropoulos, P., Salam, E. and Daniels, F. 1959 Solar Energy 4, 19-23.
Selective Radiation Coatings Preparation and High Temperature Stability.

Lampert, C.M. and Washburn, J. 1979 Proceedings 2nd Annual Conf. on Absorber Surfaces for Solar Receivers 19-30. SERI/TP-49-182.
Microstructure and Optical Properties of Black Chrome Before and After Exposure to High Temperatures.

Latham, R.V. and Brah, A.S. 1977 J. Phys. D: Appl. Phys. 10, 151-167.
The influence of surface oxidation on the electron tunnelling mechanism of microparticle charge reversal during a bouncing impact on a charged conductor.

Leig, M Van der, 1979 PhD Thesis Delft University.
Spectral-Selective Surfaces for the Thermal Conversion of Solar Energy.

Long, R.L. 1965 J. Engineering Power 87, 277-280.
A Review of Recent Air Force Research on Selective Solar Absorbers.

MacMahon, T.J. and Jasperson, S.N. 1974 Appl. Opt., 13, 2750-2751.
PbS-Al Selective Solar Absorber.

Marchini, R. and Gandy, R. 1978 J. Appl. Physl., 49, 390-391.
Selective Absorption Properties of Lead Sulfide Aluminium Coatings as a Function of Lead Sulfide Thickness.

Mash, I.D. and Motulevich, G.P. 1973 Soviet Physics J. ETP 36, 516-520.
Optical Constants and Electronic Characteristics of Titanium.

Masterson, K.D. 1977 J. of Solid State Chemistry 22, 41-49.
Selective Surfaces for Solar Thermal Conversion.

Mattox, D.M. and Sowell, R.R. 1974 J. Vac. Sci. Tecnol. 11, 793-797.
High Absorptivity Solar Absorbing Coatings.

Mattox, D.M. 1976 J. Vac. Sci. Technol. 13, 127-134.
Application of Thin Films to Solar Energy Utilization.

Meinel, A.B., McKenney, D.B. and Beauchamp, W.T. 1975 Tech. Report, NSF-RANN/SE/GI-41895 78-92.
Air Stable Selective Surfaces for Solar Energy Collectors.

Meinel, A.B. and Meinel, M.P. 1976 Applied Solar Energy: An Introduction Ch. 9. Addison-Wesley Publishing Co.

McDonald, G.E. 1975 Solar Energy 17, 119-122.
Spectral Reflectance Properties of Black Chrome for Use as a Solar Selective Coating.

McCrackin, F.L., Passaglia, E., Stromberg, R.R. and Steinberg, H.L. 1963 J. of Research of the National Bureau of Standards A - Physics and Chemistry. 67A, 363-377.
Refractive Index of Very Thin Films and the Optical Properties of Surfaces by Ellipsometry.

McKenzie, D.R. 1976 J. Opt. Soc. Am. 66, 249-253.
Selective Nature of Gold Black Deposit.

McKenzie, D.R. 1979 Appl. Phys. Lett. 34, 25-28.
Gold, Silver, Chromium, and Copper Cermet Selective Surfaces for Evacuated Solar Collectors.

Millard, J.P. and Streed, E.R. 1969 Appl. Optics, 8, 1485-1492.
A Comparison of Infrared-Emittance Measurements and Measurement Techniques.

Minard, R.C. 1962 J. Opt. Soc. Am. 52, 427-431.
Optical Measurement of Oxide Thickness on Titanium.

Moon, P. 1940 J. of the Franklin Institute, 230, 583-618.
Proposed Standard Solar-Radiation Curves for Engineering Use.

Neal, W.E.J. 1979 Applications of Surface Science 2, 445-501.
Optical Examination and Monitoring of Surfaces.

Neher, R.T. and Edwards, D.K. 1965 Appl. Optics, 4, 775-780.
Far Infrared Reflectometer for Imperfectly Diffuse Specimens.

Okuyama, M., Furusawa, K., Hamakawa, Y. 1979 Solar Energy 22, 479-482.
Ni Cermet Selective Absorber For Solar Photothermal Conversion.

Ollard, E.A. and Smith, E.B. Handbook of Electron Plating, Elsevier, New York, 1964.

Palmberg, P.W., Riach, G.E., Weber, R.E. and MacDonald, N.C. 1972 Physical Electronics Industries Inc. Handbook of Auger Electron Spectroscopy.

Peterson, R.E., and Ramsey, J.W. 1975 J. Vac. Sci. Technol. 12, 174-181. Thin Film Coatings in Solar Thermal Power Systems.

Pettit, R.B. 1975 SAND-75 0079 (June); Available from NTIS. Total Hemispherical Emittance Apparatus for Solar Selective Coating.

Pettit, R.B. and Sowell, R.R. 1976 J. Vac. Sci. Technol. 13, 596-602. Solar Absorptance and Emittance Properties of Several Solar Coatings.

Pettit, R.B. and Sowell, R.R. 1979 Silver Jubilee, ISES, Congress, Atlanta, Georgia. Thermal Ageing Characteristics of Electrodeposited Black Chrome Solar Coatings.

Pivovonsky, M. and Nagel, M. 1961, Tables of Black Body Radiation Functions, MacMillan, New York.

Roger, C.R., Yen, S.H. and Ramanathan, K.G. 1979 J. Opt. Soc. Am. 69, 1384-1390. Temperature Variation of Total Hemispherical Emissivity of Stainless Steel AISI 304.

Schmidt, R.N. and Janssen, J.E. 1965 Report NASA-SR-55, 509.

Schmidt, R.N. and Park, K.C. 1965 Appl. Optics, 4, 917-925.
High Temperature Space-Stable Selective Solar Absorber Coatings.

Seraphin, B.O. 1976 Optical Sciences Center Newsletter 10, 6-16.
Converting Solar Radiation to Heat: Challenges to Optical Material Science.

Seraphin, B.O. 1979 Topics in Applied Physics Solar Energy Conversion. Solid-State Physics Aspects 31, 5-54.
Spectrally Selective Surfaces and their Impact on Photothermal Solar Energy Conversion.

Sharma, V.C. and Hutchins, M.G. 1979 Proceedings of Jubilee ISES Congress, Atlanta.
Radiative Selectivity and the Oxidation of Stainless Steels.

Siegal, R. and Howell, J.R. 1972 Thermal Radiation and Heat Transfer (McGraw-Hill Book Company, New York).

Silo, R.S. and Mladinik, P.A. 1969 Applied Solar Energy 5, 18-25.
Solar Heaters Using Selective Surfaces.

Smith, T. 1972 J. Opt. Soc. Am. 62, 774-780.
Optical Constants of Clean Titanium and Tungsten Surfaces as a Function of Temperature.

Stalder, C. and Augustynski, J. 1979 J. Electrochem. Soc: Solid State Science and Technology, 126, 2007-2011. Photoassisted Oxidation of Water at Beryllium Doped Polycrystalline TiO_2 Electrodes.

Strong, J. 1938 Procedures in Experimental Physics, Prentice-Hall, 376.

Tabor, H. 1955 Conf. on the Use of Solar Energy, Tucson, Arizona, 2, Part 1, 24-33. Selective Radiation; Wavelength Discrimination Trans.

Tabor, H. 1961 Proc. Nat. Acad. Sci (USA) 47, 1271-1278. Solar Collectors, Selective Surfaces, and Heat Engines.

Tabor, H. 1967 ASHRE 41, Low Temperature Engineering Application to Solar Energy.

Tabor, H., Harris, J., Weinberger, H. and Doron, B., 1961 Proceedings of the United Nations Conf. on New Sources of Energy, Rome, August 21-31, 4, 618-623.

Tanaka, T. 1979 Japanese J. of Appl. Phys. 18, 1153-1155. A Method for Measuring the Photothermal Conversion Efficiency of Solar Energy.

Thekaekara, M.P. 1973 Solar Energy 14, 109-127. Solar Energy Outside the Earth's Atmosphere.

Thekaekara, M.P. 1974 Ed. The Energy Crisis and Energy from the Sun, Ch. 2, Data on Incident Solar Energy, Institute of Environmental Sciences, Mt. Prospect,II.

Thomas, A. and Richmond, J.C. 1978 Proceedings of a Seminar on Testing Solar Energy Materials and Systems, Institute of Environmental Sciences, Gaithersburg, MD, May 22-24.

Trombe, F., Foëx, M. and Phatvinh, M. 1961 Proceedings of the United Nations Conf. on New Sources of Energy, Rome, August 21-31, 4, 638-649.
Studies on Selective Surfaces for Air-Conditioning Dwellings.

Vasicek, A. 1960 Optics of Thin Films, North Holland Publishing Co., Amsterdam.

Vermilyea, D.A. 1958 Acta Metal., 6, 166-177.
The Oxidation of Tantalum at 50-300°C.

Verret, D.P. and Ramanathan, K.G. 1978 J. Opt. Soc. Am. 68, 1167-1172.
Total Hemispherical Emissivity of Tungsten.

Willrath, H. and Gammon, R.B. 1978 Solar Energy 21, 193-199.
The Measurement of Optical Properties of Selective Surfaces Using a Solar Calorimeter.

Williams, W.S., Lappin, T.A., Duffie, J.A. 1963 Trans. ASME, J. Eng. Power 85, 213-220.
Selective Radiation Properties of Particular Coatings.

Winterbottom, A.B. 1946 Trans. Farad. Soc. 42, 487-495.
Optical Methods of Studying Films on Reflecting Bases Depending on Polarisation and Interference Phenomena.

Winterbottom, A.B. 1948 J. Opt. Soc. Am. 38, 1074-1082.
Optical Determination of Thin Films on Reflecting Bases in Transparent Environments.

Wright, B. and Mason, J.J. 1978 Second Annual Solar Energy Forum, Hamburg, 1, 337-340.
Metal Foil Selective Surface on Flat Plate Solar Collector.

Yoshida, S. 1979 Thin Solid Films 56, 321-329.
Antireflection Coatings on Metals for Selective Solar Absorbers.